Neuropharmacological Studies of Sodium Channel-linked Developmental and Epileptic Encephalopathies

by

Nicholas Denomme

A dissertation submitted in partial fulfillment
of the requirements for the degree of
Doctor of Philosophy
(Pharmacology)
in the University of Michigan
2022

Doctoral Committee:

Professor Lori L. Isom, Chair
Assistant Professor William Birdsong
Professor Richard I. Hume
Professor George A. Mashour
Professor Alan V. Smrcka
Research Assistant Professor Yukun Yuan

I must Create a System, or be enslav'd by another Mans

I will not Reason & Compare: my business is to Create

William Blake (1820)

Nicholas S. Denomme

ndenomme@umich.edu

ORCID iD: 0000-0002-7631-0385

© Nicholas Denomme 2022

Dedication

Dedicated to Dr. Edward F. Domino (1924-2021)

The single most important gift I have received in my scientific journey—which has carried me to where I am today—is knowing that Dr. Ed Domino believed in me. When I first met Ed, I was lost, stuck in the vicious loop of self-doubt many young men find themselves in. I was dubious about myself, my abilities, and my value in the world.

And here was a man, 70 years my senior, who had accomplished everything in the field of psychopharmacology I could ever dream of. He not only listened to my ideas, but he also encouraged them. He saw a spark and treated me as an equal; told me that he saw “a monkey on my back.” I’ll never forget the feeling of validation that lifted my soul as I walked out of his office after our first conversation (Denomme 2018). I no longer cared what anyone else thought of me as a scientist, including myself.

I’ll forever cherish my time spent with Ed. He was a raconteur of the highest order always willing to share his wisdom. Ed taught me so much about science and life. How to: encourage everyone around you; befriend an enemy; treat women and the people you love, (and as Ronald Holz put it) “to be sure of myself while staying humble.” Thank you for everything, Dr. D. This Ph.D. is dedicated to you.

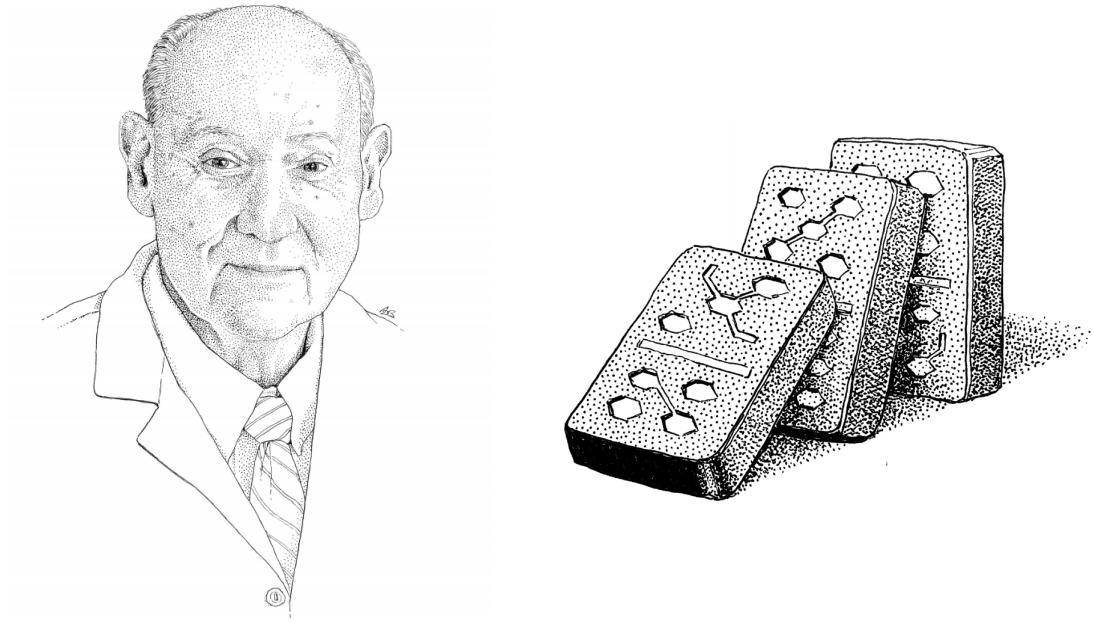


Illustration 1.1. The Domino Effect. An illustration of Dr. Ed Domino and a row of dominoes. ‘The Domino Effect’ is known as a chain reaction of falling dominoes, whose cumulative effects can be traced back to actions of the first, single member. When properly aligned, a row of dominoes can only be stopped by a lack of dominoes in line on which to lean. His family, friends, colleagues, trainees, and all human beings inspired by Ed’s life represent an infinite row of dominoes.

Acknowledgements

My graduate education has been a long, strange trip to Damascus. I must start by offering the deepest gratitude to my thesis advisor, Dr. Lori Isom. Training for the Ph.D. remains a true apprenticeship, and the apprentice walks away with not only technical knowledge from their master, but with their approach to science, their perspective on what makes good and bad science such, and even a bit of their personality. Lori Isom has shaped the scientist and human being that I am. She took a large gamble on me as a curious, disorganized, and underachieving young student. Despite my shortcomings, she always believed in me, protected me when I was weak, and grounded me when my arrogance detached me from reality. She provided true and honest emotional support. Lori is an irreplaceable pillar of biomedical research and graduate education at the University of Michigan. More importantly, she is a hero to countless aspiring female scientists, not only for her scientific excellence but because she treats everyone with respect, kindness, and encouragement. Of all the support Lori has shown me, one moment of impeccable mentorship shines brighter than the rest. It was a dark, cold evening. The halls were empty when I arrived at the laboratory to feed my hungry human embryonic kidney cells their daily ration of media. Alongside them, I too planned to indulge in the fruits of a delicious chicken potpie from Zingerman's Delicatessen. Fresh and still piping hot, I set the untouched pie down in a safe location to set my cell culture media in the water bath. Less than 5 minutes later, the whole pie had vanished.

A scoundrel had emerged from the shadows. The pharmacology potpie perp was never found. I was devastated. The next day, in the depths of my despair, Lori emerged like the sunrise on a cold Alaskan morning, holding the largest commercially available chicken potpie (weighing in at 5 pounds and 8 ounces). Chicken potpie for the graduate student's soul. This gesture bears the mark of a true mentor. Thank you for everything, Lori.

I consider myself the luckiest graduate student to grace the halls of The University of Michigan's Medical campus. I was gifted—for reasons I still do not understand—two of the most powerful and inspiring mentors one can find. Superstars of biomedical science, whose kindness and foresight somehow outweigh their intellectual prowess.

Dr. George Mashour, the man on whom nothing is lost. He who gave me an intellectual home and was there for me throughout every stage of my development as a scientist. George is Chair and Professor of Anesthesiology at Michigan, and a world-renowned powerhouse in the field of consciousness science. A true thought leader in neuroscience. Even more admirable is his relentless and wholehearted dedication to mentorship. George made me feel welcome in his research community, The Center for Consciousness Science. At every crisis and vulnerable point in the last 6 years, George was there like an oak of support. He opened my mind to philosophy and encouraged my deep interests in psychopharmacology and consciousness. George Mashour has shaped the scientist and human being that I am. Thank you for everything, George.

In addition to Lori Isom and George Mashour, I express my deep appreciation for all of the Professors on my thesis committee: Will Birdsong, Rich Hume, Alan Smrcka and Yukun Yuan. Each member of my committee was extremely helpful and impactful on my development.

Special thanks also to:

My Senpai Jacob Hull. Everything I know of neuroscience I blame on him. I remember with great pride the countless days we've spent thinking about science and life inside the medical school's second floor conference room. Jacob became the brother that I never had. He was there for me in all the pits of my frequent existential despair. He taught me how to do experiments, but more importantly, how to think. Despite his delusions of humour, I am eternally grateful for Jacob's unwavering dedication to my development. And may we all hope that one day he finally makes a good joke.

My Family, for their never-ending emotional, financial, and spiritual support throughout my life. Especially:

My Father David Denomme, for inspiring my curiosity about the natural world, belief in the ignorance of experts, and love for craftsmanship.

My Mother Shelly Sheridan, for her inspiring work ethic, leadership skills and endless love.

My Sister Jaclyn Denomme, for her boundless wisdom, sense of humor and resilience in the face of a brother perpetually complaining about graduate school.

My Aunt Elise Kapelanski for her encouragement and profound courage that helped me to carry on. Rest In Peace, Aunt Lise.

Sheri and Matthew Taylor, for their lifelong support, especially during the rough days of my master's program.

Dave Kapelanski, Karyn and Bill Kellogg, Tom and Kelly Denomme, Sharon, Melissa, Sandy and Annie Sheridan, and Sandy Macdonald, for supporting at every important milestone in my life.

Greg Taylor, for always being there for me.

All past and present members of the Isom lab. Especially:

Jim Offord, for his patience, enthusiasm, and the endless wisdom he shared with me. Rest In Peace, Jim.

Samantha Hodges, for her excellent scientific contributions to this thesis, never-ending optimism, and loving support.

Luis Lopez-Santiago and Yukun Yuan, two of my living heroes, for training me in electrophysiology and life.

Rene Caballero-Floran, a great friend, collaborator, and comedian.

Nnamdi Edokobi, for his authentic friendship and support

Allie Bouza, for saying "you'll figure it out, you always do" every time I didn't think I would.

Chunling Chen, for being a straightshooter, teaching me how to clone, and along with Yan Chen and Larissa Robinson, for their expert contributions to the genetic and rodent models used in this thesis.

All collaborators who have elevated my research with their contributions. Especially:

April Lukowski, Alison Narayan and all the molecular magicians from her lab.

Alan Smrcka for his world-class expertise in G-protein biology, as well as challenging and supporting me to become a more focused and professional scientist. I would also like to acknowledge his former graduate student, Naincy Chandan, for always providing a helping hand.

Ciria Hernandez, for patiently teaching me everything I know about automated patch clamp electrophysiology.

Nicholas Cozzi, for his longtime inspiration and mentorship of my interests in psychoactive drug research.

Tyler Ekins, for his friendship, collaborative spirit, and shared love of psychedelic neuroscience.

Justin Clark, for his insatiable curiosity, kindness, and friendship. Rest in Peace, Justin.

Hamilton Morris, a friend, and collaborator who taught me how to investigate ideas in the real world and the power of scientific storytelling.

The Professors that gave me a chance and deeply inspired me to go further: Mary Novess, Dan Swift, and Rich Hume.

All the Department of Pharmacology Professors, especially: Steve Fisher, for his mentorship of my master's degree; Jorge Iniguez-Lluhi and Emily Jutkiewicz, for their deep influence in educating me as a pharmacologist.

The Department of Pharmacology Office including Josh Daniels, Ingrid Shriner-Ward, Dar-Weia Liao, Dennis Ondreyka, Audrey Morton-Dziekan, Tom Larmee, Tom Biancalana and Elizabeth Oxford.

My Friends whom I consider Family: Michael Ambrose, Mason Amin, Ryan Ainsworth, Charlie Cashman, Alec Drean, Eli Lavender, Marcus Mallia, Max Pardington, Jack Pardington, Rene Mejia, Richie Mitchell, Fitim Sulejmani, Omead Sinai, Mike Staubach.

Alexander “Sasha” Shulgin, the preeminent psychedelic chemist. The day I opened up *PiHKAL* for the first time was the day my whole life changed. Although I never got to meet him, Shulgin’s oeuvre had a profound influence on me as a young man and will forever remain a guiding light in my life.

Reflecting on graduate school, I am especially proud of my role in building the emerging community of researchers at UM who are researching psychedelic drugs as tools to study consciousness and treat psychiatric disorders. This includes all of my colleagues from the Center for Consciousness Science and the Michigan Psychedelic Collaborative (M-PsyC), especially my lifelong friends and fellow graduate students Jon Dean, Emma Huels and Nick Glynos, whom I had the great pleasure of co-founding the still-thriving Rackham Interdisciplinary Workshop on Psychedelic Neuroscience and Therapy. Thank you for the laughter and love. To Alex Stanczyk, Nick Kolbman, and all my other pharmacology graduate student colleagues, thank you for making this possible.

Table of Contents

Dedication ..... **ii**

Acknowledgements ..... **iv**

List of Tables ..... **xii**

List of Figures ..... **xiii**

Abstract ..... **xv**

Chapter I. Introduction **1**

VGSC Structure and Function 1

VGSC α and β Subunit Expression Patterns 14

VGSC Toxicology 20

Neuromodulation of VGSCs 25

Modulation of VGSCs by G-protein βγ Subunits 32

Variants in VGSC Genes and in Genes Encoding VGSC Interacting G-proteins Result in Epilepsy 38

Pharmacology of Sodium Channel-linked DEEs 55

Subtype Selective VGSC Modulation as a Potential Treatment for Sodium Channel-linked DEE 57

Conclusion 62

Chapter II. *In Vitro* Validation of 4,9-anhydrotetrodotoxin as a $Na_v1.6$ Selective Inhibitor for the Treatment of Sodium Channel-linked Developmental and Epileptic Encephalopathy **63**

Introduction 63

Results 65

Discussion 79

Methods 88

Chapter III. Neuromodulation of Voltage-gated Sodium Channels by Gβ1γ2 Subunits: Implications for Developmental and Epileptic Encephalopathy 96

Introduction 96

Results 99

Discussion 136

Methods 144

Chapter IV. Conclusions 162

References 179

List of Tables

Table 1.1 Human voltage-gated sodium channel genes and their tissue expression…**15**
Table 1.2 Tetrodotoxin (TTX) sensitivity of voltage-gated sodium channel subtypes…**21**
Table 1.3 G protein βγ subunits genes and their corresponding proteins……**33**
Table 1.4 Sensitivity of VGSC α subunit subtypes to functional I_{Na} modulation by G protein βγ subunits when co-expressed in heterologous cells……**36**

Table 2.1 Average peak and persistent I_{Na} density and recorded in the presence of 100 nM 4,9-ah-TTX and absence (control) via whole-cell patch clamp from HEK cells stably expressing human Nav1.1, $Na_v1.3$ or $Na_v1.6$……**76**
Table 2.2 Voltage-dependence of activation and inactivation parameters recorded in the presence of 100 nM 4,9-ah-TTX and absence (control) via whole-cell patch clamp from HEK cells stably expressing human $Na_v1.1$, $Na_v1.3$ or $Na_v1.6$……...**77**
Table 2.3 Percent reduction in $Na_v1.1$ and $Na_v1.6$ peak I_{Na} from control following the perfusion of 10, 100 or 500 nM 4,9-ah-TTX……..……**78**

Table 3.1 Peak I_{Na} density @ -10 mV in HEK cells stably expressing $Na_v1.6$, $Na_v1.1$, $Na_v1.6$ and $Na_vβ1$ or $Na_v1.1$ and $Na_vβ1$ after transient co-expression of Gβ1γ2, EGFP, Gβ1γ2 + 100 nM staurosporine (ST) or $Na_vβ1$……**131**
Table 3.2 Voltage dependent properties of HEK cells stably expressing $Na_v1.1$ or $Na_v1.6$ after transient co-expression of Gβ1γ2, EGFP or $Na_vβ1$……..**132**
Table 3.3 Voltage dependent properties of HEK cells stably expressing $Na_v1.1$ and $Na_vβ1$ or $Na_v1.6$ and $Na_vβ1$ after transient co-expression of Gβ1γ2 or EGFP……..**133**
Table 3.4 Capacitance of HEK cells stably expressing $Na_v1.1$, $Na_v1.6$, $Na_v1.1$ and $Na_vβ1$ or $Na_v1.6$ and $Na_vβ1$ transiently co-expressing Gβ1γ2, Gβ1γ2 + 100 nM staurosporine, EGFP, or $Na_vβ1$……**134**
Table 3.5 Intrinsic properties and maximum firing frequency of somatosensory cortex layer 5 pyramidal neurons of *Gnb1*$^{K78R+}$ mice (blue) vs wildtype littermates at postnatal day 16-18……..**135**

List of Figures

Figure 1.1 Voltage-gated sodium channel structure topology……**2**
Figure 1.2 Sodium channel states of the action potential……...**4**
Figure 1.3 Multifunctional roles of the voltage-gated sodium channel β1 subunit…….**12**
Figure 1.4 Phylogenetic and amino acid sequence identity relationships of the rat voltage-gated sodium channel α subunits……**16**
Figure 1.5 Neurotoxin receptors sites of the voltage-gated sodium channel……..**22**
Figure 1.6 Representative example of acute perfusion of 30 μM 5-HT on I_{Na} properties in an acutely isolated wildtype P19 mouse cortical pyramidal neuron……..**31**

Figure 2.1 [^{3}H]-Saxitoxin competition binding with 4,9-ah-TTX……**66**
Figure 2.2 $Na_v1.1$, $Na_v1.3$ and $Na_v1.6$ I-V curves and I_{Na} traces in the presence and absence of 100 nM 4,9-ah-TTX……...**67**
Figure 2.3 Average peak and persistent I_{Na} density recorded in the presence and absence of 100 nM 4,9-ah-TTX via whole-cell patch clamp from HEK cells stably expressing human $Na_v1.1$, $Na_v1.3$ or $Na_v1.6$……**69**
Figure 2.4 Normalized conductance to voltage and voltage dependence of availability relationships……**70**
Figure 2.5 $Na_v1.1$ and $Na_v1.6$ peak I_{Na} traces before, during and after perfusion of 10, 100 and 500 nM 4,9-ah-TTX……**71**
Figure 2.6 Percent reduction in $Na_v1.1$ and $Na_v1.6$ peak I_{Na} by 4,9-ah-TTX……...**72**
Figure 2.7 Structures and equilibrium of tetrodotoxin, 4,9-anhydrotetrodotoxin, and 4-epi-tetrodotoxin……...**73**
Figure 2.8 Impact of pH on 4,9-ah-TTX, 4-epiTTX and TTX……..**74**
Figure 2.9 4,9-ah-TTX, 4-epiTTX and TTX in solution over time……..**75**
Figure 2.10 VGSC schematic with TTX binding site and selectivity filter residue alignment……**80**

Figure 3.1 Amino acid sequence alignment of C-tail region of human $Na_v1.2$ and human $Na_v1.6$ with proposed Gβγ binding motif……**98**
Figure 3.2 Mass spec protein profiling experiments with *Scn1b*-V5 mouse whole brain show Gβγ subunits interact with the VGSC complex through $Na_v\beta1$ subunits……..**100**
Figure 3.3 No interaction detected in coimmunoprecipitation experiments between Gβ and $Na_v\beta1$ in *Scn1b*-V5 juvenile and adult mouse whole brain……**101**
Figure 3.4 Transient transfection of Gβ1γ2 or EGFP in HEK cells stably expressing human $Na_v1.6$……...**104**
Figure 3.5 Transient transfection of Gβ1γ2 or EGFP in HEK cells stably expressing human $Na_v1.1$……...**106**

Figure 3.6 Gβ1γ2 shows differential modulation of $Na_v1.1$ vs $Na_v1.6$ persistent current in HEK cells……..**109**
Figure 3.7 Gβ1γ2 inhibition of $Na_v1.6$ but NOT $Na_v1.1$ shows acute voltage-dependent relief after prolonged hyperpolarization for 1 s at -120 mV……...**111**
Figure 3.8 Gβ1γ2 coexpression has no impact on slow inactivation properties of $Na_v1.1$ or $Na_v1.6$ at 50 Hz……..**113**
Figure 3.9 Inhibition of PKA/PKC with 100 nM staurosporine does not reduce Gβ1γ2 inhibition of $Na_v1.1$ or $Na_v1.6$……**115**
Figure 3.10 Transient co-expression of Gβ1γ2 or EGFP in HEK cells stably expressing human $Na_v1.6$ and human $Na_v\beta1$……..**117**
Figure 3.11 Transient co-expression of Gβ1γ2 or EGFP in HEK cells stably expressing human $Na_v1.1$ and human $Na_v\beta1$……..**119**
Figure 3.12 Transient co-expression of Gβ1γ2 has no effect on human $Na_v1.5$ I_{Na} properties in HEK cells……**121**
Figure 3.13 Fold change in mRNA expression levels of human Gβ, Gγ, and Gα subunits in untransfected, $Na_v1.6$ or $Na_v1.6$ and $Na_v\beta1$ stable HEK cell lines……..**124**
Figure 3.14 Baseline Gβ, Gγ, and Gα subunit gene expression in HEK cells……**125**
Figure 3.15 Western blots confirming $Na_v\beta1$ expression in HEK $Na_v1.1$ + $Na_v\beta1$ and HEK $Na_v1.6$ + $Na_v\beta1$ stable cell lines……**125**
Figure 3.16 Somatosensory cortex layer 5 pyramidal neurons of *Gnb1*$^{K78R/+}$ mice show no changes in excitability or intrinsic properties……..**128**
Figure 3.17 Spontaneous inhibitory postsynaptic currents (sIPSC) from somatosensory cortical layer 2/3 pyramidal neurons of *Gnb1*$^{K78R/+}$ mice show deficits in presynaptic inhibitory neurotransmitter release……**130**

Figure 4.1 Effects of 100 nM purified Gβ1γ2 on whole cell $Na_v1.1$ peak I_{Na} density over time using a depolarizing step from -70 mV to 0 mV repeating @ 0.2 Hz……..**168**
Figure 4.2 Acute effects of 10 μM surfen on I-V relationship of GIRK1/2 channels stably expressed in HEK cells……**170**
Figure 4.3 Various opsins that respond to different wavelengths of light and couple to different Gα subunits……**171**

Abstract

Voltage-gated sodium channels (VGSCs) allow the dynamic electrical communication between neurons in the brain with millisecond precision by controlling action potential initiation and propagation. The VGSC family of transmembrane proteins has different subtypes that are selectively expressed throughout the body to maintain proper physiological function. Both gain- and loss-of-function variants in VGSC genes that are expressed in brain can lead to malfunction of these vital proteins, causing catastrophic neurological diseases such as epilepsy. Herein, I review the structure and function of VGSCs and discuss their pharmacology considering the pathophysiology of a severe class of genetic epilepsies caused by variants in VGSC genes, known as developmental and epileptic encephalopathies (DEEs). In the following chapters, we discuss two neuropharmacological studies of DEEs linked to variants in VGSC genes, with the overarching hypothesis that small molecules targeting unique brain VGSC subtypes and neuromodulatory VGSC interacting proteins represent viable novel therapeutic strategies for treating sodium channel linked brain disease.

In Chapter II, I sought to validate a natural product, 4,9-anhydrotetrodotoxin, reported to selectively inhibit $Na_v1.6$, which is the most abundant VGSC α subunit subtype expressed in the adult brain. Because gain-of-function variants in the gene *SCN8A* are linked to DEE, selective modulation of $Na_v1.6$ has emerged as a major therapeutic

target in the field. I ultimately found that 4,9-anhydrotetrodotoxin was not selective for $Na_v1.6$ relative to other brain channels and therefore, not a useful therapeutic for treating *SCN8A*-linked DEEs.

In Chapter III, protein profiling with mass spectrometry followed by heterologous expression systems were used to discover a novel inhibitory interaction between G-protein β1γ2 subunits and brain VGSC subtypes $Na_v1.1$ and $Na_v1.6$. I found differential inhibitory effects of Gβ1γ2 on $Na_v1.1$ and $Na_v1.6$ sodium current density that showed subtype selectivity and modulation by co-expression of VGSC β1 subunits, and prepulse voltage dependence. The implications of these novel interactions for the treatment of DEEs, in particular, *GNB1*-linked DEE, are discussed.

This thesis work builds on our understanding of subtype selective sodium channel modulation with 4,9-anhydrotetrodotoxin. Additionally, this thesis builds upon our knowledge of *GNB1*-linked DEE and the potential role of altered VGSC function in this disorder. Given the significant roles of Gβ1γ2, $Na_v1.1$, and $Na_v1.6$ in regulating neurotransmission and excitability, this thesis work provides new insights into basic neuromodulatory mechanisms in the brain. More importantly, this work may lead to novel therapeutic targets for the treatment of DEEs linked to sodium channel genes and sodium channel interacting G-proteins.

Chapter I. Introduction

*Portions of this chapter have been published in *Pharmacological Reviews* (Denomme, Hull and Mashour 2019)

VGSC Structure and Function

Voltage-gated sodium channels (VGSCs) are transmembrane protein complexes responsible for the initiation and propagation of action potentials in neurons (Hille 2001). VGSCs consist of a pore-forming α-subunit (220-260 kDa) and two smaller non-pore-forming β-subunits, 30-40 kDa in size (Beneski and Catterall 1980). α-subunits alone are sufficient for Na^+ conduction and voltage sensing, at least in heterologous cells, while β-subunits modify channel expression, gating, and localization, as well as participate in cell-cell and cell-matrix adhesive interactions leading to intracellular signal transduction (Hull and Isom 2018).

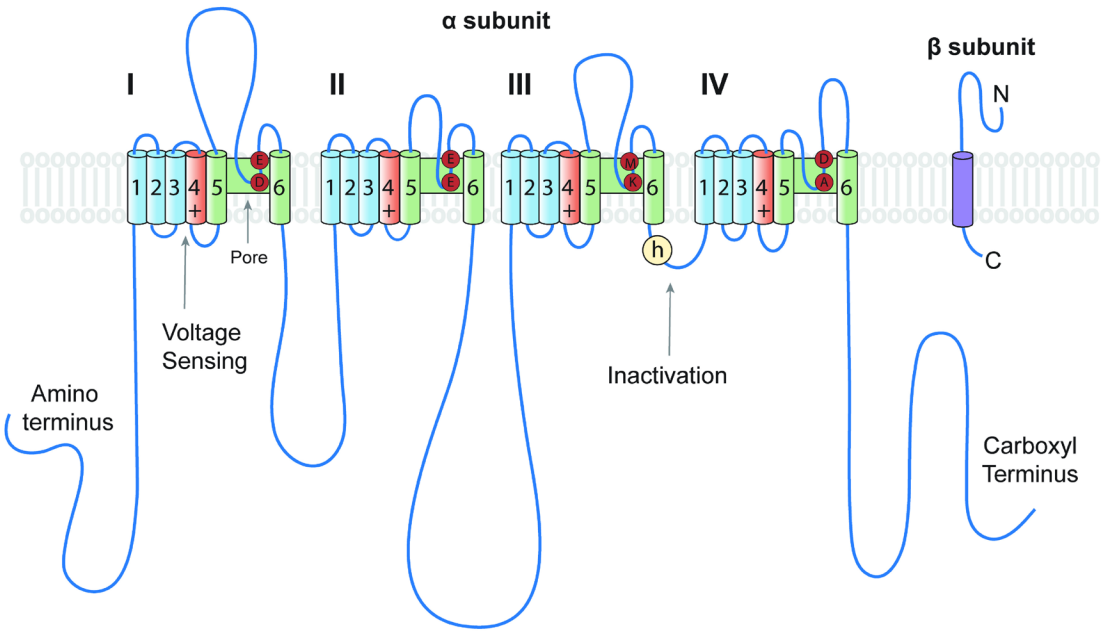


Figure 1.1 Voltage-gated sodium channel structure topology. Schematic of the eukaryotic VGSC α-subunit. Roman numerals and numbers indicate domains and segments, respectively. The pore loop regions comprised of segments S5 and S6 are highlighted in green. Voltage-sensing S4 segments are highlighted in red. The inactivation gate and "h" particle containing the IFM motif that is crucial for inactivation are highlighted in yellow. Small red circles of the re-entrant loops in each domain represent the amino acid residues that form the Na^+ ion selectivity filter.

VGSC α subunits consist of 4 pseudo-homologous domains, each composed of 6 transmembrane segments (Fig. 1.1). Segments 1-4 (S1-S4) are primarily involved in voltage sensing while S5-S6 segments form the pore. Positively charged lysine and arginine residues in the S4 helices act as voltage sensors.

α Subunit Function

VGSCs transition between several conformational states through the course of an action potential including closed, open, and inactivated states (Fig. 1.2). The predominant state of the channel at resting membrane potential is the closed state, where no Na^+ ions are conducted.

Activation: The S4 segments of each domain contain a conserved set of 4 to 7 repeating positively charged (R/K) residues that sense voltage by acting as "gating charges" that slide upward toward the extracellular milieu upon membrane depolarization to electromechanically open the pore of the channel (activation) in a "sliding helix" fashion (Catterall 1986). At rest, the sliding helix model proposes the positively charged S4 residues are drawn inward by the electrostatic force of the negative internal membrane potential. Upon sufficient depolarization to threshold, the channel opens as gating charges are driven outward in a helical path by forming ion pairs with neighboring polar or negatively charged residues in the S1-S3 segments of the pore domain (Catterall 2010). Once activated, hydrogen bonding between asparagine residues in S6 and serine resides in the S4-S5 segments is hypothesized to stabilize the channel's open (activated) state (Sheets et al. 2015).

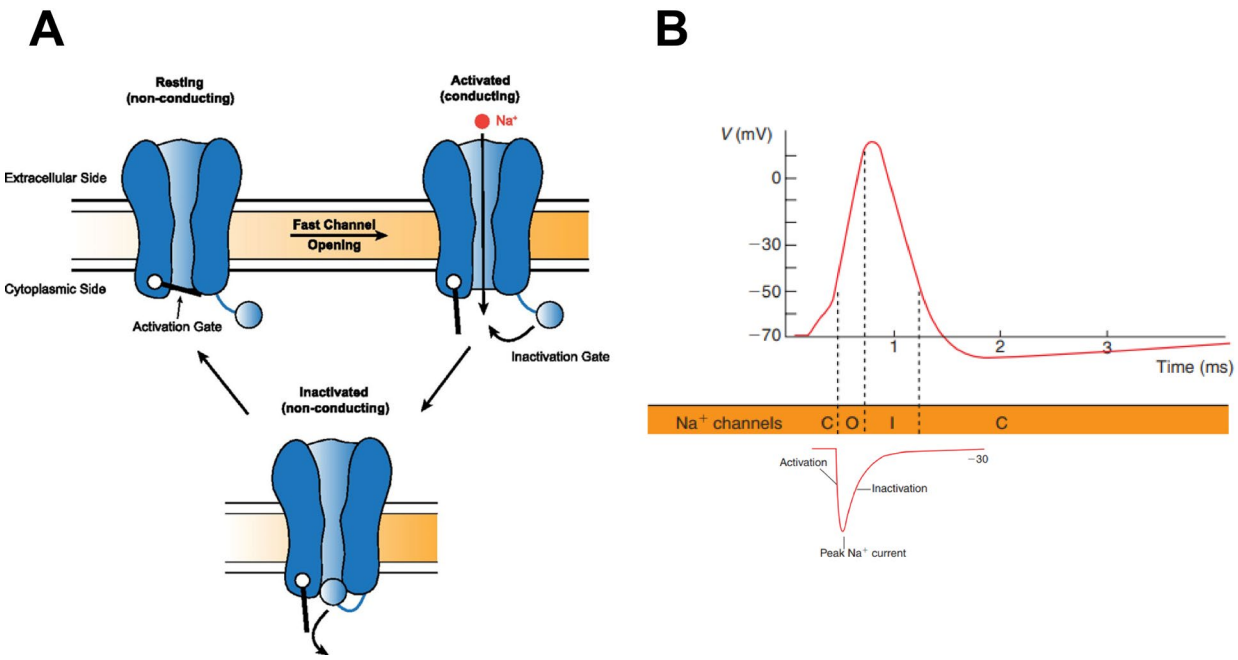


Figure 1.2 Sodium channel states during the action potential. (A) Transition states of voltage-gated sodium channels. At rest, the activation gate is closed, and the channel is in a nonconducting state. After sufficient depolarization of the membrane, the channel undergoes a conformational change to enter the activated state where both gates are open, allowing the conduction of Na^+ ions. After transitioning to the activated state, the channel undergoes fast inactivation, where intracellular residues (the inactivation gate) occlude the inside face of the channel blocking further conduction of Na^+ ions. After recovery from inactivation, the channel returns to the resting state. (B) Corresponding functional activity of sodium channels during a typical neuronal action potential. Figure modified from (Hammond 2009).

Fast Inactivation: About one millisecond after opening, fast inactivation of VGSCs begins. A set of hydrophobic residues IFM (the inactivation particle/gate) in the intracellular linker between domain III and IV swings inward to block Na^+ conduction from the inside face of the channel. Such fast inactivation (recovery time constants on the scale of milliseconds) is distinct from slow inactivation (recovery time constants on the scale of hundreds of milliseconds to seconds) which is discussed in more detail below. Recovery from fast inactivation corresponds to the absolute refractory period of an action potential. The comparatively slower rate of fast inactivation to activation and deactivation allows for timely termination of depolarization during an action potential (Hille 2001).

VGSC fast-inactivation is driven by a short loop of hydrophobic residues (IFM) on the intracellular side of the channel linking domains III and IV that forms the inactivation gate (West et al. 1992). Proposed as the “hinged lid” model of inactivation, the tethered IFM linker of domains III-IV forms a lid by occluding the intracellular face of the pore to block Na^+ conduction from the cytoplasmic side. Elucidation of the residues controlling fast-inactivation was achieved with patch clamp analysis of channel function using targeted antibodies and site-directed mutagenesis (Vassiev et al. 1988, Vassilev et al. 1989, Stuhmer et al. 1989, Patton et al. 1992). To confirm the function of this domain, restoration of mutant channels lacking inactivation was achieved using a synthetic IFM peptide (Eaholtz et al. 1994).

Hodgkin and Huxley originally proposed that VGSC inactivation was voltage-dependent but uncoupled from the activation process (Hodgkin and Huxley 1952). However, subsequent evidence showed the inactivation process is coupled to activation (Benzanilla and Armstrong 1977, Armstrong and Benzanilla 1977). More recent work highlighted the importance of the S4 segments in domain IV in coupling activation to inactivation (Capes et al. 2013). Movement of the S4 segments in domains I-III is required for activation of the channel from a closed to an open state. A second open state is achieved when the S4 segment of domain IV moves, which permits the inactivation gate binding to residues in the mouth of the pore that only become accessible once the S4 segment of domain IV has moved during the activation process. Precisely where the inactivation gate IFM residues bind is still unclear, as inactivation is disrupted by mutagenesis of residues located in multiple segments of domain IV (McPhee et a. 1994, McPhee et al. 1995, Tang et al. 1996, McPhee et al.1998). Unfortunately, recent high-resolution structures (discussed below) provide little insight into the binding site of the inactivation gate, as conditions required for structural studies often lock the channel into a closed state or block the pore with detergent (Shen et al. 2017, Yan et al. 2017, Pan et al. 2018, Shen et al. 2019).

Slow Inactivation: Narahasi was the first to discover slow inactivation in 1964, when he observed there were different times required for recovery from inactivation depending on the magnitude of the depolarizing pulse when studying action potentials in lobster giant axons (Narahashi 1964) Slow inactivation of VGSCs is a gating phenomenon that can dynamically influence synaptic integration and neuronal excitability by reducing the

number of available VGSCs through entry into a non-conducting conformation of the channel (distinct from fast inactivation) that lasts on the timescale of hundreds of milliseconds to seconds (Rudy 1978, Silva 2014).

Entry into the slow inactivated state requires repetitive or sustained depolarizations which accumulate channels in the slow inactivated state over the course of numerous action potentials (Schauf et al. 1976). Slow inactivation of VGSCs provides neurons with a temporary memory of past spiking activity (Toib et al. 1998, Marom 2010, Silva 2014). VGSC slow inactivation is robust in function, endowing neurons with the capacity to dynamically regulate firing frequency and fine-tune adaptation thresholds to the intensity of stimuli. Spike frequency adaptation is a vital mechanism for proper functioning of sensory neurons and networks. Slow inactivation of VGSCs has already been shown to be an integral component to regulating spike frequency adaptation in visual, auditory, and olfactory modalities (Fleidervish et al. 1996, Vilin and Ruben 2001, Torkkeli et al. 2001, Kim and Rieke 2003, Dhingra et al. 2005, Sarno et al. 2022). Recovery from the slow inactivated state is much slower than entry, supporting longer lasting effects on the channel than fast inactivation, which is limited to affecting fewer individual action potentials due to its fast recovery time constant. VGSC slow inactivation has the interesting property that, at depolarized potentials that support spiking (i.e., -70 mV), the recovery is slow, while at hyperpolarized potentials (i.e., < -80 mV), the recovery is much faster (Fleidervish et al. 1996, Jung et al. 1997). This voltage dependent effect is highly relevant to neuromodulation, and slow inactivation of brain VGSCs can be modulated by neurotransmitters like serotonin (5-HT), as discussed below. Slow

inactivation utilizes molecular mechanisms that differ from fast inactivation. Mutations that impair fast inactivation do not prevent slow inactivation (Rudy 1978, Featherstone et al. 1996, Vedantham et al. 1998, Todt et al. 1999, Mitrovic et al. 2000, Ong et al. 2000). Numerous mutations in VGSCs have been found to impact slow inactivation. For example, mutation of the highly conserved asparagine residues in the S6 segments to hydrophobic residues completely blocks slow inactivation (Chen et al. 2006). Patient variants that lead to impaired slow inactivation can lead to a neuromuscular disorder known as hyperkalemic periodic paralysis, as slow inactivation is involved in preventing contraction of skeletal muscle when serum K^+ is elevated (Bendahhou et al. 2002). The predominant cardiac VGSC subtype $Na_V1.5$ exhibits significantly less slow inactivation than skeletal and neuronal subtypes, and mutations in *SCN5A* (encoding $Na_V1.5$) that affect slow inactivation may be arrhythmogenic (O'Reilly 1999, Vilin and Ruben 2001). While it appears that specific VGSC domains may be involved in slow inactivation at different time scales (Silva 2014), the exact structural components of the VGSC that control slow inactivation are not yet fully understood. Due to underappreciated roles of VGSC slow inactivation in sensation and perception, neurological disease, as well as its susceptibility to neuromodulation, the basic structural and functional mechanisms of VGSC slow inactivation deserve further research.

Ion Selectivity: Selectivity of Na^+ over other ions is an essential function for the action of VGSCs. This is achieved by the precise architecture of a VGSC region known as the selectivity filter. Approximately 4.6 Å in size, the selectivity filter is composed of an inner and outer ring of charged residues. The asymmetric charge distribution of each ring

coordinates the solvated Na^+ ions as they flow through the pore (Catterall 2012). Through mutagenesis and subsequent electrophysiological analysis, four key residues (D: aspartate, E: glutamate, K: lysine, and A: alanine), each present in one of the domains, were identified as the inner ring of the mammalian VGSC selectivity filter (Lipkind and Fozzard 2008). The DEKA motif found in human VGSCs is conserved across all isoforms. Mutating the KA (lysine and alanine) of the DEKA motif to glutamate residues (EE) abolishes Na^+ selectivity of the channel and allows Ca^{2+} ions to pass through the pore (Heinemann et al. 1992). This result also highlights the high level of homology in the pore region between voltage-gated sodium and calcium channels (Backs et al. 1992).

Persistent Na^+ Current (I_{Na}): In contrast to the large transient Na^+ current (I_{Na}) produced by VGSCs in macroscopic whole-cell recordings, there is a smaller current that can be produced through incomplete fast inactivation known as persistent I_{Na}. Persistent I_{Na} (also known as late I_{Na}), named for its ability to persist at membrane potentials and time points where all VGSCs should theoretically be inactivated, accounts for roughly 1-5% of the total I_{Na} observed in whole-cell recordings from heterologous mammalian cells. Despite its small proportional size to the transient I_{Na}, persistent I_{Na} can have a significant influence on the excitability of neurons. Persistent I_{Na} is known to lower spike threshold and support repetitive and rhythmic firing of neurons by depolarizing the resting membrane potential and increasing the amplification of excitatory postsynaptic currents (Crill 1996). VGSC subtypes display variable proportions of persistent to transient current, which is thought to play a role in their functioning within and across

different neurons. Of all the brain VGSC subtypes, $Na_v1.6$ is reported to inherently pass the most persistent I_{Na}, supporting its enriched expression at the AIS. Consistent with this observation, gain-of-function variants in *SCN8A* that increase persistent I_{Na} are epileptogenic (Wagnon et al. 2016).

High-resolution structures: Dramatic advancements have occurred in pursuit of a high-resolution three-dimensional understanding of VGSC α and β subunits during my graduate studies. X-ray crystallographic analysis has been limited to prokaryotic VGSCs such as the bacterial Na_VAb channel from *Bacillus halodurans*, which has provided numerous structural insights but contains only a single domain that combines into a homotetramer and thus lacks key features of the eukaryotic VGSCs such as the intracellular loops that mediate fast inactivation (Payandeh et al. 2011, Payandeh et al. 2012, Zhang et al. 2012). Advances in cryogenic electron microscopy (Cryo-EM) have revealed exquisite structural details of eukaryotic VGSCs (Shen et al. 2017, Yan et al. 2017, Pan et al. 2018, Shen et al. 2019, Jiang et al. 2020). In 2017, the first detailed view of a eukaryotic VGSC from the American cockroach (*Periplaneta americana*) was reported. The following year, the structure of human $Na_v1.4$ co-expressed with the $\beta1$ subunit was resolved at a 3.2-Å resolution using Cryo-EM (Pan et al. 2018). These data have confirmed decades of experiments into the structural, functional, and pharmacological details of the VGSC.

β Subunits

Identification of the protein subunits of the heterotrimeric VGSC complex was first achieved in rat brain using photoaffinity labeling with a toxin derived from a deathstalker scorpion (*Leiurus hebraeus)* (Beneski and Catterall 1980). Purification and further analysis showed the VGSC complex contained one α-subunit covalently flanked by a β-subunit on one side (β2, which we now know can be substituted by β4 (Chen et al. 2012), and a non-covalently linked β-subunit on the other (β1, which we now know can be substituted by β3) (Hartshorne and Catterall 1981, Hartshorne et al. 1982, Hartshorne and Catterall 1984, Namadurai et al. 2014). Four β subunit proteins (β1- β4) and a splice variant β1B have been discovered, encoded by the genes *SCN1B-SCN4B* (Table 1.1) (O'Malley and Isom 2015). Except for β1B, VGSC β subunits are type 1 transmembrane proteins containing a large N-terminal domain connected to a short intracellular C-terminal domain by a membrane spanning segment. The extracellular N-terminal domain of each β subunit, including β1B, also contains a highly conserved immunoglobulin (Ig) loop domain—with V-set Ig homology—that is present in the Ig superfamily of cell adhesion molecules (Isom and Catterall 1996, Yu et al. 2003). The *SCN1B* splice variant, β1B, is unique in that it has no transmembrane segment and is a soluble secreted cell adhesion molecule (Patino et al 2011). The crystal structures of β1, β2, β3, and β4, in conformations with and without α subunits, have revealed two conserved extracellular cysteine residues that form an intrasubunit disulfide bond in the N-terminal domain to stabilize the Ig loop (Gilchrist et al. 2013, Namadurai et al. 2014, Das et al. 2016, Yan et al. 2017).

Although the heterologous expression of VGSC α subunits alone is sufficient for functional Na^+ conduction, the presence of β1 or β3 and β2 or β4 confers further modularity to channel function and expression (Noda et al. 1986, Recio-Pinto et al. 1987, Isom et al. 1995). β1 or β3 associate non-covalently and β2 or β4 form cysteine disulfide bonds with α subunits. In addition to modulation of channel expression and function, β subunits act as cell adhesion molecules, with roles in cellular aggregation, neurite extension, and axonal fasciculation (Figure 1.3) (Hull and Isom 2018).

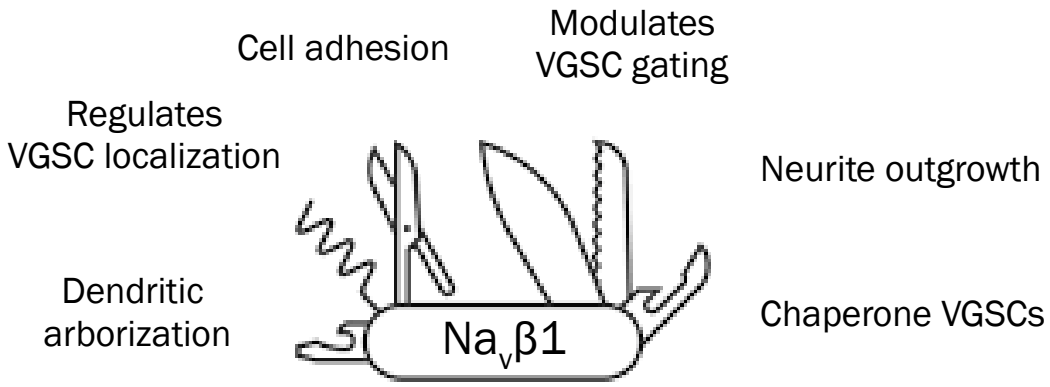


Figure 1.3 Multifunctional roles of the voltage-gated sodium channel β1 subunit

In *Xenopus* oocytes, coexpression of rat β1 and $Na_v1.2$ α subunits shifts the voltage-dependence of activation and inactivation, increases transient I_{Na} density, the rate of fast-inactivation and recovery from inactivation, and enhances VGSC surface expression (Isom et al. 1992). Similar results were observed with coexpression of β2 and $Na_v1.2$ (Isom et al. 1995), and coexpression of both β1 and β2 subunits with $Na_v1.2$ led to the highest increase in transient current density and gating/kinetic modulation

(Isom et al. 1995). Early work proposed that in the absence of β subunits, VGSC α subunits can exist in a conformation with slower gating kinetics. The presence of β1 then provides allosteric modulation which can shift the α subunits to a confirmation with faster gating kinetics (Patton et al. 1994). Limited studies show no significant effect after coexpression of β subunits on VGSC unit conductance or Na^+ selectivity in heterologous cells (Bennett Jr. et al. 1993, Schreibmayer et al. 1994).

More detailed reviews of the effects of β subunits on the gating and function of α subunits have been published (Catterall 1992, Goldin 1993 Isom et al. 1994, Adelman 1995, Gurnett and Campbell 1996, Catterall 2000). Experiments evaluating the impact of β subunits on α subunit function and trafficking in heterologous cells are variably dependent on the cell system and identity of the VGSC subunits expressed. In contrast to oocytes, coexpression of β and α subunits in Chinese hamster ovary (CHO) and human embryonic kidney (HEK) cells results in variable modulation of α subunit function and expression. These data have been reviewed in more detail (Calhoun and Isom 2014).

VGSC α and β Subunit Expression Patterns

α Subunits

Ten different human VGSC α-subunit isoforms ($Na_v1.1$- $Na_v1.9$ + Na_x) encoded by the *SCN(X)A* genes have been identified in mammalian genomes. Each VGSC subtype (denoted by the α-subunit) is uniquely distributed within and across cell and tissue types (Catterall et al. 2020) (Table 1.1).

All mammalian VGSC subtypes share greater than 75% amino acid sequence identity (Fig. 1.4) (Catterall et al. 2005). Individual VGSC subtypes have distinctive kinetic and voltage sensing properties and are strategically expressed based on these properties to optimize physiological function. While each VGSC α subunit has a wide and diverse expression pattern throughout the body, $Na_v1.1$, Nav1.2, Na_v 1.3, and $Na_v1.6$ are the most prominent central nervous system VGSCs, while the $Na_v1.7$, Nav1.8, and $Na_v1.9$ are mainly expressed in the peripheral nervous system. $Na_v1.4$ and $Na_v1.5$ are mainly expressed in skeletal and cardiac muscle, respectively (Catterall et al. 2005). The different VGSCs expressed in brain exhibit isoform enrichment in a cell type and subcellular region-specific manner.

Gene	Na_v α subunit	Primary Tissue Expression
SCN1A	$Na_v1.1$	Neurons of the Central Nervous System
SCN2A	$Na_v1.2$	Neurons of the Central Nervous System
SCN3A	$Na_v1.3$	Neurons of the Central Nervous System
SCN4A	$Na_v1.4$	Skeletal Muscle
SCN5A	$Na_v1.5$	Cardiac, denervated Skeletal Muscle
SCN8A	$Na_v1.6$	Neurons of the Central Nervous System
SCN9A	$Na_v1.7$	Neurons of the Peripheral Nervous System
SCN10A	$Na_v1.8$	Neurons of the Dorsal Root Ganglia
SCN11A	$Na_v1.9$	Neurons of the Dorsal Root Ganglia
Gene	**Na_v β subunit**	
SCN1B	β1	CNS, PNS, Cardiac
SCN1B	β1B	CNS, Cardiac
SCN2B	β2	CNS, PNS, Cardiac
SCN3B	β3	CNS, PNS, Cardiac
SCN4B	β4	CNS, PNS, Cardiac

Table 1.1 Human voltage-gated sodium channel genes and their tissue expression.

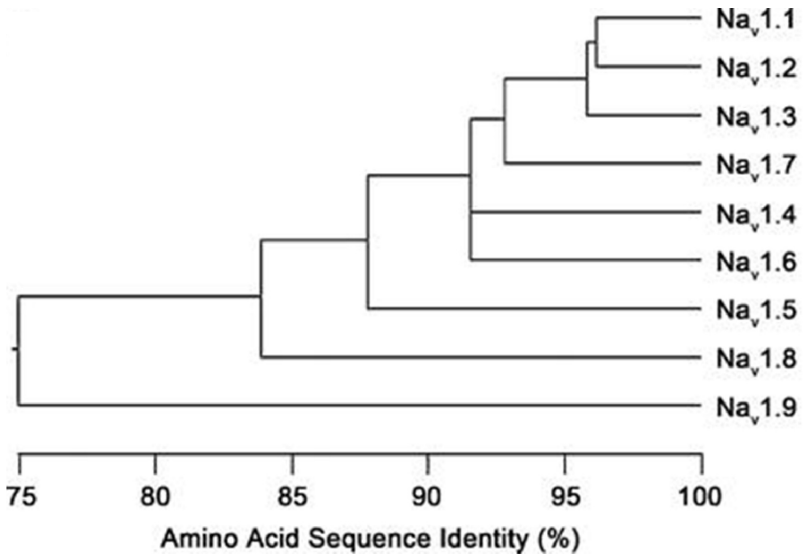


Figure 1.4 Phylogenetic and amino acid sequence identity relationships of the rat voltage-gated sodium channel α subunits. Modified from (Catterall et al. 2003).

In the adult mammalian brain, $Na_v1.1$, $Na_v1.2$, and $Na_v1.6$ are the predominant VGSCs. Their respective genes, *SCN1A*, *SCN2A,* and *SCN8A*, represent over 95% of all VGSC transcripts in the mature brain (Meisler et al. 2021). *SCN1A* mRNA expression is low in the neonatal rat and human cortex and then steadily increases with development (Beckh et al. 1989, Brysch et al.1991, Yarowsky et al. 1991, Heighway et al. 2022). Nav1.2 mRNA shows high expression in the hindbrain and cerebellum postnatally (Heighway et al. 2022). $Na_v1.1$ and $Na_v1.2$ share 93% amino acid sequence identity, while $Na_v1.1$, $Na_v1.2$, and $Na_v1.6$ exhibit 85-90% similarity. Regions of the N-termini of each of the brain subtypes show the most divergence in amino acid sequence similarity.

$Na_v1.3$ is highly expressed in the soma of neurons during development but shows reduced expression in the adult brain (Yu and Catterall 2003, Heighway et al. 2022).

In the forebrain, $Na_v1.1$ mRNA and protein are highly expressed in GABAergic inhibitory interneurons, although weaker expression exists in pyramidal neurons of the cortex and hippocampus (Westenbroek et al. 1989, Gong et al. 1999, Van Wart et al. 2007, Okaty et al. 2009). In interneurons, subcellular localization of $Na_v1.1$ protein is enriched in the cell body and to a greater degree in the axon initial segment (AIS) (Ogiwara et al. 2007). $Na_v1.2$ expression is enriched in the axons of somatostatin- but not parvalbumin-positive (PV+) interneurons of the cortex, showing further cellular subtype enrichment in VGSC expression (Li et al. 2014). $Na_v1.2$ is also expressed highly in the proximal AIS of pyramidal neurons and, during development, highly at nodes of Ranvier. $Na_v1.2$ expression is present but weaker in the cell body and dendrites of pyramidal neurons (Hu et al. 2009, Nelson et al. 2022). $Na_v1.6$ protein is highly expressed in the axons of PV+ neurons and in the distal AIS of pyramidal neurons and in nodes of Ranvier (Hu et al. 2009, Li et al. 2014). $Na_v1.6$ is also expressed in the cell body and dendrites of pyramidal neurons (Caldwell et al. 2000, Krzemien et al. 2000, Lorincz and Nusser 2010). Using photoactivation localization microscopy, one study found a 40-fold increase in the cell surface expression of $Na_v1.6$ at the AIS compared to expression at the proximal dendrites or the soma of cultured hippocampal neurons (Akin et al. 2016).

The three major adult brain VGSCs ($Na_v1.1$, $Na_v1.2$, and $Na_v1.6$) show both pre- and post-synaptic localization at synaptic terminals in the hippocampus (Johnson et al.

2017). Such localization appears to be regional/cell class specific, with the central hilus of the dentate gyrus showing predominantly presynaptic $Na_v1.1$ immunoreactivity, while in the *stratum radiatum* of CA1, Na_v 1.1, 1.2, and 1.6 exhibit stronger post-synaptic localization in spines and dendrites (Johnson et al. 2017). Although most of the work studying the cell type and sub-regional specific VGSC expression and function has focused on cortex and hippocampus, investigation has expanded to thalamic and subthalamic regions of the brain. Targeted deletion of *Scn8a* (encoding $Na_v1.6$) in PV+ neurons of the thalamic reticular nucleus of the thalamus was sufficient to generate absence epilepsy in mice, a non-convulsive seizure type that is characterized by sudden lapse of phenomenological consciousness (Makinson et al. 2017). $Na_v1.1$ is also expressed in the thalamus, with deletion of *Scn1a* in mice impacting the function of thalamic reticular neurons (Kalume et al. 2015).

β Subunits

Mammalian VGSC β-subunits are ubiquitously expressed in many cell and tissue types throughout the body (Table 1.1) (Bouza and Isom 2018). Amino acid sequence similarity is highest between β1 and β3, while β2 and β4 share higher homology with each other (Isom et al. 1992, Isom et al. 1995, Morgan et al. 2000, Yu et al. 2003, Hull and Isom 2018). Expression of β-subunits is developmentally regulated in rodents and humans, with peak CNS expression of β1B and β3 occurring in prenatal and early life, while β1, β2 and β4 peak in adulthood (Isom et al. 1992, Isom et al. 1995, Kazen-Gillespie et al. 2000, Lein et al. 2007, Patino et al. 2011, Bouza and Isom 2018). Within neurons, β1 subunits are enriched at the AIS and nodes of Ranvier (O'Malley and Isom 2015). β1

subunits are also post-translationally modified in various ways. Tyrosine phosphorylation of β1 subunits (Y181) is proposed to affect recruitment of ankyrin scaffolding proteins and subcellular localization of VGSCs (Maholtra et al. 2002, Bouza et al. 2020). Cell surface expression of β subunits is also modulated by N-linked glycosylation, which can account for up to one third of the mass of β subunits (Johnson et al. 2004). Sialic acid terminated N-linked glycosylation was required for β1 subunit mediated modulation of α subunit function (Johnson et al. 2004). β1 subunits go through regulated intramembrane proteolysis via the enzymes beta-site amyloid precursor protein cleaving enzyme-1 (BACE) and γ-secretase, generating a soluble intracellular fragment capable of nuclear translocation and transcriptional modulation (Bouza et al. 2020). Additionally, β1 subunits undergo S-palmitoylation, a reversible addition of fatty acid palmitoyl groups that can impact membrane association, protein-protein interactions, and subcellular localization (Bouza et al. 2020).

In rat neurons and in heterologous cells, co-expression of β1 and β2 subunits with α led to a five to ten-fold increase in the number of functional VGSCs expressed (Scheinman et al. 1989, Isom et al. 1995). Manipulation of the covalent disulfide bond between VGSC α-subunits and β2 or β4 impairs subcellular localization of the VGSC complex to the AIS and nodes of Ranvier (Chen et al. 2012). Similar trafficking deficits are also observed in a *SCN1B* variant linked to Genetic Epilepsy with Febrile Seizures plus (GEFS+) that disrupts the non-covalent interaction of β1 with α-subunits (Kruger et al. 2016). Expression of β1 subunits at growth cones is vital for cell adhesion and

developmental regulation of VGSC α-subunit expression and function (Brackenbury et al. 2010).

VGSC Toxicology

Much of our understanding of VGSC structure and function was built using Nature's toxins. In the early 1960s, Narahashi and colleagues used an intracellular microelectrode recording technique to show the paralytic action of the well-known puffer fish (Fugu) toxin tetrodotoxin (TTX) was blocking Na^+ influx in frog muscle fiber (Narahashi et al. 1960). TTX is a potent cyclic guanidinium VGSC pore blocker with a dioxaadamantane core found in many marine (and some terrestrial) animals. TTX is produced by microorganisms and was first isolated in 1894 from puffer fish ovaries by Japanese pharmacologist Yoshizumi Tahara (Llewellyn 2009, Suehiro 1994). He called the toxin tetrodotoxin because he first extracted it from the *Tetraodontidae* family of puffer fish. Its chemical structure was independently determined by three groups in 1964 (Woodward 1964, Tsuda 1964, Goto et al. 1965). The same year, Narahashi and colleagues published their seminal findings showing that TTX blocked the action potential by the "selective inhibition of the sodium carrying mechanism" (Narahashi et al. 1964). This ushered in a new era of neuropharmacology and provided direct pharmacological evidence that the sodium and potassium conduction mechanisms of the action potential were carried by separate molecular targets. Narahashi's pioneering work was the first detailed physiological report of a VGSC toxin, over a decade before molecular evidence of the channel proteins existed. "In fact, before that time it was

inconceivable to use a chemical or toxin to study the function of ion channels." (Narahashi 2008).

As detailed above, advances in molecular biology have allowed scientists to clone and examine isolated subtypes of VGSCs in the lab. TTX does not block all VGSC subtypes equally; having a high affinity for those expressed in the nervous system. Due to its historical significance, VGSC α-subunits are still classified based on their sensitivity to TTX (Table 1.2). $Na_v1.1$-1.4, $Na_v1.6$ and $Na_v1.7$ are 'TTX-sensitive', as half-maximal block of Na^+ conduction by TTX occurs at concentrations between 1 and 25 nM (Catterall et al. 2005). Nav1.5, Nav1.8 and Nav1.9 are referred to as 'TTX-resistant', requiring > 1μM TTX for block of half-maximal Na^+ conduction. TTX resistance in the predominant cardiac isoform ($Na_v1.5$) is conferred by a cysteine substitution for an aromatic phenylalanine or tyrosine residue present in the pore binding site of TTX-sensitive channels (Lipkind and Fozzard 1994).

TTX-Sensitive (IC_{50} < 25 nM)	
Gene	**Na_v α subunit**
SCN1A	$Na_v1.1$
SCN2A	$Na_v1.2$
SCN3A	$Na_v1.3$
SCN4A	$Na_v1.4$
SCN8A	$Na_v1.6$
SCN9A	$Na_v1.7$

TTX-Resistant (IC_{50} > 1 μM)	
Gene	**Na_v α subunit**
SCN5A	$Na_v1.5$
SCN10A	$Na_v1.8$
SCN11A	$Na_v1.9$

Table 1.2 Tetrodotoxin (TTX) sensitivity of voltage-gated sodium channel subtypes.

VGSC toxins have evolved in the form of both peptides and small-molecules, with peptides representing a majority of those discovered to date. Six classical and distinct neurotoxin receptor sites on VGSC α subunits have been characterized (Catterall 2000). A 7th site known to bind the pyrethroid class of toxins from the *Chrysanthemum* plants is also now widely accepted (Stevens et al. 2011). Neurotoxin receptor sites are classified based on the toxin's binding location and action on channel function (Fig. 1.5).

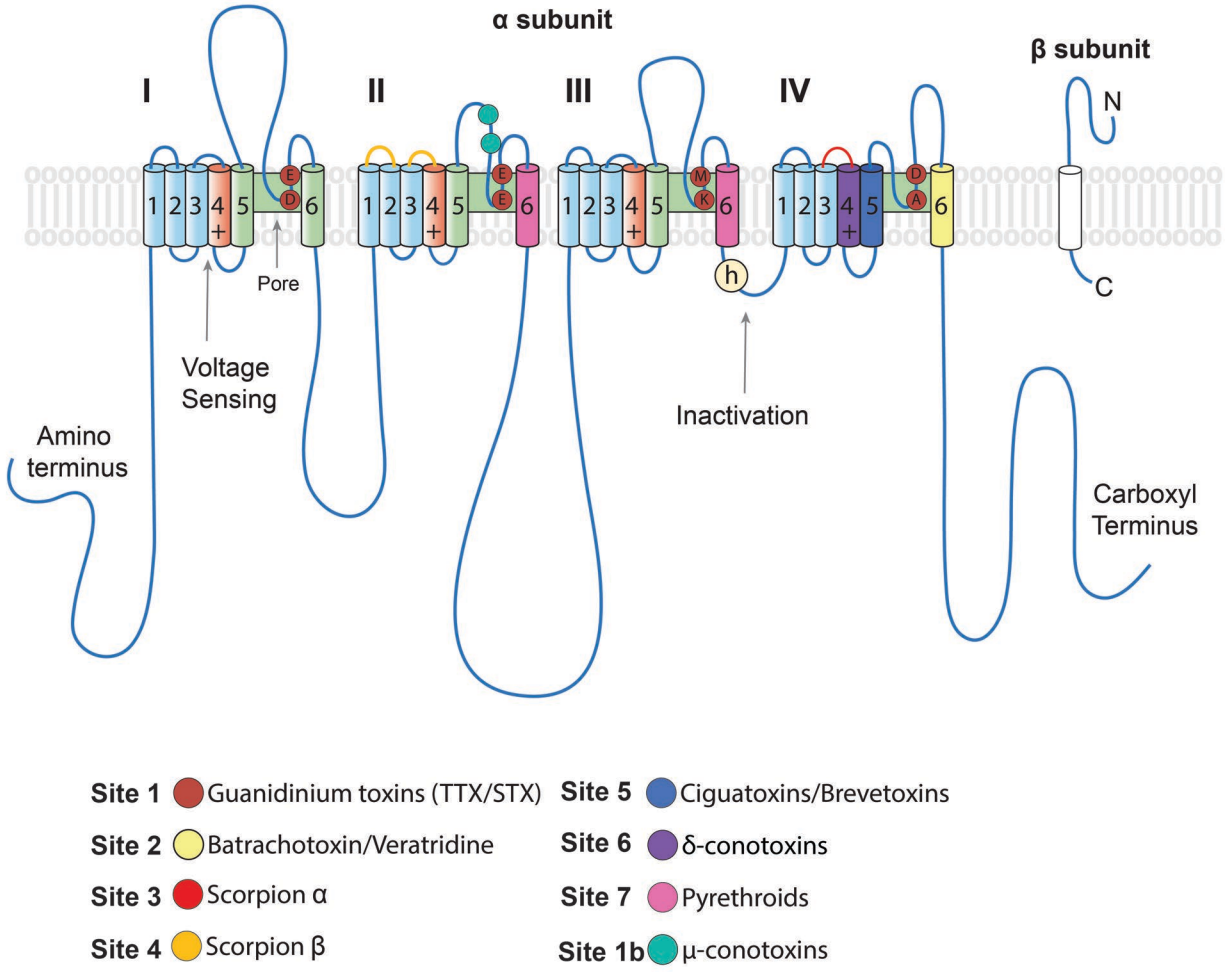


Figure 1.5 Neurotoxin receptors sites of the voltage-gated sodium channel. Modified from (Zhang et al. 2013).

There are two main methods through which VGSC toxins disrupt channel function. The first is a blockade of the pore, like the cork of a bottle. The other is an attack on one or both gating mechanisms. Toxin binding can shift or disable the activation and inactivation gates, compromising the channels' ability to conduct Na^+ ions.

Site-1 guanidinium toxins bind deep in the outer vestibule of the VGSC pore on residues that form the selectivity filter, with re-entrant pore loops of segments S5-S6 on all 4 domains. Site-1 toxins include the hydrophilic guanidinium heterocycles TTX and saxitoxin (STX), which are small molecules produced by cyanobacteria and dinoflagellates. Many aquatic species feed on these toxin-producing microorganisms, thus becoming toxin carriers themselves. The μ-conotoxins, deadly peptides found in the *Conus* genus of snails, bind at site 1b, very near the guanidinium site on the p-loops of the domain II S5-S6 segments.

Site-2 toxins are lipid-soluble VGSC activators. Well described members of this family include the steroidal alkaloids batrachotoxin and veratridine, produced by the poison dart frog and *Veratrum* family of plants, respectively.

Site-3 toxins are peptide toxins that prevent or interfere with the channel inactivation process. Studies indicate the receptor site to be located at the loops between segments S5 and S6 of domain I (Tejedor and Catterall 1988). Notable examples include the α-scorpion and sea anemone toxins. They bind with high affinity to the resting state of the channel and prevent coupling of activation to fast inactivation.

Site-4 hosts the β-scorpion toxins. These lethal peptides are promiscuous and bind to a variety of sites on all 6 segments of domains I-III. Site-4 toxins exert their toxic effects on the channel by reducing peak I_{Na} and shifting the voltage-dependence of activation.

Site 5 toxins bind to the S6 of domain I and S5 of domain IV. The lipophilic brevetoxins and ciguatoxins bind to site-5. These large molecular weight molecules are produced by dinoflagellates. Toxic action on the channel includes shifting the voltage dependence of activation as well as blocking the channel's ability to inactivate.

Site-6: The unique action of the TxVIA toxin from the *Conus textile* species of cone snail led to the identification of a new site-6. Site-6 toxins specifically disable or slow the inactivation process. Although its exact location is unclear, the location of site-6 appears to involve the S4 segment of domain IV.

Toxins can also be selective for specific VGSC subtypes, resulting in powerful research tools with therapeutic potential. To further understand the unique role each VGSC plays in normal and pathophysiological function, compounds with high affinity to a specific subtype are required. For example, the TTX derivative, 4,9-anhydro-TTX, was reported to be 40 to 160-fold more selective for $Na_v1.6$ than $Na_v1.2$-$Na_v1.8$ (Rosker et al. 2007). This selectivity could be exploited strategically to isolate the function of $Na_v1.6$ when simultaneously recording the activity of multiple VGSCs in a neuron.

Neuromodulation of VGSCs

VGSCs are affected in vivo by the action of various neuromodulators including acetylcholine, monoamines, neuropeptides, and glutamate (Cantrell and Catterall 2001). Administration of the cholinergic agonist carbachol reduces peak I_{Na} and slows fast inactivation in dissociated hippocampal neurons (Cantrell et al. 1996). This modulation was shown to act via a protein kinase C (PKC) dependent phosphorylation of VGSCs with similar effects in cortical pyramidal neurons. Cholinergic input to the hippocampus suppresses bursting activity and promotes tonic firing (Azouz et al. 1994, Alroy et al. 1999). The nucleus basalis, a major driver of cholinergic tone in the cortex, shifts cortical spiking from bursting to tonic firing, potentially utilizing modulation of VGSCs as described above (Metherate et al. 1992). Dopaminergic modulation of VGSCs is also observed. Activation of D1-like dopamine receptors, which stimulate adenylyl cyclase activity, decreases I_{Na} in acutely isolated hippocampal neurons (Cantrell et al. 1997, Cantrell et al. 1999). This modulation was shown to be protein kinase A (PKA) dependent. Alternatively, activation of D2 receptors, which are coupled to inhibition of adenylyl cyclase, increases I_{Na} in medium spiny neurons, but has an overall inhibitory effect through activation of a PKC mediated pathway. PKA and PKC phosphorylation reduce peak I_{Na} of brain VGSC subtypes in heterologous cells and intact neurons (Costa et al. 1982, Costa and Catterall 1984, Rossie and Catterall 1987, Rossie et al. 1987, Sigel and Baur 1988, Rossie and Catterall 1989, Dascal and Lotan 1991 Numann et al., 1991, Numann et al. 1991, Li et al. 1992, Surmeier et al. 1992, Sudlow and Gillette R 1995, Cantrell et al. 1996, Cantrell et al. 1996, Cantrell et al. 1997, Cantrell et al. 1999, Carr et al. 2002, Carr et al. 2003, Chen et al. 2006, Scheuer 2011). For most

VGSC subtypes, key phosphorylation sites with functional relevance are in the intracellular loop connecting domains I and II, as well as the inactivation gate (Scheuer 2011).

Phosphorylation effects on I_{Na} are mostly limited to depolarized potentials, with similar features to slow inactivation as described above, leading to the proposal that PKC and PKA modulation enhance the slow inactivation process (Carr et al. 2003). Indeed, it was found that mutation of an asparagine in S6 required for slow inactivation to alanine increased slow inactivation and potentiated the effects of PKC and PKA modulation while mutation to aspartate blocked slow inactivation and prevented modulation by PKA and PKC (West et al. 1993, Scheuer 2011). Modulation of $Na_v1.2$ by PKA and PKC exhibits synergistic modulation (Scheuer 2011). Those residues which are phosphorylated by PKC but not PKA, when mutated to block phosphorylation, also blocked the reduction in I_{Na} by PKA activation. In the absence of PKC modulation, PKA requires membrane depolarization for effective modulation, while in the presence of PKC modulation, PKA modulation occurs at all potentials (Cantrell et al. 1996). VGSC modulation by PKA also requires interaction with A Kinase Anchoring Protein 15 (AKAP15) which binds to the intracellular loop between domain I and II (Cantrell et al. 1999, Cantrell et al. 2002).

It is important to note the effects of phosphorylation on VGSC activity are specific to the cellular environment in which they are studied. Careful attention is required to understand the influence that an experimental expression system may have on the

resulting VGSC modulation observed. Not surprisingly, given the high degree of differential expression of the VGSCs in cell type and subcellular domains, the different VGSC α subunits also exhibit differential sensitivity to neuromodulation by PKA and PKC. $Na_v1.6$ is far less sensitive to PKA modulation than $Na_v1.2$ because it lacks the key serine 573 phosphorylation site (Maurice et al. 2001, Chen et al 2008, Scheuer 2011). Novel VGSC phosphorylation sites have been discovered (Berendt et al. 2010) In addition to being good substrates for PKA/PKC phosphorylation, purified brain VGSCs are dephosphorylated by protein phosphatases such as calcineurin (Gershon et al. 1992, Murphy et al. 1993). Calcineurin was shown to dephosphorylate Nav1.2 at serine residues 573 and 623, and phosphatase 2A showed effective dephosphorylation at serine 610. Both phosphatases effectively dephosphorylate serine 687 (Gershon et al.1992, Murphy et al. 1993, Scheuer 2011). One open question is the extent to which phosphatases and dephosphorylation of VGSCs is voltage-dependent. Further research into the functional role of uncharacterized VGSC phosphorylation sites and dephosphorylation activity is needed.

Serotonin (5-HT) also displays a dose-dependent neuromodulatory effect on VGSC function (Fig. 1.6). In acutely dissociated mouse prefrontal cortex (PFC) pyramidal neurons, 1 μM 5-HT reduced peak I_{Na} by ~25% from baseline at a holding potential of -70 mV (Carr et al 2002). The reduction in I_{Na} was mediated in part by a decrease in whole cell Na^+ conductance as well as a hyperpolarizing shift in the voltage-dependence of fast inactivation. Single cell reverse transcription-polymerase chain reaction (RT-PCR) analysis showed ubiquitous expression of $5\text{-}HT_2$ receptors, and most

isolated PFC pyramidal neurons expressed 5-HT_{2A} or 5-HT_{2A} and 5-HT_{2C} receptors (Carr et al. 2002). Acute perfusion of 1 μM of the 5-$HT_{2A/C}$ selective agonist 2,5-dimethoxy-4-iodoamphetamine (DOI) to acutely dissociated pyramidal neurons also led to ~25% reduction in peak I_{Na} and negatively shifted the voltage-dependence of fast inactivation (Carr et al. 2002). DOI had no effect on the fast or slow components of the fast inactivation time constant. Peak I_{Na} inhibition by acute DOI treatment was significantly reduced by Ca^{2+} chelators and Gαq, phospholipase C (PLC), and PKA/PKC inhibition (Carr et al. 2002). Additionally, DOI significantly reduced persistent I_{Na} and enhances slow inactivation in acutely dissociated PFC pyramidal neurons (Carr et al. 2002, Carr et al. 2003). In mouse PFC slices, layer V pyramidal neurons show a reduction in back-propagating dendritic action potentials, an elevation of spike threshold and increased spike failure after repetitive firing when acutely treated with 1 μM DOI (Carr et al. 2002, Carr et al. 2003). The elevation of threshold and spike failure by DOI is likely due to the enhancement of VGSC slow inactivation. I believe the robust role that slow inactivation of VGSCs plays in frequency adaptation of nearly all sensory modalities is greatly underappreciated thus far. It's attractive to speculate that many serotonergic psychedelic drugs (such as 5-$HT2_{A/C}$ agonists like DOI) may be impairing visual spatial frequency contrast adaptation by enhancing VGSC slow inactivation, ultimately leading to distorted percepts that resemble moiré patterns (Kim and Rieke 2003, Carr et al. 2003, King et al. 2015).

More recent results have shown that activation of 5-HT_{1A} receptors in PFC layer 5 pyramidal neurons differentially decreases I_{Na} in the proximal axon attributable to $Na_v1.2$

while not impacting those in the distal axon, attributable to $Na_V1.6$, showing subcellular domain-specific action of neuromodulators on VGSC function. As described above for PKA and PKC modulation, the effect of 5-HT_{1A} receptor activation on reducing I_{Na} could be attributed to enhancing slow inactivation and depolarizing the voltage dependence of activation (Yin et al. 2017).

Tricyclic antidepressants and selective 5-HT reuptake inhibitors have been shown to bind to brain VGSCs and inhibit I_{Na} in both heterologous cells and cultured neurons (McNeal et al. 1985, Nicholson et al. 2002, Lenkey et al. 2006, Dick et al. 2007). I_{Na} inhibition by 5-HT reuptake inhibitors shows similar features to 5-HT and 5-HT_2 agonists, including voltage-dependence and a hyperpolarizing shift of the inactivation curve (Lenkey et al. 2006).

The powerful impact that 5-HT-induced enhancement of slow inactivation can have on neuronal computation was recently highlighted (Navarro et al. 2020). Using a combination of computational modeling with voltage and dynamic clamp techniques in isolated and brain slice recordings from raphe neurons, Navarro and colleagues show how VGSC slow inactivation enables a neuron to act as a “molecular leaky integrator” that can encode a neuron’s spiking frequency into the fraction of available I_{Na} (Navarro et al. 2020). Because VGSCs enable the initiation of action potentials (which is also dependent on the amount of available I_{Na}), these two functions create a reciprocal feedback loop that place VGSCs as a primary controller of AP firing rates. As most brain 5-HT-producing neurons are in the raphe nuclei, the authors speculate that VGSC slow

inactivation is acting as a frequency control mechanism to stabilize the release of 5-HT (especially when acting via volume transmission) (Navarro et al. 2020). This dynamic control is likely vital for stable neurotransmission and rhythmic firing, such as in the control of respiratory pacemaker neurons in the pre-Bötzinger complex. Respiratory depression and arrest are major contributors to sudden unexpected death in epilepsy (SUDEP) (Massey et al. 2014, Stewart et al. 2020). Precisely how serotonergic modulation of respiratory networks during seizures leads to SUDEP is a current area of intense interest (Tupal and Faingold 2006, Bagdy et al. 2007, Uteshev et al. 2010, Richerson and Buchanan 2011, Faingold et al. 2014, Faingold et al. 2016, Feng and Faingold 2017, Kruse et al. 2019) and VGSCs may play a role in the pathophysiology of respiratory depression in SUDEP.

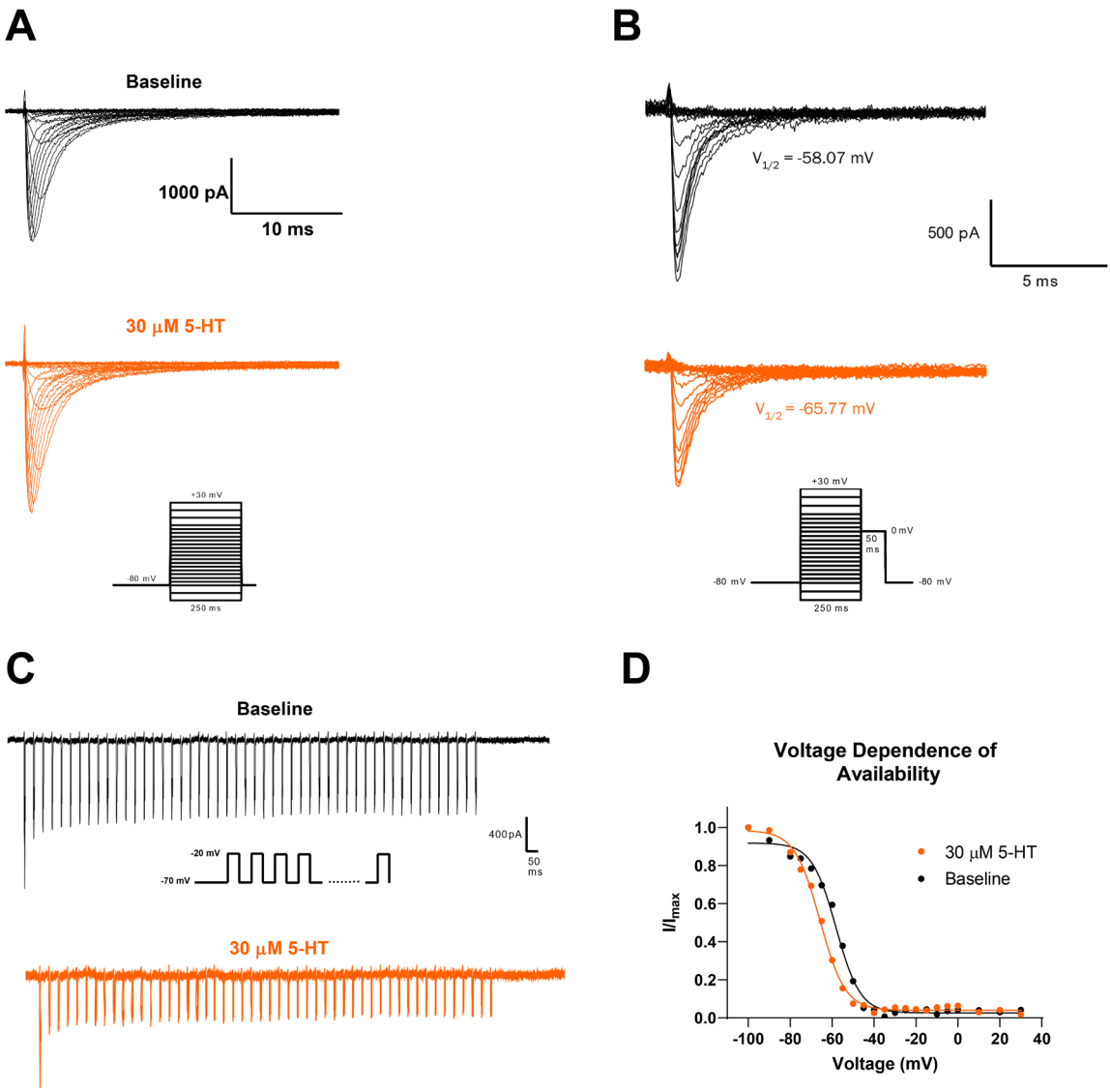


Figure 1.6 Representative example of acute perfusion of 30 μM 5-HT on I_{Na} properties in an acutely isolated wildtype P19 mouse cortical pyramidal neuron. (A) Representative traces showing the voltage-dependence of activation, (B) inactivation, (C) slow inactivation at 50 Hz, and (D) voltage-dependence of availability at baseline (black) and after perfusion of 30 μM 5-HT (orange). 30 μM 5-HT reduced peak I_{Na}, induced a hyperpolarizing shift in the voltage-dependence of fast inactivation, and enhanced slow inactivation. No changes were observed in the voltage-dependence of activation.

Modulation of VGSCs by G-protein βγ Subunits

G-protein coupled receptors (GPCRs) are seven transmembrane domain polypeptides that bind many hormonal and neurotransmitter ligands to initiate a plethora of cell signaling cascades. Upon ligand binding, GPCRs undergo a conformational shift to recruit heterotrimeric G-proteins, composed of a Gα, β, and γ subunit. The activation and subsequent conformational change of the receptors leads to the Gα subunit exchanging GDP for GTP. The binding of GTP stimulates the dissociation of Gα from the Gβγ complex, allowing both Gα and Gβγ subunits to interact with numerous downstream effectors, including many ion channels (Smrcka 2008, Dascal 2001).

G-protein Gβγ subunits are ubiquitously expressed signaling molecules involved in a vast array of intracellular signaling cascades (Fong et al. 1986, Freissmuth et al. 1989). In humans, there are five Gβ and 12 Gγ subunit genes (Table 1.3). Certain Gβ and γ subunits show selectivity for each other and all must dimerize in a $\beta\gamma$ pair for proper folding and physiological function. The direct or membrane-delimited modulation of ion channels through G-protein dependent pathways has been shown to be driven by a Gβγ complex (Hille 1994, Clapham 1994, Wickman and Clapham 1995, Clapham and Neer 1997, Dascal 2001). For example, G protein βγ subunits are known to modulate the activity of voltage-gated K^+ and Ca^{2+} ion channels (Kleuss et al. 1992, Kleuss et al. 1993, Dascal et al. 1993, Wickman et al. 1994, Reuveny et al. 1994, Diverse-Pierluissi et al. 1995, Dascal 2001). However, they also possess the ability to modulate VGSC function (Ma et al. 1997, Mantegazza et al. 2005).

Gene	Protein
Gngt1	Gγ1
Gng2	Gγ2
Gng3	Gγ3
Gng4	Gγ4
Gng5	Gγ5
Gng7	Gγ7
Gng8	Gγ8
Gng10	Gγ10
Gng11	Gγ11
Gng12	Gγ12
Gng13	Gγ13
Gngt2	Gγ14

Gene	Protein
Gnb1	Gβ1
Gnb2	Gβ2
Gnb3	Gβ3
Gnb4	Gβ4
Gnb5	Gβ5

Table 1.3 G protein βγ subunits genes and their corresponding proteins.

Modulation of brain VGSCs by a G-protein coupled signaling pathway was first reported by Catterall and colleagues (Ma et al. 1994). In CHO cells expressing rat $Na_V1.2$ as well as in acutely isolated rat hippocampal neurons, the addition of 200-500 μM GTPγS (a nonhydrolyzable analog of GTP) significantly increased peak I_{Na} in a time-dependent manner by over 200% compared to baseline. The voltage dependence of channel activation and inactivation were also negatively shifted by ~10 mV in both experimental models in the presence of GTPγS. The effect was sensitive to pertussis, but not cholera, toxin, implicating Gαi/o but not Gαs. Removing ATP or adding BAPTA to the recording pipette had no impact, suggesting that the effect of G-protein activation on VGSC function was not dependent upon phosphorylation or intracellular Ca^{2+} (Ma et al. 1994).

Transient coexpression of Gβ1γ3, Gβ5γ3, or Gβ2γ3 with rat Nav1.2 in tsA-201 cells significantly increased persistent I_{Na} and shifted the voltage-dependence of inactivation by +37 mV (Ma et al. 1997). Gβ2γ3 coexpression displayed the greatest effect on I_{Na}, increasing the number of recorded cells with >30% persistent I_{Na} from 4.6% in baseline to over 60% of the total population (Ma et al. 1997). In contrast, coexpression of Gαi1, $G\alpha i_3$, or $G\alpha o_{1A}$ with $Na_v1.2$ led to no observable changes in $Na_v1.2$ function. Addition of VGSC β1 subunits to the transfection experiment did not modulate the effect of Gβ2γ3 on $Na_v1.2$-expressed I_{Na} (Ma et al. 1997). ATP removal, PKC inhibition, or the application of calcium chelators also had little effect on the persistent I_{Na} induced by Gβγ. Co-expressing Gαi with Gβγ prevented Gβγ modulation of VGSC function, even under conditions of exogenous G-protein activation with GTPγS (Ma et al. 1997).

Marin et al. showed coimmunoprecipitation of VGSC α subunits with Gβ subunits in primary mouse cultured cortical neurons, supporting a physical association between VGSCs and Gβγ within a protein complex (Marin et al. 2001). Five-minute preincubation of neurons with 30 μM α-amino-3-hydroxy-5-methyl-4-isoxazolepropionic acid (AMPA) significantly increased the quantity of coimmunoprecipitated Gβ from baseline, suggesting that AMPA receptor activation is coupled to modulation of VGSCs through Gβγ subunits (Marin et al. 2001).

An abstract and poster were presented at the 2004 Annual Biophysical Society Meeting with the title “G-protein β1γ2 subunits directly bind to the C-terminus of $Na_v1.3$ and modulate channel properties” (Lenkowski et al. 2004), however, the results never

appeared in a peer-reviewed publication and all efforts to retrieve details of the study from the authors have been unsuccessful.

VGSC modulation by coexpression of G-protein βγ subunits has also been demonstrated in heterologous cells expressing human $Na_v1.1$ (Mantegazza et al. 2005). Coexpression of Gβγ subunits with human $Na_v1.1$ led to dramatic increases in persistent I_{Na} compared to controls. The molecular determinants for Gβγ modulation of rat $Na_v1.2$ were localized to the C-terminus of the channel, between amino acid residues 1890 and 2005 (Mantegazza et al. 2005). A putative Gβγ binding motif, QMEER, is present in the C-termini of numerous VGSC α subunit subtypes expressed in the CNS. This QxxER motif is also present on many known Gβγ effectors, including protein kinase A and adenylyl cyclase 2. Further analysis of $Na_v1.2$ using truncated and chimeric cDNA constructs showed the QxxER motif was not required for Gβγ modulation of VGSC function. Constructs of rat $Na_v1.2$ where the QxxER motif was mutated still showed modulation by Gβγ. However, constructs with truncation of the C-terminus prior to amino acid 1951 abolished the increase in persistent I_{Na} normally seen with coexpression of Gβ2γ3 and native $Na_v1.2$ (Mantegazza et al. 2005). The C-terminus of rat $Na_v1.2$ ranges from amino acid residues 1777-2005 (Mantegazza et al. 2001). These data led the authors to conclude that “The last 28 amino acid residues of the C-terminus are sufficient to support modulation [of rat $Na_v1.2$] by Gβγ when attached to the proximal C-terminal domain.” (Mantegazza et al. 2005).

Gene	Na_v α subunit	Sensitive to Gβγ Modulation
SCN1A	$Na_v1.1$	YES[3]
SCN2A	$Na_v1.2$	YES[1,3]
SCN3A	$Na_v1.3$	YES[2]
SCN4A	$Na_v1.4$	NO[3]
SCN5A	$Na_v1.5$	NO[3]
SCN8A	$Na_v1.6$	UNKNOWN

Table 1.4 Sensitivity of VGSC α subunit subtypes to functional I_{Na} modulation by G protein βγ subunits when co-expressed in heterologous cells. Ma et al. (1997)[1] Lenkowski et al. (2004)[2] Mantegazza et al. (2005)[3]

Recent evidence of a G-protein dependent pathway resulting in strong inhibition of I_{Na} in cultured and acutely isolated mouse neocortical neurons has restimulated interest in VGSC-G protein subunit interactions (Mattheisen et al. 2018). This pathway was serendipitously discovered after the observation that acute perfusion of 10 μM of the calcium-sensing G protein coupled receptor (CaSR) allosteric agonist, cinacalcet, significantly eliminated inhibitory postsynaptic current (IPSC) amplitude in cultured neurons. Further experiments in cultured neurons showed acute perfusion of 10 μM cinacalcet blocked somatic action potentials and strongly inhibited I_{Na} by over 98% in a state and time-dependent manner. Long-term incubation (50-70 minutes) of cinacalcet

resulted in a concentration-dependent inhibition of I_{Na}, with an IC_{50} of 3.5 ± 1 μM and a hill coefficient of 0.98. This experimental strategy was necessary due to the slow onset of I_{Na} inhibition and potential for confounding current run down of I_{Na} in whole cell recordings. Cinacalcet-induced I_{Na} inhibition showed slow kinetics that could be described by a single exponential with a T ~ 60 s and a delayed onset on inhibition (~75 s). Prolonged hyperpolarization of channels for 1 s at -120 mV significantly relieved the cinacalcet inhibition of I_{Na}, suggesting a transient, state-dependent effect. Another small molecule CaSR allosteric agonist, calindol, showed a similarly strong inhibition of I_{Na} at 5 μM. Surprisingly, use of *Casr*$^{-/-}$ mouse neurons or pretreatment with a CaSR antagonist had no effect on the I_{Na} inhibition induced by cinacalcet, suggesting that the observed I_{Na} inhibition is independent of the CaSR. Cinacalcet inhibition of I_{Na} was shown to be G protein dependent, as pretreatment with the GDP analog, GDPβs (which competitively inhibits GTP binding to G protein α subunits) reduced the cinacalcet inhibition of I_{Na} by over 80% from baseline conditions. Inclusion of 500 μM GTPγS in the recording pipette led to a rapid decrease (~30%) in peak I_{Na}. Pharmacological inhibition of PKA and PKC had no effect on I_{Na} inhibition by cinacalcet. Efforts to identify the identity of the GPCR mediating the I_{Na} inhibition by cinacalcet were unsuccessful, as agonism and antagonism of metabotropic glutamate receptors and $GABA_B$ receptors had no impact on this effect. These data suggest class C GPCRs are not involved in the G-protein dependent inhibition of I_{Na}. While the mechanistic details remain unclear, the authors suggest “One possible mechanism for cinacalcet-inhibition of VGSCs is the direct action of the Gβγ dimer of the G-protein complex on these channels.” (Mattheisen et al. 2018).

In her Ph. D. thesis work, Dr. Glynis Mattheisen showed a similar G-protein dependent I_{Na} inhibition in mouse cultured neocortical neurons with acute perfusion of the endocannabinoid anandamide, which acts as an agonist at the cannabinoid 1 (CB_1) GPCR (Mattheisen 2018). As with the effect of cinacalcet, anandamide activates CaSRs, but its slow, state-dependent inhibition of I_{Na} is independent of the CaSR and CB_1 receptor. Likewise, prolonged hyperpolarization at -120 mV significantly reduced anandamide inhibition of I_{Na} (Mattheisen 2018). Anandamide inhibition of VGSCs at low μM concentrations through a hyperpolarizing shift in the voltage-dependence of fast inactivation has been shown previously (Nicholson et al. 2003, Kim et al. 2005, A Kury et al. 2014, Okura et al. 2014). Antagonism of CB_1 and CB_2 receptors, or pretreatment with pertussis toxin (to inhibit Gi/o signaling) did not alter anandamide inhibition of VGSCs (Al Kury et al. 2014). In contrast to CaSR agonists, there is evidence that anandamide binds directly to VGSCs (Nicholson et al. 2003). Whether or not anandamide and cinacalcet G-protein dependent pathways inhibit VGSCs in the same manner remains poorly understood, and further investigation into the effects of G-protein dependent modulation of VGSCs is required.

Variants in VGSC Genes and in Genes Encoding VGSC Interacting G-proteins Result in Epilepsy

Epilepsy, defined by the occurrence of two or more unprovoked seizures, is one of the most common disorders of the central nervous system. Roughly 1 in 26 individuals will

develop some form of epilepsy during their lifetime (Hesdorffer et al. 2011). Many different types of epilepsies exist, varying greatly in phenotypic severity and etiology. Here we will focus on a class of severe genetic epilepsies that are collectively known as Developmental and Epileptic Encephalopathies (DEEs). DEEs are a group of clinically severe generalized epilepsies that present in the first years of life with chronic unprovoked seizures of multiple etiologies as well as encephalopathy, which refers to the maladaptive development of brain structure, function, and cognition.

Due to the prominent role of VGSC genes in shaping neuronal excitability and development, it is unsurprising that inherited or *de novo* variants in VGSC genes causing either gain- or loss-of function (GOF or LOF) can lead to severe forms of DEE. DEEs linked to variants in sodium channel genes, including *SCN1A, SCN2A, SCN3A, SCN8A*, and *SCN1B* (Meisler et al. 2021), present with severe generalized pharmacoresistant seizures starting within the first year of life. In addition to seizures, patients suffer from profound developmental, cognitive, and behavioral delays/plateaus, intellectual disability, respiratory dysfunction, cardiac arrhythmia, and ataxia. Moreover, while all patients with epilepsy are at risk for SUDEP, sodium channel-linked DEE patients have the highest risk, up to 20% (Genton et al. 2011, Cooper et al. 2016).

SCN1A

In 1978, Charlotte Dravet reported her findings on a unique pediatric epilepsy presenting with severe seizures, intellectual disability, developmental delays, and ataxia (Dravet 1978). She originally named the disorder severe myoclonic epilepsy of infancy

(SMEI), but it was renamed Dravet syndrome (DS) (Dravet 2011). DS patients present with severe generalized tonic-clonic and seizures in the first year of life. The vast majority of patients are pharmacoresistant and experience intellectual disabilities. The incidence of DS in the United States is estimated to be around 1 in 15,000 live births (Wu et al. 2015). In 2001, it was discovered that DS is caused by variants in *SCN1A*, encoding $Na_v1.1$ (Claes et al. 2001). More than 3000 DS variants in *SCN1A* have been reported in ClinVar and other databases, with over 85% *de novo* LOF resulting in haploinsufficiency of $Na_v1.1$ through premature truncation by nonsense or frameshift mutations, whole or partial gene deletion, or promotion of the expression of a nonsense-mediated decay exon (Meisler and Kearney 2005, Kearney and Meisler 2009, Isom and Knupp 2021). There is emerging evidence for a sub-group of DS patients with GOF *SCN1A* variants (Brunklaus et al. 2022). These patients have earlier onset epilepsy, e.g. in the first weeks of life, and present with a more severe phenotype.

To further understand how the paradoxical haploinsufficient LOF in a major brain VGSC subtype ($Na_v1.1$) can lead to hyperexcitability and seizures, a mouse model of DS was developed (Yu et al. 2006). In mice, heterozygous deletion of *Scn1a* recapitulates many of the key features of the human DS phenotype, including spontaneous generalized seizures and SUDEP (Yu et al. 2006). Whole cell I_{Na} recorded from acutely isolated bipolar shaped inhibitory neurons immunopositive for glutamic acid decarboxylase (67 kDa isoform) in the hippocampus at postnatal day 13-14 (P13-14) was significantly reduced in *Scn1a*$^{+/-}$ mice vs. their wildtype littermates on a C57BL/6J background. However, no difference in I_{Na} was detected in pyramidal shaped neurons. These data

laid the foundation of the disinhibition hypothesis of DS pathophysiology, in which $Na_v1.1$ LOF leads to reduced I_{Na} and hypoexcitability of cortical and hippocampal inhibitory GABAergic interneurons while hippocampal excitatory pyramidal neurons showed no differences in I_{Na} at P13-14, a subsequent study in a similar *Scn1a* mouse model showed increased pyramidal neuron I_{Na} and hyperexcitability at P22, the time of seizure on-set, implicating excitatory neurons in the mechanism of DS (Mistry et al. 2014). Further support for the disinhibition hypothesis came from a study showing the predominant localization of $Na_v1.1$ to the AIS of PV+ inhibitory interneurons of the cortex and the corresponding hypoexcitability of these PV+ fast-spiking interneurons in the DS mouse model (Ogiwara et al. 2007). Moreover, it was demonstrated that targeted heterozygous deletion of *Scn1a* in PV+ neurons is sufficient to produce seizures. Selective deletion of *Scn1a* in forebrain GABAergic interneurons of transgenic mice using the Cre-lox method driven by *Dlx*1,2 is sufficient to recapitulate the spontaneous seizures and premature death observed in global *Scn1a*$^{+/-}$ models of DS (Cheah et al. 2012). Likewise, selective deletion of *Scn1a* in vesicular GABA transporter-positive (*VGAT*+) neurons and PV+ neurons in Cre transgenic mice also leads to the DS phenotype (Ogiwara et al. 2013). Cre-dependent deletion of *Scn1a* driven by the empty spiracles homolog 1 (*Emx1*) promoter (an excitatory neuronal marker) does not lead to an epileptic phenotype but instead ameliorates SUDEP caused by gene deletion in inhibitory neurons (Ogiwara et al. 2013). The hypoexcitability of PV+ interneurons in DS mice was found to be developmentally regulated, only occurring in a transient window between P11–P21, with subsequent normalization of PV+ interneuron hypoexcitability to that of wildtype littermates by P35 (Favero et al. 2018).

Other classes of interneurons aside from PV+ interneurons have been implicated in DS pathophysiology. Cortical somatostatin-positive (SST+) interneurons are also hypoexcitable in DS mice compared to wildtype littermates (Tai et al. 2014). In addition to reduced excitability, cortical SST+ interneurons from DS mice show increased threshold and rheobase, causing a significant reduction in frequency-dependence of synaptic inhibition in neighboring excitatory layer V pyramidal neurons (Tai et al. 2014). Irregular spiking vasoactive intestinal peptide-positive (VIP+) interneurons from layer 2/3 of the somatosensory and visual cortex of DS mice show impaired excitability compared to wildtype littermates (Goff and Goldberg 2019). Treatment with the $Na_v1.1$ selective activating toxin Hm1a restored the excitability of DS VIP+ interneurons (Goff and Goldberg 2019). Together, these data show all three major classes of cortical interneurons are disrupted in mouse models of DS.

As discussed above, developmentally regulated pyramidal neuron hyperexcitability and increases in I_{Na} have been shown in DS mouse models (Mistry et al. 2014). The study of DS patient-specific variants using induced pluripotent stem (IPS) cell models has added yet another layer of nuance to our understanding. Inhibitory IPS neurons derived from DS patients have been reported to be both hyperexcitable and hypoexcitable in different studies, further highlighting the wide phenotypic variability of DS and its underlying pathophysiology (Higurashi et al. 2013, Liu et al. 2013).

SCN8A

GOF variants in the *SCN8A* gene (encoding $Na_v1.6$) can lead to a severe DEE with similar clinical presentation to DS (Larsen et al. 2015). Well over 100 pathogenic variants (see ClinVar) caused mostly by *de novo* missense mutations have been linked to *SCN8A*-DEE (Meisler et al. 2016). While many of the clinical features of *SCN8A*-DEE resemble DS, they lack the initial febrile seizures typically present in DS patients. *SCN8A*-DEE also displays a prominent component of motor dysfunction, and roughly 50% of patients are non-ambulatory (Larsen et al. 2015). Functional analysis of patient-specific *SCN8A*-DEE variants in heterologous cells has revealed a significant increase in $Na_v1.6$ activation, persistent I_{Na}, and impaired fast-inactivation leading to hyperexcitability of cortical and hippocampal pyramidal neurons as well as impaired firing of cerebellar Purkinje neurons in acute brain slices (Raman et al. 1997, Kearney et al. 2002, Veeramah et al. 2012, O'Brien and Meisler 2013, Estacio et al. 2014, Meisler et al. 2016, Lopez-Santiago et al. 2017, Johannesen et a. 2019). IPS cortical neurons derived from *SCN8A*-DEE patients show prolonged AP repolarization, increased persistent and resurgent I_{Na}, as well as shortened AIS lengths (Tidball et al. 2020). Limited evidence of GABAergic interneuron dysfunction has been observed in *Scn8a*-DEE mouse models, supporting the preferential expression of $Na_v1.6$ in excitatory pyramidal neurons as the underlying epileptogenic mechanism of *SCN8A*-DEE (Bunton-Stasyshyn et al. 2019). However, a recent study showed SST+ interneurons were hyperexcitable and hypersensitive to depolarization block due to abnormally large persistent I_{Na} in a *Scn8a*-DEE mouse model (Wengert et al. 2021).

SCN1B

Pathogenic inherited heterozygous *SCN1B* variants have been linked to cardiac dysrhythmias like Brugada syndrome and atrial fibrillation, as well as epilepsies (O'Malley and Isom 2015, Edokobi and Isom 2018). *SCN1B*-p.C121W was the first epileptic variant of *SCN1B* discovered (Wallace et al. 1998). This autosomal-dominant mutation can lead to a clinical phenotype known as genetic epilepsy with febrile seizures plus (GEFS+). *In vitro*, *SCN1B*-p.C121W shows reduced β1 cell surface expression, glycosylation, association with VGSC α subunits and trans homophilic cell adhesion capabilities compared to wildtype β1 (Krueger et al. 2016). *In vivo*, *Scn1b*-p.C121W (*Scn1b*$^{C/W}$) mice show increased susceptibility to febrile seizures compared to *Scn1b*$^{C/C}$ or *Scn1b*$^{+/-}$ mice and C121W β1 protein localization was restricted to the cell body, with little to no expression detected at the AIS (Krueger et al. 2016).

Inherited homozygous variants in *SCN1B* can lead to a devastating DEE, with clinical presentation more severe than DS (Aeby et al. 2019). An emerging number of pathogenic variants have subsequently been discovered (see ClinVar). To date, 9 patients with homozygous recessive mutations in *SCN1B* have been linked to DEE. The *SCN1B*-p.R125C variant has been reported to result in LOF, leading to a significant loss of β1 cell surface expression (Patino et al. 2009). Aside from one variant found to prevent secretion of the splice variant isoform, β1B, all *SCN1B*-linked DEE variants are located in the Ig domain. As more patients are diagnosed with *SCN1B*-linked DEE, two things are clear: *SCN1B*-linked DEE is often more clinically severe than DS, and the pathophysiological mechanisms underlying these disparities are not clearly defined. To

further define the underlying pathophysiology of *SCN1B*-linked DEE, a global *Scn1b*$^{-/-}$ mouse model was developed (Chen et al. 2004). These null mice exhibit spontaneous seizures of multiple etiologies starting around P10, ataxia, as well as ventricular and atrial cardiac arrhythmias and failure to thrive with reduced body weight (Lopez-Santiago et al. 2007, Yuan et al. 2019, Bouza et al. 2021, Ramos-Mondragon et al. 2022). Most importantly, all mice die by the age of P24 (Chen et al. 2004, Hull et al. 2020). *Scn1b* null mice also show a failure to thrive and defects in neuronal development including neuronal proliferation, pathfinding, migration, and fasciculation (Brackenbury et al. 2013, O'Malley and Isom 2015). Developmental deficits in the *Scn1b* null mouse model are observed prior to the onset of spontaneous seizures, leading to hypotheses regarding causative roles of aberrant brain development on the severity of seizures and lethality in *SCN1B*-linked DEE. Intriguingly however, targeted deletion of *Scn1b* in an adult *Scn1b*$^{flox/flox}$ mouse model following normal development is sufficient to recapitulate the phenotype of *Scn1b*$^{-/-}$ mice, including spontaneous seizures and 100% lethality from SUDEP within 20 days of *Scn1b* deletion (O'Malley et al. 2019).

Tissue specific deletion of *Scn1b* in various neuronal populations using *Scn1b*$^{flox/flox}$ mice has revealed a key role for PV+ interneurons. *Scn1b* deletion in PV+ interneurons, but not EMX+ or CAMk2a+ neurons, reproduced the seizures and SUDEP observed in the *Scn1b*$^{-/-}$ mice (Hull et al. 2020).

In addition to modulating the function of VGSC α subunits, VGSC β1 subunits can modulate multiple classes of voltage-gated K^+ channels in heterologous cell systems,

cultured neurons and brain and heart *in vivo* (Deschênes and Tomaselli 2002, Nguyen et al. 2012, Marionneau et al. 2012, Bouza et al. 2021). However, no significant differences were observed in either transient or non-inactivating K^+ currents recorded from cortical layer 6 pyramidal neurons of *Scn1b*$^{-/-}$ mice vs. wildtype littermates (Hull 2019). Alternatively, changes in K^+ currents recorded from *Scn1b*$^{-/-}$ cardiac ventricular myocytes have been observed (Bouza et al. 2021).

Although *Scn1b*$^{-/-}$ mice show spontaneous seizures and SUDEP, the seizure susceptibility of *Scn1b*$^{+/-}$ mice is similar to wild type, suggesting that a single functional *SCN1B* allele is sufficient for normal physiological function (Patino et al. 2009).

GNAO1

The recent clinical implementation of exome-based diagnostics has revealed the genetic cause for many patients with undiagnosed developmental disorders (Zhu et al. 2015). Most cases are eventually linked to pathogenic *de novo* variants (Need et al. 2012, Yang et al. 2013, Wright et al. 2015, Helbig et al. 2016). *De novo* mutations in the guanine nucleotide-binding protein α_O subunit (*GNAO1*) can lead to encephalopathy, including DEE (Nakamura et al. 2013, Law et al. 2015, Talvik et al. 2015, Saitsu et al. 2016, Ueda et al. 2016, Marce-Grau et al. 2016, Gawlinski et al. 2016, Arya et al. 2017, Gerald et al. 2018, Danti et al. 2017, Sakamoto et al. 2017, Schorling et al. 2017, Bruun et al. 2018, Feng et al. 2018). *GNAO1*-linked encephalopathy (*GNAO1*-E) patients can present with severe movement disorders, hypotonia, developmental delay, seizures,

intellectual disability, and behavioral abnormalities among other symptoms (Danti et al. 2017). A wide phenotypic spectrum is associated with *GNAO1* variants that cause neurological disease (Saitsu et al. 2016). Roughly 40% of patients have severe symptoms of movement disorder without epilepsy, while roughly 25% have epilepsy without movement disorder, and roughly 30% have both (Feng et al. 2018). Feng et al. report a strong correlation between the *in vitro* biochemical phenotype in $G\alpha_O$-dependent cAMP inhibition and the clinical pattern of epilepsy vs movement disorder (Feng et al. 2017). LOF variants showed higher correlation to DEE patients with no movement disorders, while GOF variants were found to correlate with patients displaying movement disorders with or without seizures (Feng et al. 2017). A vast majority of pathogenic *GNAO1*-E variants have been reported as missense mutations (Feng et al. 2018).

$G\alpha_O$ is prominently expressed in brain neurons where it inhibits cyclic adenosine monophosphate (cAMP) production and interacts with an array of signaling effectors. $G\alpha_O$ regulates presynaptic neurotransmission by modulating intracellular [Ca^{2+}] and has been implicated in developmental processes such as neurite outgrowth (Strittmatter et al. 1994, He et al. 2006, Bromberg et al. 2008). As with the sodium channel-linked DEEs, a better understanding of the underlying pathophysiology of *GNAO1*-E can be attained using preclinical mouse models of the human disease. *Gnao1*$^{-/-}$ mice display seizures, severe movement disorders, behavioral abnormalities hyperalgesia, and early lethality (Valenzuela et al. 1997, Jiang et al. 1998). Heterozygous *Gnao1*$^{G184S/+}$ mice show spontaneous seizures, significantly greater sensitivity to pentylenetetrazol-induced

kindling, and early lethality accompanied by epileptiform discharges with strain and sex-dependent phenotypic severity (Kehrl et al. 2014, Feng et al. 2019). *GNAO1*-p.G203R is one of the most common *GNAO1*-E variants observed clinically (Feng et al. 2019). *Gnao1*$^{G203R/+}$ results in a haploinsufficient loss of function allele (Feng et al. 2019, Feng et al. 2022). *Gnao1*$^{G203R/+}$ mice exhibit ~50% lower expression levels of $G\alpha_O$ protein in whole brain compared to wildtype littermates (Feng et al. 2022). Whole brain Gβγ protein expression was not significantly different from wildtype in *Gnao1*$^{G203R/+}$ mice, however, the reduced expression of $G\alpha_O$ led the authors to propose there would be increased free Gβγ (unbound to $G\alpha_O$) present in neurons (Feng et al. 2022). *Gnao1*$^{G203R/+}$ mice show reduced presynaptic inhibitory but not excitatory neurotransmitter release in cerebellar Purkinje neurons (Feng et al. 2022). The increased Gβγ is suggested to underlie this deficit in reduced inhibitory neurotransmission, possibly through Gβγ interactions with synaptic vesicle fusion proteins (Zurawski et al. 2016, Zurawski et al. 2017, Zurawski et al. 2019 Zurawski et al. 2022).

GNB1

Germline *de novo* variants in the guanine nucleotide-binding protein β1 subunit (*GNB1*) can lead to a neurodevelopmental disorder known as *GNB1* encephalopathy (*GNB1*-E), characterized by global developmental delay, movement disorders, intellectual disability, sensory impairments (especially visual), gastrointestinal issues, and epilepsy (Petrovski et al. 2016, Steinrucke et al. 2016, Brett et al. 2017, Lohmann et al. 2017,

Szczaluba et al. 2017, Hemati al. 2018, Jones et al. 2019, Peng et al. 2019, Endo et al. 2020, Revah-Politi et al. 2021). The first *GNB1*-E patient identified expressed the variant *GNB1*-p.K78R (c.233 A>G; p.K78R, human NM_002074, mouse NM_008142) (Colombo et al. 2019). This was reported in 2016 in a cohort of 13 *GNB1*-E patients (Petrovski et al. 2016). *GNB1*-p.I80N and p.I80T variants are the most common in *GNB1*-E patients (Petrovski et al. 2016, Hemati et al. 2018, Reddy et al. 2021). The original cohort of patients showed a spectrum of phenotypic severity, but all patients displayed global developmental delay and over 75% (10/13) suffered from seizures (Petrovski et al. 2016). More than 60 *GNB1*-E patients have been identified and roughly 60% of *GNB1*-E patients show abnormal electroencephalogram (EEG) recordings (*GNB1* Foundation, Colombo et al. 2019).

Identified pathogenic *GNB1*-E variants are primarily caused by missense mutations and most cluster in the region of amino acids 76 through 112 in Gβ1 (Pertovski et al. 2016, Hemati et al. 2018, Endo et al. 2020, Reddy et al. 2021). Many of the identified variants occur at residues involved in the Gα interface (78, 80, 89, 110) (Ford et al. 1998). The p.K78R variant also occurs at a residue predicted to be involved in the GIRK interaction interface (Whorton and MacKinnon 2013). Despite the regional clustering of *GNB1*-E variants, it does not appear that there is a clear genotype-phenotype correlation between the location of the missense mutation and phenotypic severity (Petrovski et al. 2016, Lohmann et al. 2017, Hemati al. 2018). The expansive array of downstream Gβγ effectors poses a significant challenge to the elucidation of the cellular mechanisms involved in the pathophysiology of *GNB1*-E. Further complicating the issue, the

interaction of the Gβγ subunits for any one *GNB1*-E variant may be GOF for one effector and simultaneously LOF for another. Our focus will be on the disease mechanisms involved in the epileptic component of *GNB1*-E, as this is present in most patients and according to the *GNB1* Foundation, "[…] the most urgent concern is the prevalence of epilepsy." Relevant Gβγ effectors that could play a role in the epilepsy of *GNB1*-E include voltage-gated Ca^{2+} channels (VGCCs), G-protein inwardly-rectifying K^{+} (GIRK) channels, synaptic vesicle/fusion proteins involved in neurotransmitter release, and VGSCs.

In vitro functional analysis of the neuronal signaling impairments in *GNB1*-E variants is extremely limited. Lohmann and colleagues investigated the functional effects of a panel of 10 *GNB1*-E pathogenic missense variants (L30F, R52G, G64V, H91R, A92T, P94S, P96L, A106T, D118G and K337Q) for their ability to form a functional Gβγ dimer with Gγ7 and interact G protein-coupled receptor kinase 3 (GRK3) as well as the Gαs-coupled dopamine D1 receptor (D1R) using real-time bioluminescence resonance energy transfer (BRET) (Lohmann et al. 2017). Of these 10 patients with *GNB1*-E missense variants, 7 experienced seizures (Lohmann et al. 2017). *GNB1*-E variants R52G, G64V, A92T, P94S, P96L, A106T and D118G showed significantly different functional effects from wildtype in one or more of these assays. L30F, H91R and K337Q variants showed no difference from wildtype in Gβ1γ7 dimer formation or functional signaling with GRK3 or DR1 (Lohmann et al. 2017).

Mouse models of *GNB1*-E have provided key insights into the underlying pathophysiology of the disorder. Homozygous loss of *Gnb1* is embryonically lethal in mice, with prenatal mice showing severe neurodevelopmental issues (Okae and Iwakura 2010 Georgi et al. 2013). Using CRISPR/Cas9, Colombo and colleagues generated a knock-in mouse model of *GNB1*-E using the first patient variant identified (p.K78R) (Colombo et al. 2019). *Gnb1*$^{K78R/+}$ mice recapitulate many key features of the human *GNB1*-E phenotype, including developmental delay and spontaneous 'absence-like' generalized non-convulsive seizures (Colombo et al. 2019). At P0, cortical Gβ1 expression levels at the plasma membrane were not significantly different from wildtype littermates, suggesting the K78R variant is not a functional null allele and Gβγ complexes including Gβ1 are properly trafficked to the cell surface in cortical neurons of *Gnb1*$^{K78R/+}$ mice (Colombo et al. 2019). Similarly, primary cultured cortical excitatory and inhibitory neurons from *Gnb1*$^{K78R/+}$ mice show normal levels of Gβ1 expression. *Gnb1*$^{K78R/+}$ mice of both sexes on a C57Bl/6NJ background show significantly reduced body weight compared to aged-matched wildtype littermates at P0 and P42. *Gnb1*$^{K78R/+}$ mice also display spatial learning and memory deficits in the Morris Water Maze (Colombo et al. 2019).

At P42-56, *Gnb1*$^{K78R/+}$ mice have spontaneous electrographic seizures and significantly higher susceptibility to generalized seizures (electroconvulsive threshold) compared to wildtype and (Colombo et al. 2019). The spontaneous seizure events were described as 'absence-like' because they were generalized bilateral spike and-wave discharges (SWD), a common EEG feature of absence seizures. In a one-day period, *Gnb1*$^{K78R/+}$

mice exhibited between 1000 and 3000 SWDs, while wildtype littermates rarely, if ever, displayed SWD during this time (Colombo et al. 2019). Acute treatment of *Gnb1*$^{K78R/+}$ mice with ethosuximide and valproic acid significantly reduced SWD frequency for a one-hour period following injection (likely due to short half-life), while phenytoin did not (Colombo et al. 2019). Multielectrode array recordings (MEA) of *Gnb1*$^{K78R/+}$ cultured cortical neurons showed no difference in mean firing rate compared to wildtype neurons but did display a significantly increased duration of bursting activity although overall burst frequency was significantly reduced compared to wildtype (Colombo et al. 2019). Ethosuximide, but not valproic acid, rescued this abnormal bursting phenotype in MEA recordings of *Gnb1*$^{K78R/+}$ cultured cortical neurons. VGCC Ca_v3 antagonists, ML218 and NNC 55-0396 had no effect on the abnormal bursting phenotype of Gnb*1*$^{K78R/+}$ cultured cortical neurons. The GIRK antagonist, Tertiapin Q, showed similar ameliorating effects to ethosuximide, implicating GIRK, but not Ca_v3, channels, in the pathophysiology of abnormal burst firing in MEA recordings of Gnb*1*$^{K78R/+}$ cultured cortical neurons (Colombo et al. 2019).

In *Xenopus* oocytes the *GNB1*-p.K78R mutation showed a GOF for GIRK1/2 and GIRK2 channel activation at lower RNA injection doses (0.05-0.2 ng) compared to wildtype Gβ1. At RNA injection doses ≥ 0.5 ng, the Gβ^{K78R}γ mutant activation of GIRK1/2 and GIRK 2 began to decrease from wildtype and elicited significantly lower GIRK1/2 current at an RNA injection dose of 5 ng (Colombo et al. 2019). Surface expression of Gβγ was quantified in giant excised membrane patches from oocytes with

immunofluorescence, revealing higher surface expression of the $G\beta^{K78R}\gamma$ mutant compared to wildtype (Colombo et al. 2019).

In a follow up study, *GNB1-E* variants p.K78R, p.I80N and p.I80T were assessed for their ability to modulate GIRK channels, $Ca_v2.2$ channels, and couple to Gi/o mediated GPCRs (Reddy et al. 2021). All three variants showed no significant differences from wildtype in their ability to modulate $Ca_v2.2$ channels or couple to Gi/o mediated GPCRs (Reddy et al. 2021). *In vitro*, all three mutants also showed significantly reduced binding to the C-terminal cytosolic domain of GIRK 1 and GIRK 2 subunits (Reddy et al.2021). In oocytes, the $G\beta^{K78R}\gamma$ mutant showed GOF for GIRK1/2, GIRK2 and GIRK1/3 at low RNA injection doses, but no difference or LOF at higher doses. At the 5 ng RNA injection dose, $G\beta^{I80N}\gamma$ and $G\beta^{I80T}\gamma$ showed partial or severe LOF for GIRK2 and GIRK1/3 channel activation. Surface expression of $G\beta^{K78R}\gamma$ in giant excised membrane patches from oocytes was increased compared to wildtype, while $G\beta^{I80N}\gamma$ and $G\beta^{I80T}\gamma$ showed significantly reduced expression at RNA injection doses at or below 5 ng (Reddy et al. 2021). These data highlight the complex effects that *GNB1*-E variants can have on the function of Gβγ signaling effectors involved in the regulation of neuronal excitability.

Caution should be exercised in the interpretation and translatability of whole cell two-electrode voltage clamp recordings of ion channel function in *Xenopus* oocytes. As an abnormally large and amphibious heterologous cell system there is a possibility that exogenously expressed mammalian ion channel proteins are processed differently than

they are in mammalian cells (Dascal 2001a). Further characterization of the effects pathogenic *GNB1-E* variants have on ion channel function in mammalian cells is needed.

Teng and colleagues recently published an *in vivo* characterization of absence seizures in the *Gnb1*$^{K78R/+}$ mouse model using a combination of EEG, fiber photometry, and chemogenetic methods (Teng et al. 2022). Their results revealed that SWD events in *Gnb1*$^{K78R/+}$ were highly prevalent in the awake state, and significantly reduced in non-rapid-eye-movement (REM) and REM sleep states. This finding was also observed in two other genetic models of absence epilepsy, *Stxbp1* haplodeficient mice (*Stxbp1*$^{+/-}$), a gene encoding a presynaptic protein involved in neurotransmission, as well as *Gria4* deficient mice (*Gria4*$^{-/-}$) which lack the GluR4 AMPA receptor subunit (Teng et al. 2022). This finding led to the hypothesis that sensory input drives the generation of SWD in *Gnb1*$^{K78R/+}$ mice. In support of that hypothesis, the number and duration of SWD observed in *Gnb1*$^{K78R/+}$ mice was increased during somatosensory stimulation (air puff) compared to before and after stimulation (Teng et al. 2022). Directly upon onset of the air puff, SWD incidence transiently drops and is followed by a gradual increase in frequency and duration. These data suggest sensory input has a complex involvement in synchronizing the circuits involved in SWD generation of *Gnb1*$^{K78R/+}$ mice. Disrupted thalamocortical (TC) networks are well established in absence epilepsy and SWD (Huguenard 2019). Fiber photometry combined with EEG showed excitatory TC cells are transiently activated prior to and inhibited during SWD in *Gnb1*$^{K78R/+}$ mice (Teng et al. 2022). Inhibitory cells of the thalamic reticular nucleus (TRN) show the opposite

pattern of activity to TC cells in relation to SWD. Chemogenetic activation of TC cells enhanced the occurrence of SWD, which the authors suggest further supports sensory input can regulate SWD in *Gnb1*$^{K78R/+}$ mice through activation of TC circuits (Teng et al. 2022).

As previously discussed, G-protein βγ subunits show physical and functional interactions with VGSCs in acutely isolated and cultured mouse neurons and heterologous cells (Ma et al. 1997, Marin et al. 2001, Mantegazza et al. 2005). Due to their vital role in controlling neuronal excitability and the pathophysiology of numerous DEEs, we will further explore the relationship between Gβ1γ2 subunits and brain VGSCs in Chapter III to support the hypothesis that VGSCs may be relevant Gβγ effectors promoting hyperexcitability and seizures in *GNB1*-E.

Pharmacology of Sodium Channel-linked DEEs

VGSCs are the primary targets of many local anesthetic, anti-arrhythmic, neuropsychiatric, and anti-seizure therapeutic agents. Roughly one third of all epilepsy patients are non-responsive (refractory) to available anti-seizure medications (ASMs) (Kwan and Brodie 2000, Picot et al. 2008). The risk of SUDEP is inversely related to the control of seizures, and uncontrolled tonic-clonic seizures are the best recognized risk factor for SUDEP (Ryvlin et al. 2019). Refractory patients have a 2-10 times greater risk of SUDEP than the general population (Fattorusso et al. 2021). ASMs that target VGSCs like carbamazepine, phenytoin, and lamotrigine exacerbate seizures in DS patients with LOF *SCN1A* variants and are thus contraindicated (Knupp and Wirrell

2018). Although complete seizure control is generally not achievable for sodium channel-linked DEE patients with small molecule ASMs, they have had some success in reducing seizure frequency and increasing quality of life (Löscher et al. 2020). First-line therapies for DS and *SCN1B*-linked DEE include the long-acting benzodiazepine clobazam and valproic acid, which are both broad spectrum ASMs. Patients are almost always treated with multiple ASMs concurrently. First line agents typically provide only modest reductions in seizure frequency and severity and are often combined with other second and third line “add-on” ASMs. Second and third line therapeutics include topiramate, levetiracetam, and the recent FDA approved therapeutics stiripentol, cannabidiol and fenfluramine (Strzelczyk et al. 2022). Adjunctive non-pharmacological treatment options such as vagus nerve stimulation and strict adherence to a ketogenic diet are also combined to the treatment regimen by epileptologists in some cases.

In contrast to *SCN1B*-DEE and most cases of DS caused by LOF variants leading to *SCN1A* haploinsufficency, the GOF nature of some *SCN1A* and many *SCN8A*-DEE variants does permit clinical use of broad-spectrum sodium channel blockers. *SCN1A* GOF and *SCN8A*-DEE patients do show improvement in seizure frequency and quality of life after treatment with broad-spectrum sodium channel blocking ASMs (Wagnon et al. 2016). Due to the clear evidence of increased $Na_v1.6$ function underlying most *SCN8A*-DEE variants, selective reduction of $Na_v1.6$ expression or I_{Na} with precision or small molecule therapeutics is a promising treatment strategy for this sodium channel-linked DEE. However, the relief and efficacy of VGSC blockers in *SCN8A*-DEE remains

modest and novel therapeutics are desperately needed for better seizure control and treatment of other symptoms such as ataxia and intellectual disability.

Subtype Selective VGSC Modulation as a Potential Treatment for Sodium Channel-linked DEE

Due to the highly specific role of unique VGSC subtypes in the pathophysiology of neurological disorders, especially sodium channel-linked DEEs, there is great interest in the development of subtype selective VGSC therapeutics (England and de Groot 2009). This has been a formidable task, as the high homology shared between brain VGSC α subunits minimizes the likelihood of a small molecule selectively engaging only one unique VGSC subtype. Historically, the most intense focus of VGSC subtype selective drug development has centered around $Na_v1.7$, encoded by the *SCN9A* gene. $Na_v1.7$ is highly localized to the peripheral nervous system where it plays a fundamental role in nociception. After the discovery that humans with congenital insensitivity to pain (CIP) expressed *SCN9A* LOF variants (Cox et al. 2006, Goldberg et al. 2007). as well as the observation of loss of pain sensitivity in global *SCN9A* null mice (Nassar et al. 2004, Minett et al. 2012, Gingras et al. 2014), intense efforts were poured into the development of $Na_v1.7$ selective blockers to replace opioid analgesics. Despite promising preclinical data, numerous $Na_v1.7$ selective inhibitors have failed to show efficacy in clinical trials (Alexandrou et al. 2016, DiMauro et al. 2016, Marx et al. 2016, Weiss et al. 2017, Wu et al. 2017, Focken et al. 2018, Bankar et al. 2018, Kingwell 2022). Various hypotheses for the unsuccessful development of a $Na_v1.7$ selective

blocker to date include lack of drug target engagement in the spinal cord, interplay of opioid receptors and enkephalin biosynthesis with *SCN9A* expression, and the differences in global loss of expression vs. small molecule inhibition of $Na_v1.7$ (Minett et al. 2015, Deuis et al. 2017, Kraus et al. 2021). Recent work proposed inhibition of neurotransmitter release as the principal mechanism of anosmia and analgesia in *SCN9A* null mouse models and humans with CIP (MacDonald et al. 2021).

As mentioned previously, sodium channel-linked DEEs are largely monogenetic disorders caused by variants in unique brain VGSC genes such as *SCN1A* ($Na_v1.1$) and *SCN8A* ($Na_v1.6$). In DS mice, the haploinsufficient loss of *Scn1a* leads to a roughly 50% reduction in productive *SCN1A* mRNA and $Na_v1.1$ brain protein expression (Han et al. 2020). In *SCN8A*-DEE, $Na_v1.6$ GOF drives hyperexcitability of cortical and hippocampal networks. If a small molecule or precision genetic therapy can upregulate the function of $Na_v1.1$ in DS or downregulate the function of $Na_v1.6$ in DS or *SCN8A*-DEE, this may ameliorate the hyperexcitability and seizures present in these sodium channel-linked DEE patients (Jensen et al. 2014, Johnson et al. 2022).

In support of this hypothesis, significantly decreasing $Na_v1.6$ expression prolongs the lifespan of DS mice (Martin et al. 2007). Generation of *Scn1a*$^{+/-}$/*Scn8a*$^{med\text{-}jo/+}$ double heterozygous mice, which effectively results in heterozygous deletion of *Scn8a* in the *Scn1a*$^{+/-}$ DS mouse model, no longer display early lethality (SUDEP) and a seizure threshold different from that of wildtype littermates (Martin et al. 2007). Consistent with this result, a *Scn8a* GAPmer antisense oligonucleotide (ASO) that reduces $Na_v1.6$

expression reduces seizures and SUDEP in *Scn1a* DS mice (Lenk et al. 2020, Hill and Meisler 2021).

There is also great excitement for a potential ASO treatment (STK-001) of DS (Han et al. 2020). *SCN1A* has at least one naturally occurring, developmentally regulated poison exon—an exon whose inclusion produces no protein due to nonsense mediated decay of the mRNA transcript (Carvill and Mefford 2020). This genetic failsafe can be exploited as a therapeutic target to treat haploinsufficient loss of *SCN1A* in DS with a steric block ASO that prevents inclusion of the poison exon, effectively increasing $Na_v1.1$ expression from the remaining wildtype allele (Han et al. 2020, Isom and Knupp 2021). In cultured cells, STK-001 treatment reduced the presence of *SCN1A* poison exon transcripts by over 55% (Han et al. 2020). While RNA transcript expression is not often an accurate predictor of protein expression, recent work found membrane receptors and ion channel proteins among the highest correlates of RNA transcript to protein expression levels (Bauernfeind and Babbitt 2017). *In vivo*, STK-001 administration in DS mice at P2 prevented SUDEP, significantly delayed seizure onset, and dramatically decreased seizure frequency (Han et al. 2020). Phase 2 clinical trials with STK-001 in DS patients are currently in progress (ClinicalTrials.gov Identifier: NCT04740476).

The $Na_v1.1$ selective activating disulfide-rich peptide toxin, Hm1a, leads to restoration of hypoexcitable inhibitory neuron function and significantly reduces seizures and mortality in *Scn1a*$^{+/-}$ DS mice (Richards et al. 2018). Although promising, development of the

Hm1a toxin (derived from the venom of the *Stromatopelma* family of tarantula) is highly unlikely as intracerebroventricular injection of 100 pM Hm1a led to paralysis and death of juvenile Balb/C mice in less than 2 hours (Escoubas et al. 2002). The carboxamide 3-amino-5-(4-methoxyphenyl)thiophene-2-carboxamide (AA43279) shows high selectivity and acts as an activator for $Na_v1.1$ by impairing fast inactivation (Frederiksen et al. 2017). AA43279 increases excitability of PV+ fast-spiking interneurons in rat hippocampal brain slices and the maximal electroshock seizure threshold *in vivo* (Frederiksen et al. 2017). AA43279 and two separate $Na_v1.6$-selective inhibitors (MV1369 and MV1312) all reduced spontaneous burst locomotor movements and seizure activity in *Scn1Lab*$^{-/-}$ zebrafish (a preclinical vertebrate model of DS) (Weuring et al. 2020).

Pharmacological inhibition of $Na_v1.6$, but not $Na_v1.1$, leads to reduced epileptiform activity in mouse cortical slices treated with the proconvulsant non-selective K^+ channel inhibitor 4-aminopyridine (Patel et al. 2020). Selective inhibition of $Na_v1.6$ may have implications to epilepsies beyond the treatment of sodium channel-linked DEEs: Targeted reduction of *Scn8a* expression with a short hairpin interfering RNA prevents seizure development in a mouse model of temporal lobe epilepsy (Focken et al. 2019, Wong et al. 2018). Preclinical rodent work also indicates selective inhibition of $Na_v1.1$ may be useful beyond epilepsy for neuropsychiatric disorders such schizophrenia and Parkinson's disease (von Schoubye et al. 2018, Liu et al. 2021).

In addition to the preclinical evidence for selective $Na_v1.6$ inhibition to treat seizures in DS, there is also evidence for treating *SCN8A*-DEE (Martin et al. 2007, Johnson et al. 2022). Variants in *SCN8A*, which encodes human $Na_v1.6$, have been linked to DEE, movement disorders, and cognitive impairment (Wagnon et al. 2016). In many physiologically examined *SCN8A*-DEE variants, GOF leads to excess $Na_v1.6$-mediated persistent current and hyperexcitability (Veeramah et al. 2012, Johannesen et al. 2019). The first-in-class state-dependent $Na_v1.6$ selective inhibitor, NBI-921352 (previously XEN901), is a potent aryl sulfonamide with an IC_{50} of 51 nM for $hNa_v1.6$ and > 6.9 μM IC_{50} for any other human VGSC subtype present in the central nervous system (Johnson et al. 2022). NBI-921352 is capable of restoring *SCN8A*-DEE patient-specific variant $Na_v1.6$ channel function in voltage clamp recordings of transfected heterologous cells, as well as preventing seizures in a *Scn8a*-DEE mouse model. In cortical brain slices from wildtype mice injected with 250 nM NBI-921352, no differences were observed in the current to spike frequency (F-I) relationship for fast-spiking interneurons. However, cortical pyramidal neurons showed reduced excitability, supporting the preferential expression of $Na_v1.1$ to cortical GABAergic interneurons and $Na_v1.6$ to excitatory pyramidal neurons (Johnson et al. 2022). At the time of writing, NBI-921352 is currently under evaluation in phase II clinical trials as an adjunctive therapy for *SCN8A*-DEE patients (ClinicalTrials.gov Identifier: NCT04873869).

Conclusion

Proper function of VGSCs is required for the central nervous system to operate in a healthy manner. A severe class of genetic epilepsies caused by variants in VGSC genes, known as sodium channel-linked DEEs, remain largely intractable disorders and new therapeutic strategies are desperately needed. In the following chapters, I discuss two neuropharmacological studies of DEEs linked to variants in genes encoding brain VGSCs and their interacting proteins. In Chapter II, I describe my research into the subtype selectivity of 4,9-anhydrotetrodotoxin, a natural product reported to selectively inhibit $Na_v1.6$, which is an abundant VGSC subtype expressed in the adult brain with a key role in epileptogenesis. In Chapter III, I present work investigating a novel inhibitory interaction between G-protein β1γ2 subunits and brain VGSC subtypes $Na_v1.1$ and $Na_v1.6$, and how these novel interactions may be involved in the pathophysiology of *GNB1*-encephalopathy. Together this work advances our understanding of subtype selective VGSC pharmacology and basic mechanisms of neuromodulation in both normal and pathological physiology, especially with respect to sodium channel linked-DEEs.

Chapter II. *In Vitro* Validation of 4,9-anhydrotetrodotoxin as a $Na_v1.6$ Selective Inhibitor for the Treatment of Sodium Channel-linked Developmental and Epileptic Encephalopathy

*Portions of this chapter have been published in *Neuroscience Letters* (Denomme, Lukowski, Hull, Jameson, Bouza, Narayan and Isom 2020) Nicholas Denomme performed and analyzed all experiments with the following exceptions: Dr. April Lukowski performed and analyzed mass spectrometry data shown in Figure 2.8 and Figure 2.9

Introduction

To date, ten major human VGSC α-subunit subtypes ($Na_v1.1$-1.9 plus Na_x), encoded by the *SCN*(*X*)*A* genes have been identified (Goldin 2001). Toxins have long served as pharmacological probes, playing an instrumental role in elucidating the structure and function of VGSCs (Cestele and Catterall 2000). Among the most widely used is tetrodotoxin (TTX), a potent guanidinium neurotoxin found in many species of aquatic and terrestrial organisms (Noguchi and Arakawa 2008). TTX binds with high affinity to $Na_v1.1$, $Na_v1.2$, $Na_v1.3$, $Na_v1.4$, $Na_v1.6$, and $Na_v1.7$. These channels are deemed “TTX sensitive” due to their susceptibility to half-maximal conduction blockade at nanomolar concentrations of TTX. To further understand the unique role each VGSC plays in

normal and pathophysiological function in neural networks, compounds with high affinity for a specific VGSC subtype are required (Kwong and Carr 2015). A natural derivative of TTX, 4,9-anhydro-TTX (4,9-ah-TTX) has been reported to be more selective in blocking Na^+ current (I_{Na}) mediated by $Na_v1.6$ (IC_{50} = 7.8 nM) than the other TTX sensitive VGSCs, including $Na_v1.2$ (IC_{50} = 1260 nM), $Na_v1.3$ (IC_{50} = 341 nM), $Na_v1.4$ (IC_{50} = 988 nM), and $Na_v1.7$ (IC_{50} = 1270 nM) (Rosker et al. 2007). While *SCN1A*, encoding $Na_v1.1$, has been implicated in neurological diseases (Nolan and Fink 2018), the effect of 4,9-ah-TTX on $Na_v1.1$-mediated I_{Na} has not been tested. Despite this, numerous studies have utilized 4,9-ah-TTX as a $Na_v1.6$ selective inhibitor following the initial report of its selective properties (Teramoto 2012, Hargus et al 2013, Meredith and Rennie 2018, Rogers et al. 2016, Takahara et al. 2018). In this chapter, we determine the affinity of 4,9-ah-TTX for human and mouse brain VGSCs using radioligand competition binding. We investigate the effects of 4,9-ah-TTX on human $Na_v1.1$-, $Na_v1.3$- and $Na_v1.6$-mediated I_{Na} using the whole-cell patch clamp technique in HEK cells. Finally, we use mass spectrometry to evaluate the pH and time-dependence of 4,9-ah-TTX conversion to 4-*epi*TTX and TTX, as previous reports have indicated these factors can influence the pharmacological analysis of 4,9-ah-TTX (Teramoto and Yotsu-Yamashita 2015, Tsukamoto et al. 2017). Our work shows that, while 4,9-ah-TTX administration results in significant blockade of $Na_v1.6$-mediated I_{Na} at nanomolar concentrations, it also has significant effects on $Na_v1.1$-mediated I_{Na} at similar concentrations. Thus, 4,9-ah-TTX is not useful to resolve $Na_v1.6$-specific effects in brain networks.

Results

4,9-ah-TTX binding affinity for human and mouse brain VGSCs

The binding curve of unlabeled 4,9-ah-TTX in competition with 5 nM [^{3}H]-STX for the VGSCs present in *Scn1a*$^{+/+}$ mouse whole brain membranes is shown in Fig. 2.1A. 4,9-ah-TTX showed normal steepness (Hill slope of -1.04) and was determined to have an inhibitory dissociation constant (K_i) of 63.02 nM with 95% CI (47.42 – 84.59 nM). At 10 μM, 4,9-ah-TTX displaced > 95% of the [^{3}H]-STX present. Fig. 2.1B depicts the binding curve of 4,9-ah-TTX to *Scn1a*$^{-/-}$ mouse whole brain membranes. The K_i was determined to be 87.67 nM 95% CI (68.8 - 113.5), IC_{50} of 248.6 nM with 95% CI (186.6 – 333.4), and a Hill slope of -1.08. Fig. 2.1C shows the results of 4,9-ah-TTX binding to human cortical white matter membrane preparations. The human brain binding data resulted in a K_i of 62.27 nM with 95% CI (29.2 - 136.3), IC_{50} of 172.4 nM 95% CI (85.8 – 463.4) and a Hill slope of -1.21. No significant differences in the K_i, IC_{50} or Hill slope of 4,9-ah-TTX were detected between the *Scn1a*$^{+/+}$, *Scn1a*$^{-/-}$ mouse, or human brain membranes (one-way ANOVA p=0.05).

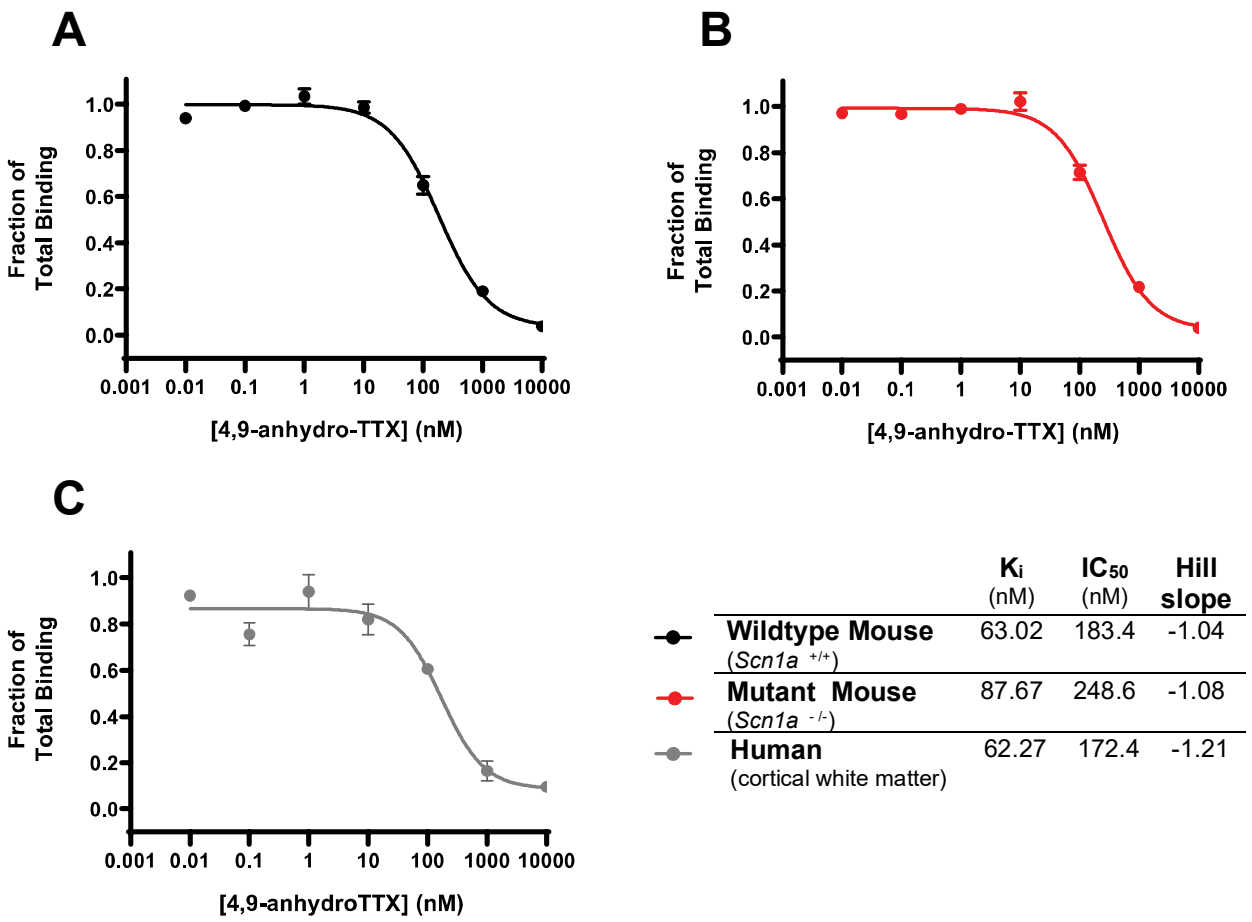


Figure 2.1. [^{3}H]-Saxitoxin competition binding with 4,9-ah-TTX. (A) Concentration response curves showing binding of 4,9-ah-TTX to human and mouse brain membrane samples in competition with 5 nM [^{3}H]-saxitoxin. Unlabeled 4,9-ah-TTX was tested at 10 µM, 1000 nM, 100 nM, 10 nM, 1 nM, 0.1 nM and 0.01 nM. (A) Binding of 4,9-ah-TTX to *Scn1a*$^{+/+}$ mouse whole brain membranes (n=4). (B) Binding of 4,9-ah-TTX to *Scn1a*$^{-/-}$ mouse whole brain membranes (n=4). (C) Binding of 4,9-ah-TTX to human cortical white matter membranes (n=2). Each data point represents the mean fraction of total specific binding ± S.E.

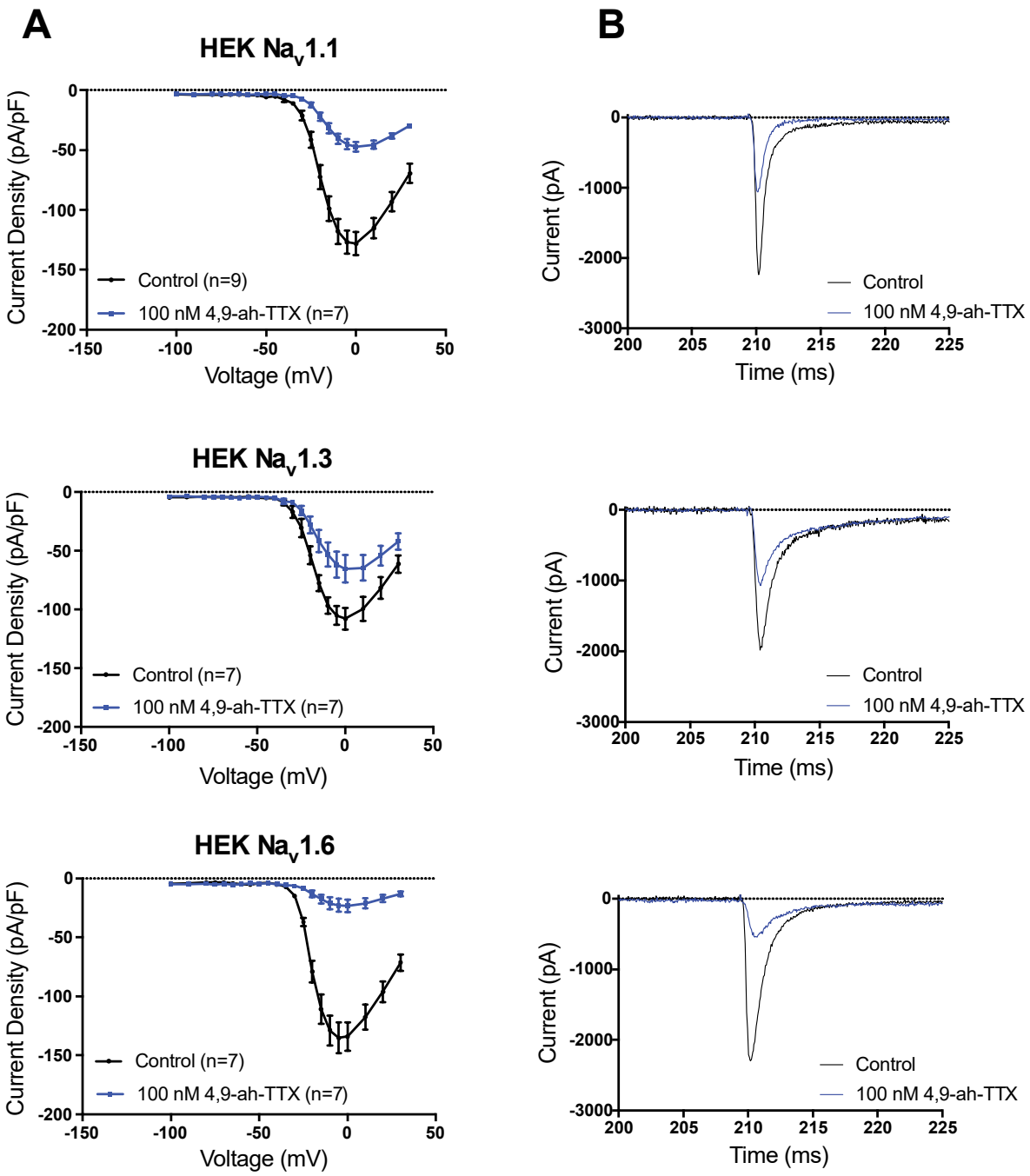


Figure 2.2 $Na_v1.1$, $Na_v1.3$ and $Na_v1.6$ I-V curves and I_{Na} traces in the presence and absence of 100 nM 4,9-ah-TTX. (A) Current-voltage (I-V) relationship obtained from recordings in the presence and absence of 100 nM 4,9-ah-TTX via whole-cell patch clamp of HEK cells stably expressing human $Na_v1.1$, $Na_v1.3$ or $Na_v1.6$. I_{Na} was evoked by stepping to different 250 ms test pulses in 5-10 mV intervals. Peak I_{Na} was normalized to cell capacitance to obtain current density. Values represent the mean ± S.E. (B) Representative peak I_{Na} traces recorded in the presence of 100 nM 4,9-ah-TTX and absence (control) via whole-cell patch clamp from HEK cells stably expressing $Na_v1.1$, $Na_v1.3$ or $Na_v1.6$. Cells were voltage-clamped at -120 mV and peak I_{Na} was elicited via stepping to a test pulse of 0 mV for 250 ms.

Effects of 100 nM 4,9-ah-TTX on I_{Na} density in human HEK-Na_v1.1, -Na_v1.3 or -Na_v1.6 cells

Fig. 2.2 shows the current-voltage (I-V) relationships for HEK-Na_v1.1, -Na_v1.3 or -Na_v1.6 cells in the presence and absence of 100 nM 4,9-ah-TTX. Differences in mean I_{Na} density evoked at 0 mV following the bathing of cells in 100 nM 4,9-ah-TTX compared to control for each cell line are shown in Table 2.1. Mean I_{Na} density in the absence of 4,9-ah-TTX (control) for HEK-Na_v1.1 was -131.6 ± 9.47, HEK-Na_v1.3 -108.7 ± 8.54 and HEK-Na_v1.6 -136.9 ± 12.72. Exposure of cells to 100 nM extracellular 4,9-ah-TTX reduced the mean peak I_{Na} density in HEK-Na_v1.1 cells by 64 ± 3% (84.31 pA/pF ± 11.39 S.E.), in HEK-Na_v1.3 cells by 39 ± 11 % (41.87 pA/pF ± 14.41 S.E.), and in HEK-Na_v1.6 cells by 83 ± 3% (113.3 ± 13.79 S.E.). The conductance-voltage (G-V) relationships for HEK-Na_v1.1, HEK-Na_v1.3 or HEK-Na_v1.6 cells in the presence and absence of 4,9-ah-TTX are shown in Fig. 2.3. The $V_{1/2}$ of activation was not significantly different in any of the cell lines tested in the presence of 100 nM extracellular 4,9-ah-TTX compared to control (Table 2.2). The slope factor (k) was not significantly different when comparing control to 100 nM 4,9-ah-TTX conditions for HEK-Na_v1.1 or HEK-Na_v1.3. In contrast, the slope factor for HEK-Na_v1.6 was significantly increased when comparing control (k = 4.857 ± 0.280) to the 100 nM 4,9-ah-TTX condition (k = 6.265 ± 0.415) (p = 0.015). The voltage dependence of availability relationship for HEK-Na_v1.1, HEK-Na_v1.3 or HEK-Na_v1.6 cells in the presence and absence of 100 nM 4,9-ah-TTX is also shown in Fig 2.3. The $V_{1/2}$ of inactivation and slope factor were not significantly

different between the control and 4,9-ah-TTX conditions for HEK-Na$_v$1.1, HEK-Na$_v$1.3 or HEK-Na$_v$1.6 (Table 2.2).

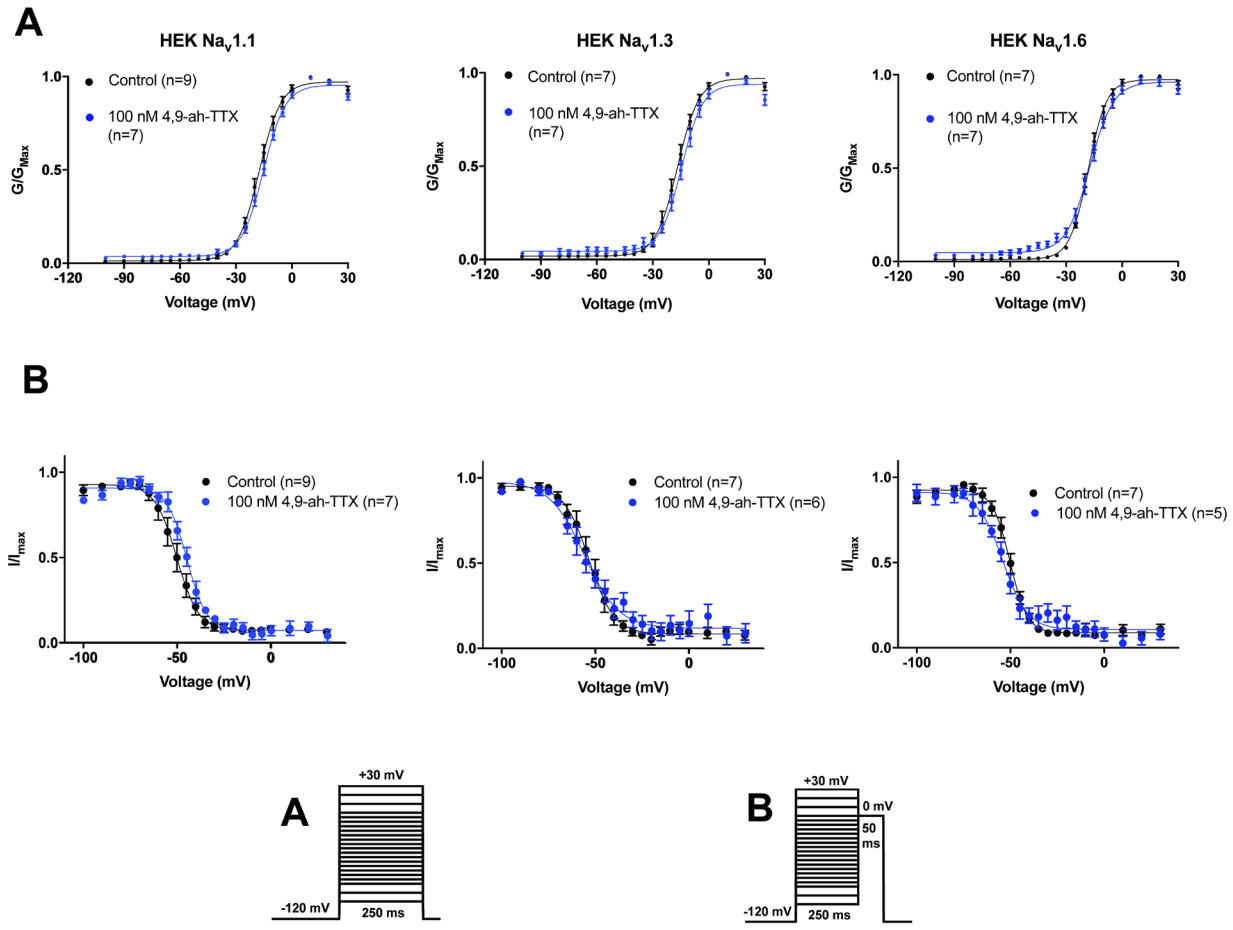


Figure 2.3 Normalized conductance to voltage and voltage dependence of availability relationships. Curves represent the voltage-dependence of steady-state activation (A) and voltage dependence of availability (B) in the presence (blue) and absence (black) of 100 nM 4,9-ah-TTX via whole-cell patch clamp from HEK cells stably expressing human Na$_v$1.1, Na$_v$1.3 or Na$_v$1.6. Corresponding voltage protocols used to elicit data analyzed in A and B are depicted at the bottom of the figure. Data points represent the mean ± S.E. Data obtained from recordings depicted in Fig. 2.2

An analysis of persistent current at a test pulse to 0 mV in the presence and absence of 100 nM 4,9-ah-TTX revealed a significant reduction (49.2%) in HEK-$Na_V1.1$ persistent I_{Na} density (Fig. 2.4). There was no significant difference in the persistent I_{Na} density observed in the control versus 100 nM 4,9-ah-TTX condition for HEK-$Na_V1.3$ or HEK-$Na_V1.6$.

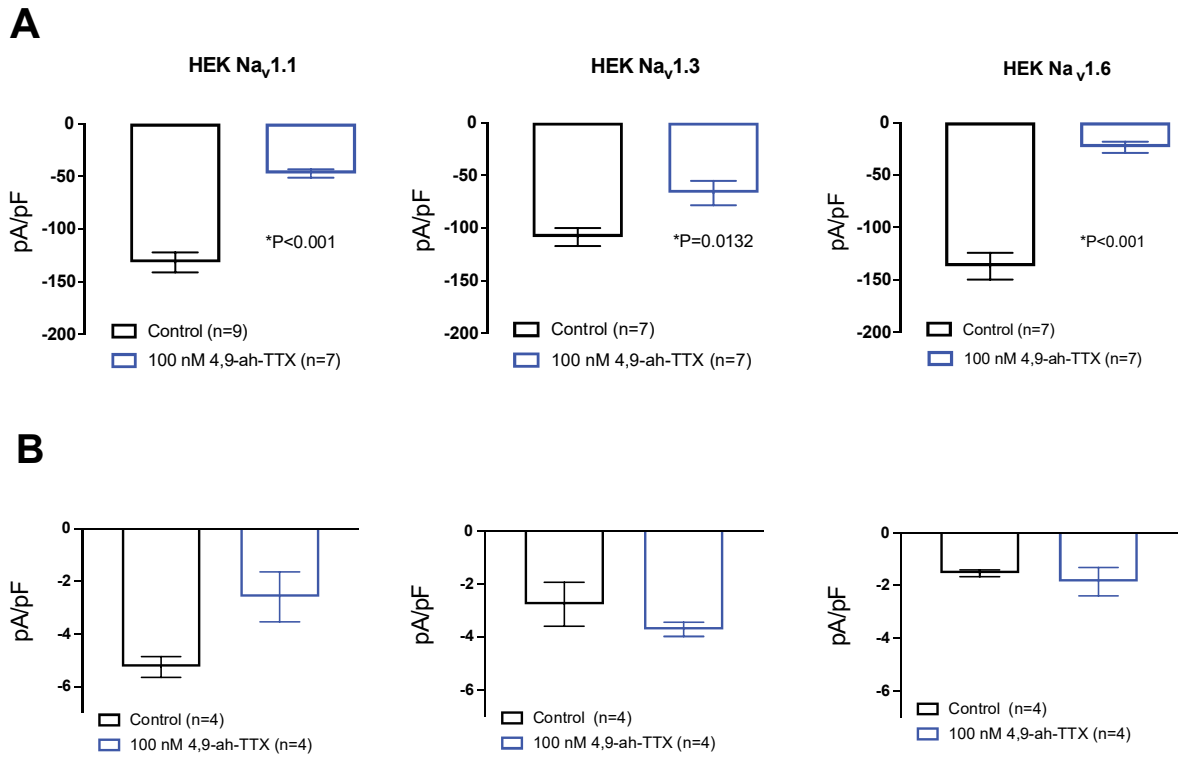


Figure 2.4 Average peak and persistent I_{Na} density recorded in the presence and absence of 100 nM 4,9-ah-TTX via whole-cell patch clamp from HEK cells stably expressing human $Na_V1.1$, $Na_V1.3$ or $Na_V1.6$. (A) Cells were voltage-clamped at -120 mV and peak I_{Na} was elicited via stepping to a test pulse of 0 mV for 250 ms. (B) Persistent I_{Na} density present in a 2 ms period 50 ms after peak I_{Na} was observed at a test pulse to 0 mV. Bar graphs represent mean ± S.E. Significant differences between control and drug treated conditions were tested using a Student's unpaired t-test. Data obtained from recordings depicted in Fig. 2.2

Reduction in $Na_v1.1$ and $Na_v1.6$ mediated peak I_{Na} following perfusion of 4,9-ah-TTX.

Perfusion of 4,9-ah-TTX onto HEK-$Na_v1.1$ and HEK-$Na_v1.6$ cells resulted in a concentration dependent reduction in peak I_{Na} (Fig. 2.5 and 2.6). $Na_v1.1$ peak I_{Na} was reduced by (11% ± 4) following the perfusion of 10 nM 4,9-ah-TTX. At 100 nM, the mean reduction in $Na_v1.1$ peak I_{Na} was (46% ± 5). The perfusion of 500 nM 4,9-ah-TTX reduced $Na_v1.1$ peak I_{Na} by (64% ± 4) (Table 3). Washout of 4,9-ah-TTX restored peak I_{Na} on average to 94.5% (range 84-106%) of baseline control in all recordings. $Na_v1.6$ peak I_{Na} was reduced by (18% ± 2) following the perfusion of 10 nM 4,9-ah-TTX. At 100 nM, the mean reduction in $Na_v1.6$ peak I_{Na} was (39% ± 2). The perfusion of 500 nM 4,9-ah-TTX reduced $Na_v1.6$ peak I_{Na} by (76% ± 2) (Table 2.3).

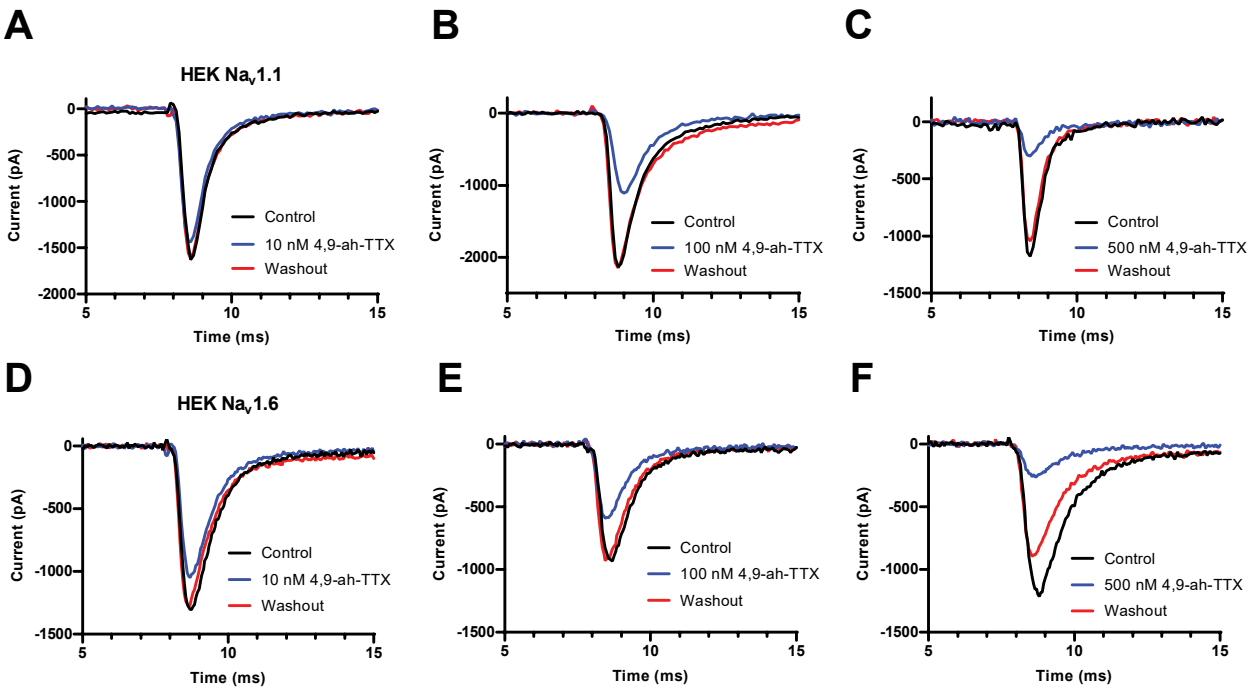


Figure 2.5 $Na_v1.1$ and $Na_v1.6$ peak I_{Na} traces before, during and after perfusion of 10, 100 and 500 nM 4,9-ah-TTX. Representative I_{Na} traces for the control (black), perfusion of 10 nM, 100 nM, and 500 nM 4,9-ah-TTX (blue) and after washout (red) via whole-cell patch clamp from HEK cells stably expressing human $Na_v1.1$ (A-C) or human $Na_v1.6$ (D-F). Cells were voltage-clamped at -120 mV and peak I_{Na} was elicited via stepping to a test pulse of 0 mV for 250 ms.

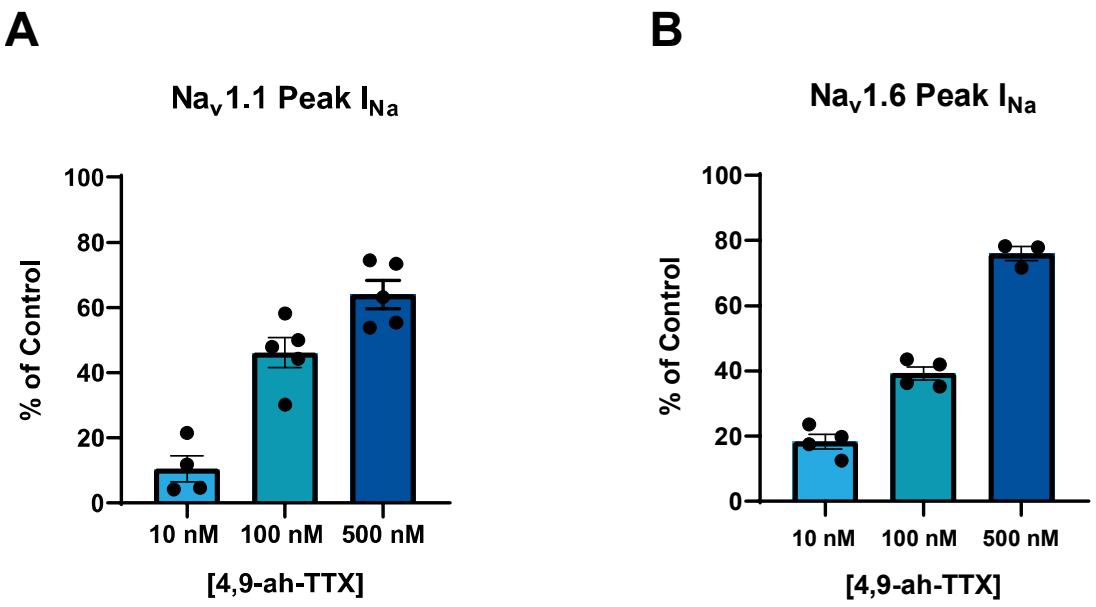


Figure 2.6 Percent reduction in Na$_v$1.1 and Na$_v$1.6 peak I$_{Na}$ by 4,9-ah-TTX. Percent reduction from control in peak I$_{Na}$ mediated by Na$_v$1.1 (A) and Na$_v$1.6 (B) following perfusion of 10 nM 4,9-ah-TTX (light blue), 100 nM 4,9-ah-TTX (cyan), and 500 nM (dark blue). Data points represent the mean ± S.E.

Time and pH dependent effects of 4,9-ah-TTX conversion to 4-epiTTX and TTX

An important consideration when testing the activity of 4,9-ah-TTX is the spontaneous equilibration that can occur between 4,9-ah-TTX, 4-epiTTX and TTX (Fig. 2.7). Relative abundances of 4,9-ah-TTX, 4-epiTTX, and TTX were monitored at different pH conditions and incubation times at ambient temperature. The results shown in Fig. 2.8 indicate that differences in pH over the range 6.4-8.4 do not significantly impact the

distribution of 4,9-ah-TTX, 4-epi-TTX, and TTX, suggesting 4,9-ah-TTX was not significantly converted to 4-epi-TTX or TTX under our analysis conditions. Assessing the relative abundances of these molecules over time similarly did not result in increased amounts of 4-epi-TTX or TTX relative to 4,9-ah-TTX; however, a significant decrease in all three molecules was observed over time, with a minute amount remaining after 5 weeks of incubation at ambient temperature, as shown in Fig. 2.9.

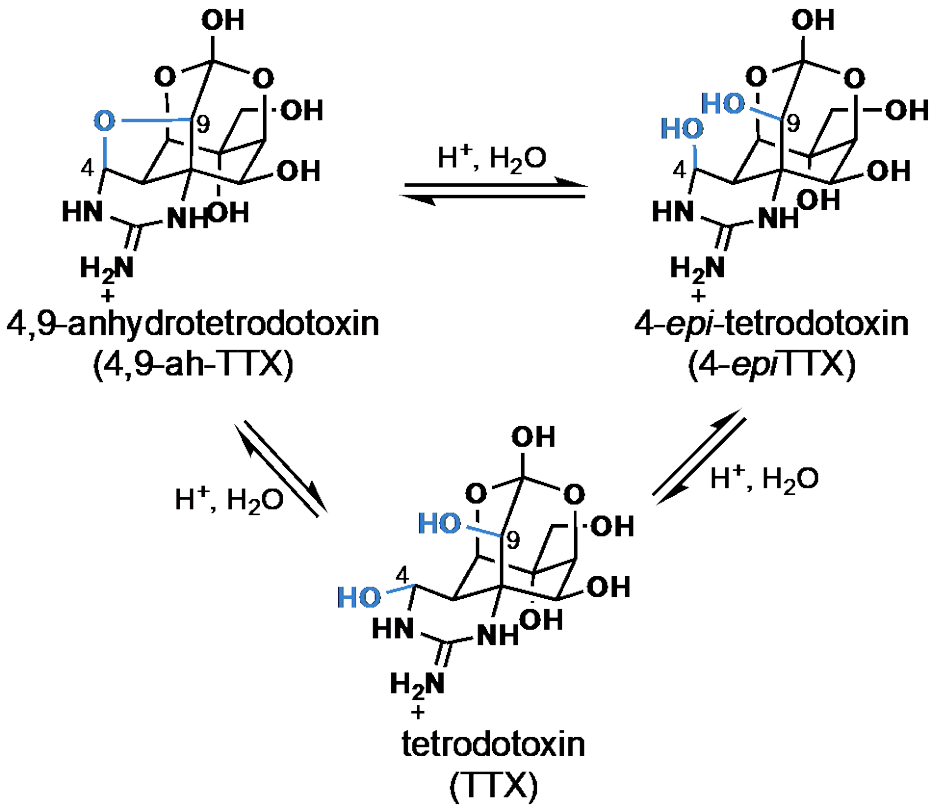
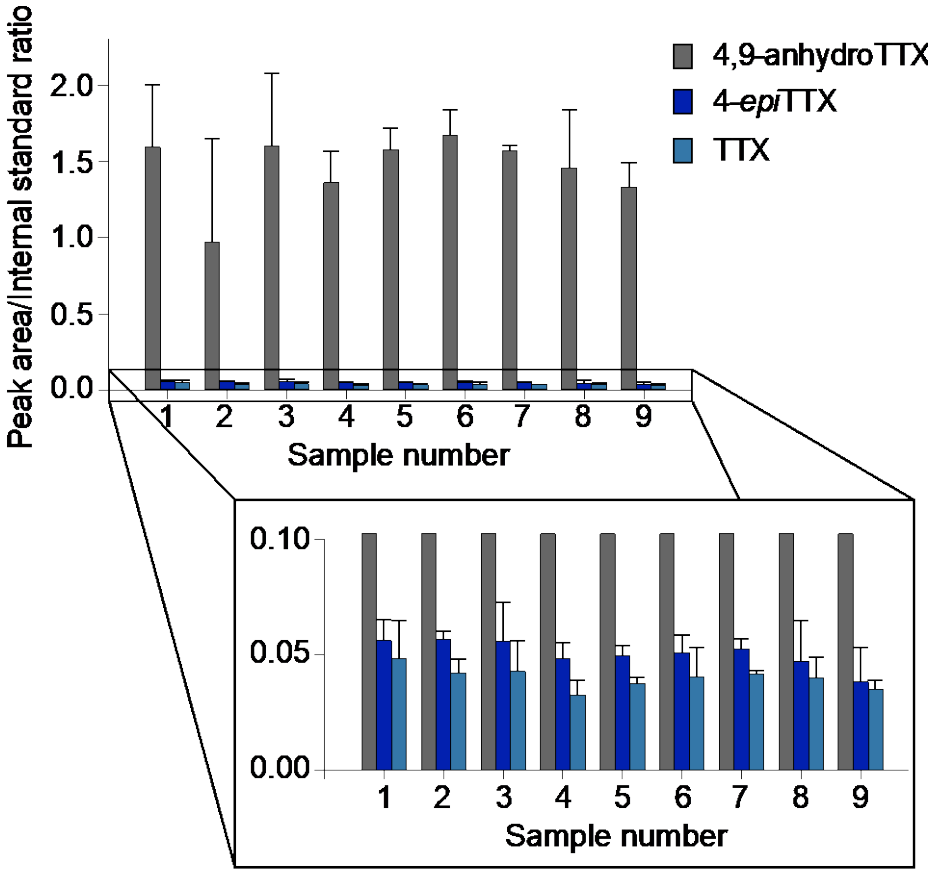


Figure 2.7 Structures and equilibrium of tetrodotoxin, 4,9-anhydrotetrodotoxin, and 4-*epi*-tetrodotoxin.



Sample	Solution	pH	Storage temp (°C)
1	1XP	7.4	–20
2	1XP	7.4	ambient
3	ER	6.4	–20
4	ER	7.0	–20
5	ER	7.35	–20
6	ER	7.35	ambient
7	ER	7.8	–20
8	ER	8.0	–20
9	ER	8.4	–20

Figure 2.8 Impact of pH on 4,9-ah-TTX, 4-epiTTX and TTX. (Top) Plot of mass spectrometry results comparing peak area/internal standard ratio based on peak integration corresponding to 4,9-ah-TTX, 4-epiTTX, and TTX. (Inset) Zoomed-in graph of represented data. (Below) Reaction conditions used in analysis. ER: external recording solution used in electrophysiology experiments. 1XP: binding buffer used in competition binding experiments.

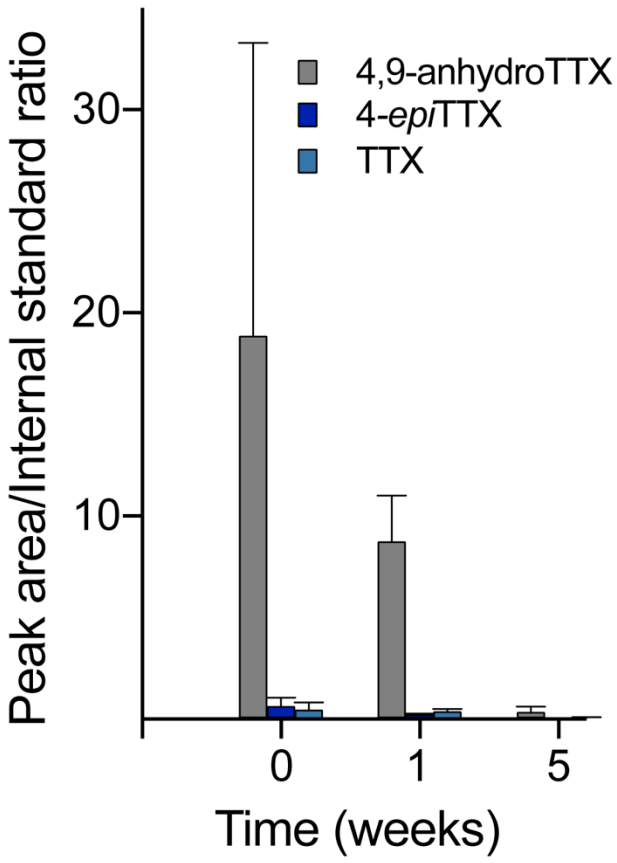


Figure 2.9 4,9-ah-TTX, 4-epiTTX and TTX in solution over time. Plot of mass spectrometry data assessing the relative abundances of 4,9-ah-TTX, 4-epi-TTX, and TTX over time comparing ratios of the analyte peak area to the peak area of the internal standard.

	Transient Na^+ Current Density (pA/pF)	
	Control	**4,9-anhydro-TTX (100 nM)**
$hNa_v1.1$	-131.6 ± 9.47	-47.24 ± 4.04
$hNa_v1.3$	-108.7 ± 8.54	-66.78 ± 11.61
$hNa_v1.6$	-136.9 ± 12.72	-23.63 ± 4.45

	Persistent Na^+ Current Density (pA/pF)	
	Control	**4,9-anhydro-TTX (100 nM)**
$hNa_v1.1$	-5.25 ± 0.39	-2.58 ± 0.94
$hNa_v1.3$	-2.77 ± 0.82	-3.71 ± 0.26
$hNa_v1.6$	-1.52 ± 0.13	-1.84 ± 0.54

Table 2.1 Average peak and persistent I_{Na} density and recorded in the presence of 100 nM 4,9-ah-TTX and absence (control) via whole-cell patch clamp from HEK cells stably expressing human $Na_v1.1$, $Na_v1.3$ or $Na_v1.6$. Values represent the mean ± S.E.

	$V_{1/2}$ of Activation (mV)			
	Control	N	4,9-anhydro-TTX (100nM)	N
hNa$_v$1.1	-17.36 ± 1.05	9	-15.31 ± 0.83	7
hNa$_v$1.3	-16.88 ± 1.58	7	-14.47 ± 1.25	7
hNa$_v$1.6	-17.97 ± 0.80	7	-17.28 ± 0.99	7

	Slope Factor (k) (mV^{-1})			
	Control	N	4,9-anhydro-TTX (100nM)	N
hNa$_v$1.1	5.501 ± 0.27	9	5.705 ± 0.14	7
hNa$_v$1.3	5.261 ± 0.24	7	5.332 ± 0.28	7
hNa$_v$1.6	4.857 ± 0.28	7	6.265 ± 0.41*	7

	$V_{1/2}$ of Inactivation (mV)			
	Control	N	4,9-anhydro-TTX (100nM)	N
hNa$_v$1.1	-50.41 ± 2.37	9	-45.14 ± 1.55	7
hNa$_v$1.3	-53.63 ± 2.21	7	-55.97 ± 1.95	6
hNa$_v$1.6	-50.73 ± 1.54	7	-55.83 ± 2.79	5

	Slope Factor (k) (mV^{-1})			
	Control	N	4,9-anhydro-TTX (100nM)	N
hNa$_v$1.1	-5.04 ± 0.22	9	-4.83 ± 0.55	7
hNa$_v$1.3	-5.85 ± 0.59	7	-9.16 ± 1.51	6
hNa$_v$1.6	-4.63 ± 0.41	7	-8.61 ± 2.17	5

Table 2.2 Voltage-dependence of activation and inactivation parameters recorded in the presence of 100 nM 4,9-ah-TTX and absence (control) via whole-cell patch clamp from HEK cells stably expressing human Na$_v$1.1, Na$_v$1.3 or Na$_v$1.6. Values represent the mean ± S.E. *p=0.0158

Reduction in Peak I_{Na} Following Perfusion of 4,9-ah-TTX				
[4,9-ah-TTX]	(% of Control)			
	Na_v 1.1	N	Na_v 1.6	N
10 nM	11% (± 4)	4	18% (± 2)	4
100 nM	46% (± 5)	5	39% (± 2)	4
500 nM	64% (± 4)	5	76% (± 2)	3

Table 2.3 Percent reduction in Na_v1.1 and Na_v1.6 peak I_{Na} from control following the perfusion of 10, 100 or 500 nM 4,9-ah-TTX. Values represent the mean ± S.E.

Discussion

TTX binds with high specificity to the VGSC pore in a 1:1 stoichiometry to occlude the conduction of Na^+ ions by forming a web of electrostatic interactions with the channel. A large body of evidence from numerous studies strongly supports that TTX interacts with a narrow region of residues within the channel involved in permeation and the selectivity of Na^+ ions (Fozzard and Lipkind 2010). Major coordinating residues are located on the membrane re-entrant P-loops (pore loops) of segments S5-S6 on all 4 domains. This region of the channel heavily influences channel conductance and ion selectivity, forming an inner and outer ring of charged amino acid residues (six carboxylates and one lysine) known as the selectivity filter (Chiamvimonvat et al. 1996, Farve et al. 1996). The asymmetric charge distribution of each ring coordinates solvated Na^+ ions as they pass through the pore (Catterall 2012). Mutagenesis and electrophysiological studies have revealed four key residues (D: aspartate, E: glutamate, K: lysine, and A: alanine), each present in one of the domains, that form the inner ring of the mammalian VGSC selectivity filter. The DEKA motif found in human VGSCs is conserved across all subtypes. Mutating K and A of the DEKA motif to glutamates, generating DEEE, abolishes Na^+ selectivity and permits Ca^{2+} to permeate the channel (Heinemann et al. 1992a). Three or four residues downstream of the DEKA selectivity filter in each domain lie the outer ring of the human VGSC selectivity filter composed of an EE(M/D)D motif (see Fig. 2.10).

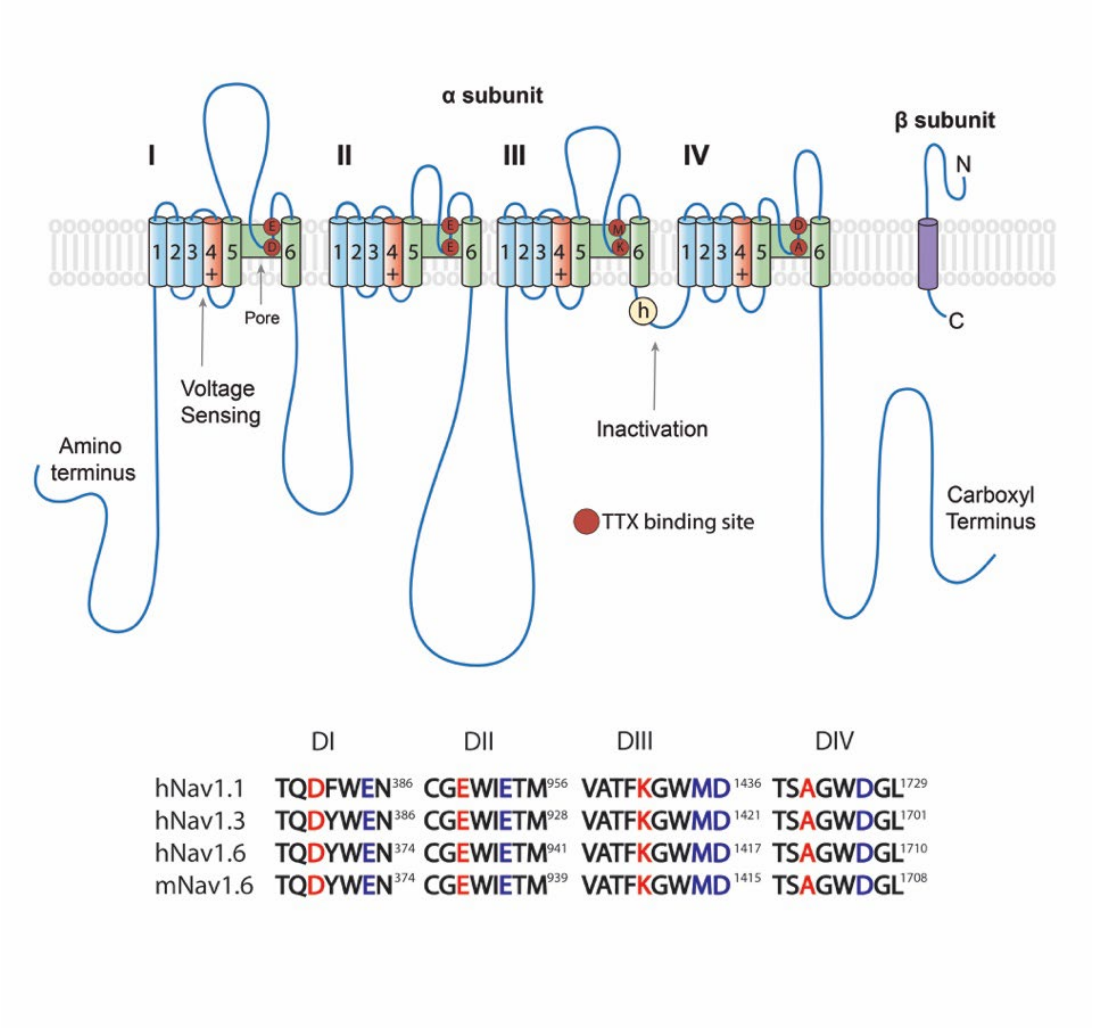


Figure 2.10. **VGSC schematic with TTX binding site and selectivity filter residue alignment.** (Top) Schematic of the mammalian voltage-gated sodium channel α and β subunit complex. Segments are labelled numerically (1-6) and domains are labeled in roman numerals (I-IV). Voltage-sensing S4 segments in each domain are labelled in light red. The pore loop regions formed by segments S5 and S6 are labelled in green. The amino acid residues representing the Na^+ ion selectivity filter and canonical TTX binding site are depicted in dark red circles. (Below) Amino acid residues of the selectivity filter in human $Na_v1.1$, $Na_v1.3$, $Na_v1.6$ or mouse $Na_v1.6$. The selectivity filter is -2 through +4 residues from the DEKA locus. The inner DEKA ring residues of each domain are shown in red. The outer EE(M/D)D ring residues of each domain are shown in blue. The following accession numbers were used to generate the basic local alignment (hNav1.1: NP_001159435.1; $hNa_v1.3$: NP_008853.3; $hNa_v1.6$: NP_055006.1; $mNa_v1.6$ NP_001070967.1)

The outer EE(M/D)D ring is comprised of four negatively charged carboxylates shown to attract Na^+ ions into the outer vestibule of the pore (Khan et al. 2002). Neutralizing mutations in the inner or outer ring of the selectivity filter, and any residues linking the two regions, can dramatically reduce TTX binding (Noda et al. 1989, Penzotti et al. 1998, Terlau et al. 1991, Fozzard and Lipkind 2010).

Another key residue in TTX binding is Y401 ($Na_v1.4$ numbering). TTX-sensitive channels have an aromatic Y/F (tyrosine or phenylalanine) at this position that is crucial for coordinating TTX in the pore (Heinemann et al. 1992b). $Na_v1.5$, $Na_v1.8$, and $Na_v1.9$ achieve “TTX-resistance” through replacement of the Y/F residue with a nonaromatic cystine (C) or serine (S) (Satin et al. 1992). Intriguingly, all the TTX-resistant VGSC subtypes are located on human chromosome 3. Adaptive resistance strategies in TTX-sensitive channels have been observed in many TTX-producing predators and their prey (Soong et al. 2006). Various species of pufferfish also possess nonaromatic substitutions for the Y/F residue present in domain I, dramatically reducing their sensitivity to TTX. Many species of newts and snakes have evolved TTX resistant $Na_v1.4$ channels via substitutions in the pore loops of domain III and IV (Toledo et al. 2016). Amino acid substitutions of the inner and outer selectivity filter ring of domain III and IV have been identified (Geffeney et al. 2002, Geffeney et al. 2005). A threonine (T) substitution of the methionine (M) in the domain III outer selectivity filter ring on $Na_v1.4$ is observed in all TTX-harboring newts and the *Thamnophis couchii* garter snake (Hanifin and Gilly 2015).

Recent high-resolution structural evidence has confirmed that TTX restricts Na^+ conduction via binding to the vestibule of the VGSC selectivity filter (Shen et al. 2018, Shen et al. 2019). Cryogenic electron microscopy studies showing TTX bound to the American cockroach sodium channel Na_vPaS reveal hydrogen bonds and salt bridges formed between the polar groups on the TTX molecule and acidic residues in the pore loop P2 helix segment of domains I, II and IV (Shen et al. 2018). The DE of the inner DEKA selectivity filter also directly binds to TTX in the Na_vPaS channel (Shen et al. 2018). In a subsequent study, the authors obtained high-resolution structural data of TTX bound to $hNa_v1.7$ (Shen et al. 2019). Inner and outer selectivity filter residues identified by previous studies were implicated in the coordination of TTX within the pore. The coordination of TTX in $hNa_v1.7$ was nearly identical to that observed in Na_vPaS, differing only in the P2 segment of domain III (Shen et al. 2019). $Na_v1.7$ contains an isoleucine in place of an aspartate that is present in the other 8 human VGSC subtypes. This outer ring aspartate likely contributes to TTX binding in $hNa_v1.1$. Aside from that difference, similar TTX coordination strategies observed by Shen et al. would be anticipated in $hNa_v1.1$, $hNa_v1.3$ and $hNa_v1.6$ (Shen et al. 2019).

It is not known which amino acid residues of VGSCs form the binding site for 4,9-ah-TTX, although it is postulated that 4,9-ah-TTX interacts with the same residues as TTX (Teramoto and Yotsu-Yamashita 2015). Xu et al. explored the differences in binding of TTX and 4,9-ah-TTX to human $Na_v1.2$ using computational modeling and molecular dynamics. The authors proposed that the H-bond interactions made between the C4 and C9 hydroxyl of TTX and the outer ring carboxylates of the human $Na_v1.2$ selectivity

filter are key factors in the greater inhibitory activity of TTX relative to 4,9-ah-TTX (Xu et al. 2018). It is important to distinguish the species used in an experimental sodium channel preparation when comparing results across studies. The original study reporting 4,9-ah-TTX to be selective for $Na_v1.6$, utilized the expression of mouse cDNA in *Xenopus* oocytes (Rosker et al. 2007). Amino acid sequence alignments shown in Fig. 10 reveal no differences when comparing the selectivity filter regions of human $Na_v1.1$, $Na_v1.3$, and $Na_v1.6$ to mouse $Na_v1.6$. Despite the high homology seen in human and rodent VGSCs, it is possible that alternative 4,9-ah-TTX binding conformations are achieved in mouse, rat, and human VGSCs, leading to different results observed across studies. To detect possible species-selective differences in 4,9-ah-TTX for mouse and human brain VGSCs, we conducted [^{3}H]-STX binding with cortical white matter membranes from neurologically normal humans (Fig. 2.1C). The lack of significant differences found in affinity and potency suggest there is no differential sensitivity of 4,9-ah-TTX for human or mouse VGSCs. Further structural studies analyzing the precise amino acid residues of each human TTX-sensitive VGSCs responsible for the coordination of 4,9-ah-TTX are required to understand potential subtype specific binding contributions.

Previous studies conducted on 4,9-ah-TTX, performed in markedly different experimental systems, have yielded variable results. Recording I_{Na} using voltage-clamp in the squid giant axon, Kao and Yasumoto reported 4,9-ah-TTX to have an IC_{50} of 298 nM (Kao and Yasumoto 1985). These experiments were performed at 7 °C with an external solution pH of 7.8. The authors noted the importance of this external pH, as the

C-10 hydroxyl of 4,9-ah-TTX has a reported pK_a of 7.95 (Goto et al. 1965). Using [^{3}H]-STX binding in rat brain synaptosomes, Yotsu-Yamashita et al. reported an equilibrium dissociation constant for 4,9-ah-TTX of 180 ± 11 nM (Yotsu-Yamashita et al. 1999). Using the two-electrode voltage clamp technique in *Xenopus* oocytes, Rosker et al. reported that 4,9-ah-TTX selectively inhibits $Na_v1.6$ with an IC_{50} of 7.8 ± 2.3 nM (Rosker et al. 2007). Teramoto et al. reported that resurgent-like I_{Na} present in isolated mouse vas deferens myocytes is abolished in the presence of 3 μM 4,9-ah-TTX (Teramoto et al. 2012). Further investigation showed that native I_{Na} in mouse vas deferens myocytes was sensitive to 4,9-ah-TTX, with a K_i of 512 nM (Takahara et al. 2018). The authors then compared this to the effects of 4,9-ah-TTX in HEK cells transiently transfected with mouse $Na_v1.6$ cDNA. In this system, the authors reported 4,9-ah-TTX to have a K_i of 112 nM for $Na_v1.6$-mediated I_{Na} and a K_i of 92 nM when $Na_v1.6$ was co-expressed with β1 subunits. Measuring I_{Na} using an automated patch clamp system in CHO and HEK cells, Rogers et al. reported an IC_{50} for 4,9-ah-TTX of 32.9 nM for $Na_v1.6$- and 1.6 μM for $Na_v1.7$-mediated I_{Na}. (Rogers et al. 2016).

4,9-ah-TTX was determined to have an inhibitory dissociation constant (K_i) of 62.03 nM for *Scn1a*$^{+/+}$ mouse brain membrane preparations in our [^{3}H]-STX binding assay, consistent with its reduced affinity for brain VGSCs compared to TTX. In *Scn1a*$^{-/-}$ mice, global expression of $Na_v1.1$ is deleted (Mistry et al. 2014). 4,9-ah-TTX shows a reduced affinity for *Scn1a*$^{-/-}$ mouse brain compared to *Scn1a*$^{+/+}$ (K_i of 87.67 nM vs. 63.02 nM), however, this difference is not statistically significant and therefore no conclusion based on these data regarding the contribution of $Na_v1.1$ to the binding activity of 4,9-ah-TTX

in mouse whole brain can be made. A heterogenous mixture of $Na_v1.1$, $Na_v1.2$, $Na_v1.5$, $Na_v1.6$, and $Na_v1.7$ are known to be present in the adult mouse whole-brain membrane preparations utilized to test 4,9-ah-TTX (Wu et al. 2002, Cheah et al. 2013, Ogiwara et al. 2018, Katz et al. 2018, Kanellopolous et al. 2018).

We showed that bathing cells in 100 nM 4,9-ah-TTX significantly reduced I_{Na} density in HEK-$Na_v1.1$ (64 ± 3%), HEK-$Na_v1.3$ (39 ± 11 %), and HEK-$Na_v1.6$ cells (83 ± 3%) compared to control. No significant changes in the $V_{1/2}$ of activation were observed when comparing control to the presence of 100 nM 4,9-ah-TTX, consistent with 4,9-ah-TTX exerting its inhibitory effects through pore-blocking action, like TTX. To confirm the observed effect was both acute and reversible, as is the case with TTX, we recorded peak I_{Na} mediated by $Na_v1.1$ and $Na_v1.6$ before, during perfusion, and after washout of 4,9-ah-TTX (Fig. 2.5). Consistent with the results we observed from the bath exposure to 4,9-ah-TTX, the perfusion of 500 nM 4,9-ah-TTX reduced $Na_v1.1$-mediated peak I_{Na} by 64% from baseline, 100 nM 4,9-ah-TTX induced a 46% reduction from baseline, and 10 nM reduced $Na_v1.1$-mediated peak I_{Na} by 11% from baseline (Table 2.3). 4,9-ah-TTX reduced $Na_v1.6$ peak I_{Na} by (76%), (39%), and (18%) at 500 nM, 100 nM and 10 nM concentrations respectively (Table 2.3). Together, these data suggest 4,9-ah-TTX has comparable inhibitory activity for human $Na_v1.1$ and $Na_v1.6$ at nanomolar concentrations.

Tetrodotoxin has long been considered a voltage and state-independent blocker, inhibiting sodium current without altering the voltage-dependence of activation or

inactivation, regardless of the original state of the channel (Catterall 1980). Reports of TTX causing a modest hyperpolarizing shift in the voltage-dependence of inactivation do exist (Heggeness and Starkus 1986). 4,9-ah-TTX was reported to induce a hyperpolarizing shift in the voltage-dependence of inactivation of $Na_v1.6$ (Rosker et al. 2007). We did not detect any shifts from baseline in the voltage-dependence of inactivation for $Na_v1.1$, $Na_v1.3$ or $Na_v1.6$ in the presence of 100 nM 4,9-ah-TTX (Table 2). Possible state-dependent effects of 4,9-ah-TTX on $Na_v1.1$ were not directly examined. Neurons expressing $Na_v1.1$ *in vivo* would rest at a more depolarized resting membrane potential (~ -65 mV) than the holding potential used in our experiments (-120 mV). Further studies examining the inhibitory activity of 4,9-ah-TTX on $hNa_v1.1$ at holding potentials from -55 to -70 mV would provide a more physiologically relevant interpretation of our findings.

Spontaneous equilibration between 4,9-ah-TTX, 4-*epi*TTX and TTX could confound pharmacology experiments with 4,9-ah-TTX (Mosher 1986). Tsukamoto et al. tested 4,9-ah-TTX on human $Na_v1.6$ mediated I_{Na} in HEK cells and reported an IC_{50} value of 294 ± 25 nM from a freshly prepared working solution. However, using a solution prepared from a stock solution that had been placed in storage for 6 months, the authors found a much greater reduction in I_{Na} following the application of 100 nM 4,9-ah-TTX, presumably due to the conversion of 4,9-ah-TTX to TTX (Tsukamoto et al. 2017). We performed analytical authentication of 4,9-ah-TTX prior to using it in our experiments to determine the level of contamination present and to validate the presence of 4,9-ah-TTX over a pH range from 6.4 to 8.4, including the pH of our

external recording solution (pH = 7.35). The relative amounts of 4,9-ah-TTX compared to 4-*epi*TTX and TTX were assessed in the extracellular recording solution using mass spectrometry. In contrast to previous findings, in our hands we found little to no evidence of 4,9-ah-TTX conversion to 4-epiTTX or TTX under the different conditions. We also assessed the relative abundances of these molecules over time at pH 7.4 and did not observe interconversion. We did find that incubating 4,9-ah-TTX at ambient temperature over the course of 5 weeks resulted in a significant decrease in the total amount of 4,9-ah-TTX without corresponding increases in 4-epiTTX or TTX, suggesting that 4,9-ah-TTX is not stable under these conditions for extended periods of time. However, the 4,9-ah-TTX used in our experiments had negligible levels of contamination from 4-epiTTX and TTX under multiple conditions.

As discussed in Chapter I, identifying a $Na_v1.6$ selective inhibitor is of great interest to VGSC biology and the development of novel therapeutics for sodium channel-linked DEEs. $Na_v1.6$ is widely expressed in the mammalian peripheral and central nervous systems as well as in the heart, although at lower levels (Schaller et al. 1995, Frasier et al. 2016). In the adult brain, $Na_v1.6$ is the most abundantly expressed VGSC subtype (Goldin 2001). Within neurons, $Na_v1.6$ is highly concentrated at the distal axon initial segment of excitatory and inhibitory neurons and nodes of Ranvier in myelinated axons (Hu et al. 2009, Lorincz and Nusser 2010). A compound with the selective properties previously reported for 4,9-ah-TTX holds great value. However, caution should be exercised when using this reagent. Our findings demonstrate that, in addition to blocking $Na_v1.6$-mediated I_{Na}, 4,9-ah-TTX has significant inhibitory effects on $Na_v1.1$-

mediated I_{Na} in the nanomolar range and thus cannot be used as a selective $Na_v1.6$ inhibitor in human cells or tissues where $Na_v1.1$ is also expressed. Despite our findings showing a lack of selectivity of 4,9-ah-TTX, the development of a $Na_v1.6$ selective inhibitor for sodium channel-linked DEE remains promising.

Methods

Cell lines

Human Embryonic Kidney (HEK) 293T cells stably expressing human VGSC α subunits $Na_v1.1$ (GenBank accession number NP_001159435.), $Na_v1.3$ (GenBank accession number NP_008853.3) or $Na_v1.6$ (GenBank accession number NP_055006.1) cDNAs were cultured in Dulbecco's Modified Eagle Medium containing (4.5 g/L D-glucose, L-glutamine, 110 mg/L sodium pyruvate, 400 μg/mL G418, 100 U/mL penicillin/streptomycin). All cells were maintained in an incubator at 37 °C with 5% CO_2 until the time of recording.

Mouse models

Mouse studies were performed in compliance with protocols approved by the University of Michigan IACUC and were in accordance with the policies of the NIH Guide for the Care and Use of Laboratory Animals. *Scn1a*^{tm1Kea} mice were a generous gift from the laboratory of Dr. Jennifer Kearney at Northwestern University (Mistry et al. 2014). The *Scn1a*^{tm1Kea} colony was maintained by breeding heterozygous (129S6.*Scn1a*$^{+/-}$) animals to 129S6/SvEvTac mice (Taconic #129SVE). For all experiments, 129S6.*Scn1a*$^{+/-}$ mice were crossed to generate -/-, +/-, and +/+ offspring. Genotyping of F1 pups was

performed by PCR amplification of mouse genomic DNA. Primers used in genotyping were: 5'-AGTCTGTACCAGGCAGAACTTG-3'; 5'-CTGTTTGCTCCATCTTGTCATC-3' and 5'-GCTTTTGAAGCGTGCAGAATGC-3'. The PCR products are 1 kb for the *Scn1a* WT allele and 650 bp for the transgenic allele. All mice were maintained on a 12:12 hour light:dark cycle and had *ad libitum* access to food and water throughout the experiments. Male and female mice were used in all experiments.

Human brain samples

De-identified, frozen, human cortical white matter samples from neurologically normal patients were obtained from the Human Brain and Spinal Fluid Resource Center in Los Angeles, CA under IRB approval (HUM00012142).

[^{3}H]-Saxitoxin Competition Binding

To measure the competitive binding of 4,9-ah-TTX to VGSCs, whole brain membranes were prepared from postnatal day (P) 10-17 mice or from frozen human brain samples as described previously (Isom et al. 1995). Equilibrium [^{3}H]-saxitoxin (STX) binding in the presence of 4,9-ah-TTX was measured at 4 °C following an incubation period of one hour using a vacuum filtration assay with a saturating concentration (5 nM) of C-11 labeled [^{3}H]-STX (20 Ci/mmol, American Radiolabeled Chemicals Inc.). In a subset of samples, 10 μM unlabeled TTX (Alomone Labs) was added to assess nonspecific binding. To quantify [^{3}H]-STX binding, counts per minute (CPM) values obtained from liquid scintillation counting (Packard Tri-carb 1900TR) were corrected for specific binding by subtraction of nonspecific (10 μM TTX) values and then converted to decays

per minute (DPM) before normalization to total protein concentration using the bicinchoninic acid (BCA) protein assay (Thermo-Fisher). A stock of 4,9-ah-TTX was diluted in 1XP binding buffer (50 nM HEPES pH 7.4, 130 mM choline chloride, 5.4 mM KCl, 80 µM MgSO4, 0.1% dextrose) to give a final concentration of 10000, 1000, 100, 10, 1, 0.1 or 0.01 nM. A 7-point concentration-response curve was generated for 4,9-ah-TTX in competition with 5 nM [^{3}H]-STX. Four independent experiments were conducted, and in each experiment, each sample was tested in duplicate. The average DPM reading of duplicate values was used for analysis. Competitive binding data were analyzed using Microsoft Excel and Graph Pad Prism v8.2 (San Diego, CA). The specific binding curve in [^{3}H]-STX (fmol)/protein (mg) was initially generated using the following one-site IC_{50} equation:

$$Y = \frac{\text{Bottom} + (\text{Top} - \text{Bottom})}{1+10^{x-log(IC_{50})}}$$

where Top and Bottom are plateaus in the units of the Y-axis. IC_{50} represents the concentration in nanomolar of unlabeled competitor that results in binding half-way between Top and Bottom values. Data were then normalized for each concentration point to the Top value obtained in the assay for each unlabeled toxin to obtain fraction of total binding. Each Y value thus represents the fraction of maximal [^{3}H]-STX displacement at the corresponding concentration (X value). To obtain K_i values from the IC_{50}, the following equation was used:

$$K_i = \frac{IC_{50}}{1 + \frac{[radioligand]}{K_d}}$$

where [^{3}H-STX] = 5 nM in each assay at equilibrium. K_d of [^{3}H]-STX = 2.5 nM. K_i = equilibrium dissociation constant of the unlabeled competitor in nM.

Whole-cell patch-clamp electrophysiology

I_{Na} was measured at room temperature using the whole-cell patch clamp technique using previously described electrophysiological methods (Chen et al. 2012). Cells were plated on 35x10 mm treated polystyrene culture dishes (Thermo-Fisher) and used for electrophysiological recordings within 1-3 days after plating. Cells were identified using an Eclipse TE300 upright microscope (Nikon). Micropipettes were obtained from 1.5 mm outer diameter capillary glass tubing (Warner Instruments) using a P-97 horizontal puller (Sutter Instrument Co.). Micropipettes were then polished using a MF-830 micro forge (Narishige) to obtain a resistance between 2.0 to 5.0 MΩ. The intracellular solution contained the following (in mM): 115 CsCl, 5 EGTA, 0.4 GTP, 2 MgATP, 0.5 $CaCl_2$, 10 HEPES, 5 Na^+ phosphocreatine, 20 tetraethylammonium chloride, pH 7.2 with CsOH. Extracellular solution contained the following (in mM): 120 NaCl, 1 $BaCl_2$, 2 $MgCl_2$, 0.2 $CdCl_2$, 1 $CaCl_2$, 20 sucrose, 10 glucose, 10 HEPES, 20 tetraethylammonium chloride, pH 7.35 with NaOH. Signals were amplified using a Multiclamp 700B amplifier (Molecular Devices). Data were acquired with a Digidata 1440A interface (Molecular Devices) and analyzed using pClamp10 offline. Pipette and whole-cell capacitance were compensated at 70%. Signals were low pass-filtered at 5 kHz, and data were sampled

at 40 kHz. For the data generated in Fig. 2, 3, 4, and Tables 1 and 2, 4,9-ah-TTX (Cayman Chemical) was evenly dissolved into the static extracellular bath solution at a concentration of 100 nM prior to recording. Cells were bathed in 4,9-ah-TTX for at least 10 minutes prior to recording. Peak I_{Na} was normalized to cell capacitance to obtain current density, used to plot I–V curves and calculate conductance with the following equation:

$$g = \frac{I}{V - V_{rev}}$$

where g is conductance, I is current, V is the test potential, and V_{rev} is the measured reversal potential. Peak currents were normalized to the maximum peak I_{Na} amplitude. The $V_{1/2}$ of activation represents the voltage of the membrane at which half-maximal conductance occurred. To determine the I_{Na} amplitude and the voltage dependence of activation, Na^+ currents were evoked by 250 ms depolarizing test pulses (from -100 to +30 mV at 5 and 10 mV intervals) from a holding potential of -120 mV. Voltage-dependence of inactivation was determined by applying a 50 ms test pulse to 0 mV after 250 ms prepulses to the same voltages as described for the voltage dependence of activation. Normalized activation and inactivation curves were fit with a Boltzmann equation:

$$\frac{1}{1 + e^{\frac{V - V_{1/2}}{k}}}$$

where $V_{1/2}$ is the membrane potential in the midpoint of the curve, and k is the slope factor. Persistent sodium current was analyzed as the average current in a 2 ms period

exactly 50 ms after the peak current was observed at a depolarizing step from -120 to 0 mV. Persistent current values were normalized to cell capacitance to obtain current density. The mean of all values obtained in the absence of 4,9-ah-TTX (control) were compared to the mean of all values obtained in the presence of 100 nM 4,9-ah-TTX. For data generated in Fig. 5, 6, and Table 3, cells were plated on coverslips (Thermo-Fisher) and extracellular solution containing 4,9-ah-TTX was perfused into the RC-26 recording chamber (Warner Instruments) by a gravity-driven perfusion system with a flow rate of 2-3 mL/min. Peak I_{Na} was evoked via a 250 ms depolarizing pulse to 0 mV from a holding potential of -120 mV. Baseline recordings were established, followed by a 3 min perfusion of 4,9-anhydro-TTX at the indicated concentrations. Extracellular recording solution was then perfused on for $\geq$ 3 minutes and a washout recording obtained. The effect of 4,9-ah-TTX was evaluated as a decrease in peak I_{Na} compared to baseline control of that cell. Series resistance was monitored throughout perfusion recordings. If access resistance changed $\geq$ 20% at any time, the recording was not included in the analysis. Signals were low pass-filtered at 10 kHz, and data were sampled at 20 kHz. Capacitive transients and leak conductance were subtracted using a P/4 protocol.

Mass Spectrometry

A 500 µM stock solution of 4,9-ah-TTX (Cayman Chemical) was prepared in 1XP binding buffer. Duplicate 10 µL samples containing 100 µM 4,9-ah-TTX were prepared in plastic 1.7 mL centrifuge tubes according to the conditions outlined in Fig. 9 varying buffer solution (1XP or external recording solution), pH (range 6.4 – 8.4), incubation

time, and storage temperature. Samples were diluted with 30 µL acetonitrile, vortexed to mix, and centrifuged at 12,000 x *g* for 20 min. 10 µL each sample was further diluted with 80 µL acetonitrile and 10 µL 0.1% formic acid in MilliQ water with 2.5 µg/mL ^{15}N-arginine as an internal standard (Cambridge Isotopes). Samples 2 and 6, indicated as being incubated for 60 min, were incubated at room temperature for 1 h prior to the first acetonitrile dilution. For assessment of time dependence, triplicate samples of 10 µL volume were prepared with 1XP buffer at pH 7.4 and incubated at ambient temperature (22 °C) for 0, 1, and 5 weeks. Samples were quenched by the addition of 30 µL acetonitrile and stored at –20 °C until prep as described previously and analysis of all samples after the 5-week timepoint.

Samples were injected in 0.5 µL volumes on a hydrophobic liquid interaction chromatography (HILIC) BEH Amide 1.7 µM, 2.1 x 100 mm UPLC column (Waters) and analyzed using an Agilent G6545A quadrupole-time of flight (Q-TOF) mass spectrometer equipped with a dual AJS ESI source and an Agilent 1290 Infinity series diode array detector, autosampler, and binary pump. Solvent A was water with 0.1% formic acid and solvent B was 95% acetonitrile, 5% water, and 0.1% formic acid. Separations were performed using a 20% solvent A isocratic method for 5 min followed by a 1 min gradient from 20% to 40% A and an 8 min re-equilibration at 20% A. Data was analyzed using MassHunter software (Agilent). The peak areas of 4,9-ah-TTX, ^{15}N-arginine, epi-TTX, and TTX were obtained by integration.

Statistical analysis

All data analysis of the recorded I_{Na} was performed using the software packages Clampfit v10.4 (Molecular Devices), Microsoft Excel, or Graph Pad Prism v8.2 (San Diego, CA). The statistical significance of differences between mean values was evaluated using Student's unpaired t-test, with $p < 0.05$ considered significant. Results are presented as mean $\pm$ S.E unless indicated otherwise.

Chapter III. Neuromodulation of Voltage-gated Sodium Channels by Gβ1γ2 Subunits: Implications for Developmental and Epileptic Encephalopathy

Nicholas Denomme performed and analyzed all experiments with the following exceptions: Dr. Samantha Hodges performed experiments and analyzed data shown in Figures 3.2, 3.3, 3.15-3.18 and Dr. Yukun Yuan performed a subset of the voltage-clamp recordings in Figure 3.14.

Introduction

As discussed in Chapter 1, VGSCs are modulated by numerous neurotransmitters through G-protein coupled receptor (GPCR) mediated signaling pathways. Most of the neuromodulatory effects on VGSCs through common GPCR neurotransmitters, e.g. dopamine and 5-HT, have been shown to occur via second messengers and protein kinases, i.e. PKA and PKC. However, there is also evidence to suggest that VGSC subtypes expressed in brain, $Na_v1.1$, $Na_v1.2$ and $Na_v1.3$, are relevant effectors of G-protein βγ subunits (Ma et al. 1997, Lenkowski et al. 2004, Mantegazza et al. 2005) and may be directly modulated in a membrane-delimited manner.

$Na_v1.6$ is prominent in the adult central nervous system and highly localized to the AIS, which is the primary site of AP initiation in brain neurons. In addition, $Na_v1.6$ is a major regulator of neuronal excitability due to its functional properties, including a hyperpolarized voltage-dependence of activation and key role in conducting high levels of persistent (or late) I_{Na} relative to the other neuronal VGSC subtypes (Raman et al. 1997, Smith et al. 1998, Rush et al. 2005). Increased persistent I_{Na} is a proposed consequence of Gβγ modulation of VGSC function, making $Na_v1.6$ a logical target for experimental evaluation. $Na_v1.2$ was proposed previously to contain a molecular determinant for Gβγ modulation at the last 28 residues of the C-terminus (Fig. 3.1B). Here, I performed sequence alignments for human $Na_v1.2$ and $Na_v1.6$ to identify a similar conserved region in the $Na_v1.6$ C-terminus that matches a proposed Gβγ binding motif (QxxER) present on numerous effectors such as adenylyl cyclase (Fig. 3.1A). Acute application of peptides containing the QxxER motif have been shown to reduce Gβγ modulation of some effectors including VGCCs (Herlitze et al. 1997, Zamponi et al. 1997). Taken together, these data suggest that Gβγ subunits may also modulate $Na_v1.6$.

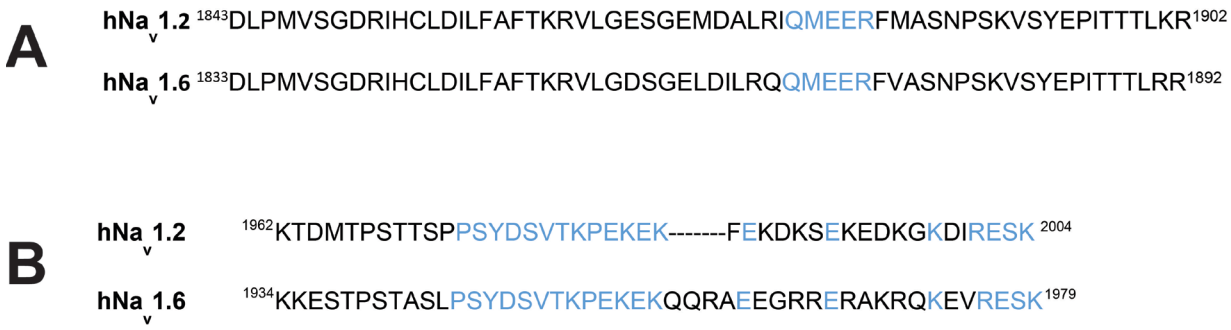


Figure 3.1 Amino acid sequence alignment of C-terminal region of human $Na_v1.2$ and human $Na_v1.6$ with proposed Gβγ binding motif (A) Proposed Gβγ binding motif (QxxER) highlighted in blue. (B) Alignment of amino acid residues in the end of the C-tail in $Na_v1.2$ and $Na_v1.6$ with homologous residues in blue. $Na_v1.2$ accession #: NP_001035232.1. $Na_v1.6$ accession #: NP_055006.1

Understanding the extent of Gβγ modulation of $Na_v1.6$ and other brain VGSCs is vital for understanding basic mechanisms of neurotransmission. Moreover, this work may provide insight into a role for VGSCs in the underlying pathophysiology of *GNB1*-linked DEE (see Chapter I). Here we investigate physical and functional interactions between brain VGSCs and Gβγ in mouse whole brain as well as the effects of transient co-expression of a prominent brain Gβγ complex, Gβ1γ2, on $Na_v1.6$ and $Na_v1.1$ in HEK cells. Finally, we perform cortical slice electrophysiology experiments as a first attempt to explore the cellular mechanisms of hyperexcitability in a mouse model of *GNB1*-E.

Results

G-protein βγ subunits interact with Na_vβ1 subunits in mouse whole brain

To identify VGSC interacting partners in brain *in vivo*, we used CRISPR-Cas9 gene editing to generate a transgenic mouse line expressing an in-frame V5 epitope tag on the C-terminus of the VGSC β1 subunit (Na_vβ1). We then performed unbiased protein profiling experiments using liquid chromatography (LC) and tandem mass spectrometry (MS/MS) in collaboration with the University of Michigan Proteomics core. In these assays, Na_vβ1 was immunoprecipitated from solubilized whole brain lysates prepared from P18 *Scn1b*-V5 epitope tagged mice (Fig. 3.2). Immunoprecipitated samples were first tested to confirm the presence of VGSC α subunits before being submitted for LC-MS/MS analysis to identify protein binding partners of the Na_vβ1 subunit. To identify protein binding partners of the Na_vβ1 subunit, Na_vβ1 was immunoprecipitated via pull-down of the V5 tag in whole brain homogenates from P18 *Scn1b*-V5 tagged mice. Positive binding partners of the Na_vβ1 subunit were identified by detection of a nonzero number of spectral counts (surrogate for relative abundance). At least 2 unique peptides per protein were required for identification. Nonspecific binding was assessed via number of spectral counts present in an immunoglobulin (IgG) control condition.

Using these methods, 2 Gβ subunits and 4 Gγ subunit proteins were observed in complex with Navβ1 and α subunits (Fig. 3.2). Gγ2, Gγ3, Gγ7 and Gγ12 subunits were found to interact in complex with Navβ1 subunits in P18 *Scn1b*-V5 mouse whole brain. Gβ1 and Gβ2 were detected in complex with Navβ1 subunits in *Scn1b*-V5 mouse whole

brain samples, however they were also detected in the IgG control samples indicating some nonspecific contamination contributed to the interaction. The increased amount of coimmunoprecipitated $Na_v\beta1$ detected in the *Scn1b*-V5 brain sample found in complex with Gβ1 or Gβ2 compared to the IgG control brain sample—coupled with the fact that Gβγ is an obligatory dimer—strongly suggests Gβγ can physically interact with the VGSC complex through $Na_v\beta1$ subunits.

Mouse Gene	Protein	Na_v β1 (V5)	Control (IgG)
Gnb1	Gβ1	139	56
Gnb2	Gβ2	120	45
Gng2	Gγ2	10	0
Gng3	Gγ3	8	0
Gng7	Gγ7	4	0
Gng12	Gγ12	2	0

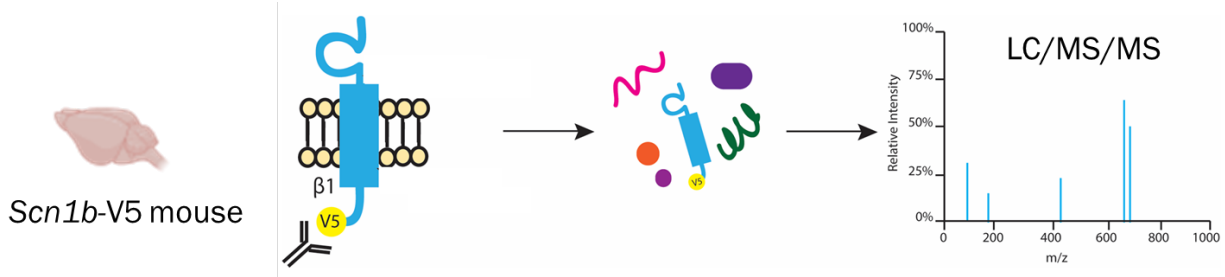


Figure 3.2. Mass spec protein profiling experiments with *Scn1b*-V5 mouse whole brain show Gβγ subunits interact with the VGSC complex through $Na_v\beta1$ subunits

To further probe the physical interaction between Gβγ subunits and brain VGSC complexes through $Na_v\beta1$ subunits found via MS, we performed coimmunoprecipitation experiments in juvenile (P18) and adult (P135) *Scn1b*-V5 mice using western blot. Using chemiluminescent detection methods, no interaction was detected in either juvenile or adult mice between $Na_v\beta1$ and Gβ subunits (Fig. 3.3). We were unable to detect the physical association between Gβγ and $Na_v\beta1$ subunits observed in LC-MS/MS coimmunoprecipitation experiments using western blot detection methods, likely due to the differences in detection sensitivity between LC-MS/MS and western blotting.

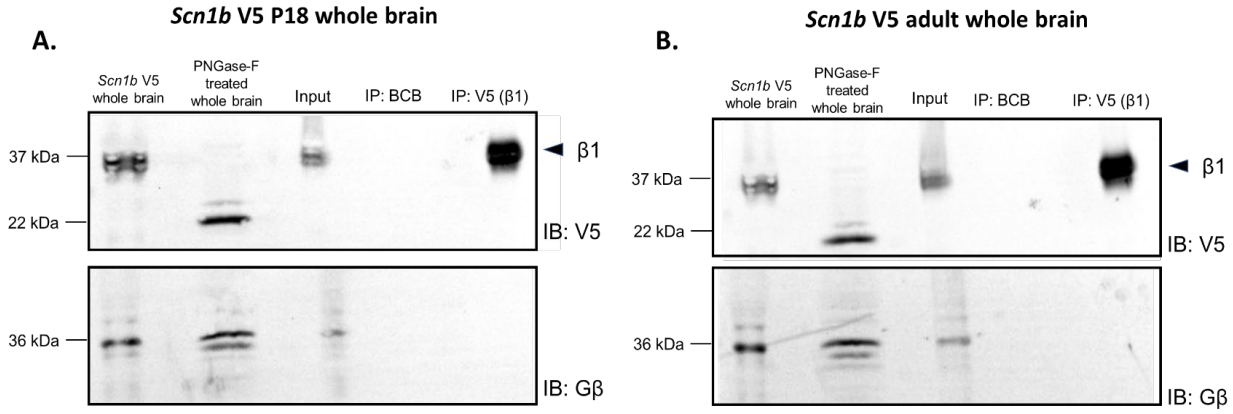
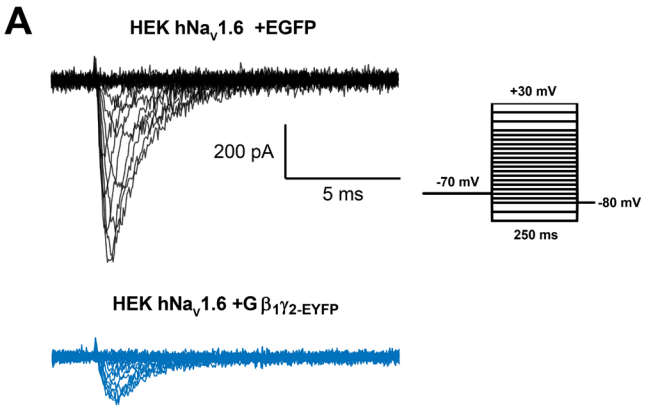


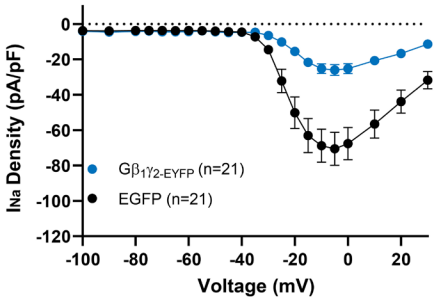
Figure 3.3. No interaction detected in coimmunoprecipitation experiments between Gβ and $Na_v\beta1$ in *Scn1b*-V5 juvenile and adult mouse whole brain. Whole cell protein lysates from P18 and adult *Scn1b*-V5 brain were immunoprecipitated (IP) with either a V5 nanobody against the V5 epitope tag on the C-terminus of β1 or with binding control beads (BCB) as a control. *Scn1b*-V5 whole brain, PNGase-F treated *Scn1b*-V5 whole brain, input samples, and IP samples were separated on a 12% SDS-PAGE gel and immunoblotted with mouse anti-V5 and anti-Gβ (B600). (A) Western blot of anti-V5 and anti-Gβ co-IP in P18 Scn1b V5 whole brain. (B) Western blot of anti-V5 and anti-Gβ co-IP in adult Scn1b V5 whole brain. N = 1 for each experiment.

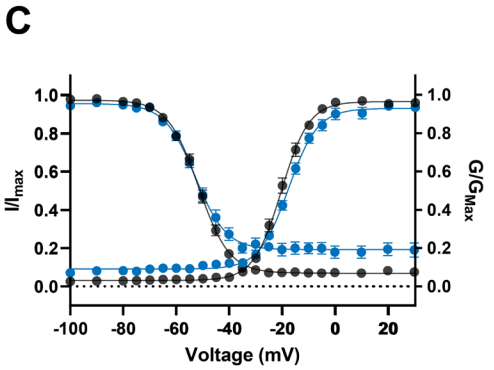
Transient coexpression of Gβ1γ2 subunits induces a subtype and voltage-dependent inhibition of $Na_v1.1$ and $Na_v1.6$ transient I_{Na} density in HEK cells .

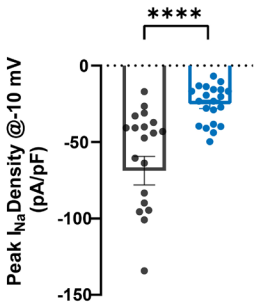
We used heterologous expression systems to test a potential functional interaction between Gβγ subunits and $Na_v1.6$. HEK cells stably expressing human $Na_v1.6$ were transiently transfected with Gβ1 plus Gγ2 tagged with enhanced yellow fluorescent protein (EYFP) or with enhanced green fluorescent protein (EGFP) as a control (Fig. 3.3). We measured whole cell I_{Na} using the voltage clamp technique. Gβ1γ2 was chosen as the Gβγ complex for this study as it is predominantly expressed in brain (Yim et al. 2017)**.** Transient coexpression of Gβ1γ2 led to a dramatic and significant inhibition of the mean $Na_v1.6$ mediated I_{Na} density compared to the EGFP control group when stepping from a -70 mV prepulse to -10 mV to elicit peak I_{Na} (Fig. 3.4D) (EGFP: -68.77 ± 9.33 pA/pF vs. Gβ1γ2: -25.28 ± 2.69 pA/pF; $P<0.0001$) (Table 3.1). To understand if there were any voltage-dependent conformations of $Na_v1.6$ that altered the sensitivity of Gβ1γ2 modulation, we recorded I_{Na} from a prepulse of -120 mV (Fig. 3.4E-H). Consistent with the results from a -70 mV prepulse, we observed a significant decrease in $Na_v1.6$ mediated I_{Na} after co-expression of Gβ1γ2 compared to co-expression of the EGFP control using a -120 mV prepulse potential (Fig. 3.4H) (EGFP: -87.70 ± 13.35 pA/pF vs Gβ1γ2: -33.10 ± 5.45 pA/pF; $P<0.0111$) (Table 3.1). No significant differences in the voltage-dependence of activation (G/Gmax) or voltage-dependence of availability (I/Imax) of $Na_v1.6$ were observed when comparing the Gβ1γ2 and EGFP conditions from both -70 and -120 mV prepulse potentials (Fig. 3.4B and 3.4F) (Table 3.2). The voltage-dependence of availability (I/I_{Max}) curves generated from the Gβ1γ2 condition

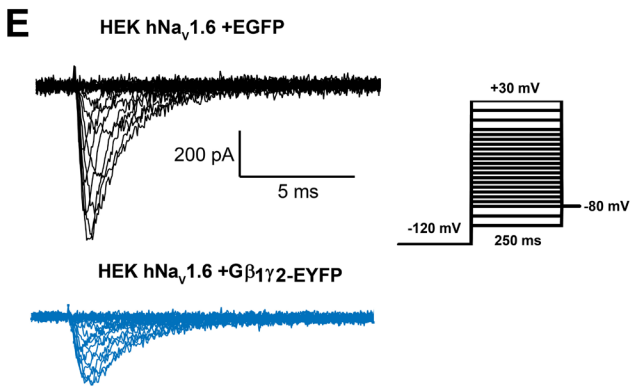
using prepulse potentials of both -70 and -120 mV (displayed in Fig. 3.4C and Fig. 3.4G, respectively) appear to show a significant non-inactivating fraction of current in the range of -40 mV to +30 mV. This is a result of the very low ratio of Nav1.6 I_{Na} compared to background noise mediated in HEK $Na_v1.6$ cells transiently expressing Gβ1γ2. The analysis of I_{Na} density was done without baseline noise subtraction, and because the dramatic inhibition of $Na_v1.6$ I_{Na} at voltage steps between -40 mV and +30 mV by Gβ1γ2 expression resulted in very low amplitudes for total Nav1.6 I_{Na}, background noise (~20-30 pA) appears to represent a significant fraction of the total $Na_v1.6$ I_{Na}. A direct analysis of non-inactivating (persistent) $Na_v1.6$ I_{Na} modulation by Gβ1γ2 expression was performed and is displayed in Fig. 3.6. Interestingly, there was also a small but significant reduction in the cell capacitance measured in HEK $Na_v1.6$ cells co-expressing Gβ1γ2 compared to the EGFP control (Gβ1γ2: 9.47 ± 0.68* pF vs EGFP: 11.90 ± 0.71 pF; P=0.017) (Table 3.4). Cell capacitance is often used as a surrogate for cell size, suggesting that co-expression of Gβ1γ2 in HEK $Na_v1.6$ cells may reduce the average size of the cell compared to cells co-expressing EGFP.

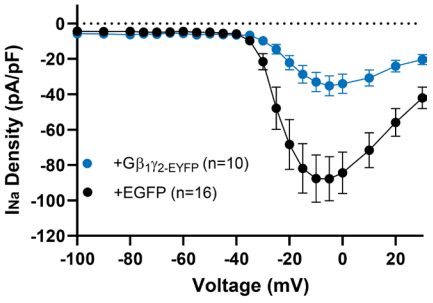

A
HEK hNaV1.6 +EGFP
200 pA
5 ms
+30 mV
-70 mV
-80 mV
250 ms
HEK hNaV1.6 +Gβ1γ2-EYFP

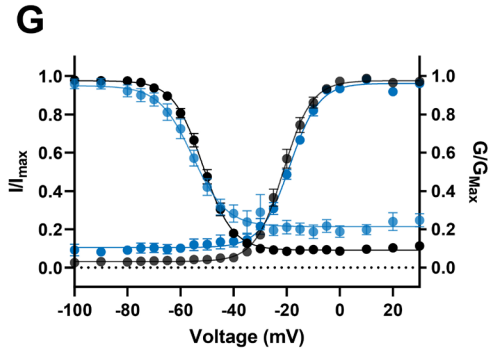

B
INa Density (pA/pF)
Gβ1γ2-EYFP (n=21)
EGFP (n=21)
Voltage (mV)


C
I/Imax
G/GMax
Voltage (mV)


D
****
Peak INa Density @-10 mV (pA/pF)


E
HEK hNaV1.6 +EGFP
200 pA
5 ms
+30 mV
-120 mV
-80 mV
250 ms
HEK hNaV1.6 +Gβ1γ2-EYFP


F
INa Density (pA/pF)
+Gβ1γ2-EYFP (n=10)
+EGFP (n=16)
Voltage (mV)


G
I/Imax
G/GMax
Voltage (mV)

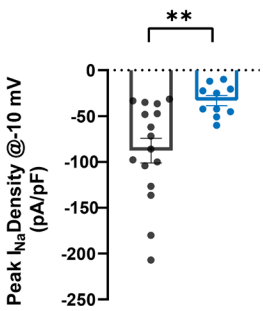
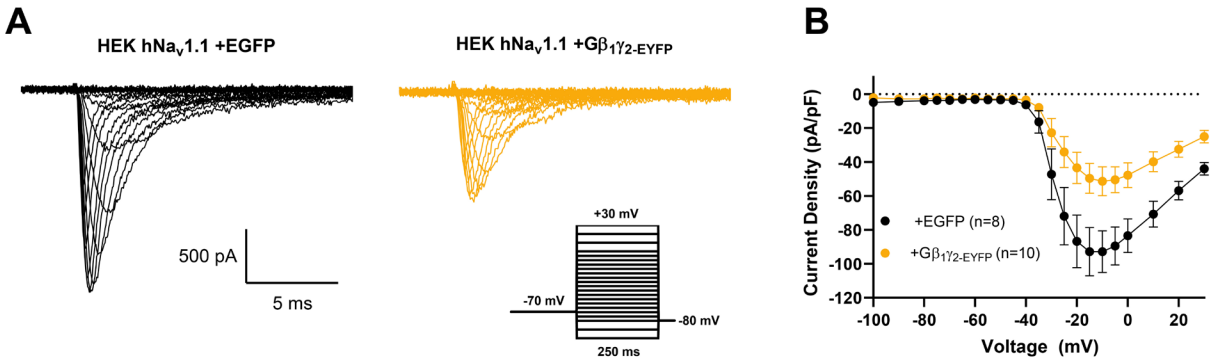
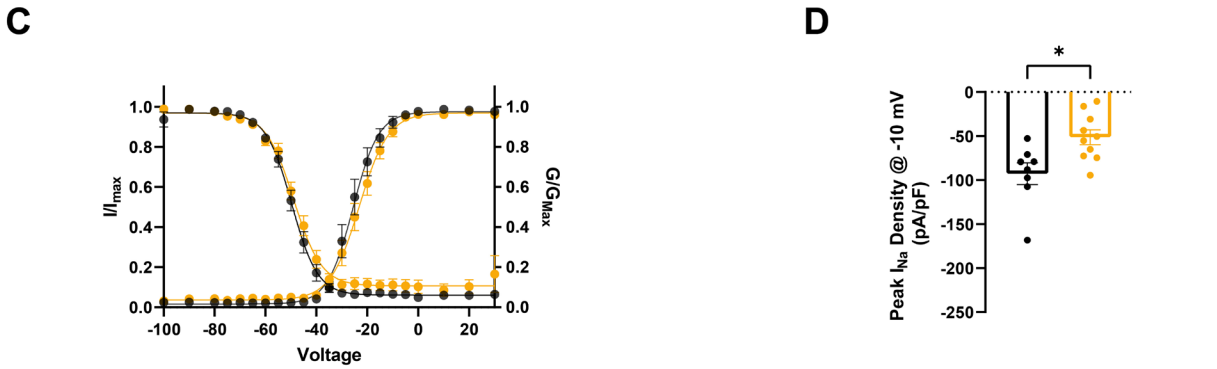
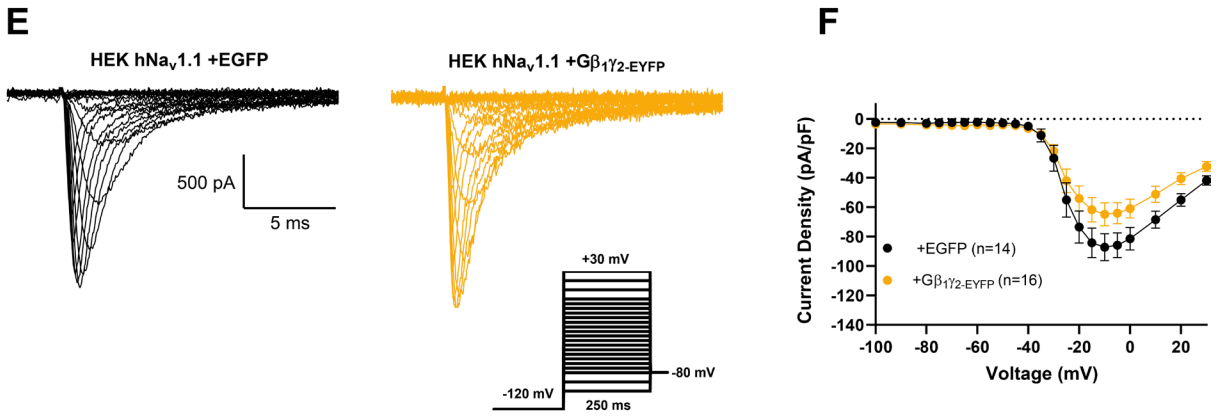

H
**
Peak INa Density @-10 mV (pA/pF)

Figure 3.4 Transient co-expression of Gβ1γ2 or EGFP in HEK cells stably expressing human $Na_v1.6$. (A) Representative I_{Na} traces evoked with a prepulse potential of -70 mV in HEK cells stably expressing $Na_v1.6$ and transiently co-transfected with Gβ1 and γ2-EYFP (blue) or EGFP only (black). (B) I-V relationship of HEK $Na_v1.6$ cells expressing Gβ1γ2-EYFP or EGFP from a prepulse of -70 mV. (C) Normalized voltage-dependence of conductance (G/Gmax) and availability (I/Imax) using a -70 mV prepulse potential. (D) Peak I_{Na} density evoked by a depolarizing step from -70 mV to -10 mV. (E) Representative I_{Na} traces of HEK $Na_v1.6$ cells expressing Gβ1γ2-EYFP or EGFP control from a prepulse of -120 mV. (F) I-V relationship of HEK $Na_v1.6$ cells expressing Gβ1γ2-EYFP or EGFP from a prepulse of -120 mV. (G) Normalized voltage-dependence of conductance(G/Gmax) and availability (I/Imax) using a prepulse potential of -120 mV. (H) Peak I_{Na} density evoked by a depolarizing step from -120 mV to -10 mV. Significance determined using a Student's unpaired t-test (****P<0.0001) (**P=0.0048)

We next asked whether Gβ1γ2 also modulated human $Na_v1.1$, another major brain VGSC subtype that is primarily localized to inhibitory interneurons and linked to DEE. Previous work has shown $Na_v1.1$ is sensitive to significant increases in persistent I_{Na} when co-expressed with Gβ2γ3 subunits (Mantegazza et al. 2005), however the effects of Gβ1γ2 have yet to be tested. Here, transient coexpression of Gβ1γ2 in HEK cells stably expressing Nav1.1 significantly reduced the mean peak I_{Na} density compared to the EGFP control group when stepping from a -70 mV prepulse to -10 mV (Fig. 3.5D) (EGFP: -92.87 ± 12.25 pA/pF vs. Gβ1γ2: -51.37 ± 8.46 pA/pF; P=0.0111) (Table 3.1). From a prepulse of -120 mV, no significant decrease in $Na_v1.1$ mediated peak I_{Na} density was observed in Gβ1γ2 vs EGFP conditions (Fig. 3.5H) (EGFP: -87.21 ± 9.15 pA/pF vs Gβ1γ2: -64.87 ± 7.79 pA/pF) (Table 3.1). No significant differences in the voltage-dependence of activation (G/Gmax) or voltage-dependence of availability (I/Imax) of $Na_v1.1$ were observed when comparing the Gβ1γ2 or EGFP conditions from both -70 and -120 mV prepulse potentials (Fig. 3.5B and 3.5F) (Table 3.2).


A
HEK hNa$_v$1.1 +EGFP
HEK hNa$_v$1.1 +Gβ$_1$γ$_{2\text{-EYFP}}$
500 pA
5 ms
+30 mV
-70 mV
-80 mV
250 ms
B
Current Density (pA/pF)
+EGFP (n=8)
+Gβ$_1$γ$_{2\text{-EYFP}}$ (n=10)
Voltage (mV)


C
I/I$_{max}$
G/G$_{Max}$
Voltage
D
*
Peak I$_{Na}$ Density @ -10 mV (pA/pF)


E
HEK hNa$_v$1.1 +EGFP
HEK hNa$_v$1.1 +Gβ$_1$γ$_{2\text{-EYFP}}$
500 pA
5 ms
+30 mV
-120 mV
-80 mV
250 ms
F
Current Density (pA/pF)
+EGFP (n=14)
+Gβ$_1$γ$_{2\text{-EYFP}}$ (n=16)
Voltage (mV)

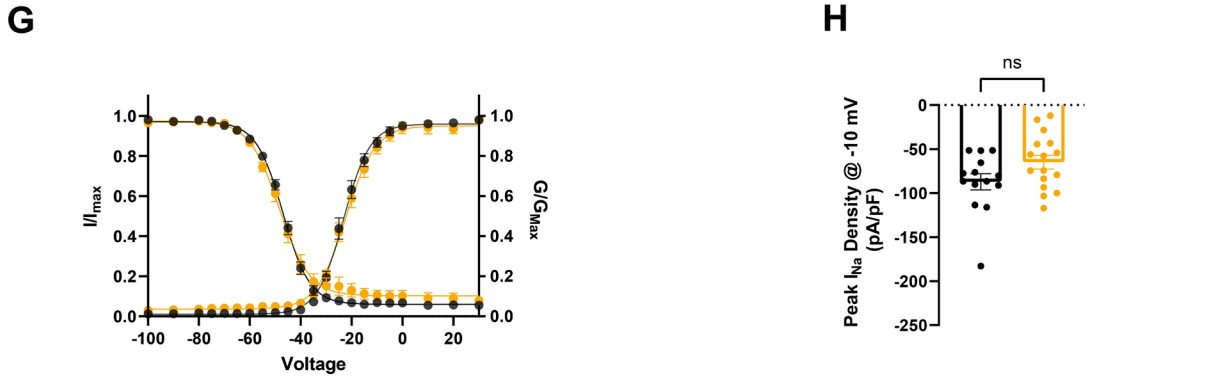

G
I/I$_{max}$
G/G$_{Max}$
Voltage
H
ns
Peak I$_{Na}$ Density @ -10 mV (pA/pF)

Figure 3.5. Transient co-expression of Gβ1γ2 or EGFP in HEK cells stably expressing human $Na_v1.1$. (A) Representative I_{Na} traces evoked with a prepulse potential of -70 mV in HEK cells stably expressing $Na_v1.1$ and transiently co-transfected with Gβ1 and γ2-EYFP (orange) or EGFP only (black). (B) I-V relationship of HEK $Na_v1.1$ cells expressing Gβ1γ2-EYFP or EGFP from a prepulse of -70 mV. (C) Normalized voltage-dependence of conductance (G/Gmax) and availability (I/Imax) using a -70 mV prepulse potential. (D) Peak I_{Na} density evoked by a depolarizing step from -70 mV to -10 mV. (E) Representative I_{Na} traces of HEK $Na_v1.1$ cells expressing Gβ1γ2-EYFP or EGFP control from a prepulse of -120 mV. (F) I-V relationship of HEK $Na_v1.1$ cells expressing Gβ1γ2-EYFP or EGFP from a prepulse of -120 mV. (G) Normalized voltage-dependence of conductance (G/Gmax) and availability (I/Imax) using a prepulse potential of -120 mV. (H) Peak I_{Na} density evoked by a depolarizing step from -120 mV to -10 mV. Significance determined using a Student's unpaired t-test (*P=0.0111)

Gβ1γ2 co-expression modulates both $Na_v1.1$- and $Na_v1.6$-mediated persistent I_{Na} in HEK cells

We next sought to examine the impact of Gβ1γ2 co-expression on $Na_v1.1$ and $Na_v1.6$ mediated persistent I_{Na} at a voltage step from -70 to -10 mV (Fig. 3.6). Persistent I_{Na} density was quantified as the average I_{Na} density measured in a 2 ms period 50 ms after the peak transient I_{Na} was observed in each cell. Transient co-expression of Gβ1γ2 led to a significant decrease in the mean persistent I_{Na} density compared to the EGFP control condition for $Na_v1.6$ (Fig. 3.6A) (EGFP: -2.83 ± 0.70 pA/pF vs Gβ1γ2: -1.18 ± 0.15 pA/pF; P=0.0393*) but not $Na_v1.1$ (Fig. 3.6E) (EGFP: -3.64 ± 0.89 pA/pF vs Gβ1γ2: -4.53 ± 1.75 pA/pF; P=0.6256). When plotting persistent I_{Na} density as a percentage of the transient peak I_{Na} density, no significant differences were detected in Gβ1γ2 vs. EGFP conditions for $Na_v1.6$ (Fig. 3.6B) (EGFP: 3.70 ± 0.63% vs Gβ1γ2: 4.10 ± 0.75%; P=0.6896) or Nav1.1 (Fig. 3.6F) (EGFP: 4.74 ± 0.97% vs Gβ1γ2: 9.75 ± 2.88%; P=0.0676). However, a subset of the HEK $Na_v1.1$ cells co-expressing Gβ1γ2

produced a dramatic amount of persistent I_{Na} density. 30% of HEK $Na_v1.1$ cells co-expressing Gβ1γ2 produced >20% persistent/peak I_{Na} density while 0% of cells from the EGFP condition did, suggesting the effects of Gβ1γ2 variably impact $Na_v1.1$ persistent I_{Na} in a proportion of cells, similar to results observed previously (Mantegazza et al. 2005).

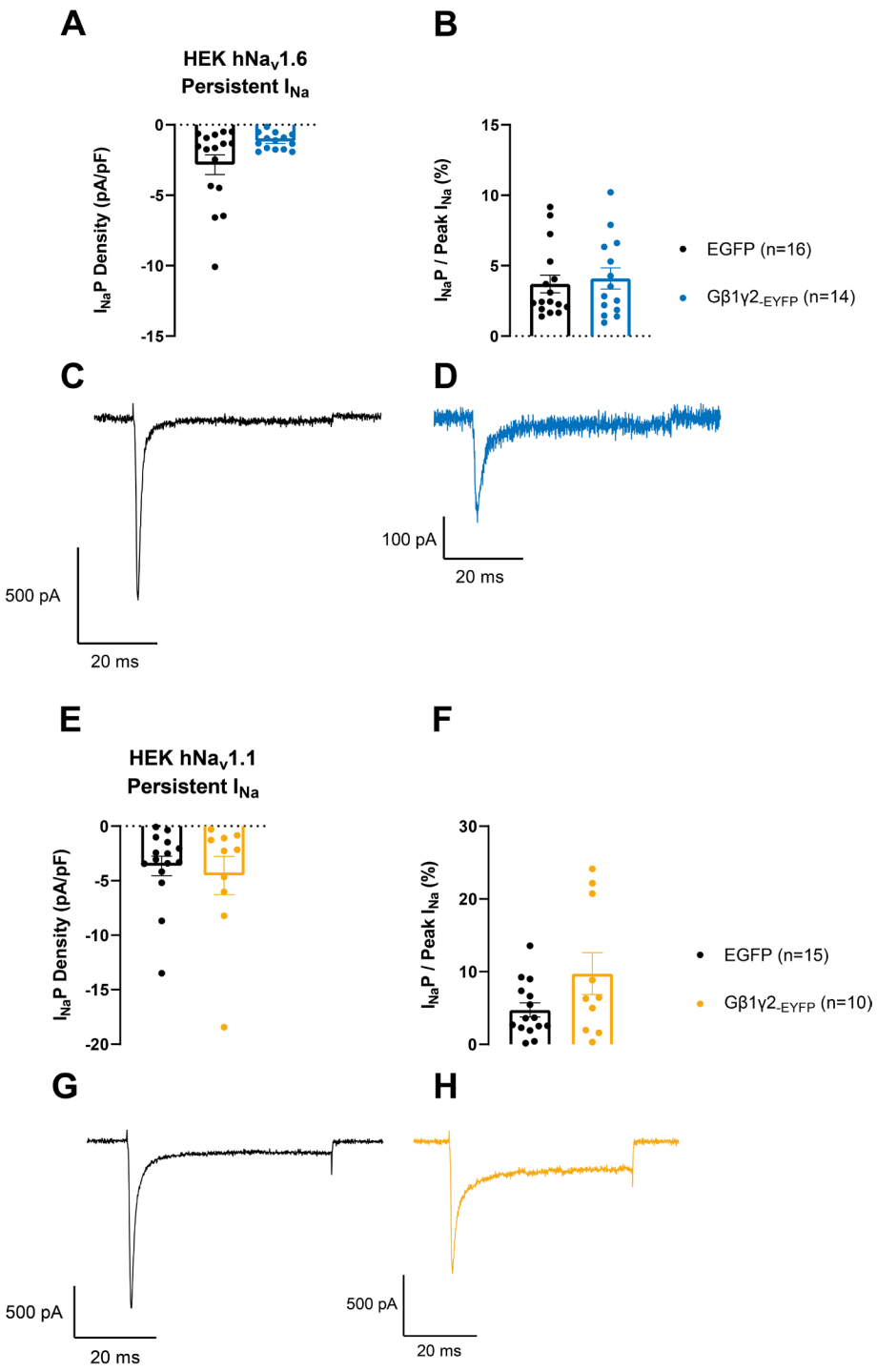


Figure 3.6 Gβ1γ2 shows differential modulation of $Na_v1.1$ vs $Na_v1.6$ persistent current in HEK cells. (A) Average persistent I_{Na} density in HEK cells stably expressing $Na_v1.6$ transiently co-transfected with Gβ1 and γ2-EYFP (blue) or EGFP only (black). (B) Persistent I_{Na} as a percentage of the peak transient current. (C & D) Representative traces evoked by a depolarizing step from -70 mV to -10 mV. (E) Average persistent I_{Na} density in HEK cells stably expressing $Na_v1.1$ transiently co-transfected with Gβ1 and γ2-EYFP (orange) or EGFP only (black). (F) Persistent I_{Na} as a percentage of the peak transient I_{Na}. (G & H) Representative traces evoked by a depolarizing step from -70 mV to -10 mV.

Gβ1γ2 inhibition of $Na_v1.6$ but not $Na_v1.1$ shows acute voltage-dependent relief

Membrane-delimited modulation of high-voltage-activated N- and P/Q-type VGCCs (i.e. $Ca_v2.2$) by Gβγ subunits shows an acute voltage-dependent relief that can be elicited using a double pulse protocol (Bean 1989, Ikeda 1996, Zamponi and Snutch 1998). By dramatically depolarizing the channel to positive membrane potentials (+100 mV), the VGCC exists in a confirmation that shows a reduced affinity for Gβγ subunits. Experiments using a similar depolarizing double pulse protocol (Zampoini and Snutch 1998) to examine voltage-dependent relief of Gβ1γ2 inhibition of $Na_v1.1$ and $Na_v1.6$ were performed (data not shown), however, prolonged depolarization of HEK cells expressing VGSCs was compromising to cell heath and membrane stability. To investigate the acute nature of Gβ1γ2 inhibition of $Na_v1.1$ and $Na_v1.6$ mediated peak I_{Na} density, we recorded peak I_{Na} using a double pulse protocol stepping from -70 to 0 mV (for 250 ms) before and after holding the membrane at a hyperpolarized potential of -120 mV for 1 s (Fig 3.7). Prolonged hyperpolarization of VGSCs was reported to relieve the G-protein dependent inhibition of VGSCs by cinacalcet and anandamide (See Chapter I; Mattheisen et al. 2018, Mattheisen 2018). Here, using the double pulse protocol, the ratio of the second I_{Na} peak after prolonged hyperpolarization was significantly increased compared to the first I_{Na} peak (P2/P1) in HEK $Na_v1.6$ cells co-expressing Gβ1γ2 compared to EGFP (Fig. 3.7A-B) (EGFP: 1.089 ± 0.018 vs Gβ1γ2: 1.16 ± 0.022; P=0.0305*). In HEK $Na_v1.1$ cells, there was no significant difference in the P1/P2 peak I_{Na} density ratio between (EGFP: 1.05 ± 0.011 vs Gβ1γ2: 1.05 ± 0.019; P=0.9805).

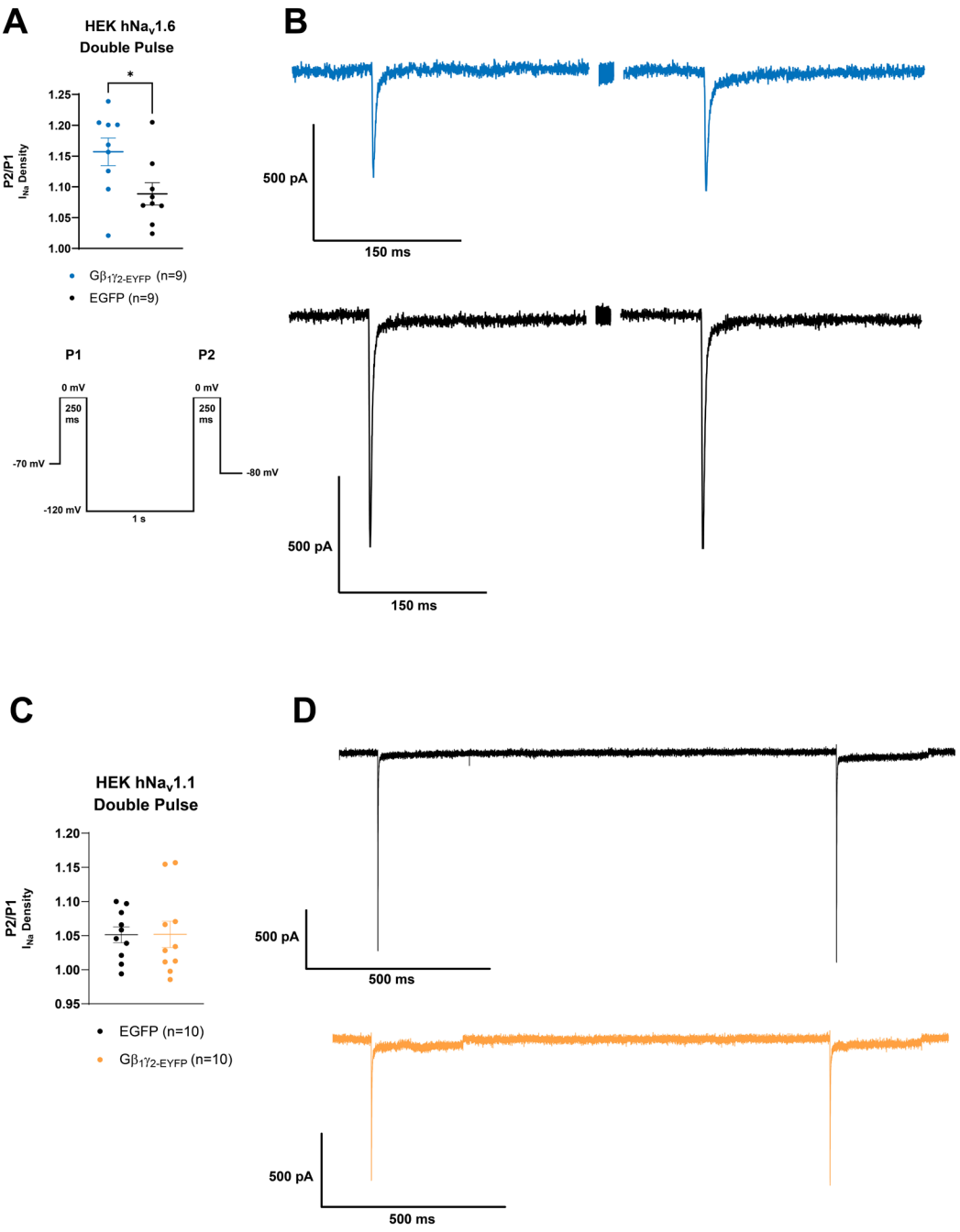


Figure 3.7 Gβ1γ2 inhibition of $Na_v1.6$ but NOT $Na_v1.1$ shows acute voltage-dependent relief after prolonged hyperpolarization for 1s at -120 mV. (A) Ratio of pulse 2 to pulse 1 (P2/P1) peak I_{Na} density after prolonged hyperpolarization for 1 s at -120 mV in HEK $Na_v1.6$ cells co-expressing Gβ1 and γ2-EYFP (blue) or EGFP only (black). (B) Representative traces from $Na_v1.6$ double pulse protocol for Gβ1γ2 (blue) and EGFP (black) conditions. (C) P2/P1 peak I_{Na} density ratio after prolonged hyperpolarization for 1 s at -120 mV in HEK $Na_v1.1$ cells co-expressing Gβ1 and γ2-EYFP (orange) or EGFP only (black). (D) Representative traces from $Na_v1.1$ double pulse protocol for Gβ1γ2 (blue) and EGFP (black) conditions. Significance in A determined using a Student's unpaired t-test (*P=0.0305)

Transient coexpression of Gβ1γ2 subunits has no effect on slow inactivation of $Na_v1.1$ or $Na_v1.6$ in HEK cells.

Enhancement of slow inactivation is a common feature of GPCR-mediated neuromodulation of VGSCs (see Chapter I). To determine whether slow inactivation contributes to the Gβ1γ2 inhibition of $Na_v1.1$ or $Na_v1.6$, we measured slow inactivation at a stimulation frequency of 50 Hz after co-expression of Gβ1γ2 or EGFP in HEK cells (Fig. 3.8). 50 Hz slow inactivation, quantified as % of the initial peak I_{Na} density remaining after the 50^{th} pulse, of $Na_v1.6$ showed no significant differences between the Gβ1γ2 and EGFP conditions (Fig. 3.8A-B) (EGFP: 35.37 ± 4.97% vs Gβ1γ2: 24.98 ± 4.33%; P=0.1352). In HEK cells, $Na_v1.1$ also showed no significant differences in 50 Hz slow inactivation when comparing the Gβ1γ2 or EGFP co-expression conditions (Fig. 3.8C-D) (EGFP: 38.22 ± 4.77% vs Gβ1γ2: 31.89 ± 3.24%; P=0.288).

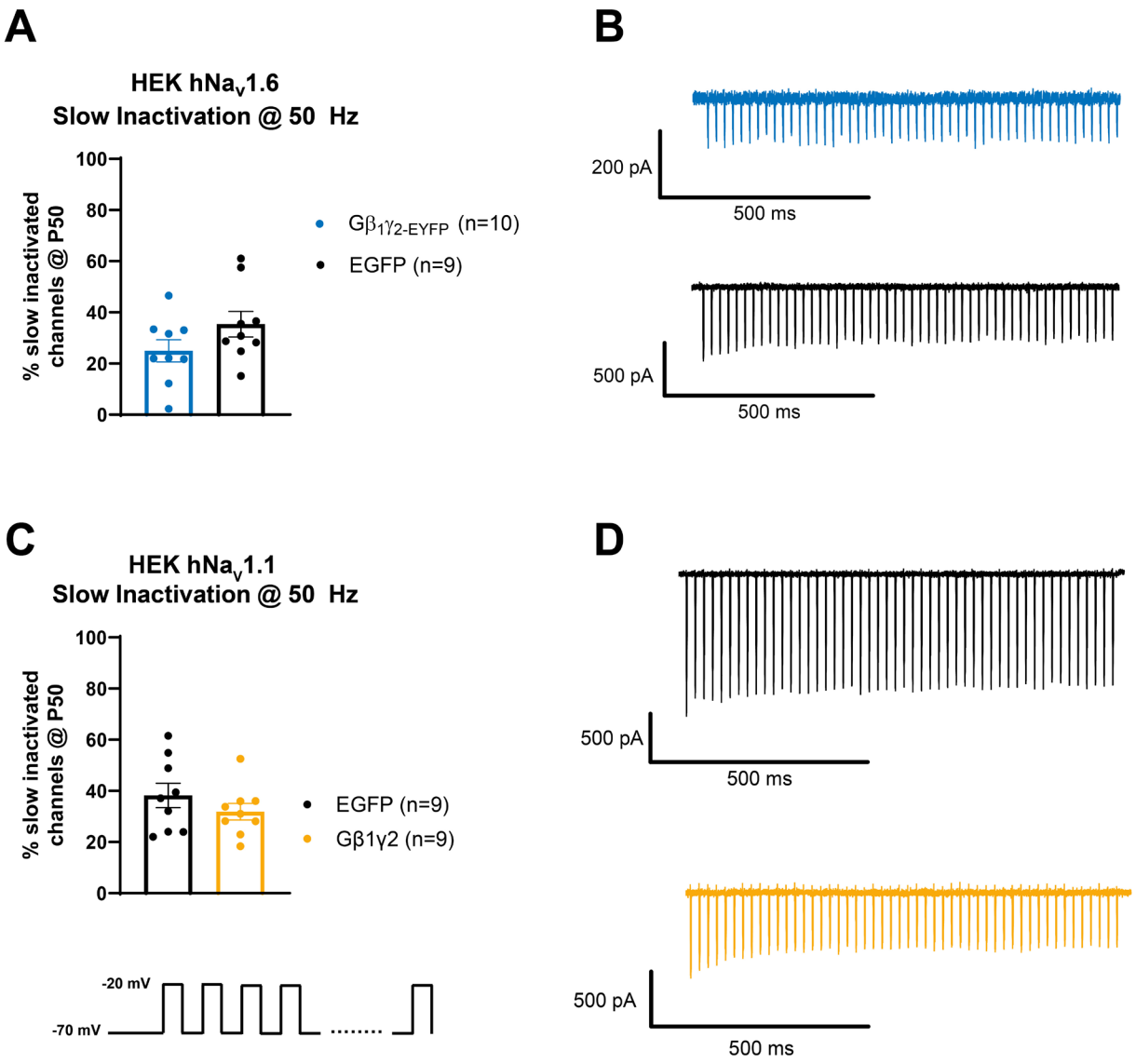


Figure 3.8. Gβ1γ2 coexpression has no impact on slow inactivation properties of $Na_v1.1$ or $Na_v1.6$ at 50 Hz. (A) Quantification of % slow inactivated channels at pulse 50 (P50) elicited using repeating depolarizing steps from -70 mV to -20 mV at 50 Hz in HEK $Na_v1.6$ cells co-expressing Gβ1γ2-EYFP (blue) or EGFP (black). (B) Representative traces of $Na_v1.6$ 50 Hz slow inactivation in Gβ1γ2 (blue) or EGFP (black) conditions. (C) % slow inactivated channels at 50 Hz in HEK $Na_v1.1$ cells co-expressing Gβ1γ2-EYFP (orange) or EGFP (black). (D) Representative traces of $Na_v1.1$ 50 Hz slow inactivation in Gβ1γ2 (orange) or EGFP (black) conditions.

PKA/PKC inhibition does not significantly reduce Gβ1γ2 inhibition of $Na_v1.1$- or $Na_v1.6$-mediated I_{Na}

PKA and PKC are downstream targets of both Gα and Gβγ subunits and are well-documented contributors to GPCR-mediated neuromodulation of VGSCs (see Chapter I). To ask whether PKA or PKC-mediated phosphorylation contributes to Gβ1γ2-mediated inhibition of $Na_v1.1$- or $Na_v1.6$-mediated I_{Na}, we recorded from HEK $Na_v1.1$ or $Na_v1.6$ cells co-expressing Gβ1γ2 in the presence and absence of 100 nM staurosporine (ST), which is a potent PKA/PKC inhibitor. From a -70 mV prepulse, $Na_v1.1$ peak I_{Na} density was not significantly increased in the presence of 100 nM ST (Fig. 3.9A-B) (Gβ1γ2: -51.37 ± 8.46 pA/pF vs Gβ1γ2 + 100 nM ST: -79.76 ± 10.74 pA/pF; P=0.0511) (Table 3.1). Likewise, using a -120 mV prepulse potential, no significant changes in $Na_v1.1$ peak I_{Na} density were observed in the presence of 100 nM ST (Fig. 3.9C-D) (Gβ1γ2: -64.87 ± 7.79 pA/pF vs Gβ1γ2 + 100 nM ST: -74.38 ± 9.69 pA/pF; P=0.4613) (Table 3.1). Preincubation of the PKA/PKC inhibitor (ST) had no effect on the Gβ1γ2 inhibition of $Na_v1.6$ I_{Na} density using a -70 mV prepulse (Fig. 3.9E-F) (Gβ1γ2: -25.28 ± 2.69 pA/pF vs Gβ1γ2 + 100 nM ST: -25.43 ± 6.06 pA/pF; P=0.9798) (Table 3.1) or -120 mV prepulse potential (Fig. 3.9G-H) (Gβ1γ2: -33.10 ± 5.45 pA/pF vs Gβ1γ2 + 100 nM ST: -28.33 ± 8.63 pA/pF; P=0.6298) (Table 3.1).

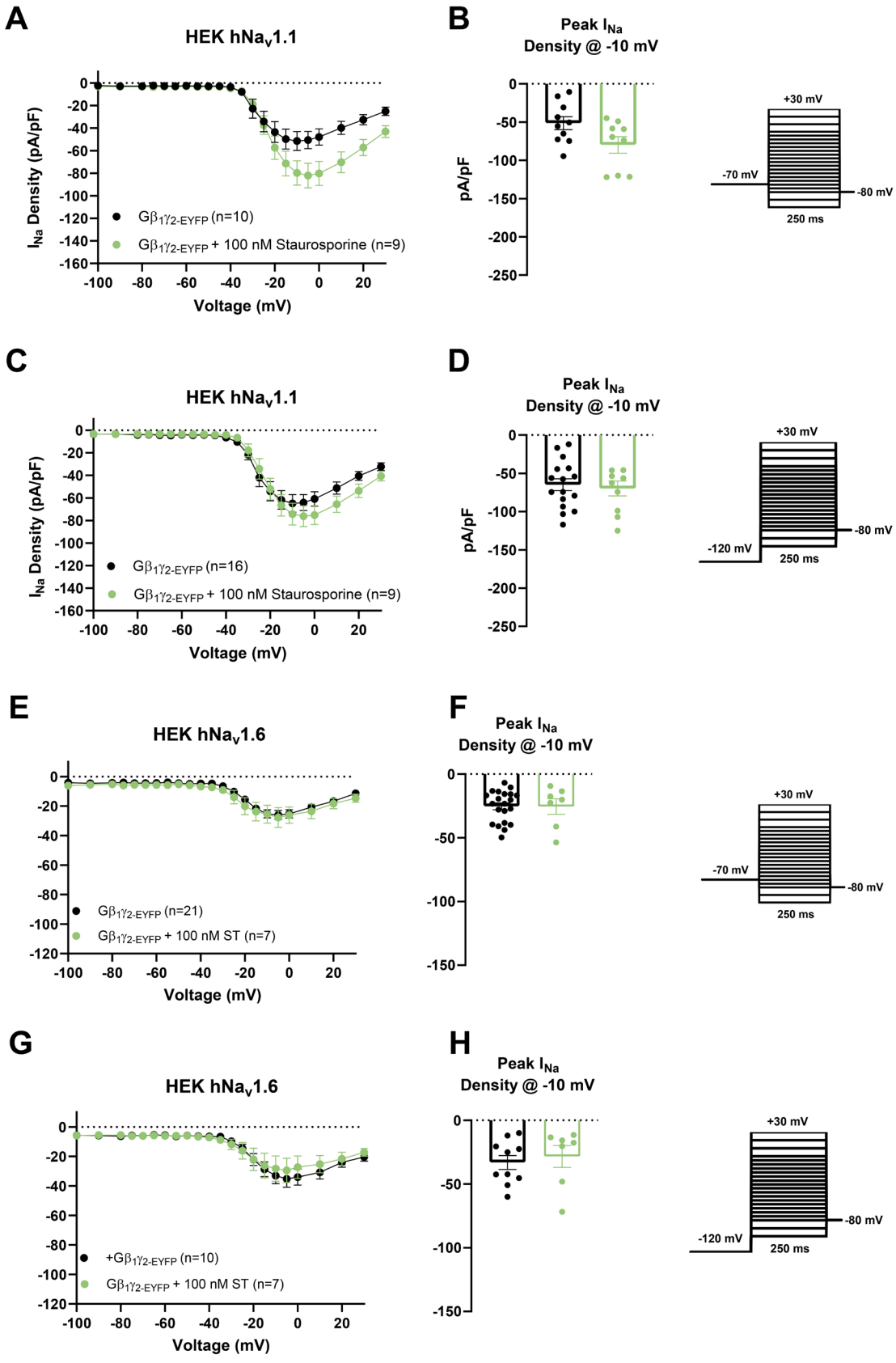

A
HEK hNaV1.1
INa Density (pA/pF)
Gβ1γ2-EYFP (n=10)
Gβ1γ2-EYFP + 100 nM Staurosporine (n=9)
Voltage (mV)
B
Peak INa Density @ -10 mV
pA/pF
+30 mV
-70 mV
-80 mV
250 ms
C
HEK hNaV1.1
INa Density (pA/pF)
Gβ1γ2-EYFP (n=16)
Gβ1γ2-EYFP + 100 nM Staurosporine (n=9)
Voltage (mV)
D
Peak INa Density @ -10 mV
pA/pF
+30 mV
-120 mV
-80 mV
250 ms
E
HEK hNaV1.6
Gβ1γ2-EYFP (n=21)
Gβ1γ2-EYFP + 100 nM ST (n=7)
Voltage (mV)
F
Peak INa Density @ -10 mV
+30 mV
-70 mV
-80 mV
250 ms
G
HEK hNaV1.6
+Gβ1γ2-EYFP (n=10)
Gβ1γ2-EYFP + 100 nM ST (n=7)
Voltage (mV)
H
Peak INa Density @ -10 mV
+30 mV
-120 mV
-80 mV
250 ms

Figure 3.9 Inhibition of PKA/PKC with 100 nM staurosporine does not reduce Gβ1γ2 inhibition of $Na_v1.1$ or $Na_v1.6$. (A) I-V relationship and (B) peak I_{Na} density from a prepulse of -70 mV in HEK cells stably expressing $Na_v1.1$ transiently co-transfected with Gβ1γ2-EYFP (black) or Gβ1γ2-EYFP + 100 nM staurosporine (green). (C) I-V relationship and (D) peak I_{Na} density from a prepulse of -120 mV in HEK cells stably expressing $Na_v1.1$ transiently co-transfected with Gβ1γ2-EYFP (black) or Gβ1γ2-EYFP + 100 nM staurosporine (green). (E) I-V relationship and (F) peak I_{Na} density from a prepulse of -70 mV in HEK cells stably expressing $Na_v1.6$ transiently co-transfected with Gβ1γ2-EYFP (black) or Gβ1γ2-EYFP + 100 nM staurosporine (green). (G) I-V relationship and (H) peak I_{Na} density from a prepulse of -120 mV in HEK cells stably expressing $Na_v1.6$ transiently co-transfected with Gβ1γ2-EYFP (black) or Gβ1γ2-EYFP + 100 nM staurosporine (green).

Inclusion of $Na_v\beta1$ subunits prevents Gβ1γ2 inhibition of $Na_v1.1$- but not of $Na_v1.6$-mediated I_{Na}

Our original finding that Gβγ subunits can associate in a protein complex with $Na_v\beta1$ subunits in whole brain was observed in coimmunoprecipitation experiments where $Na_v\beta1$ subunits were used as the probe to detect protein-protein interactions (Fig. 3.2). The role of $Na_v\beta1$ subunits in Gβγ modulation of VGSCs is largely unknown. To gain insight into this mechanism, we recorded I_{Na} in HEK cells stably expressing $Na_v1.6$ plus $Na_v\beta1$ or $Na_v1.1$ plus $Na_v\beta1$, with transient co-expression of Gβ1γ2 or EGFP.

Fig. 3.10 shows the impact of stable $Na_v\beta1$ expression on Gβ1γ2 modulation of $Na_v1.6$-mediated I_{Na} properties in HEK cells. In the presence of Navβ1, we still observed Gβ1γ2 inhibition of peak $Na_v1.6$ I_{Na} density at a prepulse potential of -70 (Fig. 3.10D) (EGFP: -124.9 ± 24.07 pA/pF vs Gβ1γ2: -42.59 ± 8.87 pA/pF; P=0.0033*) (Table 3.1) and -120 mV (Fig. 3.10H) (EGFP: -120.6 ± 22.42 pA/pF vs Gβ1γ2: -47.72 ± 8.77 pA/pF; P=0.0038*) (Table 3.1). No changes were observed in the voltage-dependence of activation or availability when comparing the Gβ1γ2 and EGFP conditions at a prepulse potential of -70 mV (Fig. 3.10C) or -120 mV (Fig. 3.10G) (Table 3.3).

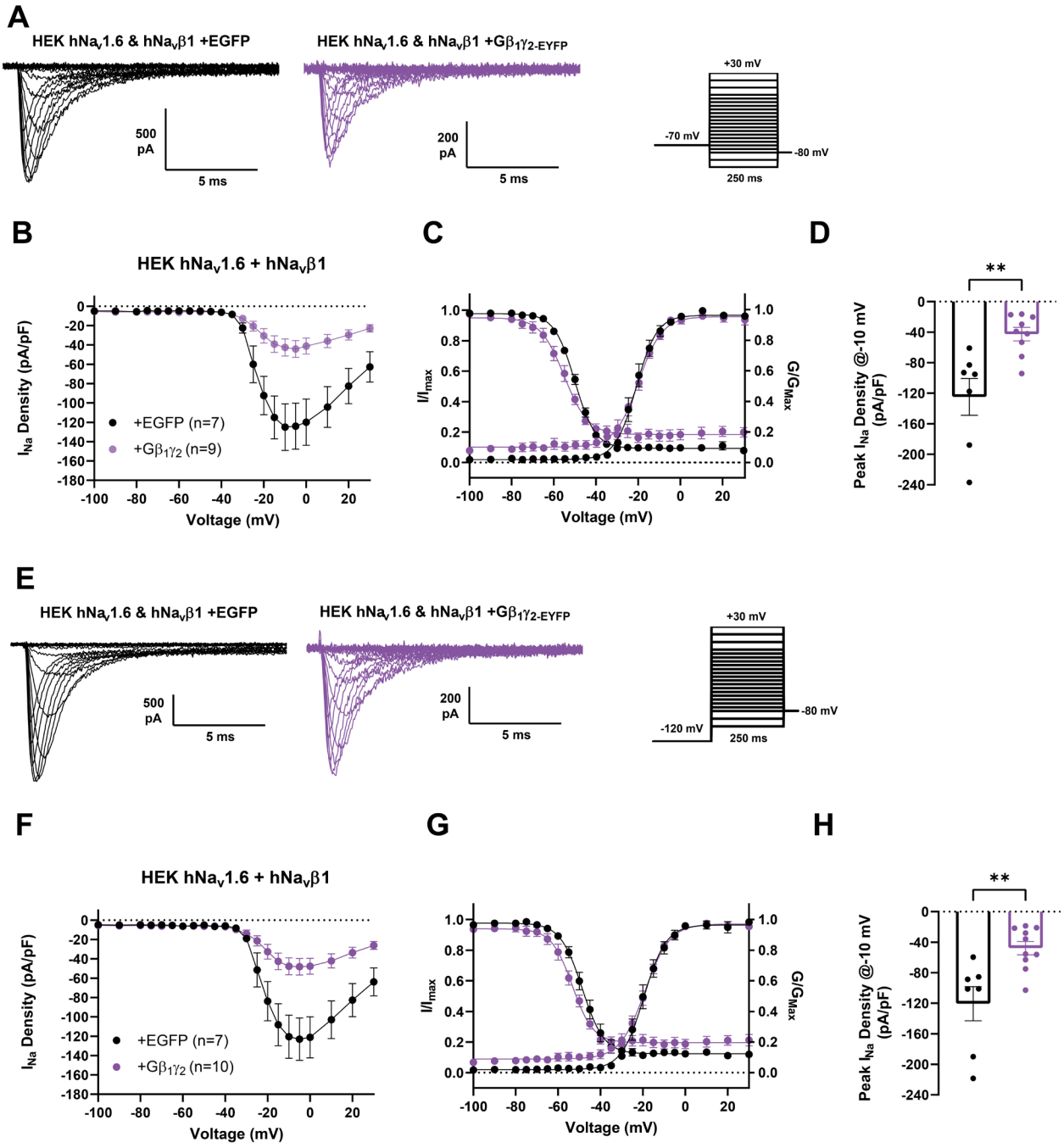


Figure 3.10 Transient co-expression of Gβ1γ2 or EGFP in HEK cells stably expressing human $Na_v1.6$ and human $Na_v\beta1$. (A) Representative I_{Na} traces evoked with a prepulse potential of -70 mV in HEK cells stably expressing $Na_v1.6$ and $Na_v\beta1$ transiently co-transfected with Gβ1 and γ2-EYFP (purple) or EGFP only (black). (B) I-V relationship from a prepulse of -70 mV. (C) Normalized voltage-dependence of conductance (G/Gmax) and availability (I/Imax) using a -70 mV prepulse potential. (D) Peak I_{Na} density evoked by a depolarizing step from -70 mV to -10 mV. (E) Representative I_{Na} traces of HEK $Na_v1.6$ and $Na_v\beta1$ cells expressing Gβ1γ2-EYFP or EGFP control from a prepulse of -120 mV. (F) I-V relationship from a prepulse of -120 mV. (G) Normalized voltage-dependence of conductance (G/Gmax) and availability (I/Imax) using a prepulse potential of -120 mV. (H) Peak I_{Na} density evoked by a depolarizing step from -120 mV to -10 mV. Significance determined using a Student's unpaired t-test

Fig. 3.11 shows the impact of stable $Na_v\beta1$ expression on Gβ1γ2 modulation of $Na_v1.1$-mediated I_{Na} properties in HEK cells. In contrast to Nav1.6, the presence of $Na_v\beta1$ subunits prevented Gβ1γ2 inhibition of peak $Na_v1.1$ I_{Na} density at a prepulse potential of -70 (Fig. 3.10D) (EGFP: -93.53 ± 15.95 pA/pF vs Gβ1γ2: -80.52 ± 13.69 pA/pF; P=0.5417) (Table 3.1) and -120 mV (Fig. 3.10H) (EGFP: -98.31 ± 16.54 pA/pF vs Gβ1γ2: -69.04 ± 11.82 pA/pF; P=0.1540) (Table 3.1). No changes were observed in the voltage-dependence of activation or availability when comparing the Gβ1γ2 and EGFP conditions at a prepulse potential of -70 mV (Fig. 3.11C) or -120 mV (Fig. 3.11G) (Table 3.3).

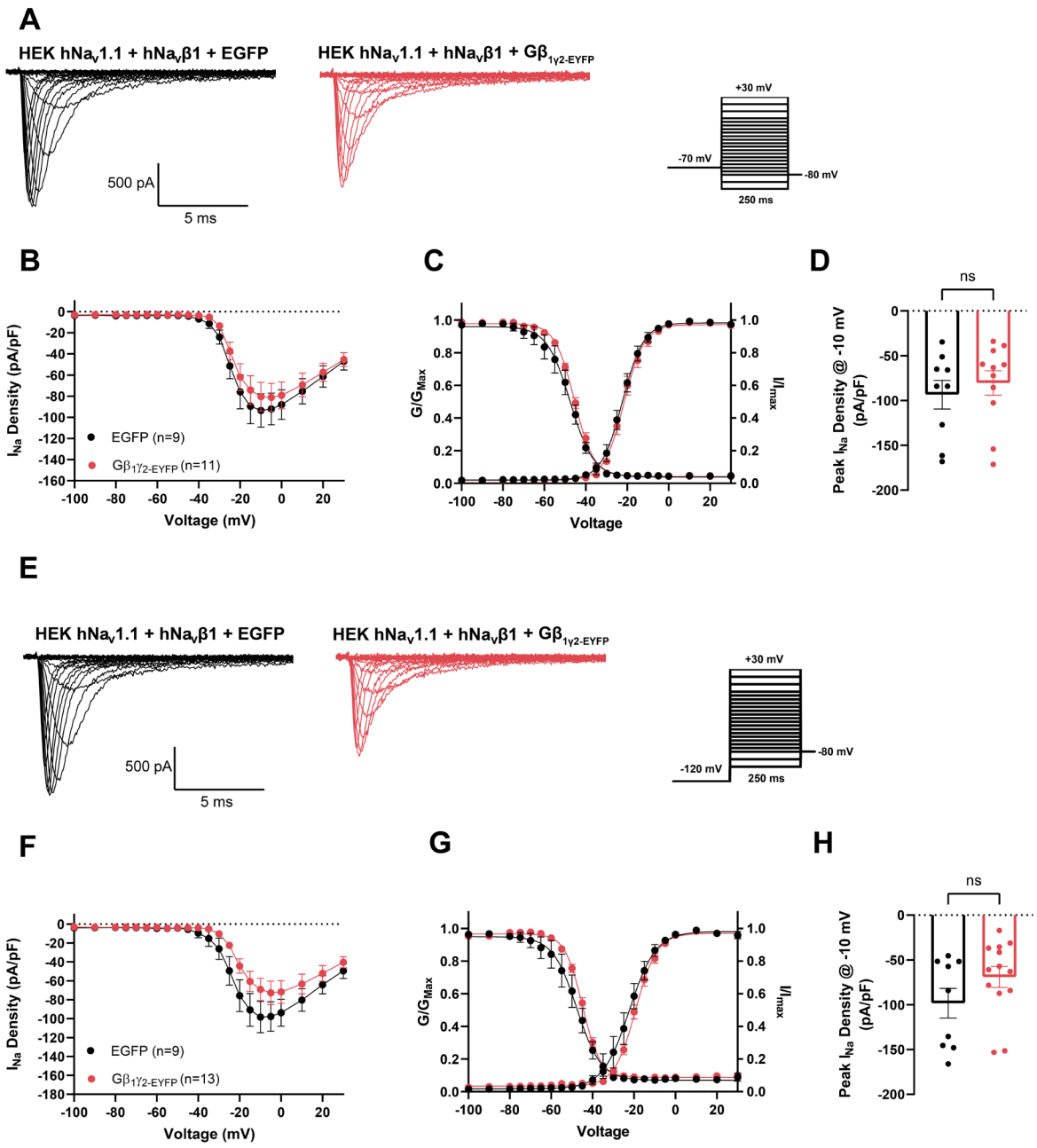


Figure 3.11 Transient co-expression of Gβ1γ2 or EGFP in HEK cells stably expressing human $Na_v1.1$ and human $Na_vβ1$. (A) Representative I_{Na} traces evoked with a prepulse potential of -70 mV in HEK cells stably expressing $Na_v1.1$ and $Na_vβ1$ transiently co-transfected with Gβ1 and γ2-EYFP (red) or EGFP only (black). (B) I-V relationship from a prepulse of -70 mV. (C) Normalized voltage-dependence of conductance (G/Gmax) and availability (I/Imax) using a -70 mV prepulse potential. (D) Peak I_{Na} density evoked by a depolarizing step from -70 mV to -10 mV. (E) Representative I_{Na} traces of HEK $Na_v1.1$ and $Na_vβ1$ cells expressing Gβ1γ2-EYFP or EGFP control from a prepulse of -120 mV. (F) I-V relationship from a prepulse of -120 mV. (G) Normalized voltage-dependence of conductance (G/Gmax) and availability (I/Imax) using a prepulse potential of -120 mV. (H) Peak I_{Na} density evoked by a depolarizing step from -120 mV to -10 mV. Significance determined using a Student's unpaired t-test

Transient co-expression of Gβ1γ2 has no impact on $Na_v1.5$ I_{Na} properties

$Na_v1.5$ is the predominant VGSC α subunit expressed in adult cardiac tissue (Catterall et al. 2020). Previous studies have shown that $Na_v1.5$ lacks sensitivity to modulation by coexpression of various Gβγ subunits in heterologous cells (Mantegazza et al. 2005). However, the sensitivity of $Na_v1.5$ to modulation by Gβ1γ2 subunits (a prominent Gβγ complex expressed in brain) has not been tested. Fig. 3.12 shows no significant Gβ1γ2 inhibition of $Na_v1.5$ I_{Na} density at a prepulse potential of -70 (Fig. 3.12C) (EGFP: -60.40 ± 12.00 pA/pF vs Gβ1γ2: -39.02 ± 13.52 pA/pF; P=0.7794) and -120 mV (Fig. 3.12F) (EGFP: -172.5 ± 11.54 pA/pF vs Gβ1γ2: -185.20 ± 39.56 pA/pF; P=0.2643). No changes were observed in the voltage-dependence of activation or availability when comparing the Gβ1γ2 and EGFP conditions at a prepulse potential of -70 mV (Fig. 3.12B) or -120 mV (Fig. 3.12E). These data suggest that Gβ1γ2 subunits do not functionally interact with the major cardiac VGSC subtype, $Na_v1.5$, in HEK cells. However, these data represent a small sample size of cells (n=6-7) and due to the cell-to-cell variance observed in $Na_v1.5$ peak I_{Na} density, further analysis of the impact of Gβ1γ2 on $Na_v1.5$ is required. This finding is important for any future therapeutic efforts that attempt to target Gβ1γ2, as functional engagement of $Na_v1.5$ may produce dangerous adverse cardiac effects.

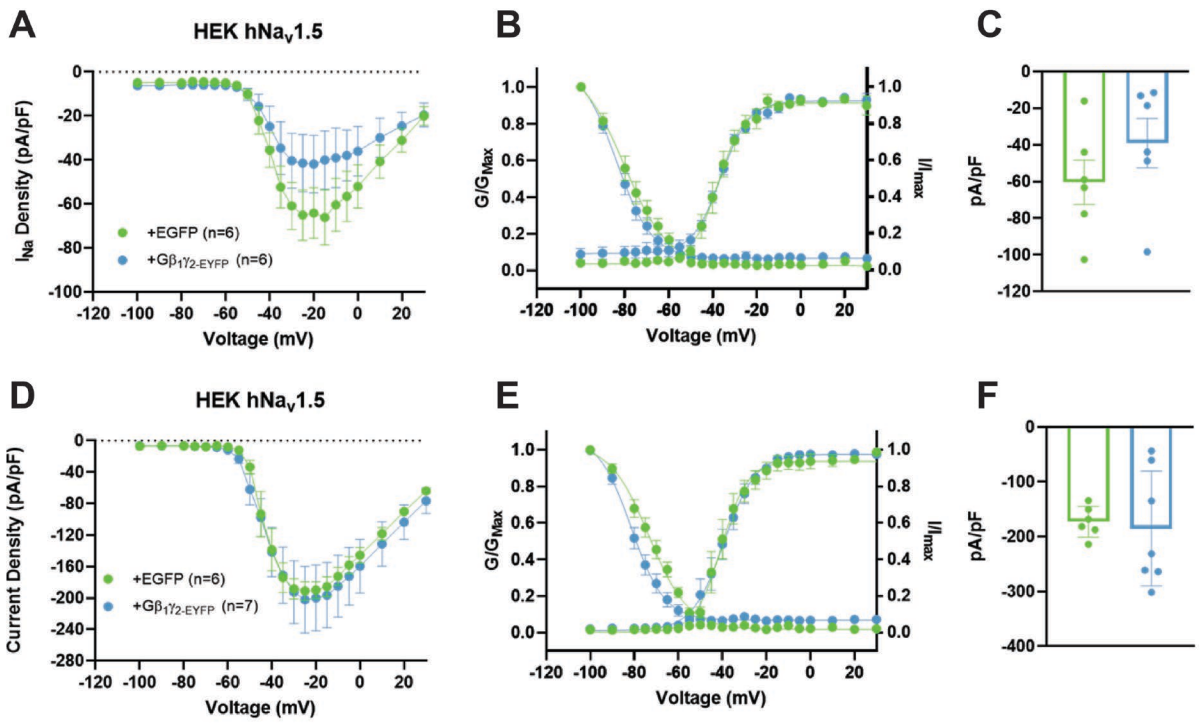


Figure 3.12. Transient co-expression of Gβ1γ2 has no effect on human $Na_v1.5$ I_{Na} properties in HEK cells. (A) I-V relationship of HEK $Na_v1.5$ cells expressing Gβ1γ2-EYFP (blue) or EGFP (green) from a prepulse of -70 mV. (B) Normalized voltage-dependence of conductance (G/Gmax) and availability (I/Imax) using a -70 mV prepulse potential. (C) Peak I_{Na} density evoked by a depolarizing step from -70 mV to -10 mV. (D) I-V relationship of HEK $Na_v1.5$ cells expressing Gβ1γ2-EYFP or EGFP from a prepulse of -120 mV. (E) Normalized voltage-dependence of conductance (G/Gmax) and availability (I/Imax) using a prepulse potential of -120 mV. (F) Peak I_{Na} density evoked by a depolarizing step from -120 mV to -10 mV.

Changes in mRNA expression of human Gβ, Gγ, and Gα subunits in HEK cells after stable expression of $Na_v1.6$ or $Na_v1.6$ and $Na_v\beta1$

Based on previous work demonstrating that the intracellular domain of $Na_v\beta1$ can undergo regulated intramembrane proteolysis and regulate transcription in the nucleus (Bouza et al. 2021), we examined whether stable expression of $Na_v\beta1$ affects G-protein subunit mRNA expression in HEK cells. We isolated mRNA from untransfected, $Na_v1.6$, and $Na_v1.6$ + $Na_v\beta1$ stable HEK cell lines and then performed RT-qPCR experiments to examine endogenous Gα, Gβ, and Gγ subunit mRNA expression (Fig. 3.13). We found that *GNAQ* was significantly different across cell lines ($p=0.0012$), with reduced overall *GNAQ* expression in the presence of $Na_v\beta1$ ($p<0.05$). *GNAO1* was significantly different across cell lines ($p<0.0001$), with $Na_v1.6$ HEK and $Na_v1.6$ + $Na_v\beta1$ HEK cells having increased expression compared to control ($p<0.0001$). *GNAI1* and *GNAS* did not differ between cell lines.

$Na_v1.6$ + $Na_v\beta1$ HEK cells had reduced mRNA expression of *GNB1* ($p<0.05$), *GNB4* ($p<0.001$), and *GNB5* ($p<0.05$) compared to $Na_v1.6$ HEK and control lines. *GNB2* was significantly reduced in $Na_v1.6$ + $Na_v\beta1$ HEK cells compared to control HEK cells ($p<0.01$). *GNB3* expression was downregulated in both $Na_v1.6$ HEK cells and $Na_v1.6$ + $Na_v\beta1$ HEK cells compared to control ($p<0.05$).

$Na_v1.6$ + $Na_v\beta1$ HEK cells had reduced mRNA expression of *GNG1* ($p<0.01$), *GNG2* ($p<0.0001$), *GNG7* ($p<0.001$), *GNG10* ($p<0.001$), compared to $Na_v1.6$ HEK and

untransfected control cell lines. The addition of $Na_v\beta1$ further reduced expression of these genes in comparison to HEK cells expressing $Na_v1.6$, suggesting potential transcriptional regulation of Gγ subunit mRNA expression by the $Na_v\beta1$ intracellular domain. *GNGT2* expression was reduced in both $Na_v1.6$ HEK cells and $Na_v1.6$ + $Na_v\beta1$ HEK cells compared to control ($p<0.001$), while the addition of $Na_v\beta1$ increased expression compared to HEK $Na_v1.6$ cells ($p<0.05$). *GNG3* ($p<0.01$), *GNG8* ($p<0.01$), and *GNG11* ($p<0.0001$) expression was decreased in both $Na_v1.6$ HEK cells and $Na_v1.6$ + $Na_v\beta1$ HEK cells compared to control. *GNG4* was significantly increased in both $Na_v1.6$ HEK cells and $Na_v1.6$ + $Na_v\beta1$ HEK cells compared to control ($p<0.0001$), while the inclusion of $Na_v\beta1$ reduced expression when compared to HEK $Na_v1.6$ cells ($p<0.0001$). *GNG12* expression was downregulated in $Na_v1.6$ + $Na_v\beta1$ HEK cells compared to $Na_v1.6$ HEKs ($p<0.05$) and *GNG13* expression was reduced in $Na_v1.6$ + $Na_v\beta1$ HEK cells compared to control cell lines ($p<0.05$).

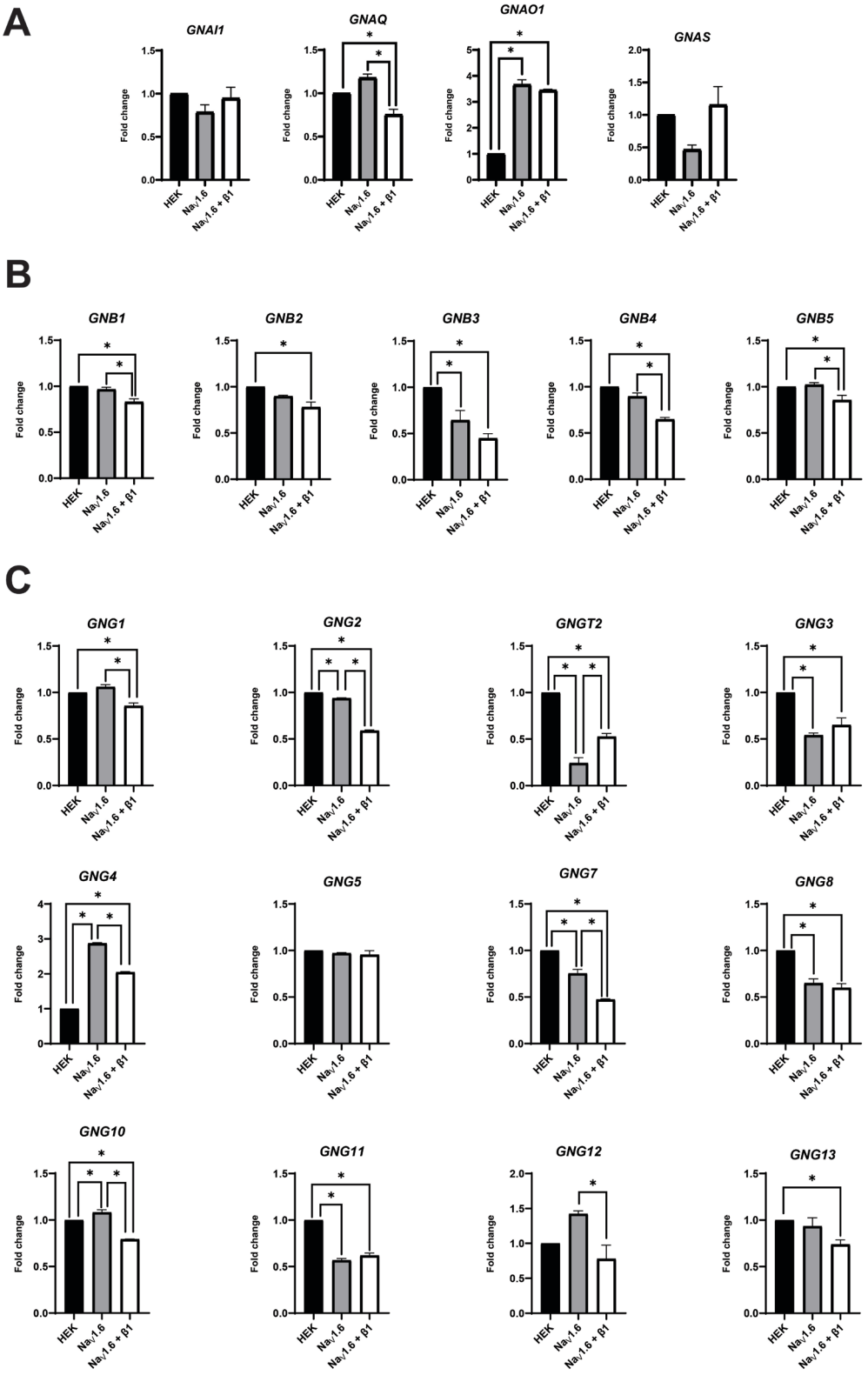


Figure 3.13 Fold change in mRNA expression levels of human Gβ, Gγ, and Gα subunits in untransfected, $Na_v1.6$ or $Na_v1.6$ and $Na_v\beta1$ stable HEK cell lines.

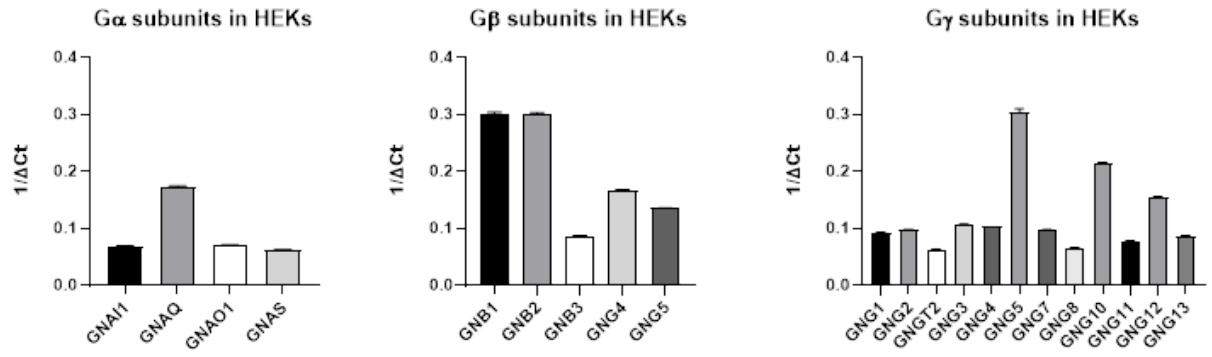


Figure 3.14 Baseline human Gβ, Gγ, and Gα subunit gene expression in HEK cells. (A) Gβ subunits, (B) Gγ subunits, (C) Gα subunits. Gene expression measurements on individual samples were performed in triplicate. The inverse of each ΔCt (delta cycle threshold) value was averaged for each gene and compared across subunits within each family. Data are expressed as mean ± SEM. N = 3 for each experiment.

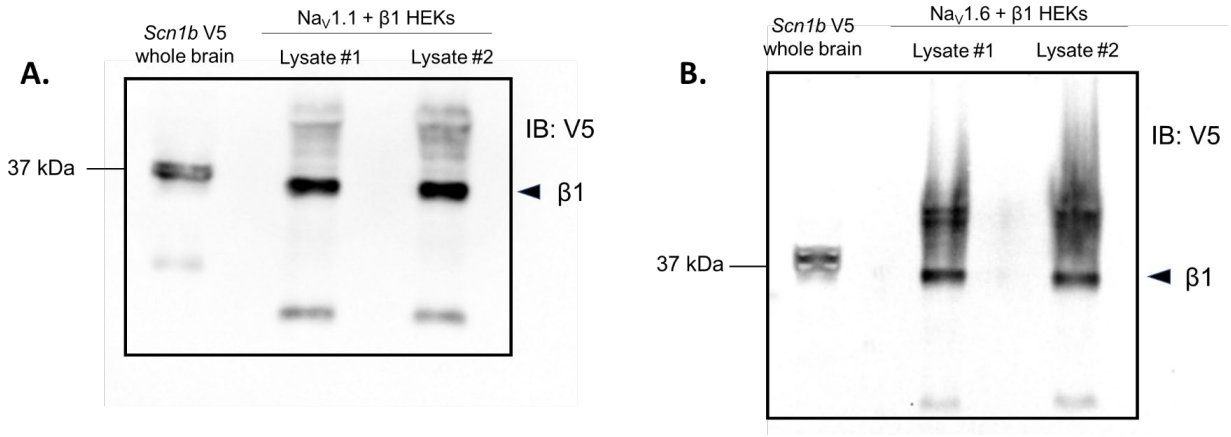


Figure 3.15 Western blots confirming Na$_v$β1 expression in (A) HEK Na$_v$1.1 + Na$_v$β1 and (B) HEK Na$_v$1.6 + Na$_v$β1 stable cell lines. N=2 for each experiment.

Investigation of neuronal firing properties of Gnb1$^{K78R/+}$ mice

GNB1-E is a devastating neurological disorder characterized by global developmental delays, motor, cognitive and sensory impairments, and seizures (Chapter I). The first patient that was identified with a pathogenic *GNB1*-E variant in published reports expressed the variant *GNB1*-p.K78R (c.233 A>G; p.K78R) (Petrovski et al. 2016). *Gnb1*$^{K78R/+}$ mice recapitulate many key features of the human *GNB1*-E phenotype, including developmental delay and spontaneous 'absence-like' generalized non-convulsive seizures (Colombo et al. 2019).

As a first attempt to understand differences in electrical excitability due to variants in Gβ subunits, we recorded from cortical layer 5 (L5) pyramidal neurons in brain slices prepared from *Gnb1*$^{K78R/+}$ mice. L5 pyramidal neurons are considered to be primary output units of the cortex that have dendrites spanning all layers capable of integrating local and long-range excitatory and inhibitory inputs from other cortical and subcortical regions (Larkum et al. 2009, Larkum 2013).

To investigate the contribution of L5 pyramidal neurons to the hyperexcitable networks underlying the epilepsy observed in *Gnb1*$^{K78R/+}$ mice, we performed current clamp recordings to assess the injection current to AP firing frequency relationship (F-I) and intrinsic properties of L5 pyramidal neurons in the somatosensory cortex vs. wildtype littermates at P16-18 (Fig. 3.16). We observed no significant differences in the F-I relationship and max firing frequency between *Gnb1*$^{K78R/+}$ vs wildtype L5 pyramidal

neurons (Fig.3.16A-B) (Table 3.5). Likewise, we also observed no significant changes in the resting membrane potential, AP threshold, 1st AP peak amplitude, 1st AP minimum dV/dt, 1st AP maximum dV/dt, input resistance or spike half-width (Fig. 3.16C) (Table 3.5).

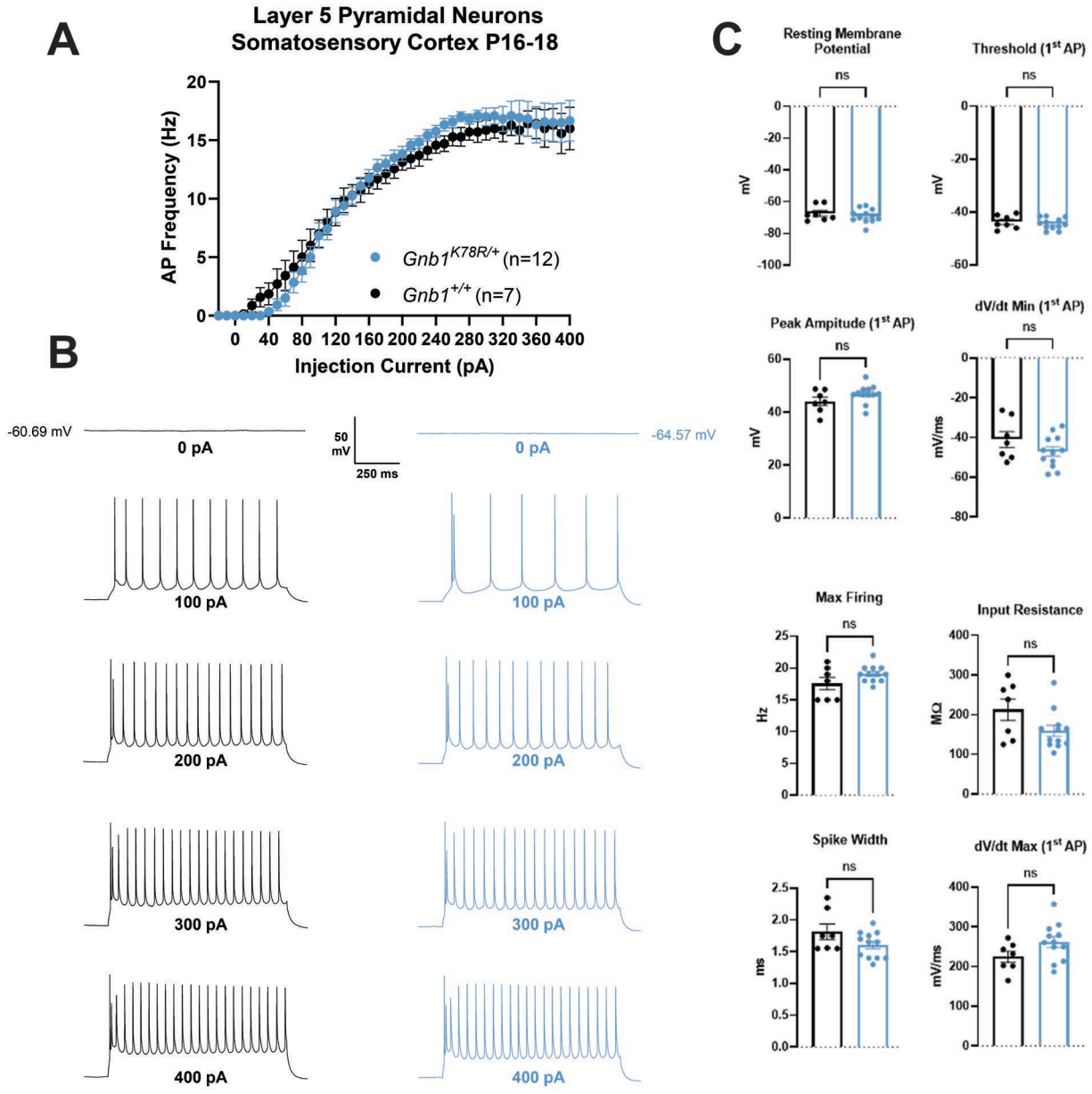


Figure 3.16 Somatosensory cortex layer 5 pyramidal neurons of Gnb1$^{K78R/+}$ mice show no changes in excitability or intrinsic properties. (A) Injection current to AP firing frequency relationship of somatosensory cortex L5 pyramidal neurons in Gnb1$^{K78R/+}$ (blue) vs. wildtype (black). (B) Representative AP trains at 0, 100, 200, 300 and 400 pA current injections in Gnb1$^{K78R/+}$ (blue) vs. wildtype (black). (C) Intrinsic properties of L5 pyramidal neurons.

Somatosensory cortical layer 2/3 pyramidal neurons of Gnb1$^{K78R/+}$ mice show deficits in presynaptic inhibitory neurotransmitter release

Based on previous reports hypothesizing that haploinsufficient loss of *Gnao1 can* increase levels of free Gβγ and lead to reduced presynaptic inhibitory neurotransmitter release in *Gnao1*^{G203R} mutant mice (Feng et al. 2022), we hypothesized that *Gnb1*$^{K78R/+}$ mice may show deficits in cortical inhibitory neurotransmission. To examine inhibitory neurotransmission, we performed voltage clamp recordings of spontaneous inhibitory postsynaptic currents (sIPSC) in layer 2/3 pyramidal neurons from slices of the somatosensory cortex of *Gnb1*$^{K78R/+}$ mice vs. wildtype littermates at P16-18 (3.17). Experimental conditions using pharmacological blockers of glutamate receptor-mediated excitatory postsynaptic currents and symmetric external and internal [Cl-] recording solutions resulted in inward GABAergic currents. No significant difference was observed in the sIPSC decay time constant (Fig. 3.17C) (*Gnb1*$^{K78R/+}$: 28.85 ± 2.66 ms vs : *Gnb1*$^{+/+}$ 26.63 ± 3.57; P=0.6206) or amplitude (Fig. 3.17D) (*Gnb1*$^{K78R/+}$: 28.14 ± 4.80 pA vs : *Gnb1*$^{+/+}$ 26.01 ± 2.68 pA; P=0.7157) when comparing *Gnb1*$^{K78R/+}$ vs. wildtype. L2/3 pyramidal neurons of *Gnb1*$^{K78R/+}$ mice showed significantly reduced sIPSC frequency compared to wildtype (Fig. 3.17E) (*Gnb1*$^{K78R/+}$: 0.796 ± 0.20 Hz vs *Gnb1*$^{+/+}$: 2.42 ± 0.41 Hz; P=0.0026**). The significant reduction in L2/3 pyramidal neuron sIPSC frequency, but not amplitude, suggests *Gnb1*$^{K78R/+}$ have a presynaptic disruption in cortical inhibitory transmission.

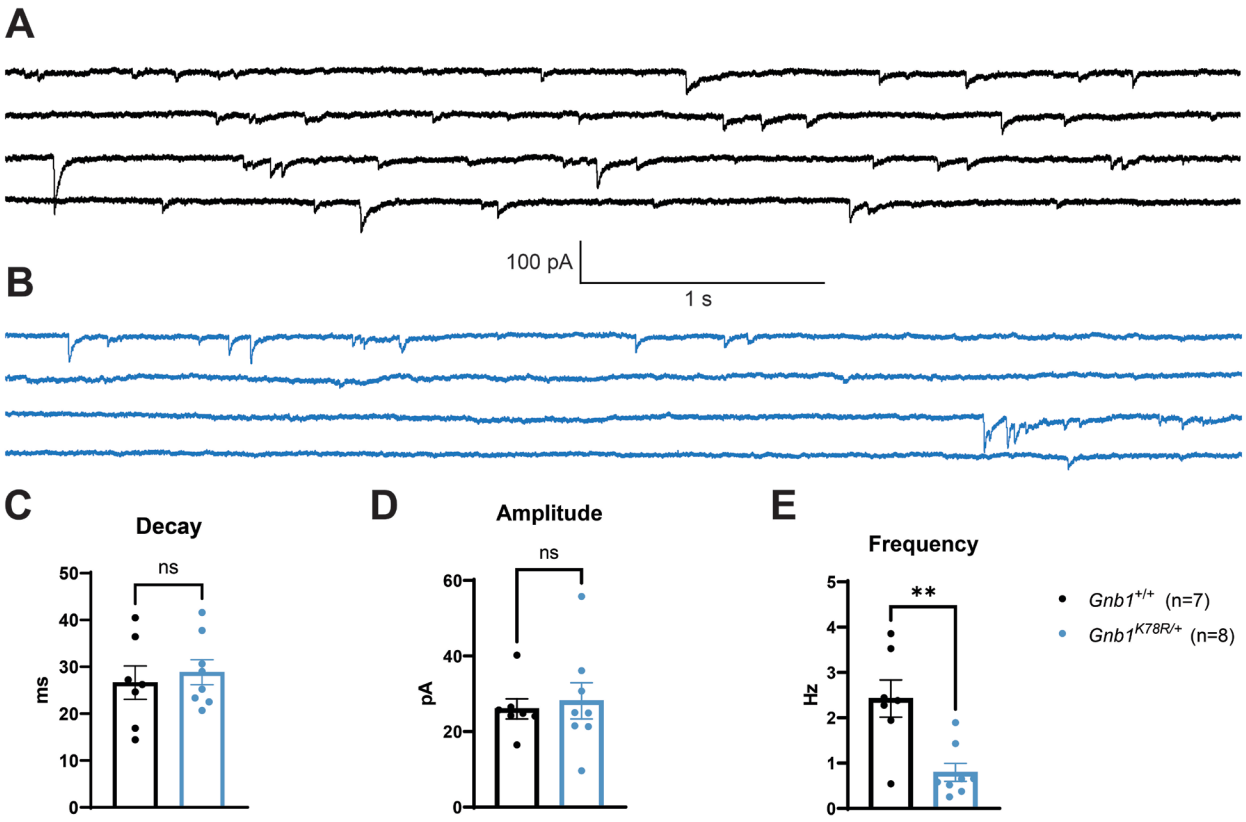


Figure 3.17 Spontaneous inhibitory postsynaptic currents (sIPSC) from somatosensory cortical layer 2/3 pyramidal neurons of *Gnb1*$^{K78R/+}$ mice show deficits in presynaptic inhibitory neurotransmitter release. (A) Representative sIPSC traces from wildtype *Gnb1*$^{+/+}$ mice. (B) Representative sIPSC traces from *Gnb1*$^{K78R/+}$ mice. (C) sIPSC decay time constant (D) amplitude and (E) frequency from wildtype *Gnb1*$^{+/+}$ (black) and *Gnb1*$^{K78R/+}$ (blue) layer 2/3 pyramidal neurons.

$Na_v1.6$ (-70 mV Prepulse)	Peak I_{Na} Density (pA/pF)
Gβ1γ2 (n=21)	-25.28 ± 2.69
EGFP (n=21)	-68.77 ± 9.33
Gβ1γ2 + 100 nM ST (n=7)	-25.43 ± 6.06
$Na_vβ1_{2A\text{-}EGFP}$ (n=7)	-110.7 ± 29.80

$Na_v1.1$ (-70 mV Prepulse)	Peak I_{Na} Density (pA/pF)
Gβ1γ2 (n=10)	-51.37 ± 8.46
EGFP (n=8)	-92.87 ± 12.25
Gβ1γ2 + 100 nM ST (n=9)	-79.76 ± 10.74
$Na_vβ1_{2A\text{-}EGFP}$ (n=4)	-143.8 ± 48.12

$Na_v1.6$ (-120 mV Prepulse)	Peak I_{Na} Density (pA/pF)
Gβ1γ2 (n=10)	-33.10 ± 5.45
EGFP (n=16)	-87.70 ± 13.35
Gβ1γ2 + 100 nM ST (n=7)	-28.33 ± 8.63
$Na_vβ1_{2A\text{-}EGFP}$ (n=7)	-119.9 ± 30.92

$Na_v1.1$ (-120 mV Prepulse)	Peak I_{Na} Density (pA/pF)
Gβ1γ2 (n=16)	-64.87 ± 7.79
EGFP (n=14)	-87.21 ± 9.15
Gβ1γ2 + 100 nM ST (n=10)	-74.38 ± 9.68
$Na_vβ1_{2A\text{-}EGFP}$ (n=6)	-148.2 ± 35.57

$Na_v1.6$ & $Na_vβ1$ (-70 mV Prepulse)	Peak I_{Na} Density (pA/pF)
Gβ1γ2 (n=9)	-42.59 ± 8.87
EGFP (n=7)	-124.9 ± 24.07

$Na_v1.1$ & $Na_vβ1$ (-70 mV Prepulse)	Peak I_{Na} Density (pA/pF)
Gβ1γ2 (n=13)	-80.52 ± 13.69
EGFP (n=11)	-93.53 ± 15.95

$Na_v1.6$ & $Na_vβ1$ (-120 mV Prepulse)	Peak I_{Na} Density (pA/pF)
Gβ1γ2 (n=10)	-47.72 ± 8.77
EGFP (n=7)	-120.6 ± 22.42

$Na_v1.1$ & $Na_vβ1$ (-120 mV Prepulse)	Peak I_{Na} Density (pA/pF)
Gβ1γ2 (n=11)	-69.04 ± 11.82
EGFP (n=9)	-98.31 ± 16.54

Table 3.1 Peak I_{Na} density @ -10 mV in HEK cells stably expressing $Na_v1.6$, $Na_v1.1$, $Na_v1.6$ and $Na_vβ1$ or $Na_v1.1$ and $Na_vβ1$ after transient co-expression of Gβ1γ2, EGFP, Gβ1γ2 + 100 nM staurosporine (ST) or $Na_vβ1$.

$Na_v1.1$ (-70 mV Prepulse)	**$V_{1/2}$ Activation (mV)**	**$V_{1/2}$ Inactivation (mV)**	**Activation Slope Factor (mV^{-1})**	**Inactivation Slope Factor (mV^{-1})**
Gβ1γ2 (n=10)	-23.19 ± 0.48	-48.95 ± 0.61	5.69 ± 0.42	-5.47 ± 0.53
EGFP (n=8)	-25.64 ± 0.49	-49.71 ± 0.38	5.03 ± 0.42	-5.08 ± 0.33
Na_vβ1 (n=4)	-23.06 ± 1.08	-47.65 ± 0.42	6.43 ± 0.93	-4.84 ± 0.36

$Na_v1.1$ (-120 mV Prepulse)	**$V_{1/2}$ Activation (mV)**	**$V_{1/2}$ Inactivation (mV)**	**Activation Slope Factor (mV^{-1})**	**Inactivation Slope Factor (mV^{-1})**
Gβ1γ2 (n=16)	-22.29 ± 0.42	-48.43 ± 0.53	5.74 ± 0.36	-5.90 ± 0.46
EGFP(n=14)	-23.18 ± 0.32	-46.99 ± 0.28	5.19 ± 0.28	-5.27 ± 0.24
Na_vβ1 (n=6)	-27.43 ± 1.04	-48.01 ± 0.33	6.18 ± 0.91	-4.84 ± 0.29

$Na_v1.6$ (-70 mV Prepulse)	**$V_{1/2}$ Activation (mV)**	**$V_{1/2}$ Inactivation (mV)**	**Activation Slope factor** (mV^{-1})	**Inactivation Slope factor** (mV^{-1})
Gβ1γ2 (n=21)	-17.76 ± 0.39	-52.78 ± 0.60	5.50 ± 0.33	-5.82 ± 0.52
EGFP (n=21)	-20.45 ± 0.26	-51.55 ± 0.28	5.21 ± 0.23	-5.81 ± 0.24
Na_vβ1 (n=7)	-26.89 ± 0.60	-53.94 ± 0.25	5.36 ± 0.52	-5.68 ± 0.22

$Na_v1.6$ (-120 mV Prepulse)	**$V_{1/2}$ Activation (mV)**	**$V_{1/2}$ Inactivation (mV)**	**Activation Slope factor (mV^{-1})**	**Inactivation Slope factor (mV^{-1})**
Gβ1γ2 (n=10)	-18.82 ± 0.46	-55.50 ± 0.99	5.45 ± 0.40	-6.35 ± 0.86
EGFP (n=16)	-21.30 ± 0.31	-51.64 ± 0.32	5.33 ± 0.27	-5.58 ± 0.27
Na_vβ1 (n=7)	-25.07 ± 0.60	-53.12 ± 0.26	5.65 ± 0.52	-5.55 ± 0.22

Table 3.2 Voltage dependent properties of HEK cells stably expressing $Na_v1.1$ or $Na_v1.6$ after transient co-expression of Gβ1γ2, EGFP or Na_vβ1.

$Na_v1.6$ & $Na_v\beta1$ (-70 mV Prepulse)	**$V_{1/2}$ Activation (mV)**	**$V_{1/2}$ Inactivation (mV)**	**Activation Slope Factor (mV^{-1})**	**Inactivation Slope Factor (mV^{-1})**
Gβ1γ2(n=9)	-20.27 ± 0.59	-55.07 ± 0.71	5.58 ± 0.51	-5.65 ± 0.61
EGFP (n=7)	-21.33 ± 0.42	-50.08 ± 0.24	4.90 ± 0.36	-4.86 ± 0.21

$Na_v1.6$ & $Na_v\beta1$ (-120 mV Prepulse)	**$V_{1/2}$ Activation (mV)**	**$V_{1/2}$ Inactivation (mV)**	**Activation Slope Factor (mV^{-1})**	**Inactivation Slope Factor (mV^{-1})**
Gβ1γ2 (n=10)	-19.10 ± 0.49	-53.30 ± 0.64	5.88 ± 0.42	-4.92 ± 0.55
EGFP (n=7)	-19.59 ± 0.47	-48.64 ± 0.48	5.26 ± 0.40	-5.14 ± 0.41

$Na_v1.1$ & $Na_v\beta1$ (-70 mV Prepulse)	**$V_{1/2}$ Activation (mV)**	**$V_{1/2}$ Inactivation (mV)**	**Activation Slope Factor (mV^{-1})**	**Inactivation Slope Factor (mV^{-1})**
Gβ1γ2 (n=11)	-21.57 ± 0.31	-44.93 ± 0.22	4.86 ± 0.27	-4.27 ± 0.19
EGFP (n=9)	-22.34 ± 0.39	-47. 63 ± 0.82	5.09 ± 0.33	-5.78 ± 0.71

$Na_v1.1$ & $Na_v\beta1$ (-120 mV Prepulse)	**$V_{1/2}$ Activation (mV)**	**$V_{1/2}$ Inactivation (mV)**	**Activation Slope Factor (mV^{-1})**	**Inactivation Slope Factor (mV^{-1})**
Gβ1γ2 (n=13)	-19.25 ± 0.29	-44.93 ± 0.22	5.12 ± 0.25	-4.27 ± 0.19
EGFP (n=9)	-22.29 ± 0.72	-47.63 ± 0.82	6.38 ± 0.62	-5.78 ± 0.71

Table 3.3 Voltage dependent properties of HEK cells stably expressing $Na_v1.1$ and $Na_v\beta1$ or $Na_v1.6$ and $Na_v\beta1$ after transient co-expression of Gβ1γ2 or EGFP.

$Na_v1.1$	Capacitance (pF)
Gβ1γ2 (n=16)	14.3 ± 0.85
EGFP (n=14)	16.18 ± 0.91
$Na_vβ1_{2A\text{-}EGFP}$ (n=6)	12.56 ± 2.32
Gβ1γ2 + 100 nM ST (n=9)	14.11 ± 0.79

$Na_v1.1$ & $Na_vβ1$	Capacitance (pF)
Gβ1γ2 (n=13)	15.04 ± 1.41
EGFP (n=9)	13.13 ± 1.45

$Na_v1.6$	Capacitance (pF)
Gβ1γ2 (n=27)	9.47 ± 0.68*
EGFP (n=23)	11.90 ± 0.71
$Na_vβ1_{2A\text{-}EGFP}$ (n=7)	11.72 ± 1.00
Gβ1γ2 + 100 nM ST (n=7)	5.15 ± 1.07

$Na_v1.6$ & $Na_vβ1$	Capacitance (pF)
Gβ1γ2 (n=10)	7.51 ± 0.62
EGFP (n=7)	9.34 ± 1.67

Table 3.4 Capacitance of HEK cells stably expressing Nav1.1, Nav1.6, $Na_v1.1$ and $Na_vβ1$ or $Na_v1.6$ and $Na_vβ1$ transiently co-expressing Gβ1γ2, Gβ1γ2 + 100 nM staurosporine, EGFP, or $Na_vβ1$. Gβ1γ2 Gβ1γ2 vs. EGFP (P=0.017) Significance determined using a Student's unpaired t-test (*P=0.017)

	Gnb1$^{+/+}$ (n=7)	*Gnb1*$^{K78R/+}$ (n=12)
Resting V_m (mV)	-67.23 ± 1.86	-68.98 ±1.26
Input Resistance (MΩ)	212. ± 27.12	159.5 ± 14.05
Max Firing Rate (Hz)	17.57 ± 0.97	19.08 ± 0.38
Spike Width (ms)	1.81 ± 0.12	1.60 ± 0.06
1st AP Peak Voltage (mV)	44.08 ± 1.61	46.90 ± 0.98
1st AP Max dv/dt (mV/ms)	224.3 ± 13.92	261.6 ± 13.56
1st AP Min dv/dt (mV/ms)	-40.98 ± 3.96	-47.10 ± 2.33
1st AP Threshold (mV)	-43.75 ± 0.97	-44.37 ± 0.62

Table 3.5 Intrinsic properties and maximum firing frequency of somatosensory cortex layer 5 pyramidal neurons of Gnb1^{K78R+} mice (blue) vs wildtype littermates at postnatal day 16-18.

Discussion

Gβγ modulation of neuronal excitability through ion channel effectors has been largely focused on voltage-gated Ca^{2+} and K^+ channels, however, evidence suggests VGSCs deserve further investigation (see Chapter I). Our work shows that Gβ1, Gβ2, Gγ2, Gγ3, Gγ7 and Gγ12 associate in a protein complex with $Na_v\alpha$ and β1 subunits in P18 mouse whole brain. Furthermore, we provide evidence for functional association of these important signaling molecules.

Transient expression of Gβ1γ2 decreases $Na_v1.6$ I_{Na} density and shows acute voltage-dependent prepulse relief

$Na_v1.6$ is the most abundant VGSC expressed in the adult brain (Goldin 2001). Despite its biological prominence, the sensitivity of $Na_v1.6$ to modulation by Gβγ subunits was unknown prior to this study. Elucidating the extent of G-protein βγ subunit modulation of VGSCs expressed in brain neurons, including $Na_v1.6$, is critical for understanding neurotransmission and the development of novel treatments for neurological disorders. Our works shows that transient co-expression of Gβ1γ2 in HEK cells stably expressing human $Na_v1.6$ induces a significant decrease in peak whole cell I_{Na} density. The decrease in $Na_v1.6$ I_{Na} density was significant at a prepulse potential of both -70 mV and -120 mV, indicating Gβ1γ2 can reduce $Na_v1.6$ I_{Na} at depolarized potentials close to the resting membrane potential in neurons (-70 mV) and when all VGSCs are available at hyperpolarized potentials (-120 mV). Surprisingly, no shifts in the voltage-dependence of activation or inactivation of $Na_v1.6$ were induced by the co-expression of Gβ1γ2 in

HEK cells. This suggests that the Gβ1γ2 inhibits $Na_v1.6$-mediated current by reducing I_{Na} density without altering the voltage-dependence of gating. Furthermore, we showed that preincubation with staurosporine had no effect on the Gβ1γ2 inhibition of $Na_v1.6$ at -70 or -120 mV prepulse potentials. This evidence suggests PKA/PKC inhibition does not play a role in the inhibition of $Na_v1.6$ in HEK cells. Acute prepulse relief of Gβγ inhibition of $Ca_v2.2$ channels has been well established as evidence for the membrane-delimited modulation of VGCCs by Gβγ (Zamponi and Currie 2013). Our work shows that Gβ1γ2 inhibition of $Na_v1.6$ peak I_{Na} density in HEK cells shows acute voltage-dependent prepulse relief after prolonged hyperpolarization for 1 s at -120 mV. Taken together, this work provides strong evidence that Gβ1γ2 may inhibit brain Nav1.6 channels in a membrane-delimited manner.

Transient expression of Gβ1γ2 decreases $Na_v1.1$ I_{Na} only at depolarized membrane potentials

Coexpression of Gβ1γ2 in HEK cells stably expressing human $Na_v1.1$ also led to a significant decrease in I_{Na} density from a prepulse potential of -70 mV, but not -120 mV. This voltage-dependence of Gβ1γ2 modulation of $Na_v1.1$ suggests that $Na_v1.1$ is more sensitive to modulation by Gβ1γ2 at depolarized membrane potentials. This could be due to a voltage-dependent confirmation of the channel enhancing sensitivity to Gβ1γ2, or enhanced activity of downstream signaling effectors such at depolarized potentials that are contributing to the inhibition of $Na_v1.1$. No shifts in the voltage-dependence of

activation or inactivation of $Na_v1.1$ were observed after the coexpression of Gβ1γ2 subunits. PKA/PKC inhibition insignificantly reduced the inhibition of $Na_v1.1$-mediated I_{Na} by Gβ1γ2 at a prepulse of -70 mV. Staurosporine is a broad-spectrum kinase inhibitor with an IC_{50} < 30 nM for PKA and PKC (Meggio et al. 1995). It is possible that other kinases could be contributing to the Gβ1γ2 inhibition of $Na_v1.1$ in HEK cells that were not affected by staurosporine preincubation.

In contrast to $Na_v1.6$, the Gβ1γ2 inhibition of $Na_v1.1$ did not show any voltage-dependent prepulse relief after 1 s hyperpolarization of the membrane to -120 mV. This observation, coupled with the lack of Gβ1γ2 inhibition of $Na_v1.1$ at -120 mV prepulse potentials, suggests that downstream effectors or 2nd messengers are involved in the functional interaction between Gβ1γ2 and $Na_v1.1$.

Transient expression of Gβ1γ2 leads to variable effects on $Na_v1.6$ and $Na_v1.1$ persistent I_{Na}

One of the major findings from previous reports of transient co-expression of Gβγ subunits with VGSCs in heterologous cells was a dramatic increase in persistent I_{Na} (Mantegazza et al. 2005). However, this effect was only observed with certain Gβγ subunit combinations (i.e., Gβ2γ3) and only in a proportion of cells tested. We observed similarly complex effects on persistent I_{Na} in HEK $Na_v1.6$ and $Na_v1.1$ cells after transient coexpression of Gβ1γ2. We detected a significant decrease in the mean $Na_v1.6$ persistent I_{Na} density compared to cells expressing EGFP, however, when normalized

as a ratio of the transient peak I_{Na} there was no significant change in $Na_v1.6$ persistent I_{Na} induced by Gβ1γ2. At present, it is unclear why the observed reduction in unnormalized $Na_v1.6$ persistent I_{Na} is not observed when normalized to peak transient current. It is possible that Gβ1γ2 is producing a similarly uniform inhibition of both transient and persistent components of Nav1.6 mediated I_{Na}. These data motivate further evaluation into the modulation of $Na_v1.6$ persistent I_{Na} by Gβ1γ2.

The mean persistent I_{Na} density and normalized persistent to peak I_{Na} density mediated by $Na_v1.1$ did not show any significant changes after transient co-expression of Gβ1γ2. Intriguingly, there were a subset of HEK $Na_v1.1$ cells tested that showed dramatic increases (>20%) in persistent to peak I_{Na} density. 30% of HEK $Na_v1.1$ cells co-expressing Gβ1γ2 produced >20% persistent/peak I_{Na} density while 0% of cells from the EGFP condition did. This finding suggests inherent variability in the effects of Gβ1γ2 on persistent I_{Na}, which is consistent with previous reports using other Gβγ subunit combinations. Another factor complicating the analysis of Gβ1γ2 on persistent I_{Na} in HEK cells is the baseline intrinsic variability of persistent I_{Na} observed. Cell to cell variability in persistent I_{Na} is common and is likely confounding the interpretation of Gβ1γ2 modulation of persistent I_{Na} in HEK cells. Nevertheless, given the vital and dynamic impact of persistent I_{Na} on neuronal firing properties, further work examining the impact of Gβγ subunits (especially Gβ1γ2) on persistent I_{Na} in neurons is warranted.

Co-expression of Gβ1γ2 did not affect the accumulation of slow inactivated $Na_v1.1$ or $Na_v1.6$-mediated I_{Na} in HEK cells using a 50 Hz train of depolarizing steps. This was surprising as GPCR neuromodulation of VGSCs by monoamines can enhance slow inactivation of VGSCs in acutely isolated neurons (Carr et al. 2003). Giving the very limited set of proteins and excitability-enabling components present in HEK cells compared to the rich repertoire of molecular machinery expressed in neurons, the lack of observed Gβ1γ2 modulation of $Na_v.1$ or $Na_v1.6$ slow inactivation in HEK cells should be interpreted with caution and deserves further experimentation in native neuronal preparations.

Co-expression of Na_vβ1 subunits alters Gβ1γ2 inhibition of $Na_v1.1$ but not $Na_v1.6$ mediated I_{Na}

Na_vβ1 subunits associate with all neuronal VGSC α subunits, including $Na_v1.6$ and $Na_v1.1$. Understanding the role of Na_vβ1 subunits in Gβ1γ2 modulation of VGSC activity, and thus neuronal excitability, is important to fully understand this signal transduction cascade. Na_vβ1 coexpression with $Na_v1.1$, but not $Na_v1.6$, abolishes I_{Na} inhibition by Gβ1γ2. These data suggest Na_vβ1 may compete with the Gβ1γ2 complex in its interaction with VGSC α subunits. These data also raise the hypothesis that Gβ1γ2 (or an indirect signaling effector activated by Gβ1γ2) may differ between $Na_v1.6$ and $Na_v1.1$ subtypes.

One potential limitation of my experiments performed in HEK cells is the endogenous expression of Gβγ subunits and other VGSC subtypes that may contribute to the observed whole cell I_{Na} properties. In a recent review of the endogenous voltage-gated ion channels present in HEK-293 cells (Zhang et al. 2022) multiple studies have indicated low background endogenous expression of TTX-sensitive VGSCs, typically producing current amplitudes around 50-200 pA (depending on the composition of the recording solutions used) (Zhang et al. 2022). The endogenous TTX-sensitive I_{Na} present in HEK-293 cells is primarily associated with $Na_v1.7$, and trace amounts of $Na_v1.2$, $Na_v1.3$, and $Na_v1.5$ were also detected (He and Soderlund 2010, Zhang et al. 2022)

Under normal physiological conditions, the classical dissociation model of the heterotrimeric Gαβγ complex proposes that ligand or constitutive activation of a GPCR permits Gβγ subunits to become 'free' to modulate signaling effectors after dissociation from the activated GTP-bound Gα subunit. Whether or not free Gβγ subunits exist under physiological conditions that can modulate effectors without originally being released from Gα subunits is still under debate. The experiments performed in HEK cells throughout this chapter used a transient overexpression of Gβ1γ2 subunits that presumably leads to chronically elevated levels of free Gβ1γ2 that would not be observed physiologically. This limitation is important to consider when interpreting how these data would compare to endogenous modulation of VGSC function by Gβ1γ2 subunits released via GPCR activation. Further work is needed to identify and link a specific GPCR to Gβγ modulation of VGSCs, preferably in a neuronal system with

greater similarity to physiological conditions. Potential experimental methods to investigate the effects of endogenous Gβγ subunits on VGSC function in neurons are discussed in Chapter 4.

Another limitation of these experimental interpretations that will be explored in future experiments is the effect of transient overexpression of Gβ1γ2 on the cell surface expression of VGSCs. Free Gβγ subunits are known to translocate to numerous organelles and modulate the expression of membrane proteins. One possible explanation for the significant decrease in whole cell I_{Na} after co-expression of Gβ1γ2 is the downregulation of VGSC expression or trafficking to the membrane. We plan to test this hypothesis using [^{3}H]-saxitoxin binding assays in HEK cells stably expressing $Na_v1.1$ or $Na_v1.6$ and comparing total vs membrane expression of VGSCs between cells transiently expressing Gβ1γ2 vs. EGFP.

Collectively, these data show the neuronal VGSC subtypes $Na_v1.1$ and $Na_v1.6$ are relevant effectors of Gβ1γ2 signaling in heterologous cells. Given the significant role of Gβγs in neurotransmission and neuropharmacology, as well as the roles of $Na_v1.1$ and $Na_v1.6$ in controlling neuronal excitability, these data motivate further characterization of this functional interaction in native neuronal preparations.

Gnb1$^{K78R/+}$ *mice show deficits in cortical layer 2/3 presynaptic inhibitory transmitter release*

Unbiased exome sequencing has revealed the breadth of biological processes implicated in epilepsy. Over 100 new genes have been implicated in epilepsy since the implementation of next generation sequencing (Knowles et al. 2022). These genes include chromatin remodelers, transcription factors, synaptic proteins, and cell signaling proteins, including G-proteins, highlighting the diversity of pathogenic mechanisms implicated in epilepsy and moving the disorder beyond channelopathies. Despite this rapid progress, we lack the animal and cellular models, as well as the experimental paradigms, to study how pathogenic variants in non-ion-channel genes cause epilepsy. Moreover, our growing appreciation for the genetic causes of epilepsy has not yet translated into new therapeutic options for the ~30% of patients with refractory epilepsy.

Our work presented here on *Gnb1*$^{K78R/+}$ mice represents the first investigation of a *GNB1*-E mouse model using brain slice electrophysiology. *Gnb1*$^{K78R/+}$ mice display spontaneous seizures and SWD involving the cortex on EEG (Teng et al. 2022). For this reason, we hypothesized cortical layer 5 pyramidal neurons may be intrinsically hyperexcitable. Surprisingly, we observed no differences in the F-I relationship, or any active or passive membrane properties of somatosensory cortical layer 5 pyramidal neurons of *Gnb1*$^{K78R/+}$ mice vs. their wildtype littermates at P16-18. These data suggest the hyperexcitability underlying seizures in *Gnb1*$^{K78R/+}$ mice are not driven by layer 5 pyramidal neurons and may exist in other brain regions or cell types. Layer 5 pyramidal

neurons represent a major unit of computation and integration within the cortex that serve as a primary output of cortical excitability. They also sit downstream in the hierarchy of feedforward sensory input in cortical columns, suggesting the hyperexcitability driving epileptogenesis in *Gnb1*$^{K78R/+}$ mice may be in layers further upstream in the hierarchy such as layer 4 or layer 2/3. This hypothesis is further supported by recent study showing that sensory input reinforces SWD in *Gnb1*$^{K78R/+}$ mice (Teng et al. 2022), suggesting a bottom-up regulation of epileptogenesis in *Gnb1*$^{K78R/+}$ mice.

Methods

Cell lines

Human Embryonic Kidney (HEK) 293T cells stably expressing human VGSC α subunits $Na_v1.1$ (accession #: NP_001159435.) or $Na_v1.6$ (accession #: NP_055006.1) cDNAs were cultured in Dulbecco's Modified Eagle Medium containing (4.5 g/L D-glucose, L-glutamine, 10% heat-inactivated FBS, 110 mg/L sodium pyruvate, 200 µg/mL G418, 100 U/mL penicillin/streptomycin). HEK cells stably expressing human $Na_v1.1$ and $Na_vβ1$ (accession #: NP_001028.1) or $Na_v1.6$ and $Na_vβ1$ were cultured in the same media with the addition of 200 µg/mL hygromycin. HEK cells stably expressing GIRK1/2 subunits were a generous gift from Dr. Alan Smrcka cultured under the same conditions described above using G418 selection and maintenance. All cells were maintained in an incubator at 37°C with 5% CO_2 until the time of recording.

Plasmids and transient transfections

For transient transfections, a synthesis-optimized human wildtype $Na_v\beta1$-V5 cDNA was generated by gBLOCK from Integrated DNA technologies. The bicistronic cDNA construct included an in-frame $Na_v\beta1$ C-terminal V5 epitope tag followed by a self-cleaving 2A peptide and enhanced green fluorescent protein (EGFP) to facilitate immunodetection of transiently expressed $Na_v\beta1$. Using the Gateway cloning system, this construct was moved from pENTR-SD/D-TOPO to pcDNAdest40 via LR Clonase reaction according to the manufacturers' protocol.

For $Na_v\beta1$ stable lines, wildtype $Na_v\beta1$ cDNA was generated by PCR using human $Na_v\beta1$ cDNA using pcDNA3 as the template. The cDNA was inserted into pcDNA3.1 Hygro(+). cDNA was amplified by PCR to remove the stop codon and then inserted into pcDNA3.1/V5–HIS using the pcDNA3.1/V5–HIS TOPO TA Expression kit (Invitrogen), according to the instructions of the manufacturer, to produce the V5–HIS-tagged $Na_v\beta1$ subunits with the Hygro(+) cassette. Gβ1 and Gγ2 plasmids were a generous gift from Dr. Alan Smrcka. *Ovis aries* AVI (ELNDIFEAQKIEWHE)-tagged-Gβ1 and enhanced YFP (EYFP)- tagged Gγ2 were in a pCI-neo vector. HEK stable cell lines expressing wildtype $Na_v\beta1$ were confirmed via western blot (Fig. 3.15) Cells transiently transfected by EGFP alone were used for control experiments. Sequences for all plasmids were confirmed and PCR primers and conditions for all reactions are available on request

To generate $Na_v1.6$ or $Na_v1.1$ ± $Na_v\beta1$ stable HEK cell lines, 1 µg cDNAs were transfected with 5 µL Lipofectamine 2000. Approximately 48 hours after transfection, cells were passed into fresh media containing 600 µg/mL G418 or hygromycin. The cells were incubated for approximately 1 week until individual colonies were isolated and grown until confluent and subsequently passaged for biochemical characterization. Electrophysiological experiments involving Gβ1γ2 used transient transfection. A total of 1 µg of each cDNA was transfected with 5 µL Lipofectamine 2000. Approximately 24 hours after transfection, cells were plated onto poly-D-lysine-coated coverslips glass cover slips for whole cell recordings. EYFP or EGFP-positive cells were identified via fluorescence and whole cell recordings were performed approximately 24–48 hours after final plating.

Mouse Models

Animals were housed in the Unit for Laboratory Animal Medicine at the University of Michigan. All procedures were performed in accordance with the NIH and approved by the University of Michigan IACUC. All mice were maintained on a 12:12 h light:dark cycle and had *ad libitum* access to food and water throughout the experiments. Male and female mice were used in all experiments.

Gnb1$^{K78R/+}$ mice were a generous gift from Drs. Yueqing Peng and Wayne Frankel from Columbia University. *Gnb1*$^{K78R/+}$ mice were generated using CRISPR/Cas9 as described in (Colombo et al. 2019). For *Gnb1* genotyping, DNA was extracted from the tail and

PCR was performed using the following primers: Forward: CGAGCATTGAGATCCTCTTTC; Reverse: GTCATCATTGCTCCATCAACAG. The restriction enzyme HinfI was used to distinguish wildtype from *Gnb1*$^{K78R/+}$ mice. All *Gnb1* mice were used for experiments between postnatal day (P16-P18).

Scn1b-V5 knock-in mice were generated using CRISPR/Cas9 technology to add a V5 epitope tag to the carboxyl terminus of the mouse *Scn1b* gene. Exon 5 of ensemble gene model transcript *Scn1b*-001 (ENSMUSE00000533876) encodes the carboxyl terminus of the protein. The CRISPOR algorithm (Haeussler et al. 2016) was used to identify specific guide RNA targets (gRNA). gRNA predicted to cut the chromosome near codon 218 were subcloned in plasmid pX330-U6-Chimeric_BB-CBh-hSpCas9 (Cong et al. 2013) and tested to determine if they cause chromosome breaks. pX330 plasmids were co-electroporated with a puromycin selection plasmid into mouse ES cells. After drug selection, surviving cells were pooled and genomic DNA was prepared. PCR with primers spanning the predicted cut site was used to generate amplicons for Sanger sequencing. The process is essentially as described (Mashiko et al. 2014, Sakurai et al. 2014). Sequence chromatograms of amplicons were evaluated to determine if small insertions/deletions caused by non-homologous endjoining (NHEJ) repair of chromosome breaks were present. gRNA C60G3 was found to be the most active, which targets the sequence 5’ CTGGCGATGCGCAGACCCGT (PAM=CGG) 3’ with a high specificity score (CFD score of 96, Doench et al. 2016). After determining that C60G3 caused chromosome breaks 5 ng/μL of the pX330 plasmid was combined with 10 ng/μL of a single stranded oligonucleotide DNA donor (Integrated DNA

Technologies). The CRISPR reagents were microinjected into fertilized mouse eggs produced by mating super-ovulated C57BL/6J female mice (Jackson Laboratory stock no. 000664) to C57BL/6J male mice as described (Van Keuren et al. 2009). Generation zero founder (G0) pups were identified by Sanger sequencing of amplicons spanning exon 5 and the V5 tag. G0 founders were mated with wild type C57BL/6J mice to obtain germline transmission of the *Scnb1-V5* mutant. The use of high specificity sgRNA and ESPCAS9 makes an off-target hit in mouse models highly unlikely (Anderson et al. 2018). The sequence of the single stranded oligonucleotide DNA donor was:

CCTTCCCTTGCACAGCTCAGAATACCTGGCCATTACATCCGAGAGCAAAGAAAACT GTACAGGCGTCCAGGTGGCTGAA**GGCAAGCCTATCCCTAACCCTCTCCTCGGCCT CGATTCTACC**tagCGCTGGTAAGGTTGATGGAAAGACGGGATCCTGCGCATCGCCA GCCAGGAGGGCTCAGGGACACACTCTTAAGTCT

Exon 5 is underlined. The V5 coding sequence is shown in bold. Lower case letters indicate the termination codon

LC/MS/MS proteomics

To identify protein binding partners of the VGSC β1 subunit, $Na_V\beta1$ was immunoprecipitated via pull-down of the V5 tag in whole brain homogenates from postnatal day 18 (P18) *Scn1b*-V5 tagged mice. V5 ($Na_V\beta1$) and IgG control immunoprecipitation samples were subjected to in-gel proteolytic digestion using trypsin. Samples were reduced with DTT, alkylated with iodoacetamide, and incubated at 37°C overnight in the presence of trypsin. The digests were analyzed using nano

LC/MS/MS on a Orbitrap Lumos Fusion mass spectrometer. Gradient elution was over a 10 cm 75 μm ID C18 column at 400 nL/min, with a 30 min gradient employed. MS/MS data were searched against the NCBI mouse protein database using the Mascot and X-Tandem! search engines. The parameters for all LC/MS/MS searches were as follows: Type of search: MS/MS Ion Search; Taxonomy: Uniprot mouse (concatenated forward and reverse plus common contaminants); Enzyme: Trypsin; Fixed modifications: Carbamidomethyl (C); Variable modifications: Glu/Gln->pyro-Glu, Ammonia-loss, Deamidated (Q,N), Oxidation (M), Acetyl (n); Mass values: Monoisotopic; Protein Mass: unrestricted; Peptide Mass Tolerance : ± 20 PPM; Fragment Mass Tolerance: ± 0.8 Da; Max Missed Cleavages: 2. Mascot output files were analyzed and filtered in Scaffold, to assess false discovery rates and allow for only correct protein identifications. At least 2 unique peptides per protein were required for identification and Scaffold Protein and Peptide Prophet thresholds were set at 99% (proteins) and 95% (peptides), respectively.

Co-immunoprecipitation and western blotting

To further examine the interaction between $Na_V\beta1$ and Gβγ subunits, $Na_V\beta1$ was immunoprecipitated in whole cell protein lysate preparations from P18 (juvenile) and P135 (adult) *Scn1b*-V5 mouse whole brain. Brains were lysed in Pierce™ RIPA lysis buffer (ThermoFisher) with Complete protease inhibitors (PIs) (Sigma Aldrich) at a concentration of 2X and homogenized by hand with a dounce homogenizer, followed by sonication and incubation on ice for 30min. Samples were centrifuged at 14,000 g/rcf for

5 min at 4°C, followed by the supernatant being stored at -80°C. For V5 nanobody co-immunoprecipitations, ChromoTek V5-Trap Agarose (Proteintech), consisting of an anti-V5 nanobody/VHH coupled to agarose beads, and binding control beads (BCB) as a control, were diluted in dilution buffer: 60 mM Tris/HCl (pH 7.5), 180 mM NaCl, 1% Triton X-100, and 6mM EDTA (pH 8.0) with 2X PIs and washed 3 times (2,500 g/rcf, 5min) at 4°C. Brain lysates were diluted in dilution buffer prior to being added to V5-Trap beads and incubated for 1hr. at 4°C with end-over-end mixing. Protein-bead complexes were washed 3X with wash buffer (50 mM Tris/HCl (pH 7.5), 150 mM NaCl, 0.02% SDS, 5 mM EDTA (pH 8.0) with 0.1% Triton X-100 followed by washed 1X in wash buffer without 0.1% Triton X-100. Complexes were eluted in 2X sample buffer (1 M Tris/HCl pH 8.8, bromophenol blue, 40% glycerol, 5% sodium dodecyl sulfate, 5% β-mercaptoethanol, 1% dithiothreitol) and heated at 85°C for 5 min to dissolve immunocomplexes from beads. Samples were stored at -80°C until used for western blotting.

Co-immunoprecipitation and input control samples were separated by SDS-PAGE on 12% polyacrylamide gels and transferred to Hybond-P polyvinyl difluoride (PVDF) membranes overnight. Membranes were blocked for 1 hour in either 5% milk, 1% Bovine serum albumin (BSA) (for V5) or 3% BSA (for Gβ) diluted in 1X Tris-buffered saline with 0.1% Tween 20 detergent (TBST). Membranes were then incubated overnight at 4°C in either mouse anti-V5 (1:1000, Invitrogen #R960-25) or rabbit anti-Gβ (B600) (1:10,000) primary antibodies diluted in 5% milk, 1% BSA or 3% BSA diluted in 1X TBST, respectively. Membranes were washed 3X (5min each) in 1X TBST,

incubated in HRP-conjugated goat anti-mouse (1:1000, BioRad #1706516) or anti-rabbit secondary antibodies (1:1000, ThermoFisher #32460) for 1hr at room temperature, followed by three 5min. washes in 1X TBST. Immunoreactive bands were detected with West Dura chemiluminescent substrate and imaged on an iBrightFL1000.

RT-qPCR

Total RNA was isolated from HEK, $Na_V1.6$ HEKs, and $Na_V1.6$ + $Na_V\beta1$ HEK stable cell lines using the Qiagen RNeasy Plus kit according to manufacturer's instructions. Cells were lysed through a sterile, 18-guage hypodermic needle and vortexed for 30 s. RNA samples were run on a NanoDrop One Spectrophotometer (ThermoFisher Scientific) to ensure adequate concentration and purity and stored at -80°C until use. cDNA was generated from 0.5-1 µg of RNA using Reverse Transcriptase SuperScript III (RT SS III), random primers (Invitrogen), and dNTPs (Invitrogen). RNA, random primers, and dNTPs were incubated at 65°C for 5 min. Salt buffers, 0.1M DTT, RNase Out, and RT SS III were added, and reactions were incubated at 25°C for 5 min, 50°C for 60 min, and at 70°C for 15 min. cDNA was kept undiluted (*GNGT2*, *GNAS*, *GNG3*) or diluted 1:3 in RNase-free water (all other genes). Quantitative PCR was performed using SYBR Green (Applied Biosystems) and gene-specific primers (Integrated DNA Technologies) on a QuantStudio 7 Flex Real-Time PCR System (Applied Biosystems). Gene-specific

measurements of each cDNA sample were run in triplicate, along with the endogenous control gene (*GAPDH*) used for normalization. For comparison of G protein subunit expression across HEK cell lines, $Na_v1.6$ HEKs and $Na_v1.6$ + $Na_v\beta1$ expression was compared to baseline HEK expression levels with relative expression levels of each gene quantified using the comparative threshold ($2^{-\Delta\Delta Ct}$) method of quantification. Data are presented as the fold change in gene expression ± SEM. Statistical significance ($p < 0.05$) between genotypes was determined using a two-way ANOVA. To examine baseline G protein subunit expression in HEKs, inverse delta comparative threshold (ΔCt) values were compared for Gα, Gβ, and Gγ subunits. The following primers were used: *GNAI1* forward: CTAGGTCTCCATCCGTAAAGTG, *GNAI1* reverse: GGGAAACAAGAACGAAACTCTG, *GNAQ* forward: CTCAGTCATGCACTCACAAAGAT, *GNAQ* reverse: CATCAGGAGGGAGGTATGAATTAG, *GNAO1* forward: GCTCTTCGACTCCATCTGTAAC, *GNAO1* reverse: CAGGAAAGCAGATGGTCAAAGGTG, *GNAS* forward: GCAGACAGATGCGCAAAGAAGC, *GNAS* reverse: GCTTTTACCAGATTCTCCAGCAC, *GNB1* forward: TCGTCTCTGGTGCTTGTGATGC, *GNB1* reverse: GTCGTCTGAGCCAGTGGCAAAT, *GNB2* forward: TGTTGCCGCTTCCTGGATGACA**,** *GNB2* reverse: CACTGTGTCCAGCAAAACCCAC, *GNB3* forward: GAGTCGGACATCAACGCCATCT, *GNB3* reverse: ATGCCGCAGATGATGCTCTCGT, *GNB4* forward: CTGGTGCTTGTGATGCCTCTTC, *GNB4* reverse: AGAGCCAGTGGCGAAGGCATAT, *GNB5* forward: GGAAGGTGATCGTGTGGGATTC, *GNB5* reverse: CAAGCAATGGCACATCCCGATG,

GNG1 forward: GCTCAAGAAAGAAGTGACACTGG, *GNG1* reverse:

TCACACAGCCTCCTTTGAGCTC, *GNG2* forward:

ATGGAAGCCAATATCGACAGGATA, *GNG2* reverse:

CTTCTCCCTAAACGGGTTTTCTG, *GNGT2* forward:

CTGACCTTGCTGGGAACACTCT, *GNGT2* reverse:

GTAAGTGCTTCCTAAGGACTGCC, *GNG3* forward:

GATTGAAGCCAGCTTGTGTCGG, *GNG3* reverse: GGGTTCTCCGAAGTGGGCACA,

GNG4 forward: CTCCAGATTCAGCCTCCGTTTTG, *GNG4* reverse:

TGCCATAGGTCTGGAAGAGGTG, *GNG5* forward:

CCTCTGCTGACTGGAGTATCTTC, *GNG5* reverse:

CTGGATCATAAGGAGTGGTTTGG, *GNG7* forward:

CAAAGCGGCGTCTGACCTCATG, *GNG7* reverse:

GGTTTCTTGTCCTTAAAGGGGTTC, *GNG8* forward: CCGCAACCATGTCCAACAAC,

GNG8 reverse: CCTTCATGCGGTCGATGTTCAC, *GNG10* forward:

GGGAGCAGATTCTTAGCAAAC, *GNG10* reverse: GCCACAACTACAAAGCAGAG,

GNG11 forward: CTCCAAACCCTGCGTCAATG, *GNG11* reverse:

CATAGATGTGGCTTGGCCTTG, *GNG12* forward: CGTTCTGCGATATGCCCAGTTC,

GNG12 reverse: AAAAGAATGTCTCATTAAGTGAAGCA, *GNG13* forward:

GGGTTGTTCTTCATCAGGTCG, *GNG13* reverse: GATGAAGAAAGAGGTGGAGAGC.

Western blot in HEK cells

Western blotting was performed to confirm expression of $Na_v\beta1$ in HEK $Na_v1.1$ + $Na_v\beta1$ and HEK $Na_v1.6$ + $Na_v\beta1$ stable cell lines. Cells were lysed in Pierce™ RIPA lysis buffer (ThermoFisher) with Complete PIs (Sigma Aldrich) at a concentration of 2X. Samples were vortexed and sonicated at 20% for 10 pulses every 10 min during a 30 min. incubation on ice, followed by centrifugation at 14,000 g/rcf for 5 min. at 4°C and the supernatant stored at -80°C. Protein concentration of samples was determined with a bicinchoninic acid (BCA) assay and measured with a Multiskan SkyHigh Microplate Spectrophotometer (ThermoFIsher). Lysates were diluted in 2X sample buffer (1M Tris/HCl pH 8.8, bromophenol blue, 40% glycerol, 5% sodium dodecyl sulfate, 5% β-mercaptoethanol, 1% dithiothreitol) and samples separated by SDS-PAGE on a 12% gel, followed by being transferred to Hybond-P polyvinyl difluoride (PVDF) membranes overnight. Membranes were blocked in 5% milk, 1% BSA for 1hr. and incubated in mouse anti-V5 (1:1000, Invitrogen #R960-25) overnight. The following day, membranes were washed 3X (5min each) in 1X TBST, incubated in HRP-conjugated goat anti-mouse (1:1000, BioRad #1706516) secondary antibody for 1hr at room temperature, followed by being washed 3X in 1X TBST. Immunoreactive bands were detected with West Dura chemiluminescent substrate and imaged on an iBrightFL1000 to confirm expression of V5 ($Na_v\beta1$) in the HEK stable cell lines.

Whole cell Na^+ Current (I_{Na}) recording

I_{Na} was measured at RT (22–25°C) using the manual whole cell patch clamp technique with previously described electrophysiological methods (Chen et al. 2012). Cells were plated on 12 mm diameter clear glass poly-D-lysine-coated coverslips (Neuvitro) and used for electrophysiological recordings within 48 hours after plating. Cells were identified via fluorescence with an A1R upright confocal microscope (Nikon). Micropipettes were obtained from 1.5 mm outer diameter capillary glass tubing (Harvard Apparatus) using a P-97 horizontal puller (Sutter Instrument Co.). Micropipettes were then polished using a MF-830 micro forge (Narishige) to obtain a resistance between 2.0 to 5.0 MΩ. The intracellular solution contained the following (in mM): 1 NaCl, 125 N-methyl-D-glucamine, 2 $MgCl_2$, 10 EGTA, 40 HEPES, 5 phosphocreatine-tris, 2 Mg-ATP, 0.2 Na_2-GTP, 0.1 leupeptin, 270-275 mOsm (pH 7.2 with H_2SO_4). Extracellular solution contained the following (in mM): 120 NaCl, 1 $BaCl_2$, 2 $MgCl_2$, 0.2 $CdCl_2$, 1 $CaCl_2$, 20 sucrose, 10 glucose, 10 HEPES, 10 tetraethylammonium chloride, 300-305 mOsm (pH 7.35 with NaOH). Signals were amplified using a Multiclamp 700B amplifier (Molecular Devices). Data were acquired with a Digidata 1440A interface (Molecular Devices) and analyzed using pClamp10 offline. Pipette and whole cell capacitance were fully compensated, and series resistance was predicted and compensated at 50%. If access resistance changed ≥ 20% at any time, the recording was not included in the analysis. Signals were low pass-filtered at 10 kHz and data were sampled at 20 kHz. Residual linear capacity and leak currents were eliminated using online P/4 subtraction.

I_{Na} was normalized to cell capacitance to obtain I_{Na} density, used to plot I–V curves and calculate conductance with the following equation:

$$g = \frac{I}{V - V_{rev}}$$

where g is conductance, I is current, V is the test potential, and V_{rev} is the measured reversal potential. Peak currents were normalized to the maximum peak I_{Na} amplitude. The $V_{1/2}$ of activation represents the voltage of the membrane at which half-maximal conductance occurred. To determine the I_{Na} amplitude and the voltage dependence of activation, Na^+ currents were evoked by 250 ms depolarizing test pulses (from -120 to +30 mV at 5 and 10 mV intervals) from a prepulse potential of -70 or -120 mV. Voltage-dependence of inactivation (availability) was determined by applying a 50 ms test pulse to 0 mV after 250 ms prepulses to the same voltages as described for the voltage dependence of activation. Normalized activation (G/Gmax) and inactivation (I/Imax) curves were fit with a Boltzmann equation:

$$\frac{1}{1 + e^{\frac{V - V_{1/2}}{k}}}$$

where $V_{1/2}$ is the membrane potential in the midpoint of the curve, and k is the slope factor. Persistent I_{Na} was analyzed as the average current in a 2 ms period exactly 50 ms after the peak I_{Na} was observed at a depolarizing step from -70 to -10 mV. Persistent I_{Na} values were normalized to cell capacitance to obtain persistent I_{Na} density.

Slow inactivation was elicited using a 50 Hz train of 2 ms depolarizing pulses from -70 to -20 mV with a 48 ms recovery period between pulses to remove fast inactivation and a holding potential of -80 mV. Slow inactivation was quantified as the % of the initial peak I_{Na} density remaining after the 50^{th} pulse compared to the first depolarizing pulse.

Acute voltage-dependent relief of Gβ1γ2 inhibition of HEK $Na_v1.1$ and $Na_v1.6$ in Fig. 3.7 was assessed using a double pulse protocol by eliciting peak I_{Na} using an initial depolarizing step from -70 to 0 mV for 250 ms before and after holding the membrane at a hyperpolarized potential of -120 mV for 1 s. A holding potential of -80 mV was used. Acute relief of I_{Na} inhibition was quantified by dividing the peak I_{Na} density observed in the second pulse (P2) by the peak I_{Na} density observed in the first pulse (P1) to obtain a P2/P1 ratio.

To inhibit PKA/PKC, HEK cells stably expressing human $Na_v1.1$ or $Na_v1.6$ were pre-incubated for 2 hours prior to whole cell recording with 100 nM staurosporine (Cayman Chemical). Staurosporine was also added to the recording chamber at a concentration of 100 nM to maintain PKA/PKC inhibition the duration of electrophysiological recordings.

To test the acute effects of purified Gβ1γ2 subunits, a generous gift from Dr. Alan Smrcka of 46 μM Gβ1-His6-γ2 in a stock solution containing 50 mM NaCl, 20 mM HEPES, 1% CHAPS, and protease inhibitors at pH 8.0 was diluted with a solution containing 0.1% CHAPS then directly added to the intracellular I_{Na} recording pipette

solution (described above) to give final purified Gβ1γ2 concentrations between 20 and 100 nM in 0.02% CHAPS. I_{Na} recordings were then performed immediately after gaining whole cell access as purified Gβ1γ2 subunits were assumed to diffuse into the cytoplasm immediately after rupturing the membrane.

Whole cell GIRK1/2 recording

K^+ current from HEK cells stably expressing GIRK1/2 channel subunits was performed with the same whole cell methods describe above except for the use of different solutions and voltage clamp protocols. The intracellular solution contained the following (in mM): 130 KCl, 20 NaCl, 5 EGTA, 5.46 $MgCl_2$, 2 Mg-ATP, 0.2 Na-GTP, 10 HEPES (pH 7.4). Extracellular solution contained the following (in mM): 20 KCl, 120 mM NaCl, 0.5 $CaCl_2$, 2 $MgCl_2$, 10 HEPES (pH 7.4). The amplitude and I-V relationship of GIRK1/2 currents were evoked using 1 s long hyperpolarizing voltage steps from +50 mV to -120 mV in -10 mV intervals) from a holding potential of -50 mV (E_K = 50 mV with 20 mM K_{out}). GIRK currents were recorded at baseline and subtracted from currents elicited in the presence of 1 mM Ba^{2+} then normalized to cell capacitance to obtain current density which was used to plot I-V curves.

Brain Slice Preparation

Acute brain slices were prepared as described previously (Hull et al. 2020) Briefly, mice were anesthetized with isoflurane anesthesia and decapitated. Brains were carefully

removed from the skull and placed in ice-cold carbogen-aerated slice solution containing (in mM): 110 sucrose, 62.5 NaCl, 2.5 KCl, 6 $MgCl_2$, 1.25 KH_2PO_4, 26 $NaHCO_3$, 0.5 $CaCl_2$, 20 D-glucose, pH 7.35-7.40. Brains were blocked and slices were cut using a vibrating microtome (Electron Microscopy Sciences) in 250 µm thick coronal sections from prefrontal cortex. Slices were incubated in an aerated holding chamber containing slice solution for 30 minutes at room temperature and then incubated in 1:1 slice:artificial cerebrospinal solution (ACSF) for 30 minutes at 35°C. ACSF contained in mM (125 NaCl, 2.5 KCl, 1 $MgCl_2$, 1.25 KH_2PO_4, 26 $NaHCO_3$, 2 $CaCl_2$, and 20 D-glucose (pH 7.35-7.40). Slices were then aerated in a holding chamber containing 100% ACSF for at least 30 min at room temperature before recording.

Action potential recording and analysis

Individual brain slices were placed in an RC-26 recording chamber (Warner Instruments) and superfused with aerated ACSF at a flowrate of 2-3 mL/min. Layer 2/3 or 5 pyramidal neurons were identified based on their soma size, shape, and location using an A1R upright confocal microscope (Nikon) equipped with IR-DIC optics and a 40X water immersion objective. Only vertically oriented pyramidal cells were selected for recording. Recording electrodes had a resistance of 4-8 MΩ with solutions containing (in mM): 140 K-Gluconate, 4 NaCl, 0.5 $CaCl_2$, 10 HEPES, 5 EGTA, 5 phosphocreatine, 2 Mg-ATP, and 0.4 GTP (pH 7.2-7.3 with KOH). The junction potential was calculated to be 14.3 mV using the P-clamp junction potential calculator and all values presented in the study as uncorrected values. Following break in at -94.3 mV in

voltage clamp mode, the resting membrane potential was defined as the membrane potential in current clamp <10 s after initial break in for baseline. Repetitive action potential firing was elicited in whole-cell current clamp from the resting membrane potential in 1 s long current injections in 10 pA steps from -20 pA to +400 pA. There was a 1 s long 0 pA current injection between each sweep. Data were acquired at 20 kHz and were filtered at 10 kHz. Cells with an access resistance measured in voltage clamp >20 MΩ or RMP more depolarized than -64.3 mV were not used. Access resistance and pipette capacitance were compensated using bridge balance. Whole cell capacitance was measured using P-clamp whole cell capacitance compensation in voltage clamp with 10 mV depolarizing steps from -94.3 mV. Automated action potential (AP) quantification and analysis was performed using custom MATLAB (MathWorks) software. APs were defined as the voltage crossing 0 mV after a dV/dt>10 mV/ms, defined here as the AP threshold. Input resistance was calculated using Ohm's law with a -10 pA current injection from the resting membrane potential after 250 ms.

Spontaneous inhibitory postsynaptic current (sIPSC) recordings

sIPSCs were recorded in layer 2/3 pyramidal cells from somatosensory cortical slices prepared as described above. The pipette solution consisted of (in mM) 140 CsCl; 0.4 GTP; 2 Mg-ATP; 0.5 $CaCl_2$; 5 Na_2-Phosphocreatine; 5 EGTA-CsOH; 10 HEPES (pH 7.3 adjusted with CsOH). Nearly symmetric external and internal [Cl^-] resulted in inward currents that were strictly GABAergic when the cells were held in voltage clamp at −70 mV after constant perfusion of 10 μM 6-cyano-7-nitroquinoxaline-2,3-dione (CNQX)

and 100 µM amino-5-phosphonopentanoic acid (APV) in the external solution to block glutamate receptor-mediated excitatory postsynaptic currents. As with all other patch clamp recordings performed in this thesis work, acute application of drugs was achieved via gravity-powered perfusion with a flow rate of 2-3 mL/min. sIPSCS were recorded for 2 min at a sampling rate of 10 kHz and filtered at 2 kHz with a Digidata 1440A interface and analyzed using pClamp10 or 11 (Molecular Devices, Sunnyvale, CA). All experiments were carried out at RT (22–25°C). The mean decay time constants, frequency and amplitudes of sIPSCs were analyzed using MiniAnalysis 6.0.3 programs (Synaptosoft Inc., Decatur, GA). Unless otherwise specified, synaptic events per cell collected over a 2 min period were averaged to calculate the decay, frequency, and amplitude of sIPSC. Cumulative probability distributions were calculated by sampling 100 random events from each neuron and combining across neurons to compare conditions. All results were plotted in GraphPad Prism (GraphPad; LaJolla, CA). Data are presented as mean value ± SEM, where n or N represent number of cells or animals, respectively. Statistical significance was determined using unpaired Student's t-test unless stated otherwise. A P value < 0.05 was deemed significant.

Statistical analysis

All data analysis of the recorded I_{Na} was performed using the software packages Clampfit v10.4 (Molecular Devices), Microsoft Excel, Graph Pad Prism v9.0 (San Diego, CA). Active and passive neuronal properties of brain slice recordings were analyzed using custom MATLAB (MathWorks) software. Results are presented as mean ± S.E unless indicated otherwise.

Chapter IV. Conclusions

This thesis work advances knowledge in two areas of neuropharmacology that are relevant to the treatment of developmental and epileptic encephalopathies: selective inhibition of the major brain voltage-gated sodium channel (VGSC) subtype $Na_v1.6$, and in extending our understanding of basic neuromodulatory mechanisms involving VGSCs and G-protein βγ subunits. Together, the intellectual advancements presented in this thesis may provide new ideas for the treatment of sodium channel and *GNB1*-linked developmental and epileptic encephalopathies.

Subtype Selective Small Molecule Therapeutics for Sodium Channel-linked DEE

Small molecules selectively targeting structural regions of unique VGSC α subunits have largely failed to achieve clinical efficacy thus far. VGSC subtypes display very high amino acid sequence homology and even minor off-target engagement of other subtypes can lead to dangerous side effects. In Chapter II, we showed the previously reported $Na_v1.6$ selective inhibitor, 4,9-anhydrotetrodotoxin (4,9-ah-TTX), also blocks $Na_v1.1$ at low nanomolar concentrations. This finding suggests 4,9-ah-TTX is an inappropriate reagent to experimentally isolate $Na_v1.6$ activity *in vitro*. Moreover, it dramatically narrows the selectivity index of 4,9-ah-TTX and discourages further efforts to develop the compound as a $Na_v1.6$ selective therapeutic (see WIPO Patent #: WO2007110220A1). In hindsight, the discovery that 4,9-ah-TTX inhibits $Na_v1.1$ I_{Na} at comparable concentrations used to inhibit $Na_v1.6$ is not that surprising. The active site that 4,9-ah-TTX binds to on $Na_v1.6$ is hypothesized to be very similar to that of TTX itself, which binds deep in the outer vestibule of the pore where the residues forming the Na^+ selectivity filter are located (neurotoxin receptor site 1). This region of the channel is identical in amino acid sequence between human $Na_v1.6$ and $Na_v1.1$ (see Fig. 2.10), and even surrounding residues show very high homology between the two subtypes. New ideas and creative approaches are needed for subtype selective VGSC small molecules to succeed as useful therapeutics.

One approach to enhance selectivity involves targeting the C-terminal domain of brain VGSCs, as they show higher amino acid sequence divergence and are a common site for protein-protein interactions with other signaling molecules. For example, recent research has explored fibroblast growth factor (FGF) polypeptides as VGSC interacting proteins for their subtype selective therapeutic potential (Ali et al. 2016). FGF-14 shows a selective interaction with the C-terminal domain of $Na_v1.6$ and the therapeutic potential of this functional relationship is currently being explored for selective small molecule drug development (Lou et al. 2005, Laezza et al. 2009, Ali et al. 2016, Ali et al. 2018, Singh et al. 2021).

This thesis work further supports the idea that the VGSC α subunit homology problem may be successfully circumvented to create selective VGSC small molecules by targeting signaling proteins that uniquely interact with the C-terminus of specific subtypes. G protein βγ subunits are thought to bind to the distal C-terminus of $Na_v1.2$ and presumably other brain VGSC subtypes, like $Na_v1.6$. Our work showing a differential functional interaction of Gβ1γ2 with brain VGSC subtypes may be due to differences in the way the Gβ1γ2 interacts with the C-terminus of $Na_v1.1$, $Na_v1.2$ or $Na_v1.6$. Further characterization of the Gβγ binding site and subtype variation in this binding site are needed to advance this pursuit.

Gβγ Modulation of VGSCs

In his elegant review of G-protein modulation of ion channels (Dascal 2001), Dr. Nathan Dascal set forth four criteria that must be experimentally satisfied to determine direct activation of an ion channel by G-proteins:

1. “GPCR ligand is shown to modulate the activity of the ion channel AND G-proteins themselves are implicated in ion channel regulation.”
2. “The G-protein mimics the effect of the hormone or neurotransmitter in a “membrane-delimited” fashion-“directness” of the channel regulation by G proteins”
3. “The G protein subunit physically interacts with the channel.”
4. “Prevention of G protein binding to its binding site abolishes the regulation.”

Some but not all conditions of the four criteria listed above have been experimentally satisfied to support direct Gβγ modulation of VGSCs (Ma et al. 1994, Ma et al. 1997, Mantegazza et al. 2005, Mattheisen et al. 2018). I will review the previous evidence (and lack thereof) for each criterion and incorporate any further advancements presented in this thesis work to support direct Gβγ modulation of brain VGSCs.

#1: GPCR ligand is shown to modulate the activity of the ion channel AND G-proteins themselves are implicated in ion channel regulation.

Multiple GPCR ligands present in neurons have been shown to modulate VGSC function, including dopaminergic activation of D1 and D2-like dopamine GPCRs, cholinergic activation of muscarinic acetylcholine GPCRs and serotonergic activation of $5HT_{1A}$, $5\text{-}HT_2$ GPCRs (Cantrell and Catterall 2001). However, evidence suggests the I_{Na} modulation produced after ligand activation of these GPCRs is mediated almost exclusively through PKA, PKC or phosphorylation-dependent pathways (Scheuer and Catterall 2006, Scheuer 2011). Alternatively, G-proteins themselves have been implicated, as addition of GTPγS to the intracellular pipette solution has been shown to modulate I_{Na} in multiple studies (Ma et al. 1994, Mattheisen et al. 2018). Mattheisen and colleagues provided strong evidence for satisfying criteria #1 by showing that acute application of the GPCR ligands, anandamide and cinacalcet, inhibit I_{Na} in cultured cortical neurons (Mattheisen 2018, Mattheisen et al. 2018). This GPCR mediated I_{Na} inhibition is significantly reduced in the presence of GDPβS, suggesting a G-protein dependent effect. However, surprisingly, selective deletion of the GPCR thought to mediate the ligand action (CB_1 for anandamide and CaSR for cinacalcet) did not impact the I_{Na} inhibition. These results leave open questions about the identity of the GPCR(s) driving G-protein mediated I_{Na} modulation in neurons, and if Gβγ subunits are the necessary G-proteins in this pathway.

#2: The G-protein mimics the effect of the hormone or neurotransmitter in a "membrane-delimited" fashion-"directness" of the channel regulation by G proteins.

In the context of G-protein modulation of ion channels, the term membrane-delimited is defined as a direct effect on the function of an ion channel exerted by the G-protein(s) that is *independent* of diffusible 2nd messengers and cytoplasmic signaling proteins. Of the four criteria needed to satisfy direct Gβγ modulation of brain VGSCs, #2 is lacking the most experimental evidence thus far. Interestingly, Surmeier and Kitai found that D2-agonist mediated decrease of I_{Na} in striatonigral neurons was observed in the whole cell configuration but absent in the cell-attached configuration, suggesting a membrane-delimited pathway (Surmeier and Kitai 1993). This observation is far from conclusive, and the direct effects of acutely applied exogenous Gβγ subunits or endogenously activated Gβγ subunits need to be demonstrated for proper satisfaction of criterion #2. I attempted to test the acute effects of Gβγ subunits on VGSC function using whole cell patch clamp with two different methods. One method involved the inclusion of purified Gβ1γ2 subunits into the intracellular pipette solution and the other employed a small molecule activator of endogenous Gβγ. Both were unsuccessful, as methodological complications deemed the results uninterpretable when testing intracellular purified Gβγ subunits in whole cell I_{Na} recordings.

No experiment evaluating the acute effects of purified Gβγ subunits on VGSC function in heterologous cells or neurons has been reported yet. I attempted to evaluate the acute effects of purified Gβ1γ2 on HEK $Na_v1.1$ peak I_{Na} density over time (Fig. 4.1), but

numerous complications including confirming the diffusion and concentration of exogenous Gβ1γ2, and use of the CHAPS detergent to maintain solubility of purified Gβ1γ2 subunits causing disruption of the GΩ seal ultimately compromised a useful interpretation of the results.

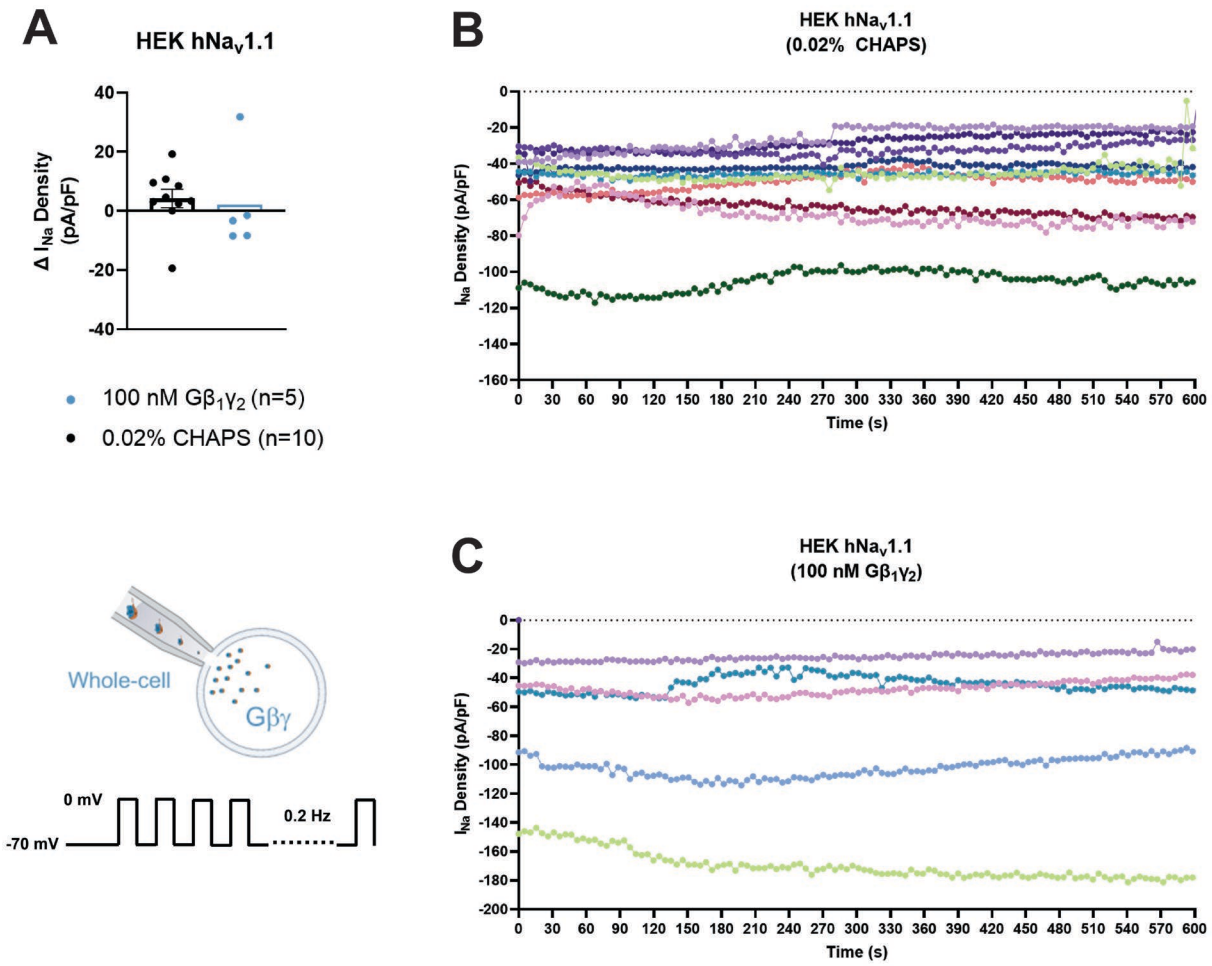


Figure 4.1 Effects of 100 nM purified Gβ1γ2 on whole cell $Na_v1.1$ peak I_{Na} density over time using a depolarizing step from -70 mV to 0 mV repeating @ 0.2 Hz. (A) Change in $Na_v1.1$ peak I_{Na} density after an approximately 10 min diffusion of purified Gβγ. (B) Control time course of peak I_{Na} density with 0.02% intracellular CHAPS. (C) Time course of peak I_{Na} density during diffusion of 100 nM purified Gβ1γ2 + 0.02% intracellular CHAPS. Each data point in B and C represents the peak HEK $Na_v1.1$ I_{Na} density measured in a step from -70 mV to 0 mV every 4.9 s.

Surfen (1,3-bis(4-amino-2-methylquinolin-6-yl)urea) is a small molecule reported to dissociate Gβ1γ2 from Gα-GDP when applied to intact cells without inducing nucleotide exchange in the Gα subunit *in vitro* (Surve et al. 2014). I attempted to use this tool to activate endogenous or exogenously expressed Gβγ subunits while recording $Na_V1.6$ I_{Na} in HEK cells but observed no effects (data not shown). Attempts to validate surfen as a tool to explore endogenous Gβγ modulation of GIRK1/2 channels (a known target of membrane-delimited Gβγ modulation) expressed in HEK cells showed no difference in whole cell GIRK I-V relationships in the presence of 10 μM surfen compared to baseline. Therefore, we deemed surfen not useful for further experimental pursuit of membrane delimited Gβγ modulation of VGSCs.

My attempts to advance evidence in support of criterion #2 were unsuccessful and more work is needed to better understand the acute and direct impact of Gβγ subunits on VGSC function in neurons. Inside-out patch recordings in the presence and absence of acutely perfused purified Gβγ subunits from membrane patches of neurons or even heterologous cells expressing brain VGSCs may reveal many insights. Alternative methods involving the use of animal opsins (especially those that use bistable pigments) that respond to different wavelengths of light stimulation and are directly coupled to various Gα subunits (Fig. 4.3) may one day be used in a noninvasive manner to probe the direct effects of endogenous Gβγ on VGSC function. Strategic expression of animal opsins while using optogenetic patch clamp electrophysiology techniques to directly dissociate endogenous Gβγ from Gα would permit the evaluation of endogenous Gβγ modulation of VGSC function in neuronal preparations.

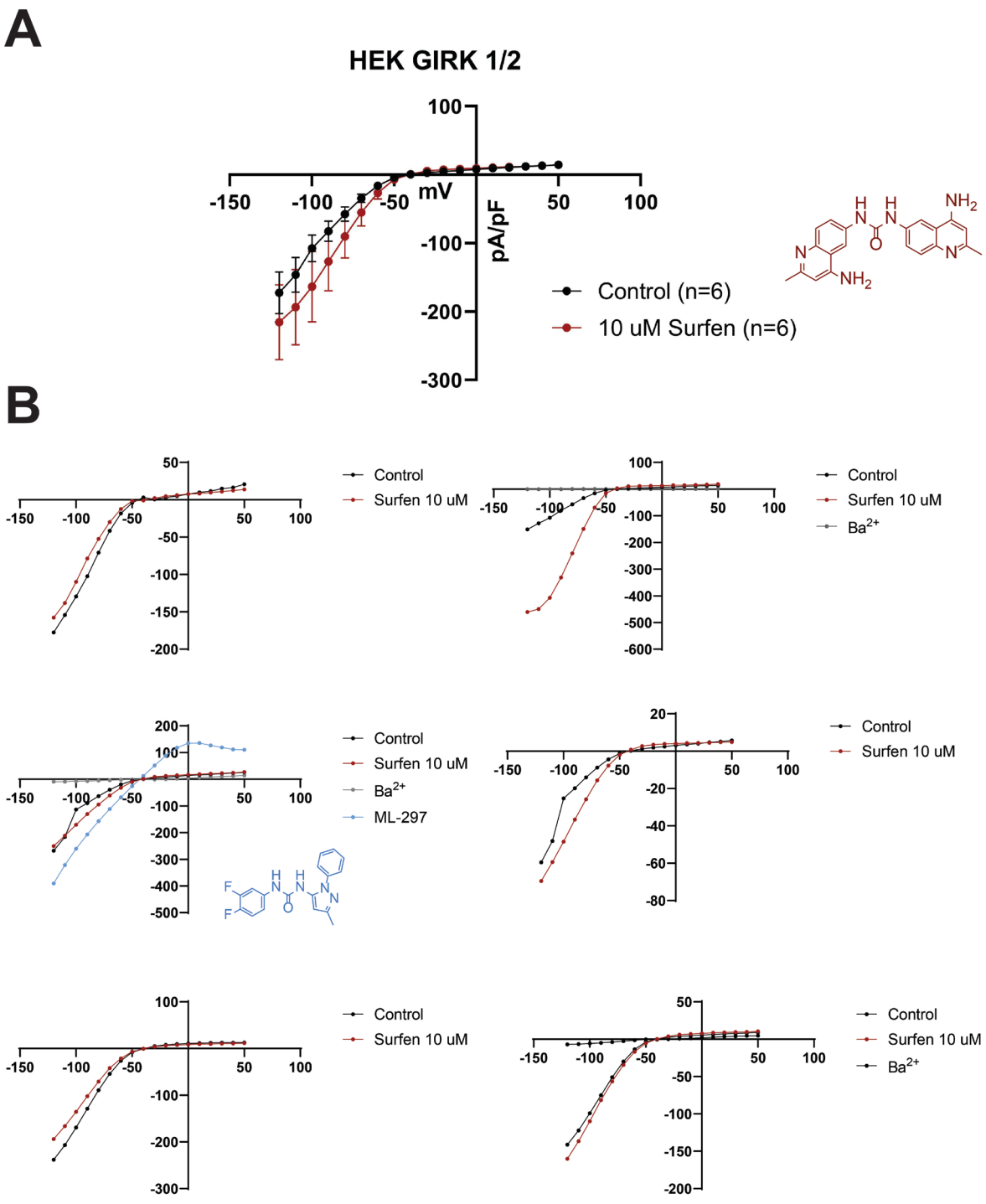


Figure 4.2 Acute effects of 10 μM surfen on I-V relationship of GIRK1/2 channels stably expressed in HEK cells. (A) I-V curve of GIRK1/2 channels in the presence and absence (control) of 10 μM surfen hydrate. (B) Representative individual I-V curves of cells at baseline (control), 10 μM surfen (red), 1 mM Ba^{2+} (grey), or 10 μM of the GIRK activator ML-297 (blue).

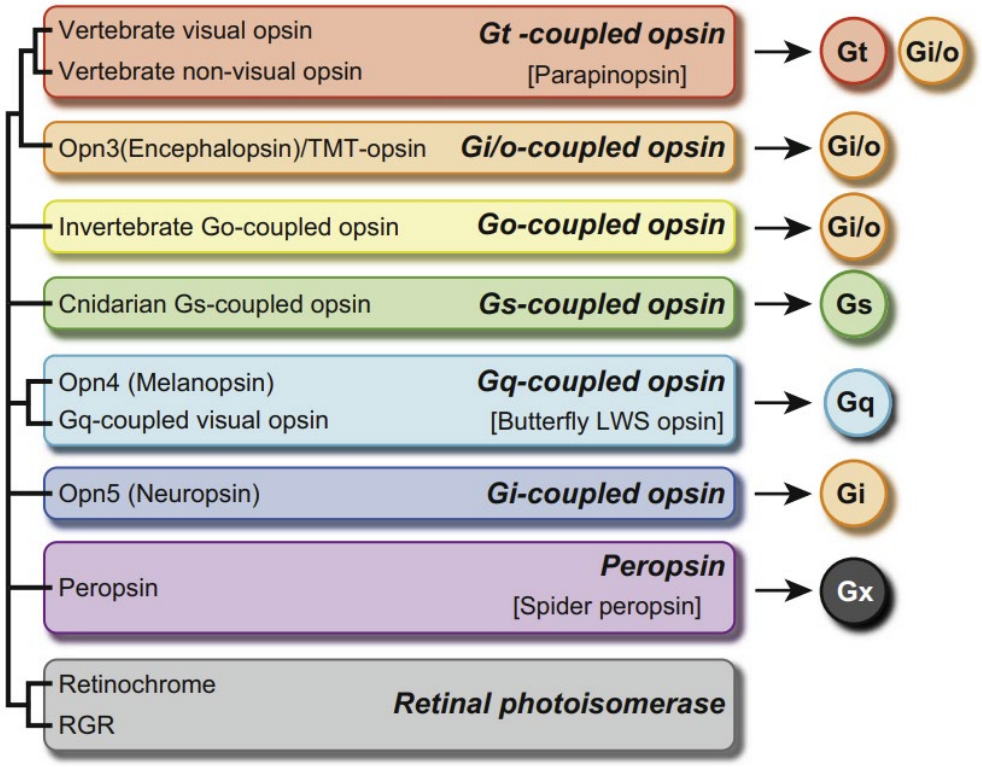


Figure 4.3 Various opsins that respond to different wavelengths of light and couple to different Gα subunits. (Adapted from Terakita et al. 2015)

#3: The G protein subunit physically interacts with the channel.

Gβ subunits coimmunoprecipitate with VGSC Gα subunits in mouse culture cortical neurons, supporting the physical association between Gβγ and VGSCs in a complex, but does not provide information on direct protein-protein interactions (Marin et al. 2001). This thesis work presents evidence of physical and functional interactions between Gβγ subunits and the VGSC complex through $Na_v\beta1$ subunits in mouse whole brain (Fig.3.2). Further work is needed to provide more convincing support for the physical interaction between Gβγ and VGSC α subunits in physiologically relevant neuronal environments such as whole brain preparations. The gold standard to convincingly support a physical interaction would be X-ray crystallographic or Cryo-EM analysis of Gβγ in complex with a VGSC. Mantezzaga et al. proposed that the distal portion of the C-terminus (last 28 amino acid residues) are necessary for Gβγ modulation of $Na_v1.2$ persistent I_{Na} (Mantezzaga et al. 2005). This thesis work motivates deeper investigation into the C-terminus as the site of interaction for Gβγ modulation of $Na_v1.6$, and if this region is the same site determining Gβγ modulation of persistent and transient I_{Na} in brain VGSC subtypes.

#4: Prevention of G protein binding to its binding site abolishes the regulation.

As previously mentioned, the binding site of Gβγ subunits to brain VGSC α subunits is not completely understood yet. Studies using truncation mutants and chimeras of $Na_v1.2$ with other subtypes suggest the binding site is located on the last 28 amino acid residues of the C-terminus of $Na_v1.2$ (Mantezzaga et al. 2005). A synthetic peptide containing the proposed QxxER Gβγ binding motif derived from adenylyl cyclase 2 (AC2: QEHAQEPERQYMHIGTMVEFAYALVGK) reversed the effect of transiently co-expressed Gβ2γ3 on $Na_v1.2$ I_{Na} when added to the intracellular recording pipette at 100 μM (Ma et al. 1997). The AC2 peptide has been previously shown to block Gβγ modulation of numerous effectors including K^+ channels, GRK2, and PLCβ (Chen et al. 1995, Ma et al. 1997). Another synthetic peptide (DALRIQMEERFMASNPSKVSYEPIT) derived from a region in the distal C-terminus in rat $Na_v1.2$ (hypothesized as the Gβγ binding site) also reversed the effect of Gβ2γ3 on $Na_v1.2$ (Ma et al.1997). Prevention of Gβ2γ3 binding to $Na_v1.2$ by co-expression of Gαi or Gαo also significantly reduced Gβ2γ3 modulation of $Na_v1.2$ I_{Na} (Ma et al. 1997).

The experiments presented in this thesis did not directly attempt to prevent Gβ1γ2 binding to $Na_v1.6$ or $Na_v1.1$. Our co-immunoprecipitation/LS-MS/MS experiments indicate that $Na_v\beta1$ subunits associate with Gβγ in mouse whole brain. We also showed that coexpression of $Na_v\beta1$ can disrupt the Gβ1γ2 modulation of $Na_v1.1$, but not $Na_v1.6$. This raises the question of if Gβ1γ2 binds to $Na_v1.1$ at a site overlapping with the

$Na_v1.1$/$Na_v\beta1$ interface. More research is needed to understand the binding site of Gβγ subunits to brain VGSC subtypes. A greater understanding of the structural details involved in the physical interaction between Gβγ and VGSC α and β subunits will likely reveal key functional insights into this important neuromodulatory relationship.

Much progress has been made in the study of Gβγ modulation of VGSCs. The work presented in this thesis has expanded our understanding of VGSC $Na_v1.6$, $Na_v1.1$ and $Na_v\beta1$ subunits as targets of Gβγ signaling, however, many knowledge gaps remain. Hopefully these advancements will motive further study of this neuromodulatory signaling pathway in heterologous cells, and most importantly, native neuronal preparations.

Cellular and Circuit Level Origins of Epilepsy in *Gnb1*$^{K78R/+}$ Mice

Recent evidence has shown that *Gnb1*$^{K78R/+}$ mice display spontaneous seizures and spike and wave discharges (SWD) *in vivo* (Teng et al. 2022), an EEG hallmark of absence epilepsy. It is well established that absence epilepsy is a disorder of thalamocortical (TC) networks. Widespread synchrony is prominent in absence networks, as action potential firing is highly synchronized in thalamocortical loops during the spike phase of SWD. Indeed, Teng and colleagues recently provided *in vivo* evidence that TC circuits are involved in the SWD *Gnb1*$^{K78R/+}$ phenotype (Teng et al. 2022). The thalamic reticular nucleus (TRN) and TC areas are two subcortical regions highly influential in absence epilepsy. Inhibitory neurons of the TRN and excitatory TC neurons are thought to be primary cell types involved in generating SWD (Huguenard 2019). The TRN is comprised of GABAergic neurons that provide both feedforward and feedback inhibition to excitatory TC relay neurons of various thalamic nuclei. TC relay neurons show high expression of low-voltage-activated T-type VGCCs ($Ca_v3.1$), endowing them with the ability to fire bursts of action potentials after hyperpolarization. Teng et al. proposed that SWD are a pathophysiological transformation of sleep spindles and, based on the observation that SWD occur predominately in the awake state in multiple mouse models of absence epilepsy (including *Gnb1*$^{K78R/+}$ mice), hypothesized that sensory input stimulates greater frequency and duration of SWD in *Gnb1*$^{K78R/+}$ mice (Teng et al. 2022). This is an intriguing hypothesis, however, there is a difference between a positive correlation of SWD occurrence in the awake state and

sensory input regulating the generation of SWD. More research characterizing the relationship between sensory input and SWD incidence using methods with better temporal and spatial resolution than fiber photometry is needed to support this claim.

As a pharmacologist trying to understand the pathophysiological mechanisms underlying a particular aspect of disease, my training has taught me to follow the mechanism of action of drugs that are shown to be effective in treating those symptoms. Ethosuximide (ETX) has shown efficacy in reducing the bursting activity of *Gnb1*$^{K78R/+}$ cultured neurons *in vitro* and suppressing SWD of *Gnb1*$^{K78R/+}$ mice *in vivo* (Colombo et al. 2019). ETX and related succinimides are thought to block T-type Ca_v3 channels to exert their anti-absence effects. ETX was shown to inhibit T-type Ca^{2+} channels in acutely dissociated thalamocortical neurons at concentrations between 250-750 μM (Coulter et al. 1989, Coulter et al. 1990, Huguenard and Prince 1994). However, T-type Ca_v3 channels being the primary anti-absence mechanism of ETX is somewhat controversial (Crunelli and Leresche 2022) because ETX also inhibits numerous ion channels (including VGSCs and GIRK channels) at therapeutic concentrations (0.5 -1 mM) in neurons and heterologous cells (Marfia et al. 2000, Kobayashi et al. 2009). Reddy and colleagues proposed that GIRK inhibition is the primary anti-absence mechanism of ETX in treating SWD in *Gnb1*$^{K78R/+}$ mice (Reddy et al. 2021). To my knowledge, virtually all the work showing direct action of ETX on GIRK channels has been performed in Xenopus oocytes and further work in mammalian cells and neuronal preparations is required to test this hypothesis.

This thesis work highlights a major role for $Na_v1.6$ inhibition by Gβ1γ2, which may be a relevant interaction in the epilepsy phenotype of *Gnb1*$^{K78R/+}$ mice and *GNB1*-E patients. Interestingly, the Gβ^{K78R}γ mutant shows increased levels of expression in oocytes compared to wildtype Gβγ (Reddy et al. 2021), although Colombo and colleagues saw no difference in Gβ1 expression of P0 *Gnb1*$^{K78R/+}$ cortex compared to wildtype (Colombo et al. 2019). Nevertheless, if *GNB1*-E patient neurons have increased free Gβγ levels or if the Gβ^{K78R}γ mutant shows GOF for the interaction with $Na_v1.6$, this could lead to pathological inhibition of $Na_v1.6$. Makinson et al. showed that knockdown of *Scn8a* in TRN cells is sufficient to induce absence epilepsy (Makinson et al. 2017). Selective deletion of *Scn8a* in excitatory and/or inhibitory neurons leads to absence seizures (Makinson et al. 2017). It's hypothesized that loss of *Scn8a* disrupts the excitability of TRN neurons and recurrent TRN synaptic inhibition. Additionally, the loss of *Scn8a* leads to hypoexcitable cortical circuits which leads to convulsive seizure protection (Makinson et al. 2017). Collectively, these data highlight the need to further explore the implications of Gβγ inhibition of $Na_v1.6$ in the cellular and circuit level mechanisms underlying the epilepsy of *GNB1*-E.

Our work showing a significant reduction in sIPSC frequency, but not amplitude, suggests *Gnb1*$^{K78R/+}$ mice have a deficit in presynaptic inhibitory neurotransmission of cortical layer 2/3 pyramidal neurons. One possible reason for this result is the difference in whole cell evaluation of intrinsic firing properties of layer 5 pyramidal neurons could mask the cortical network deficits that are present when recording postsynaptic

currents. A preferential deficit in inhibitory transmitter release has been proposed as a primary mechanism in the *Gnao1* encephalopathy mouse model (Feng et al. 2022). The authors propose that *Gnao1* haplodeficient mice have more free Gβγ available due to the reduced expression of Gαo. In turn, the increased Gβγ may lead to greater inhibition of synaptic proteins involved in vesicle formation and fusion such as SNARE and SNAP-25. This hypothesis motivated our experimental assessment of cortical inhibitory transmission in the *Gnb1*$^{K78R/+}$ mouse model. We were quite surprised to find a reduction in presynaptic inhibitory transmission, and future directions will include an analysis of excitatory postsynaptic currents in *Gnb1*$^{K78R/+}$ cortical networks.

Further supporting a deficit in presynaptic inhibitory transmission as the primary candidate for a cellular mechanism of epilepsy in *Gnb1*$^{K78R/+}$ mice, Gβ1γ2 has been shown to regulate Ca^{2+}-triggered vesicular exocytosis (Blackmer et al. 2005). Using rotating disk electrode voltammetry, Blackmer et al. assessed the impact of over 15 Gβ1 mutants on Gβ1γ1 and Gβ1γ2 inhibition of Ca^{2+}-triggered norepinephrine secretion in PC12 cells. The Gβ1 K78A mutant showed the highest potency for inhibiting Ca^{2+}-triggered norepinephrine secretion (Blackmer et al. 2005). This result highlights the K78 residue as a key site in Gβ1γ2 interactions with synaptic machinery. Moreover, these data further support the disruption in Gβ1γ2 inhibition of GABAergic release as a lead candidate for the epileptic mechanism of the *Gnb1*$^{K78R/+}$ mouse model of *GNB1*-E.

References

Adelman JP (1995) Proteins that interact with the pore-forming subunits of voltage-gated ion channels. *Current Opinion in Neurobiology* **5**:286-295.

Aeby A, Sculier C, Bouza AA, Askar B, Lederer D, Schoonjans AS, Vander Ghinst M, Ceulemans B, Offord J, Lopez-Santiago LF and Isom LL SCN1B-linked early infantile developmental and epileptic encephalopathy. *Annals of Clinical and Translational Neurology*.

Akin EJ, Sole L, Johnson B, el Beheity M, Masson J-B, Krapf D and Tamkun MM (2016) Single-Molecule Imaging of Na(v)1.6 on the Surface of Hippocampal Neurons Reveals Somatic Nanoclusters. *Biophysical Journal* **111**:1235-1247.

Alexandrou AJ, Brown AR, Chapman ML, Estacion M, Turner J, Mis MA, Wilbrey A, Payne EC, Gutteridge A, Cox PJ, Doyle R, Printzenhoff D, Lin Z, Marron BE, West C, Swain NA, Storer RI, Stupple PA, Castle NA, Hounshell JA, Rivara M, Randall A, Dib-Hajj SD, Krafte D, Waxman SG, Patel MK, Butt RP and Stevens EB (2016) Subtype-Selective Small Molecule Inhibitors Reveal a Fundamental Role for Nav1.7 in Nociceptor Electrogenesis, Axonal Conduction and Presynaptic Release. *Plos One* **11**.

Ali SR, Liu Z, Nenov MN, Folorunso O, Singh A, Scala F, Chen H, James TF, Alshammari M, Panova-Elektronova NI, White MA, Zhou J and Laezza F (2018) Functional Modulation of Voltage-Gated Sodium Channels by a FGF14-Based Peptidomimetic. *Acs Chemical Neuroscience* **9**:976-987.

Ali SR, Singh AK and Laezza F (2016) Identification of Amino Acid Residues in Fibroblast Growth Factor 14 (FGF14) Required for Structure-Function Interactions with Voltage-gated Sodium Channel Nav1.6. *Journal of Biological Chemistry* **291**:11268-11284.

Allen AS, Berkovic SF, Cossette P, Delanty N, Dlugos D, Eichler EE, Epstein MP, Glauser T, Goldstein DB, Han Y, Heinzen EL, Hitomi Y, Howell KB, Johnson MR, Kuzniecky R, Lowenstein DH, Lu Y-F, Madou MRZ, Marson AG, Mefford HC, Nieh SE, O'Brien TJ, Ottman R, Petrovski S, Poduri A, Ruzzo EK, Scheffer IE, Sherr EH, Yuskaitis CJ, Abou-Khalil B, Alldredge BK, Bautista JF, Boro A, Cascino GD, Consalvo D, Crumrine P, Devinsky O, Fiol M, Fountain NB, French J, Friedman D, Geller EB, Glynn S, Haut SR, Hayward J, Helmers SL, Joshi S, Kanner A, Kirsch HE, Knowlton RC, Kossoff E, Kuperman R, McGuire SM, Motika PV, Novotny EJ, Paolicchi JM, Parent JM, Park K, Shellhaas RA, Shih JJ, Singh R, Sirven J, Smith MC, Sullivan J, Thio LL, Venkat A, Vining EPG, Von Allmen GK, Weisenberg JL, Widdess-Walsh P and Winawer MR (2013) De novo mutations in epileptic encephalopathies. *Nature* **501**:217-+.

Alroy G, Su HL and Yaari Y (1999) Protein kinase C mediates muscarinic block of intrinsic bursting in rat hippocampal neurons. *Journal of Physiology-London* **518**:71-79.

Anderson KR, Haeussler M, Watanabe C, Janakiraman V, Lund J, Modrusan Z, Stinson J, Bei Q, Buechler A, Yu C, Thamminana SR, Tam L, Sowick M-A, Alcantar T, O'Neil N, Li J, Ta L, Lima L, Roose-Girma M, Rairdan X, Durinck S and Warming S (2018) CRISPR off-target analysis in genetically engineered rats and mice. *Nature Methods* **15**:512-+.

Armstrong CM and Bezanilla F (1977) Inactivation of sodium channel .2. gating current experiments. *Journal of General Physiology* **70**:567-590.

Arya R, Spaeth C, Gilbert DL, Leach JL and Holland KD (2017) GNAO1-associated epileptic encephalopathy and movement disorders: c.607G> A variant represents a probable mutation hotspot with a distinct phenotype. *Epileptic Disorders* **19**:67-75.

Azouz R, Jensen MS and Yaari Y (1994) Muscarinic modulation of intrinsic burst firing in rat hippocampal-neurons. *European Journal of Neuroscience* **6**:961-966.

Backx PH, Yue DT, Lawrence JH, Marban E and Tomaselli GF (1992) Molecular localization of an ion-binding site within the pore of mammalian sodium-channels. *Science* **257**:248-251.

Bagdy G, Kecskemeti V, Riba P and Jakus R (2007) Serotonin and epilepsy. *Journal of Neurochemistry* **100**:857-873.

Bankar G, Goodchild SJ, Howard S, Nelkenbrecher K, Waldbrook M, Dourado M, Shuart NG, Lin S, Young C, Xie Z, Khakh K, Chang E, Sojo LE, Lindgren A, Chowdhury S, Decker S, Grimwood M, Andrez J-C, Dehnhardt CM, Pang J, Chang JH, Safina BS, Sutherlin DP, Johnson JP, Jr., Hackos DH, Robinette CL and Cohen CJ (2018) Selective Na(V)1.7 Antagonists with Long Residence Time Show Improved Efficacy against Inflammatory and Neuropathic Pain. *Cell Reports* **24**:3133-3145.

Bauernfeind AL and Babbitt CC (2017) The predictive nature of transcript expression levels on protein expression in adult human brain. *Bmc Genomics* **18**.

Bean BP (1989) Neurotransmitter inhibition of neuronal calcium currents by changes in channel voltage dependence. *Nature* **340**:153-156.

Beckh S, Noda M, Lubbert H and Numa S (1989) Differential regulation of 3 sodium-channel messenger-rnas in the rat central nervous-system during development. *Embo Journal* **8**:3611-3616.

Bendahhou S, Cummins TR, Kula RW, Fu YH and Ptacek LJ (2002) Impairment of slow inactivation as a common mechanism for periodic paralysis in DIIS4-S5. *Neurology* **58**:1266-1272.

Beneski DA and Catterall WA (1980) Covalent labeling of protein-components of the sodium-channel with a photoactivable derivative of scorpion toxin. *Proceedings of the National Academy of Sciences of the United States of America-Biological Sciences* **77**:639-643.

Bennett PB, Makita N and George AL (1993) A molecular-basis for gating mode transitions in human skeletal-muscle na+ channels. *Febs Letters* **326**:21-24.

Berendt FJ, Park K-S and Trimmer JS (2010) Multisite Phosphorylation of Voltage-Gated Sodium Channel alpha Subunits from Rat Brain. *Journal of Proteome Research* **9**:1976-1984.

Bezanilla F and Armstrong CM (1977) Inactivation of sodium channel .1. sodium current experiments. *Journal of General Physiology* **70**:549-566.

Bouza AA, Edokobi N, Hodges SL, Pinsky AM, Offord J, Piao L, Zhao Y-T, Lopatin AN, Lopez-Santiago LF and Isom LL (2021) Sodium channel beta 1 subunits participate in regulated intramembrane proteolysis-excitation coupling. *Jci Insight* **6**.

Bouza AA and Isom LL (2018) Voltage-Gated Sodium Channel beta Subunits and Their Related Diseases, in *Voltage-Gated Sodium Channels: Structure, Function and Channelopathies* (Chahine M ed) pp 423-450.

Bouza AA, Philippe JM, Edokobi N, Pinsky AM, Offord J, Calhoun JD, Lopez-Floran M, Lopez-Santiago LF, Jenkins PM and Isom LL (2020) Sodium channel?1 subunits are post-translationally modified by tyrosine phosphorylation,S-palmitoylation, and regulated intramembrane proteolysis. *Journal of Biological Chemistry* **295**:10380-10393.

Brackenbury WJ, Calhoun JD, Chen C, Miyazaki H, Nukina N, Oyama F, Ranscht B and Isom LL (2010) Functional reciprocity between Na+ channel Na(v)1.6 and beta 1 subunits in the coordinated regulation of excitability and neurite outgrowth. *Proceedings of the National Academy of Sciences of the United States of America* **107**:2283-2288.

Brackenbury WJ, Yuan Y, O'Malley HA, Parent JM and Isom LL (2013) Abnormal neuronal patterning occurs during early postnatal brain development of Scn1b-null mice and precedes hyperexcitability. *Proceedings of the National Academy of Sciences of the United States of America* **110**:1089-1094.

Brett M, Lai AHM, Ting T-W, Tan A-M, Foo R, Jamuar S and Tan E-C (2017) Acute lymphoblastic leukemia in a child with a de novo germline gnb1 mutation. *American Journal of Medical Genetics Part A* **173**:550-552.

Bromberg KD, Iyengar R and He JC (2008) Regulation of neurite outgrowth by G(i/o) signaling pathways. *Frontiers in Bioscience-Landmark* **13**:4544-4557.

Brunklaus A, Brünger T, Feng T, Fons C, Lehikoinen A, Panagiotakaki E, Vintan M, Symonds J, Andrew J, Arzimanoglou A, Delima S, Gallois J, Hanrahan D, Lesca G, MacLeod S, Marjanovic D, McTague A, Nuñez-Enamorado N, Perez-Palma E, Perry M, Pysden K, Russ-Hall S, Scheffer I, Sully K, Syrbe S, Vaher U, Velayutham M, Vogt J, Weiss S, Wirrell E, Zuberi S, Lal D, Møller R, Mantegazza M, Cestèle S (2022) The gain of function SCN1A disorder spectrum: novel epilepsy phenotypes and therapeutic implications, *Brain*

Bruun TUJ, DesRoches C-L, Wilson D, Chau V, Nakagawa T, Yamasaki M, Hasegawa S, Fukao T, Marshall C and Mercimek-Andrews S (2018) Prospective cohort study for identification of underlying genetic causes in neonatal encephalopathy using whole-exome sequencing. *Genetics in Medicine* **20**:486-494.

Brysch W, Creutzfeldt OD, Luno K, Schlingensiepen R and Schlingensiepen KH (1991) Regional and temporal expression of sodium-channel messenger-rnas in the rat-brain during development. *Experimental Brain Research* **86**:562-567.

Bunton-Stasyshyn RKA, Wagnon JL, Wengert ER, Barker BS, Faulkner A, Wagley PK, Bhatia K, Jones JM, Maniaci MR, Parent JM, Goodkin HP, Patel MK and Meisler MH (2019) Prominent role of forebrain excitatory neurons in SCN8A encephalopathy. *Brain* **142**:362-375.

Caldwell JH, Schaller KL, Lasher RS, Peles E and Levinson SR (2000) Sodium channel Na(v)1.6 is localized at nodes of Ranvier, dendrites, and synapses. *Proceedings of the National Academy of Sciences of the United States of America* **97**:5616-5620.

Cantrell AR, Ma JY, Scheuer T and Catterall WA (1996) Muscarinic modulation of sodium current by activation of protein kinase C in rat hippocampal neurons. *Neuron* **16**:1019-1026.

Cantrell AR, Smith RD, Goldin AL, Scheuer T and Catterall WA (1997) Dopaminergic modulation of sodium current in hippocampal neurons via cAMP-dependent phosphorylation of specific sites in the sodium channel alpha subunit. *Journal of Neuroscience* 17:7330-7338.

Cantrell AR, Scheuer T and Catterall WA (1999) Voltage-dependent neuromodulation of Na+ channels by D1-like dopamine receptors in rat hippocampal neurons. *Journal of Neuroscience* 19:5301-5310.

Cantrell AR and Catterall WA (2001) Neuromodulation of Na+ channels: An unexpected form of cellular plasticity. *Nature Reviews Neuroscience* **2**:397-407.

Cantrell AR, Tibbs VC, Yu FH, Murphy BJ, Sharp EM, Qu YS, Catterall WA and Scheuer T (2002) Molecular mechanism of convergent regulation of brain Na+ channels by protein kinase C and protein kinase A anchored to AKAP-15. *Molecular and Cellular Neuroscience* 21:63-80.

Capes DL, Goldschen-Ohm MP, Arcisio-Miranda M, Bezanilla F and Chanda B (2013) Domain IV voltage-sensor movement is both sufficient and rate limiting for fast inactivation in sodium channels. *Journal of General Physiology* **142**:101-112.

Carvill GL and Mefford HC (2020) Poison exons in neurodevelopment and disease. *Current Opinion in Genetics & Development* **65**:98-102.

Catterall WA (1980) NEUROTOXINS THAT ACT ON VOLTAGE-SENSITIVE SODIUM-CHANNELS IN EXCITABLE-MEMBRANES. *Annual Review of Pharmacology and Toxicology* **20**:15-43.

Catterall WA, Schmidt JW, Messner DJ and Feller DJ (1986) Structure and biosynthesis of neuronal sodium-channels. *Annals of the New York Academy of Sciences* **479**:186-203

Catterall WA (1992) Cellular and molecular-biology of voltage-gated sodium-channels. *Physiological Reviews* **72**:S15-S48.

Catterall WA (2000) From ionic currents to molecular mechanisms: The structure and function of voltage-gated sodium channels. *Neuron* **26**:13-25.

Catterall WA, Goldin AL and Waxman SG (2005) International Union of Pharmacology. XLVII. Nomenclature and structure-function relationships of voltage-gated sodium channels. *Pharmacological Reviews* **57**:397-409.

Catterall WA (2012) Voltage-gated sodium channels at 60: structure, function and pathophysiology. *Journal of Physiology-London* **590**:2577-2589.

Catterall W, Lenaeus MJ and Gamal El-Din T (2020) Structure and Pharmacology of Voltage-Gated Sodium and Calcium Channels. *Annual Review Pharmacology and Toxicology **60***:133-154

Carr DB, Cooper DC, Ulrich SL, Spruston N and Surmeier DJ (2002) Serotonin receptor activation inhibits sodium current and dendritic excitability in prefrontal cortex via a protein kinase C-dependent mechanism. *Journal of Neuroscience* 22:6846-6855.

Carr DB, Day M, Cantrell AR, Held J, Scheuer T, Catterall WA and Surmeier DJ (2003) Transmitter modulation of slow, activity-dependent alterations in sodium channel availability endows neurons with a novel form of cellular plasticity. *Neuron* 39:793-806.

Cestele S and Catterall WA (2000) Molecular mechanisms of neurotoxin action on voltage-gated sodium channels. *Biochimie* **82**:883-892.

Cheah CS, Westenbroek RE, Roden WH, Kalume F, Oakley JC, Jansen LA and Catterall WA (2013) Correlations in timing of sodium channel expression, epilepsy, and sudden death in Dravet syndrome. *Channels* **7**:468-472.

Cheah CS, Yu FH, Westenbroek RE, Kalume FK, Oakley JC, Potter GB, Rubenstein JL and Catterall WA (2012) Specific deletion of Na(V)1.1 sodium channels in inhibitory interneurons causes seizures and premature death in a mouse model of Dravet syndrome. *Proceedings of the National Academy of Sciences of the United States of America* **109**:14646-14651.

Chen J, DeVivo M, Dingus J, Harry A, Li J, Sui J, Carty DJ, Blank JL Exton JH, Stoffel RH, Inglese J, Lefkowitz RJ, Logothetis DE, Hildebrandt JD and Iyengar RA (1995) region of adenylyl cyclase 2 critical for regulation by G protein beta gamma subunits. *Science* **268**:1166-1169.

Chen CL, Westenbroek RE, Xu XR, Edwards CA, Sorenson DR, Chen YA, McEwen DP, O'Malley HA, Bharucha V, Meadows LS, Knudsen GA, Vilaythong A, Noebels JL, Saunders TL, Scheuer T, Shrager P, Catterall WA and Isom LL (2004) Mice lacking sodium channel beta 1 subunits display defects in neuronal excitability, sodium channel expression, and nodal architecture. Journal of Neuroscience 24:4030-4042.

Chen YA, Yu FH, Surmeier DJ, Scheuer T and Catterall WA (2006) Neuromodulation of Na+ channel slow inactivation via cAMP-dependent protein kinase and protein kinase C. Neuron 49:409-420.

Chen Y, Yu FH, Sharp EM, Beacham D, Scheuer T and Catterall WA (2008) Functional properties and differential neuromodulation of Na(v)1.6 channels. Molecular and Cellular Neuroscience 38:607-615.

Chen CL, Calhoun JD, Zhang YQ, Lopez-Santiago L, Zhou N, Davis TH, Salzer JL and Isom LL (2012) Identification of the Cysteine Residue Responsible for Disulfide Linkage of Na+ Channel alpha and beta 2 Subunits. *Journal of Biological Chemistry* **287**:39061-39069.

Chen R and Chung SH (2014) Mechanism of tetrodotoxin block and resistance in sodium channels. *Biochemical and Biophysical Research Communications* **446**:370-374.

Chiamvimonvat N, PerezGarcia MT, Tomaselli GF and Marban E (1996) Control of ion flux and selectivity by negatively charged residues in the outer mouth of rat sodium channels. *Journal of Physiology-London* **491**:51-59.

Claes L, Del-Favero J, Ceulemans B, Lagae L, Van Broeckhoven C and De Jonghe P (2001) De novo mutations in the sodium-channel gene SCN1A cause severe myoclonic epilepsy of infancy. *American Journal of Human Genetics* **68**:1327-1332.

Clapham DE (1994) Direct g-protein activation of ion channels. *Annual Review of Neuroscience* **17**:441-464.

Clapham DE and Neer EJ (1997) G protein beta gamma subunits. *Annual Review of Pharmacology and Toxicology* **37**:167-203.

Colombo S, Petri S, Shalomov B, Reddy HP, Tabak G, Dhindsa RS, Gelfman S, Teng S, Krizay D, Rafikian EE, Bera AK, Yang M, Boland MJ, Peng Y, Frankel WN, Dascal N and Goldstein DB (2019) G protein-coupled potassium channels implicated in mouse and cellular models of GNB1 Encephalopathy. *bioRxiv*:697235.

Cong L, Ran FA, Cox D, Lin S, Barretto R, Habib N, Hsu PD, Wu X, Jiang W, Marraffini LA and Zhang F (2013) Multiplex Genome Engineering Using CRISPR/Cas Systems. *Science* **339**:819-823.

Cooper MS, McIntosh A, Crompton DE, McMahon JM, Schneider A, Farrell K, Ganesan V, Gill D, Kivity S, Lerman-Sagie T, McLellan A, Pelekanos J, Ramesh V, Sadleir L, Wirrell E and Scheffer IE (2016) Mortality in Dravet syndrome. *Epilepsy Research* **128**:43-47.

Costa MRC, Casnellie JE and Catterall WA (1982) Selective phosphorylation of the alpha-subunit of the sodium-channel by camp-dependent protein-kinase. *Journal of Biological Chemistry* **257**:7918-7921.

Costa MRC and Catterall WA (1984) Phosphorylation of the alpha-subunit of the sodium-channel by protein kinase-c. *Cellular and Molecular Neurobiology* **4**:291-297.

Cox JJ, Reimann F, Nicholas AK, Thornton G, Roberts E, Springell K, Karbani G, Jafri H, Mannan J, Raashid Y, Al-Gazali L, Hamamy H, Valente EM, Gorman S, Williams R, McHale DP, Wood JN, Gribble FM and Woods CG (2006) An SCN9A channelopathy causes congenital inability to experience pain. *Nature* **444**:894-898.

Coulter DA, Huguenard JR, Prince DA (1989) Specific petit mal anticonvulsants reduce calcium currents in thalamic neurons. *Neuroscience Letters* **98**:74–78.

Coulter DA, Huguenard JR, Prince DA (1990) Differential effects of petit mal anticonvulsants and convulsants on thalamic neurones: calcium current reduction. *Br J Pharmacol* **100**:800–806.

Crill WE (1996) Persistent sodium current in mammalian central neurons. *Annual Review of Physiology* **58**:349-362.

Crunelli V, Leresche L (2022) Block of Thalamic T-Type Ca2+ Channels by Ethosuximide Is Not the Whole Story. *Epilepsy Currents* 2(2):53-56.

Danti FR, Galosi S, Romani M, Montomoli M, Carss KJ, Raymond FL, Parrini E, Bianchini C, McShane T, Dale RC, Mohammad SS, Shah U, Mahant N, Ng J, McTague A, Samanta R, Vadlamani G, Valente EM, Leuzzi V, Kurian MA and Guerrini R (2017) GNAO1 encephalopathy Broadening the phenotype and evaluating treatment and outcome. *Neurology-Genetics* **3**.

Das S, Gilchrist J, Bosmans F and Van Petegem F (2016) Binary architecture of the Na(v)1.2-beta 2 signaling complex. *Elife* **5**.

Dascal N (2001a) Voltage clamp recordings from Xenopus oocytes. *Current protocols in neuroscience* **6**.

Dascal N (2001b) Ion-channel regulation by G proteins. Trends in Endocrinology and Metabolism 12:391-398.

Dascal N and Lotan I (1991) Activation of protein-kinase-c alters voltage dependence of a na+ channel. *Neuron* **6**:165-175.

Dascal N, Schreibmayer W, Lim NF, Wang WZ, Chavkin C, Dimagno L, Labarca C, Kieffer BL, Gaveriauxruff C, Trollinger D, Lester HA and Davidson N (1993) Atrial g-protein-activated k+-channel - expression cloning and molecular-properties. *Proceedings of the National Academy of Sciences of the United States of America* **90**:10235-10239.

Denomme N (2018) The Domino Effect: Ed Domino's early studies of Psychoactive Drugs. *Journal of Psychoactive Drugs* **50**:298-305.

Denomme N, Hull JM and Mashour GA (2019) Role of Voltage-Gated Sodium Channels in the Mechanism of Ether-Induced Unconsciousness. *Pharmacological Reviews* **71**:450-466.

Denomme N, Lukowski AL, Hull JM, Jameson MB, Bouza AA, Narayan ARH and Isom LL (2020) The voltage-gated sodium channel inhibitor, 4,9-anhydrotetrodotoxin, blocks human Na(v)1.1 in addition to Na(v)1.6. *Neuroscience Letters* **724**.

Deschenes I and Tomaselli GF (2002) Modulation of Kv4.3 current by accessory subunits. *Febs Letters* **528**:183-188.

Deuis JR, Dvorakova LS and Vetter I (2017) Methods Used to Evaluate Pain Behaviors in Rodents. *Frontiers in Molecular Neuroscience* **10**.

Dhingra NK, Freed MA and Smith RG (2005) Voltage-gated sodium channels improve contrast sensitivity of a retinal ganglion cell. *Journal of Neuroscience* **25**:8097-8103.

Dick IE, Brochu RM, Purohit Y, Kaczorowski GJ, Martin WJ and Priest BT (2007) Sodium channel blockade may contribute to the analgesic efficacy of antidepressants. *Journal of Pain* **8**:315-324.

DiMauro EF, Altmann S, Berry LM, Bregman H, Chakka N, Chu-Moyer M, Bojic EF, Foti RS, Fremeau R, Gao H, Gunaydin H, Guzman-Perez A, Hall BE, Huang H, Jarosh M, Korneook T, Lee J, Ligutti J, Liu D, Moyer BD, Ortuno D, Rose PE, Schenkel LB, Taborn K, Wang J, Wang Y, Yu V and Weiss MM (2016) Application of a Parallel Synthetic Strategy in the Discovery of Biaryl Acyl Sulfonamides as Efficient and Selective Na(V)1.7 Inhibitors. *Journal of Medicinal Chemistry* **59**:7818-7839.

Diverse-Pierluissi M, Goldsmith PK and Dunlap K (1995) Transmitter-mediated inhibition of n-type calcium channels in sensory neurons involves multiple gtp-binding proteins and subunits. *Neuron* **14**:191-200.

Doench JG, Fusi N, Sullender M, Hegde M, Vaimberg EW, Donovan KF, Smith I, Tothova Z, Wilen C, Orchard R, Virgin HW, Listgarten J and Root DE (2016) Optimized sgRNA design to maximize activity and minimize off-target effects of CRISPR-Cas9. *Nature Biotechnology* **34**:184-+.

Dravet C (1978). Les epilepsies graves de l'enfant. *Vie Med*. **8**:543-548)

Dravet C (2011) The core Dravet syndrome phenotype. *Epilepsia* **52**:3-9.

Eaholtz G, Scheuer T and Catterall WA (1994) Restoration of inactivation and block of open sodium-channels by an inactivation gate peptide. *Neuron* **12**:1041-1048.

Edokobi N and Isom LL (2018) Voltage-Gated Sodium Channel beta 1/beta 1B Subunits Regulate Cardiac Physiology and Pathophysiology. *Frontiers in Physiology* **9**.

Endo W, Ikemoto S, Togashi N, Miyabayashi T, Nakajima E, Hamano S-i, Shibuya M, Sato R, Takezawa Y, Okubo Y, Inui T, Kato M, Sengoku T, Ogata K, Hamanaka K, Mizuguchi T, Miyatake S, Nakashima M, Matsumoto N and Haginoya K (2020) Phenotype-genotype correlations in patients with GNB1 gene variants,

including the first three reported Japanese patients to exhibit spastic diplegia, dyskinetic quadriplegia, and infantile spasms. *Brain & Development* **42**:199-204.

England S and de Groot MJ (2009) Subtype-selective targeting of voltage-gated sodium channels. *British Journal of Pharmacology* **158**:1413-1425.

Escoubas P, Diochot S, Celerier ML, Nakajima T and Lazdunski M (2002) Novel tarantula toxins for subtypes of voltage-dependent potassium channels in the Kv2 and Kv4 subfamilies. *Molecular Pharmacology* **62**:48-57.

Estacion M, O'Brien JE, Conravey A, Hammer MF, Waxman SG, Dib-Hajj SD and Meisler MH (2014) A novel de novo mutation of SCN8A (Na(v)1.6) with enhanced channel activation in a child with epileptic encephalopathy. *Neurobiology of Disease* **69**:117-123.

Faingold CL, Kommajosyula SP, Long X, Plath K and Randall M (2014) Serotonin and sudden death: Differential effects of serotonergic drugs on seizure-induced respiratory arrest in DBA/1 mice. *Epilepsy & Behavior* **37**:198-203.

Faingold CL, Randall M, Zeng C, Peng S, Long X and Feng H-J (2016) Serotonergic agents act on 5-HT3 receptors in the brain to block seizure-induced respiratory arrest in the DBA/1 mouse model of SUDEP. *Epilepsy & Behavior* **64**:166-170.

Fattorusso A, Matricardi S, Mencaroni E, Dell'Isola GB, Di Cara G, Striano P and Verrotti A (2021) The Pharmacoresistant Epilepsy: An Overview on Existant and New Emerging Therapies. *Frontiers in Neurology* **12**.

Favero M, Sotuyo NP, Lopez E, Kearney JA and Goldberg EM (2018) A Transient Developmental Window of Fast-Spiking Interneuron Dysfunction in a Mouse Model of Dravet Syndrome. *Journal of Neuroscience* **38**:7912-7927.

Favre I, Moczydlowski E and Schild L (1996) On the structural basis for ionic selectivity among Na+, K+, and Ca2+ in the voltage-gated sodium channel. *Biophysical Journal* **71**:3110-3125.

Featherstone DE, Richmond JE and Ruben PC (1996) Interaction between fast and slow inactivation in Skm1 sodium channels. *Biophysical Journal* **71**:3098-3109.

Feng H, Khalil S, Neubig RR and Sidiropoulos C (2018) A mechanistic review on GNAO1-associated movement disorder. *Neurobiology of Disease* **116**:131-141.

Feng H, Larrivee CL, Demireva EY, Xie H, Leipprandt JR and Neubig RR (2019) Mouse models of GNAO1-associated movement disorder: Allele- and sex-specific differences in phenotypes. *Plos One* **14**.

Feng H, Sjogren B, Karaj B, Shaw V, Gezer A and Neubig RR (2017) Movement disorder in GNAO1 encephalopathy associated with gain-of-function mutations. *Neurology* **89**:762-770.

Feng H, Yuan Y, Williams MR, Roy AJ, Leipprandt JR and Neubig RR (2022) Mice with monoallelic GNAO1 loss exhibit reduced inhibitory synaptic input to cerebellar Purkinje cells. *Journal of Neurophysiology* **127**:607-622.

Feng H-J and Faingold CL (2017) Abnormalities of serotonergic neurotransmission in animal models of SUDEP. *Epilepsy & Behavior* **71**:174-180.

Fleidervish IA, Friedman A and Gutnick MJ (1996) Slow inactivation of Na+ current and slow cumulative spike adaptation in mouse and guinea-pig neocortical neurones in slices (vol 493, pg 83, 1996). *Journal of Physiology-London* **494**:907-907.

Focken T, Burford K, Grimwood ME, Zenova A, Andrez J-C, Gong W, Wilson M, Taron M, Decker S, Lofstrand V, Chowdhury S, Shuart N, Lin S, Goodchild SJ, Young C, Soriano M, Tari PK, Waldbrook M, Nelkenbrecher K, Kwan R, Lindgren A, de Boer G, Lee S, Sojo L, DeVita RJ, Cohen CJ, Wesolowski SS, Johnson JP, Jr., Dehnhardt CM and Empfield JR (2019) Identification of CNS-Penetrant Aryl Sulfonamides as Isoform-Selective Na(V)1.6 Inhibitors with Efficacy in Mouse Models of Epilepsy. *Journal of Medicinal Chemistry* **62**:9618-9641.

Focken T, Chowdhury S, Zenova A, Grimwood ME, Chabot C, Sheng T, Hemeon I, Decker SM, Wilson M, Bichler P, Jia Q, Sun S, Young C, Lin S, Goodchild SJ, Shuart NG, Chang E, Xie Z, Li B, Khakh K, Bankar G, Waldbrook M, Kwan R, Nelkenbrecher K, Tari PK, Chahal N, Sojo L, Robinette CL, White AD, Chen C-A, Zhang Y, Pang J, Chang JH, Hackos DH, Johnson JP, Cohen CJ, Ortwine DF, Sutherlin DP, Dehnhardt CM and Safina BS (2018) Design of Conformationally Constrained Acyl Sulfonamide Isosteres: Identification of N-(1,2,4 Triazolo 4,3-a pyridin-3-yl)methane-sulfonamidesas Potent and Selective hNa(v)1.7 Inhibitors for the Treatment of Pain. *Journal of Medicinal Chemistry* **61**:4810-4831.

Fong HKW, Hurley JB, Hopkins RS, Miakelye R, Johnson MS, Doolittle RF and Simon MI (1986) repetitive segmental structure of the transducin beta-subunit - homology with the cdc4 gene and identification of related messenger-rnas. *Proceedings of the National Academy of Sciences of the United States of America* **83**:2162-2166.

Ford CE, Skiba NP, Bae HS, Daaka YH, Reuveny E, Shekter LR, Rosal R, Weng GZ, Yang CS, Iyengar R, Miller RJ, Jan LY, Lefkowitz RJ and Hamm HE (1998) Molecular basis for interactions of G protein beta gamma subunits with effectors. *Science* **280**:1271-1274.

Fozzard HA and Lipkind GM (2010) The Tetrodotoxin Binding Site Is within the Outer Vestibule of the Sodium Channel. *Marine Drugs* **8**:219-234.

Franceschetti S, Taverna S, Sancini G, Panzica F, Lombardi R and Avanzini G (2000) Protein kinase C-dependent modulation of Na+ currents increases the excitability of rat neocortical pyramidal neurones. *Journal of Physiology-London* **528**:291-304.

Frasier CR, Wagnon JL, Bao YO, McVeigh LG, Lopez-Santiago LF, Meisler MH and Isom LL (2016) Cardiac arrhythmia in a mouse model of sodium channel SCN8A epileptic encephalopathy. *Proceedings of the National Academy of Sciences of the United States of America* **113**:12838-12843.

Frederiksen K, Lu D, Yang J, Jensen HS, Bastlund JF, Larsen PH, Liu H, Crestey F, Dekermendjian K, Badolo L, Laursen M, Hougaard C, Yang C, Svenstrup N and Grunnet M (2017) A small molecule activator of Na(v)1.1 channels increases fast-spiking interneuron excitability and GABAergic transmission in vitro and has anti-convulsive effects in vivo. *European Journal of Neuroscience* **46**:1887-1896.

Freissmuth M, Casey PJ and Gilman AG (1989) G-proteins control diverse pathways of transmembrane signaling. *Faseb Journal* **3**:2125-2131.

Gawlinski P, Posmyk R, Gambin T, Sielicka D, Chorazy M, Nowakowska B, Jhangiani SN, Muzny DM, Bekiesinska-Figatowska M, Bal J, Boerwinkle E, Gibbs RA, Lupski JR and Wiszniewski W (2016) PEHO Syndrome May Represent Phenotypic Expansion at the Severe End of the Early-Onset Encephalopathies. *Pediatric Neurology* **60**:83-87.

Geffeney S, Brodie ED and Ruben PC (2002) Mechanisms of adaptation in a predator-prey arms race: TTX-resistant sodium channels. *Science* **297**:1336-1339.

Geffeney SL, Fujimoto E, Brodie ED and Ruben PC (2005) Evolutionary diversification of TTX-resistant sodium channels in a predator-prey interaction. *Nature* **434**:759-763.

Genton P, Velizarova R and Dravet C (2011) Dravet syndrome: The long-term outcome. *Epilepsia* **52**:44-49.

Georgi B, Voight BF and Bucan M (2013) From Mouse to Human: Evolutionary Genomics Analysis of Human Orthologs of Essential Genes. *Plos Genetics* **9**.

Gerald B, Ramsey K, Belnap N, Szelinger S, Siniard AL, Balak C, Russell M, Richholt R, De Both M, Claasen AM, Schrauwen I, Huentelman MJ, Craig DW, Rangasamy S and Narayanan V (2018) Neonatal epileptic encephalopathy caused by de novo GNAO1 mutation misdiagnosed as atypical Rett syndrome:

Cautions in interpretation of genomic test results. *Seminars in Pediatric Neurology* **26**:28-32.

Gershon E, Weigl L, Lotan I, Schreibmayer W and Dascal N (1992) Protein kinase-a reduces voltage-dependent na+ current in xenopus oocytes. *Journal of Neuroscience* **12**:3743-3752.

Gilchrist J, Das S, Van Petegem F and Bosmans F (2013) Crystallographic insights into sodium-channel modulation by the beta 4 subunit. *Proceedings of the National Academy of Sciences of the United States of America* **110**:E5016-E5024.

Gingras J, Smith S, Matson DJ, Johnson D, Nye K, Couture L, Feric E, Yin R, Moyer BD, Peterson ML, Rottman JB, Beiler RJ, Malmberg AB and McDonough SI (2014) Global Nav1.7 Knockout Mice Recapitulate the Phenotype of Human Congenital Indifference to Pain. *Plos One* **9**.

Goff KM and Goldberg EM (2019) Vasoactive intestinal peptide-expressing interneurons are impaired in a mouse model of Dravet syndrome. *Elife* **8**.

Goldberg YP, MacFarlane J, MacDonald ML, Thompson J, Dube MP, Mattice M, Fraser R, Young C, Hossain S, Pape T, Payne B, Radomski C, Donaldson G, Ives E, Cox J, Younghusband HB, Green R, Duff A, Boltshauser E, Grinspan GA, Dimon JH, Sibley BG, Andria G, Toscano E, Kerdraon J, Bowsher D, Pimstone SN, Samuels ME, Sherrington R and Hayden MR (2007) Loss-of-function mutations in the Na(v)1.7 gene underlie congenital indifference to pain in multiple human populations. *Clinical Genetics* **71**:311-319.

Goldin AL (1993) Accessory subunits and sodium channel inactivation. *Current opinion in neurobiology* **3**:272-277.

Goldin AL (2001) Resurgence of sodium channel research. *Annual Review of Physiology* **63**:871-894.

Goldin AL, Snutch T, Lubbert H, Dowsett A, Marshall J, Auld V, Downey W, Fritz LC, Lester HA, Dunn R, Catterall WA and Davidson N (1986) Messenger-rna coding for only the alpha-subunit of the rat-brain na-channel is sufficient for expression of functional channels in xenopus-oocytes. *Proceedings of the National Academy of Sciences of the United States of America* **83**:7503-7507.

Gong B, Rhodes KJ, Bekele-Arcuri Z and Trimmer JS (1999) Type I and type II Na^+ channel alpha-subunit polypeptides exhibit distinct spatial and temporal patterning, and association with auxiliary subunits in rat brain. *Journal of Comparative Neurology* **412**:342-352.

Goto T, Kishi Y, Takahash.S and Hirata Y (1965) Tetrodotoxin. *Tetrahedron* **21**:2059-&.

Gurnett CA and Campbell KP (1996) Transmembrane auxiliary subunits of voltage-dependent ion channels. *Journal of Biological Chemistry* **271**:27975-27978.

Haeussler M, Schoenig K, Eckert H, Eschstruth A, Mianne J, Renaud J-B, Schneider-Maunoury S, Shkumatava A, Teboul L, Kent J, Joly J-S and Concordet J-P (2016) Evaluation of off-target and on-target scoring algorithms and integration into the guide RNA selection tool CRISPOR. *Genome Biology* **17**.

Hammond C (2009). *Cellular and Molecular Neurophysiology*

Han Z, Chen C, Christiansen A, Ji S, Lin Q, Anumonwo C, Liu C, Leiser SC, Meena, Aznarez I, Liau G and Isom LL (2020) Antisense oligonucleotides increase Scn1a expression and reduce seizures and SUDEP incidence in a mouse model of Dravet syndrome. *Science Translational Medicine* **12**.

Hanifin CT and Gilly WF (2015) Evolutionary history of a complex adaptation: Tetrodotoxin resistance in salamanders. *Evolution* **69**:232-244.

Hargus NJ, Nigam A, Bertram EH and Patel MK (2013) Evidence for a role of Na(v)1.6 in facilitating increases in neuronal hyperexcitability during epileptogenesis. *Journal of Neurophysiology* **110**:1144-1157.

Hartshorne RP and Catterall WA (1981) Purification of the saxitoxin receptor of the sodium-channel from rat-brain. *Proceedings of the National Academy of Sciences of the United States of America-Biological Sciences* **78**:4620-4624.

Hartshorne RP and Catterall WA (1984) The sodium-channel from rat-brain - purification and subunit composition. *Journal of Biological Chemistry* **259**:1667-1675.

Hartshorne RP, Messner DJ, Coppersmith JC and Catterall WA (1982) The saxitoxin receptor of the sodium-channel from rat-brain - evidence for 2 non-identical beta-subunits. *Journal of Biological Chemistry* **257**:3888-3891.

He JC, Neves SR, Jordan JD and Iyengar R (2006) Role of the G(o/i) signaling network in the regulation of neurite outgrowth. *Canadian Journal of Physiology and Pharmacology* **84**:687-694.

He B and Soderlund DM (2010) Human embryonic kidney (HEK293) cells express endogenous voltage-gated sodium currents and Na(v)1.7 sodium channels. *Neuroscience Letters* **469**:268-272.

Heggeness ST and Starkus JG (1986) Saxitoxin and tetrodotoxin - electrostatic effects on sodium-channel gating current in crayfish axons. *Biophysical Journal* **49**:629-643.

Heighway J, Sedo A, Garg A, Eldershaw L, Perreau V, Berecki G, Reid CA, Petrou S and Maljevic S (2022) Sodium channel expression and transcript variation in the developing brain of human, Rhesus monkey, and mouse. *Neurobiology of Disease* **164**.

Heinemann SH, Teriau H, Stuhmer W, Imoto K and Numa S (1992a) Calcium-channel characteristics conferred on the sodium-channel by single mutations. *Nature* **356**:441-443.

Heinemann SH, Terlau H and Imoto K (1992b) Molecular-basis for pharmacological differences between brain and cardiac sodium-channels. *Pflugers Archiv-European Journal of Physiology* **422**:90-92.

Helbig KL, Hagman KDF, Shinde DN, Mroske C, Powis Z, Li S, Tang S and Helbig I (2016) Diagnostic exome sequencing provides a molecular diagnosis for a significant proportion of patients with epilepsy. *Genetics in Medicine* **18**:898-905.

Hemati P, Revah-Politi A, Bassan H, Petrovski S, Bilancia CG, Ramsey K, Griffin NG, Bier L, Cho MT, Rosello M, Lynch SA, Colombo S, Weber A, Haug M, Heinzen EL, Sands TT, Narayanan V, Primiano M, Aggarwal VS, Millan F, Sattler-Holtrop SG, Caro-Llopis A, Pillar N, Baker J, Freedman R, Kroes HY, Sacharow S, Stong N, Lapunzina P, Schneider MC, Mendelsohn NJ, Singleton A, Ramey VL, Wou K, Kuzminsky A, Monfort S, Weiss M, Doyle S, Iglesias A, Martinez F, McKenzie F, Orellana C, van Gassen KLI, Palomares M, Bazak L, Lee A, Bircher A, Basel-Vanagaite L, Hafstrom M, Houge G, Goldstein DB, Anyane-Yeboa K, Grp CRR and Study DDD (2018) Refining the phenotype associated with GNB1 mutations: Clinical data on 18 newly identified patients and review of the literature. *American Journal of Medical Genetics Part A* **176**:2259-2275.

Herlitze S, Hockerman GH, Scheuer T and Catterall WA (1997) Molecular determinants of inactivation and G protein modulation in the intracellular loop connecting domains I and II of the calcium channel alpha(1A) subunit. *Proceedings of the National Academy of Sciences of the United States of America* **94**:1512-1516.

Hesdorffer DC, Tomson T, Benn E, Sander JW, Nilsson L, Langan Y, Walczak TS, Beghi E, Brodie MJ, Hauser A and Subco ICE (2011) Combined analysis of risk factors for SUDEP. *Epilepsia* **52**:1150-1159.

Higurashi N, Uchida T, Lossin C, Misumi Y, Okada Y, Akamatsu W, Imaizumi Y, Zhang B, Nabeshima K, Mori MX, Katsurabayashi S, Shirasaka Y, Okano H and Hirose S (2013) A human Dravet syndrome model from patient induced pluripotent stem cells. *Molecular Brain* **6**.

Hill SF and Meisler MH (2021) Antisense oligonucleotide therapy for neurodevelopmental disorders. *Developmental neuroscience* **43**:247-252.

Hille B (1994) Modulation of ion-channel function by g-protein-coupled receptors. Trends in Neurosciences 17:531-536.

Hille B (2001) Ion Channels of Excitable Membranes. 3rd Edition.

Hodgkin AL and Huxley AF (1952) The dual effect of membrane potential on sodium conductance in the giant axon of loligo. *Journal of Physiology-London* **116**:497-506.

Hu WQ, Tian CP, Li T, Yang MP, Hou H and Shu YS (2009) Distinct contributions of Na(v)1.6 and Na(v)1.2 in action potential initiation and backpropagation. *Nature Neuroscience* **12**:996-U961.

Huguenard, JR and Prince DA (1994) Intrathalamic rhythmicity studied in vitro: nominal T-current modulation causes robust antioscillatory effects. *Journal of Neurosci*ence **14**:5485–5502.

Huguenard J (2019) Current controversy: spikes, bursts, and synchrony in generalized absence epilepsy: unresolved questions regarding thalamocortical synchrony in absence epilepsy. *Epilepsy Currents* **19**:105-111.

Hull JM and Isom LL (2018) Voltage-gated sodium channel beta subunits: The power outside the pore in brain development and disease. *Neuropharmacology* **132**:43-57.

Hull JM (2019) The Role of the Voltage Gated Sodium Channel Gene Scn1b in Neuronal Excitability and Network Synchrony

Hull JM, O'Malley HA, Chen C, Yuan Y, Denomme N, Bouza AA, Anumonwo C, Lopez-Santiago LF and Isom LL (2020) Excitatory and inhibitory neuron defects in a mouse model of Scn1b-linked EIEE52. *Annals of Clinical and Translational Neurology* **7**:2137-2149.

Ikeda SR (1996) Voltage-dependent modulation of N-type calcium channels by G-protein beta gamma subunits. *Nature* **380**:255-258.

Imendra KG, Fujiyama R, Miyamato T, Okada Y and Sato T (2000) Serotonin inhibits voltage-gated sodium current by cyclic adenosine monophosphate-dependent mechanism in bullfrog taste receptor cells. *Neuroscience Letters* **294**:151-154.

Isom LL and Catterall WA (1996) Na+ channel subunits and Ig domains. *Nature* **383**:307-308.

Isom LL, Dejongh KS and Catterall WA (1994) Auxiliary subunits of voltage-gated ion channels. *Neuron* **12**:1183-1194.

Isom LL, Dejongh KS, Patton DE, Reber BFX, Offord J, Charbonneau H, Walsh K, Goldin AL and Catterall WA (1992) Primary structure and functional expression of the beta-1-subunit of the rat-brain sodium-channel. *Science* **256**:839-842.

Isom LL and Knupp KG (2021) Dravet Syndrome: Novel Approaches for the Most Common Genetic Epilepsy. *Neurotherapeutics* **18**:1524-1534.

Isom LL, Ragsdale DS, Dejongh KS, Westenbroek RE, Reber BFX, Scheuer T and Catterall WA (1995a) Structure and function of the beta-2 subunit of brain sodium-channels, a transmembrane glycoprotein with a cam motif. *Cell* **83**:433-442.

Isom LL, Scheuer T, Brownstein AB, Ragsdale DS, Murphy BJ and Catterall WA (1995b) Functional coexpression of the beta-1 and type iia alpha-subunits of sodium-channels in a mammalian-cell line. *Journal of Biological Chemistry* **270**:3306-3312.

Jensen HS, Grunnet M and Bastlund JF (2014) Therapeutic potential of Na(v)1.1 activators. *Trends in Pharmacological Sciences* **35**:113-118.

Jiang D, Shi H, Tonggu L, El-Din TMG, Lenaeus MJ, Zhao Y, Yoshioka C, Zheng N and Catterall WA (2020) Structure of the Cardiac Sodium Channel. *Cell* **180**:122-+.

Jiang MS, Gold MS, Boulay G, Spicher K, Peyton M, Brabet P, Srinivasan Y, Rudolph U, Ellison G and Birnbaumer L (1998) Multiple neurological abnormalities in mice deficient in the G protein G(o). *Proceedings of the National Academy of Sciences of the United States of America* **95**:3269-3274.

Johannesen KM, Gardena E, Encinas AC, Lehesjoki A-E, Linnankivi T, Petersen MB, Lund ICB, Blichfeldt S, Miranda MJ, Pal DK, Lascelles K, Procopis P, Orsini A, Bonuccelli A, Giacomini T, Helbig I, Fenger CD, Sisodiya SM, Hernandez-Hernandez L, Krithika S, Rumple M, Masnada S, Valente M, Cereda C, Giordano L, Accorsi P, Burki S, Mancardi M, Korff C, Guerrini R, von Spiczak S, Hoffman-Zacharska D, Mazurczak T, Coppola A, Buono S, Vecchi M, Hammer MF, Varesio C, Veggiotti P, Lal D, Bruenger T, Zara F, Striano P, Rohholi G and Moller RS (2019) The spectrum of intermediate SCN8A-related epilepsy. *Epilepsia* **60**:830-844.

Johnson D, Montpetit ML, Stocker PJ and Bennett ES (2004) The sialic acid component of the beta(1) subunit modulates voltage-gated sodium channel function. *Journal of Biological Chemistry* **279**:44303-44310.

Johnson KW, Herold KF, Milner TA, Hemmings HC, Jr. and Platholi J (2017) Sodium channel subtypes are differentially localized to pre- and post-synaptic sites in rat hippocampus. *Journal of Comparative Neurology* **525**:3563-3578.

Johnson JP, Focken T, Khakh K, Tari PK, Dube C, Goodchild SJ, Andrez J-C, Bankar G, Bogucki D, Burford K, Chang E, Chowdhury S, Dean R, de Boer G, Decker S, Dehnhardt C, Feng M, Gong W, Grimwood M, Hasan A, Hussainkhel A, Jia Q, Lee S, Li J, Lin S, Lindgren A, Lofstrand V, Mezeyova J, Namdari R, Nelkenbrecher K, Shuart NG, Sojo L, Sun S, Taron M, Waldbrook M, Weeratunge D, Wesolowski S, Williams A, Wilson M, Xie Z, Yoo R, Young C, Zenova A, Zhang W, Cutts AJ, Sherrington RP, Pimstone SN, Winquist R, Cohen CJ, Empfield JR and Chanda B (2022) NBI-921352, a first-in-class, Na(V)1.6 selective, sodium channel inhibitor that prevents seizures in Scn8a gain-of-function mice, and wild-type mice and rats. *Elife* **11**.

Jones HF, Morales-Briceno H, Barwick K, Lewis J, Sanchis-Juan A, Raymond FL, Stewart K, Waugh M-C, Mahant N, Kurian MA, Dale RC and Mohammad SS (2019) Myoclonus-dystonia caused by GNB1 mutation responsive to deep brain stimulation. *Movement Disorders* **34**:1079-1080.

Jung HY, Mickus T and Spruston N (1997) Prolonged sodium channel inactivation contributes to dendritic action potential attenuation in hippocampal pyramidal neurons. *Journal of Neuroscience* **17**:6639-6646.

Kalume F, Oakley JC, Westenbroek RE, Gile J, de la Iglesia HO, Scheuer T and Catterall WA (2015) Sleep impairment and reduced interneuron excitability in a mouse model of Dravet Syndrome. *Neurobiology of Disease* **77**:141-154.

Kanellopoulos AH, Koenig J, Huang HL, Pyrski M, Millet Q, Lolignier S, Morohashi T, Gossage SJ, Jay M, Linley JE, Baskozos G, Kessler BM, Cox JJ, Dolphin AC, Zufall F, Wood JN and Zhao J (2018) Mapping protein interactions of sodium channel Na(V)1.7 using epitope-tagged gene-targeted mice. *Embo Journal* **37**:427-445.

Kao CY and Yasumoto T (1985) Actions of 4-epitetrodotoxin and anhydrotetrodotoxin on the squid axon. *Toxicon* **23**:725-729.

Katz E, Stoler O, Scheller A, Khrapunsky Y, Goebbels S, Kirchhoff F, Gutnick MJ, Wolff F and Fleidervish IA (2018) Role of sodium channel subtype in action potential generation by neocortical pyramidal neurons. *Proceedings of the National Academy of Sciences of the United States of America* **115**:E7184-E7192.

Kazen-Gillespie KA, Ragsdale DS, D'Andrea MR, Mattei LN, Rogers KE and Isom LL (2000) Cloning, localization, and functional expression of sodium channel beta 1A subunits. *Journal of Biological Chemistry* **275**:1079-1088.

Kearney J and Meisler M (2009). Genetics: Single Gene Mutations in Inherited and Sporadic Epilepsy. In *Encyclopedia of Basic Epilepsy Research* 369-374

Kearney JA, Buchner DA, de Haan G, Adamska M, Levin SI, Furay AR, Albin RL, Jones JM, Montal M, Stevens MJ, Sprunger LK and Meisler MH (2002) Molecular and pathological effects of a modifier gene on deficiency of the sodium channel Scn8a (Na(v)1.6). *Human Molecular Genetics* **11**:2765-2775.

Kehrl JM, Sahaya K, Dalton HM, Charbeneau RA, Kohut KT, Gilbert K, Pelz MC, Parent J and Neubig RR (2014) Gain-of-function mutation in Gnao1: A murine model of epileptiform encephalopathy (EIEE17)? *Mammalian Genome* **25**:202-210.

Khan A, Romantseva L, Lam A, Lipkind G and Fozzard HA (2002) Role of outer ring carboxylates of the rat skeletal muscle sodium channel pore in proton block. *Journal of Physiology-London* **543**:71-84.

Kim KJ and Rieke F (2003) Slow Na+ inactivation and variance adaptation in salamander retinal ganglion cells. *Journal of Neuroscience* **23**:1506-1516.

King JL, Lowe MP and Crowder NA (2015) Contrast adaptation is spatial frequency specific in mouse primary visual cortex. *Neuroscience* **310**:198-205.

Kingwell K (2022) Navigating a new path to Nav1.7 for pain. *Nature Reviews Drug Discovery* **21**:18-18.

Kleuss C, Scherubl H, Hescheler J, Schultz G and Wittig B (1992) Different beta-subunits determine g-protein interaction with transmembrane receptors. *Nature* **358**:424-426.

Kleuss C, Scherubl H, Hescheler J, Schultz G and Wittig B (1993) Selectivity in signal transduction determined by gamma-subunits of heterotrimeric g-proteins. *Science* **259**:832-834.

Knowles JK, Helbig I, Metcalf CS, Lubbers LS, Isom LL, Demarest S, Goldberg E, George AL, Jr., Lerche H, Weckhuysen S, Whittemore V, Berkovic SF and Lowenstein DH (2022) Precision medicine for genetic epilepsy on the horizon: recent advances, present challenges and suggestions for continued progress. *Epilepsia* Online ahead of print.

Knupp KG and Wirrell EC (2018) Treatment Strategies for Dravet Syndrome. *Cns Drugs* **32**:335-350.

Kobayashi T, Hirai H, Iino M, Fuse I, Mitsumura K, Washiyama K, Kasai S and Ikeda K (2009) Inhibitory effects of the antiepileptic drug ethosuximide on G protein-activated inwardly rectifying K+ channels. *Neuropharmacology*, **56**(2), pp.499-506.

Kraus RL, Zhao F, Pall PS, Zhou D, Vardigan JD, Danziger A, Li Y, Daley C, Ballard JE, Clements MK, Klein RM, Holahan MA, Greshock TJ, Kim RM, Layton ME, Burgey CS, Serra J, Henze DA and Houghton AK (2021) Na(v)1.7 target modulation and efficacy can be measured in nonhuman primate assays. *Science Translational Medicine* **13**.

Kruger LC and Isom LL (2016) Voltage-Gated Na+ Channels: Not Just for Conduction. *Cold Spring Harbor Perspectives in Biology* **8**.

Kruse SW, Dayton KG, Purnell BS, Rosner JI and Buchanan GF (2019) Effect of monoamine reuptake inhibition and alpha(1) blockade on respiratory arrest and death following electroshock-induced seizures in mice. *Epilepsia* **60**:495-507.

Krzemien DM, Schaller KL, Levinson SR and Caldwell JH (2000) Immunolocalization of sodium channel isoform NaCh6 in the nervous system. *Journal of Comparative Neurology* **420**:70-83.

Kwan P and Brodie MJ (2000) Early identification of refractory epilepsy. *New England Journal of Medicine* **342**:314-319.

Kwong K and Carr MJ (2015) Voltage-gated sodium channels. *Current Opinion in Pharmacology* **22**:131-139.

Laezza F, Lampert A, Kozel MA, Gerber BR, Rush AM, Nerbonne JM, Waxman SG, Dib-Hajj SD and Ornitz DM (2009) FGF14 N-terminal splice variants differentially modulate Nav1.2 and Nav1.6-encoded sodium channels. *Molecular and Cellular Neuroscience* **42**:90-101.

Larkum M (2013) A cellular mechanism for cortical associations: an organizing principle for the cerebral cortex. *Trends in Neurosciences* **36**:141-151.

Larkum ME, Nevian T, Sandler M, Polsky A and Schiller J (2009) Synaptic Integration in Tuft Dendrites of Layer 5 Pyramidal Neurons: A New Unifying Principle. *Science* **325**:756-760.

Larsen J, Carvill GL, Gardella E, Kluger G, Schmiedel G, Barisic N, Depienne C, Brilstra E, Mang Y, Nielsen JEK, Kirkpatrick M, Goudie D, Goldman R, Jaehn JA, Jepsen B, Gill D, Doecker M, Biskup S, McMahon JM, Koeleman B, Harris M, Braun K, de Kovel CGF, Marini C, Specchio N, Djemie T, Weckhuysen S, Tommerup N, Troncoso M, Troncoso L, Bevot A, Wolff M, Hjalgrim H, Guerrini R, Scheffer IE, Mefford HC, Moller RS and Euro ERESCCRP (2015) The phenotypic spectrum of SCN8A encephalopathy. *Neurology* **84**:480-489.

Law C-Y, Chang ST-L, Cho SY, Yau EK-C, Ng GS-F, Fong N-C and Lam C-W (2015) Clinical whole-exome sequencing reveals a novel missense pathogenic variant

of GNAO1 in a patient with infantile-onset epilepsy. *Clinica Chimica Acta* **451**:292-296.

Lein ES, Hawrylycz MJ, Ao N, Ayres M, Bensinger A, Bernard A, Boe AF, Boguski MS, Brockway KS, Byrnes EJ, Chen L, Chen L, Chen T-M, Chin MC, Chong J, Crook BE, Czaplinska A, Dang CN, Datta S, Dee NR, Desaki AL, Desta T, Diep E, Dolbeare TA, Donelan MJ, Dong H-W, Dougherty JG, Duncan BJ, Ebbert AJ, Eichele G, Estin LK, Faber C, Facer BA, Fields R, Fischer SR, Fliss TP, Frensley C, Gates SN, Glattfelder KJ, Halverson KR, Hart MR, Hohmann JG, Howell MP, Jeung DP, Johnson RA, Karr PT, Kawal R, Kidney JM, Knapik RH, Kuan CL, Lake JH, Laramee AR, Larsen KD, Lau C, Lemon TA, Liang AJ, Liu Y, Luong LT, Michaels J, Morgan JJ, Morgan RJ, Mortrud MT, Mosqueda NF, Ng LL, Ng R, Orta GJ, Overly CC, Pak TH, Parry SE, Pathak SD, Pearson OC, Puchalski RB, Riley ZL, Rockett HR, Rowland SA, Royall JJ, Ruiz MJ, Sarno NR, Schaffnit K, Shapovalova NV, Sivisay T, Slaughterbeck CR, Smith SC, Smith KA, Smith BI, Sodt AJ, Stewart NN, Stumpf K-R, Sunkin SM, Sutram M, Tam A, Teemer CD, Thaller C, Thompson CL, Varnam LR, Visel A, Whitlock RM, Wohnoutka PE, Wolkey CK, Wong VY, Wood M, Yaylaoglu MB, Young RC, Youngstrom BL, Yuan XF, Zhang B, Zwingman TA and Jones AR (2007) Genome-wide atlas of gene expression in the adult mouse brain. *Nature* **445**:168-176.

Lenk GM, Jafar-Nejad P, Hill SF, Huffman LD, Smolen CE, Wagnon JL, Petit H, Yu W, Ziobro J, Bhatia K, Parent J, Giger RJ, Rigo F and Meisler MH (2020) Scn8a Antisense Oligonucleotide Is Protective in Mouse Models of SCN8A Encephalopathy and Dravet Syndrome. *Annals of Neurology* **87**:339-346.

Lenkey N, Karoly R, Kiss JP, Szasz BK, Vizi ES and Mike A (2006) The mechanism of activity-dependent sodium channel inhibition by the antidepressants fluoxetine and desipramine. *Molecular Pharmacology* 70:2052-2063.

Lenkowski PW, Stevens EB, Yusaf SP, Patel MK (2004) G-protein β1γ2 subunits directly bind to the C-terminus of Nav1.3 and modulate channel properties. *Biophys J* 87a: 881

Li M, West JW, Lai Y, Scheuer T and Catterall WA (1992) Functional modulation of brain sodium channels by cAMP-dependent phosphorylation. *Neuron* **8**:1151-1159.

Lipkind GM and Fozzard HA (2008) Voltage-gated Na channel selectivity: The role of the conserved domain III lysine residue. *Journal of General Physiology* **131**:523-529.

Liu W, Lao W, Zhang R and Zhu H (2021) Altered expression of voltage gated sodium channel Nav1.1 is involved in motor ability in MPTP-treated mice. *Brain Research Bulletin* **170**:187-198.

Liu Y, Lopez-Santiago LF, Yuan Y, Jones JM, Zhang H, O'Malley HA, Patino GA, O'Brien JE, Rusconi R, Gupta A, Thompson RC, Natowicz MR, Meisler MH, Isom LL and Parent JM (2013) Dravet Syndrome Patient-Derived Neurons Suggest a Novel Epilepsy Mechanism. *Annals of Neurology* **74**:128-139.

Llewellyn LE (2009) Sodium channel inhibiting marine toxins. *Marine toxins as research tools*:67-97.

Lohmann K, Masuho I, Patil DN, Baumann H, Hebert E, Steinrücke S, Trujillano D, Skamangas NK, Dobricic V and Hüning I (2017) Novel GNB1 mutations disrupt assembly and function of G protein heterotrimers and cause global developmental delay in humans. *Human molecular genetics* **26**:1078-1086.

Lopez-Santiago LF, Meadows LS, Ernst SJ, Chen C, Malhotra JD, McEwen DP, Speelman A, Noebels JL, Maier SKG, Lopatin AN and Isom LL (2007) Sodium channel Scn1b null mice exhibit prolonged QT and RR intervals. *Journal of molecular and cellular cardiology* **43**:636-647.

Lopez-Santiago LF, Yuan Y, Wagnon JL, Hull JM, Frasier CR, O'Malley HA, Meisler MH and Isom LL (2017) Neuronal hyperexcitability in a mouse model of SCN8A epileptic encephalopathy. *Proceedings of the National Academy of Sciences* **114**:2383-2388.

Lorincz A and Nusser Z (2010) Molecular Identity of Dendritic Voltage-Gated Sodium Channels. *Science* **328**:906-909.

Lou JY, Laezza F, Gerber BR, Xiao M, Yamada KA, Hartmann H, Craig AM, Nerbonne JM and Ornitz DM (2005) Fibroblast growth factor 14 is an intracellular modulator of voltage-gated sodium channels. *The Journal of physiology* **569**:179-193.

Löscher W, Potschka H, Sisodiya SM and Vezzani A (2020) Drug resistance in epilepsy: clinical impact, potential mechanisms, and new innovative treatment options. *Pharmacological reviews* **72**:606-638.

Ma JY, Catterall WA and Scheuer T (1997) Persistent sodium currents through brain sodium channels induced by G protein beta gamma subunits. *Neuron* 19:443-452.

Ma JY, Li M, Catterall WA and Scheuer T (1994) Modulation of brain na+ channels by a g-protein-coupled pathway. *Proceedings of the National Academy of Sciences of the United States of America* 91:12351-12355.

MacDonald DI, Sikandar S, Weiss J, Pyrski M, Luiz AP, Millet Q, Emery EC, Mancini F, Iannetti GD and Alles SR (2021) A central mechanism of analgesia in mice and humans lacking the sodium channel NaV1. 7. *Neuron* **109**:1497-1512. e1496.

Makinson CD, Tanaka BS, Sorokin JM, Wong JC, Christian CA, Goldin AL, Escayg A and Huguenard JR (2017) Regulation of Thalamic and Cortical Network Synchrony by Scn8a. *Neuron* 93:1165

Malhotra JD, Koopmann MC, Kazen-Gillespie KA, Fettman N, Hortsch M and Isom LL (2002) Structural requirements for interaction of sodium channel β1 subunits with ankyrin. *Journal of Biological Chemistry* **277**:26681-26688.

Mantegazza M, Yu FH, Catterall WA, Scheuer T (2001) Role of the C-terminal domain in inactivation of brain and cardiac sodium channels. *Proceedings of the National Academy of Sciences* **98**: 15348-15353.

Mantegazza M, Yu FH, Powell AJ, Clare JJ, Catterall WA and Scheuer T (2005) Molecular determinants for modulation of persistent sodium current by G-protein beta gamma subunits. Journal of Neuroscience 25:3341-3349.

Marcé-Grau A, Dalton J, López-Pisón J, García-Jiménez MC, Monge-Galindo L, Cuenca-León E, Giraldo J and Macaya A (2016) GNAO1 encephalopathy: further delineation of a severe neurodevelopmental syndrome affecting females. *Orphanet journal of rare diseases* **11**:1-9.

Marin P, Fagni L, Torrens Y, Alcaraz G, Couraud F, Bockaert J, Glowinski J and Prémont J (2001) AMPA receptor activation induces association of G-beta protein with the alpha subunit of the sodium channel in neurons. *European Journal of Neuroscience* **14**:1953-1960.

Marionneau C, Carrasquillo Y, Norris AJ, Townsend RR, Isom LL, Link AJ and Nerbonne JM (2012) The sodium channel accessory subunit Navβ1 regulates neuronal excitability through modulation of repolarizing voltage-gated K+ channels. *Journal of Neuroscience* **32**:5716-5727.

Marfia G, Cope DW, Robinson DR, Eugene D, Crunelli V, Leresche N (2000) Ethosuximide decreases the persistent Na+ current and the Ca2+ activated K+ current of rat cortical pyramidal neurones in vitro. *Soc Neurosci Abstr* **26**: 662.1.

Marom S (2010) Neural timescales or lack thereof. *Progress in neurobiology* **90**:16-28.

Martin MS, Tang B, Papale LA, Yu FH, Catterall WA and Escayg A (2007) The voltage-gated sodium channel Scn8a is a genetic modifier of severe myoclonic epilepsy of infancy. *Human molecular genetics* **16**:2892-2899.

Marx IE, Dineen TA, Able J, Bode C, Bregman H, Chu-Moyer M, DiMauro EF, Du B, Foti RS and Fremeau Jr RT (2016) Sulfonamides as selective NaV1. 7 inhibitors: optimizing potency and pharmacokinetics to enable in vivo target engagement. *ACS medicinal chemistry letters* **7**:1062-1067.

Mashiko D, Young SA, Muto M, Kato H, Nozawa K, Ogawa M, Noda T, Kim YJ, Satouh Y and Fujihara Y (2014) Feasibility for a large scale mouse mutagenesis by injecting CRISPR/Cas plasmid into zygotes. *Development, growth & differentiation* **56**:122-129.

Massey CA, Sowers LP, Dlouhy BJ and Richerson GB (2014) Mechanisms of sudden unexpected death in epilepsy: the pathway to prevention. *Nature Reviews Neurology* **10**:271-282.

Mattheisen GB, Tsintsadze T and Smith SM (2018) Strong G-Protein-Mediated Inhibition of Sodium Channels. Cell Reports 23:2770-2781.

Mattheisen G-protein regulation of voltage-gated sodium channels by allosteric modulators of the calcium-sensing receptor. (2018)

Maurice N, Tkatch T, Meisler M, Sprunger LK and Surmeier DJ (2001) D1/D5 dopamine receptor activation differentially modulates rapidly inactivating and persistent sodium currents in prefrontal cortex pyramidal neurons. *Journal of Neuroscience* **21**:2268-2277.

McNeal ET, Lewandowski GA, Daly JW and Creveling C (1985) [^{3}H] Batrachotoxinin A 20. alpha.-benzoate binding to voltage-sensitive sodium channels: a rapid and quanitative assay for local anesthetic activity in a variety of drugs. *Journal of medicinal chemistry* **28**:381-388.

McPhee JC, Ragsdale DS, Scheuer T and Catterall WA (1994) A mutation in segment IVS6 disrupts fast inactivation of sodium channels. *Proceedings of the National Academy of Sciences* **91**:12346-12350.

McPhee JC, Ragsdale DS, Scheuer T and Catterall WA (1995) A critical role for transmembrane segment IVS6 of the sodium channel α subunit in fast inactivation. *Journal of Biological Chemistry* **270**:12025-12034.

McPhee JC, Ragsdale DS, Scheuer T and Catterall WA (1998) A critical role for the S4-S5 intracellular loop in domain IV of the sodium channel α-subunit in fast inactivation. *Journal of Biological Chemistry* **273**:1121-1129.

Meggio F, Deana AD, Ruzzene M, Brunati AM, Cesaro L, Guerra B, Meyer T, Mett H, Fabbro D and Furet P (1995) Different susceptibility of protein kinases to staurosporine inhibition: kinetic studies and molecular bases for the resistance of protein kinase CK2. *European Journal of Biochemistry* **234**:317-322.

Meisler MH, Helman G, Hammer MF, Fureman BE, Gaillard WD, Goldin AL, Hirose S, Ishii A, Kroner BL and Lossin C (2016) SCN8A encephalopathy: research progress and prospects. *Epilepsia* **57**:1027-1035.

Meisler MH, Hill SF and Yu W (2021) Sodium channelopathies in neurodevelopmental disorders. *Nature Reviews Neuroscience* **22**:152-166.

Meisler MH and Kearney JA (2005) Sodium channel mutations in epilepsy and other neurological disorders. *Journal of Clinical Investigation* **115**:2010-2017.

Meredith FL and Rennie KJ (2018) Regional and Developmental Differences in Na+ Currents in Vestibular Primary Afferent Neurons. *Frontiers in Cellular Neuroscience* **12**:14.

Metherate R, Cox CL and Ashe JH (1992) Cellular bases of neocortical activation: modulation of neural oscillations by the nucleus basalis and endogenous acetylcholine. *Journal of Neuroscience* **12**:4701-4711.

Miller AR, Hawkins NA, McCollom CE and Kearney JA (2014) Mapping genetic modifiers of survival in a mouse model of Dravet syndrome. *Genes Brain and Behavior* **13**:163-172.

Minett MS, Nassar MA, Clark AK, Passmore G, Dickenson AH, Wang F, Malcangio M and Wood JN (2012) Distinct Nav1. 7-dependent pain sensations require different sets of sensory and sympathetic neurons. *Nature communications* **3**:1-9.

Minett MS, Pereira V, Sikandar S, Matsuyama A, Lolignier S, Kanellopoulos AH, Mancini F, Iannetti GD, Bogdanov YD and Santana-Varela S (2015) Endogenous opioids contribute to insensitivity to pain in humans and mice lacking sodium channel Nav1. 7. *Nature communications* **6**:1-8.

Mistry AM, Thompson CH, Miller AR, Vanoye CG, George AL and Kearney JA (2014) Strain- and age-dependent hippocampal neuron sodium currents correlate with epilepsy severity in Dravet syndrome mice. *Neurobiology of Disease* **65**:1-11.

Mitrovic N, George AL and Horn R (2000) Role of domain 4 in sodium channel slow inactivation. *Journal of General Physiology* **115**:707-717.

Moczydlowski EG (2013) The molecular mystique of tetrodotoxin. *Toxicon* **63**:165-183.

Morgan K, Stevens EB, Shah B, Cox PJ, Dixon AK, Lee K, Pinnock RD, Hughes J, Richardson PJ and Mizuguchi K (2000) β3: an additional auxiliary subunit of the voltage-sensitive sodium channel that modulates channel gating with distinct kinetics. *Proceedings of the National Academy of Sciences* **97**:2308-2313.

Mosher HS (1986) The chemistry of tetrodotoxin. *Annals of the New York Academy of Sciences* **479**:32-43.

Murphy BJ, Rossie S, De Jongh K and Catterall W (1993) Identification of the sites of selective phosphorylation and dephosphorylation of the rat brain Na+ channel alpha subunit by cAMP-dependent protein kinase and phosphoprotein phosphatases. *Journal of Biological Chemistry* **268**:27355-27362.

Nakamura K, Kodera H, Akita T, Shiina M, Kato M, Hoshino H, Terashima H, Osaka H, Nakamura S and Tohyama J (2013) De Novo mutations in GNAO1, encoding a Gαo subunit of heterotrimeric G proteins, cause epileptic encephalopathy. *The American Journal of Human Genetics* **93**:496-505.

Namadurai S, Balasuriya D, Rajappa R, Wiemhöfer M, Stott K, Klingauf J, Edwardson JM, Chirgadze DY and Jackson AP (2014) Crystal structure and molecular imaging of the Nav channel β3 subunit indicates a trimeric assembly. *Journal of Biological Chemistry* **289**:10797-10811.

Narahashi T (1964) Restoration of action potential by anodal polarization in lobster giant axons. *Journal of cellular and comparative physiology* **64**:73-96.

Narahashi T (2008) Tetrodotoxin—A brief history—. *Proceedings of the Japan Academy, Series B* **84**:147-154.

Narahashi T, Deguchi T, Urakawa N and Ohkubo Y (1960) Stabilization and rectification of muscle fiber membrane by tetrodotoxin. *American Journal of Physiology-Legacy Content* **198**:934-938.

Narahashi T, Moore JW and Scott WR (1964) Tetrodotoxin blockage of sodium conductance increase in lobster giant axons. *Journal of General Physiology* **47**:965-&.

Nassar MA, Stirling LC, Forlani G, Baker MD, Matthews EA, Dickenson AH and Wood JN (2004) Nociceptor-specific gene deletion reveals a major role for Nav1. 7 (PN1) in acute and inflammatory pain. *Proceedings of the National Academy of Sciences* **101**:12706-12711.

Navarro MA, Salari A, Lin JL, Cowan LM, Penington NJ, Milescu M and Milescu LS (2020) Sodium channels implement a molecular leaky integrator that detects action potentials and regulates neuronal firing. *Elife* **9**:e54940.

Need AC, Shashi V, Hitomi Y, Schoch K, Shianna KV, McDonald MT, Meisler MH and Goldstein DB (2012) Clinical application of exome sequencing in undiagnosed genetic conditions. *Journal of medical genetics* **49**:353-361.

Nelson JW, Randolph PB, Shen SP, Everette KA, Chen PJ, Anzalone AV, An M, Newby GA, Chen JC, Hsu A and Liu DR (2022) Engineered pegRNAs improve prime editing efficiency. *Nature biotechnology* **40**:402-410.

Nguyen HM, Miyazaki H, Hoshi N, Smith BJ, Nukina N, Goldin AL and Chandy KG (2012) Modulation of voltage-gated K+ channels by the sodium channel β1 subunit. *Proceedings of the National Academy of Sciences of the United States of America* **109**:18577-18582.

Nicholson GM, Blanche T, Mansfield K and Tran Y (2002) Differential blockade of neuronal voltage-gated Na(+) and K(+) channels by antidepressant drugs. *Eur J Pharmacol* **452**:35-48.

Nicholson RA, Liao C, Zheng J, David LS, Coyne L, Errington AC, Singh G and Lees G (2003) Sodium channel inhibition by anandamide and synthetic cannabimimetics in brain. *Brain Research* **978**:194-204.

Noda M, Ikeda T, Suzuki H, Takeshima H, Takahashi T, Kuno M and Numa S (1986) Expression of functional sodium channels from cloned cDNA. *Nature* **322**:826-828.

Noda M, Suzuki H, Numa S and Stuhmer W (1989) A single point mutation confers tetrodotoxin and saxitoxin insensitivity on the sodium channel-ii. *Febs Letters* **259**:213-216.

Noguchi T and Arakawa O (2008) Tetrodotoxin - Distribution and accumulation in aquatic organisms, and cases of human intoxication. *Marine Drugs* **6**:220-242.

Nolan D and Fink J (2018) Genetics of epilepsy. *Handbook of clinical neurology* **148**:467-491.

Numann R, Catterall WA and Scheuer T (1991) Functional modulation of brain sodium channels by protein kinase C phosphorylation. *Science* **254**:115-118.

O'Brien JE and Meisler MH (2013) Sodium channel SCN8A (Nav1.6): properties and de novo mutations in epileptic encephalopathy and intellectual disability. *Front Genet* **4**:213.

O'Malley HA, Hull JM, Clawson BC, Chen C, Owens-Fiestan G, Jameson MB, Aton SJ, Parent JM and Isom LL (2019a) Scn1b deletion in adult mice results in seizures and SUDEP. *Annals of Clinical and Translational Neurology* **6**:1121-1126.

O'Malley HA and Isom LL (2015) Sodium channel β subunits: emerging targets in channelopathies. *Annu Rev Physiol* **77**:481-504.

O'Reilly JP, Wang SY, Kallen RG and Wang GK (1999) Comparison of slow inactivation in human heart and rat skeletal muscle Na+ channel chimaeras. *J Physiol* **515 (Pt 1)**:61-73.

Ogiwara I, Iwasato T, Miyamoto H, Iwata R, Yamagata T, Mazaki E, Yanagawa Y, Tamamaki N, Hensch TK, Itohara S and Yamakawa K (2013) Nav1.1 haploinsufficiency in excitatory neurons ameliorates seizure-associated sudden death in a mouse model of Dravet syndrome. *Human Molecular Genetics* **22**:4784-4804.

Ogiwara I, Miyamoto H, Morita N, Atapour N, Mazaki E, Inoue I, Takeuchi T, Itohara S, Yanagawa Y, Obata K, Furuichi T, Hensch TK and Yamakawa K (2007) Na_v1.1 Localizes to Axons of Parvalbumin-Positive Inhibitory Interneurons: A Circuit Basis for Epileptic Seizures in Mice Carrying an Scn1a Gene Mutation. *The Journal of Neuroscience* **27**:5903-5914.

Ogiwara I, Miyamoto H, Tatsukawa T, Yamagata T, Nakayama T, Atapour N, Miura E, Mazaki E, Ernst SJ, Cao DZ, Ohtani H, Itohara S, Yanagawa Y, Montal M, Yuzaki M, Inoue Y, Hensch TK, Noebels JL and Yamakawa K (2018) Nav1.2 haplodeficiency in excitatory neurons causes absence-like seizures in mice. *Communications Biology* **1**:16.

Okae H and Iwakura Y (2010) Neural tube defects and impaired neural progenitor cell proliferation in Gbeta1-deficient mice. *Dev Dyn* **239**:1089-1101.

Okaty BW, Miller MN, Sugino K, Hempel CM and Nelson SB (2009) Transcriptional and electrophysiological maturation of neocortical fast-spiking GABAergic interneurons. *The Journal of neuroscience : the official journal of the Society for Neuroscience* **29**:7040-7052.

Ong BH, Tomaselli GF and Balser JR (2000) A structural rearrangement in the sodium channel pore linked to slow inactivation and use dependence. *Journal of General Physiology* **116**:653-661.

Pan X, Li Z, Zhou Q, Shen H, Wu K, Huang X, Chen J, Zhang J, Zhu X, Lei J, Xiong W, Gong H, Xiao B and Yan N (2018) Structure of the human voltage-gated sodium channel Na(v)1.4 in complex with β1. *Science* **362**.

Patel RR, Ping X, Patel SR, McDermott JS, Krajewski JL, Chi XX, Nisenbaum ES, Jin X and Cummins TR (2020) Preferential Pharmacological Inhibition of Nav1.6, but not Nav1.1, Abolishes Epileptiform Activity Induced by 4-AP in Mouse Cortical Slices. *bioRxiv*:2020.2005.2029.124693.

Patino GA, Brackenbury WJ, Bao Y, Lopez-Santiago LF, O'Malley HA, Chen C, Calhoun JD, Lafreniere RG, Cossette P, Rouleau GA and Isom LL (2011) Voltage-Gated Na+ Channel beta 1B: A Secreted Cell Adhesion Molecule Involved in Human Epilepsy. *Journal of Neuroscience* **31**:14577-14591.

Patino GA, Claes LR, Lopez-Santiago LF, Slat EA, Dondeti RS, Chen C, O'Malley HA, Gray CB, Miyazaki H, Nukina N, Oyama F, De Jonghe P and Isom LL (2009) A

functional null mutation of SCN1B in a patient with Dravet syndrome. *J Neurosci* **29**:10764-10778.

Patton DE, Isom LL, Catterall WA and Goldin AL (1994) The adult-rat brain beta(1) subunit modifies activation and inactivation gating of multiple sodium-channel alpha-subunits. *Journal of Biological Chemistry* **269**:17649-17655.

Patton DE, West JW, Catterall WA and Goldin AL (1992) Amino acid residues required for fast Na(+)-channel inactivation: charge neutralizations and deletions in the III-IV linker. *Proc Natl Acad Sci U S A* **89**:10905-10909.

Payandeh J, Gamal El-Din TM, Scheuer T, Zheng N and Catterall WA (2012) Crystal structure of a voltage-gated sodium channel in two potentially inactivated states. *Nature* **486**:135-139.

Payandeh J, Scheuer T, Zheng N and Catterall WA (2011) The crystal structure of a voltage-gated sodium channel. *Nature* **475**:353-358.

Peng J, Pang N, Wang Y, Wang XL, Chen J, Xiong J, Peng P, Zhu CH, Kessi MB, He F and Yin F (2019) Next-generation sequencing improves treatment efficacy and reduces hospitalization in children with drug-resistant epilepsy. *CNS Neurosci Ther* **25**:14-20.

Penzotti JL, Fozzard HA, Lipkind GM and Dudley SC (1998) Differences in saxitoxin and tetrodotoxin binding revealed by mutagenesis of the Na+ channel outer vestibule. *Biophysical Journal* **75**:2647-2657.

Petrovski S, Küry S, Myers CT, Anyane-Yeboa K, Cogné B, Bialer M, Xia F, Hemati P, Riviello J, Mehaffey M, Besnard T, Becraft E, Wadley A, Politi AR, Colombo S, Zhu X, Ren Z, Andrews I, Dudding-Byth T, Schneider AL, Wallace G, Rosen ABI, Schelley S, Enns GM, Corre P, Dalton J, Mercier S, Latypova X, Schmitt S, Guzman E, Moore C, Bier L, Heinzen EL, Karachunski P, Shur N, Grebe T, Basinger A, Nguyen JM, Bézieau S, Wierenga K, Bernstein JA, Scheffer IE, Rosenfeld JA, Mefford HC, Isidor B and Goldstein DB (2016) Germline De Novo Mutations in GNB1 Cause Severe Neurodevelopmental Disability, Hypotonia, and Seizures. *Am J Hum Genet* **98**:1001-1010.

Picot MC, Baldy-Moulinier M, Daurès JP, Dujols P and Crespel A (2008) The prevalence of epilepsy and pharmacoresistant epilepsy in adults: a population-based study in a Western European country. *Epilepsia* **49**:1230-1238.

Raman IM, Sprunger LK, Meisler MH and Bean BP (1997) Altered Subthreshold Sodium Currents and Disrupted Firing Patterns in Purkinje Neurons of Scn8a Mutant Mice. *Neuron* **19**:881-891.

Ramos-Mondragon R, Edokobi N, Hodges SL, Wang S, Bouza AA, Canugovi C, Scheuing C, Juratli L, Abel WR, Noujaim SF, Madamanchi NR, Runge MS, Lopez-Santiago LF and Isom LL (2022) Neonatal Scn1b-null mice have sinoatrial node dysfunction, altered atrial structure, and atrial fibrillation. *Jci Insight* **7**.

Recio-Pinto E, Duch DS, Levinson SR and Urban BW (1987) Purified and unpurified sodium channels from eel electroplax in planar lipid bilayers. *Journal of General Physiology* **90**:375-395.

Reddy HP, Yakubovich D, Keren-Raifman T, Tabak G, Tsemakhovich VA, Pedersen MH, Shalomov B, Colombo S, Goldstein DB, Javitch JA, Bera AK and Dascal N (2021) Encephalopathy-causing mutations in Gβ(1) (GNB1) alter regulation of neuronal GIRK channels. *iScience* **24**:103018.

Reuveny E, Slesinger PA, Inglese J, Morales JM, Iñiguez-Lluhi JA, Lefkowitz RJ, Bourne HR, Jan YN and Jan LY (1994) Activation of the cloned muscarinic potassium channel by G protein βγ subunits. *Nature* **370**:143-146.

Revah-Politi A, Sands TT, Colombo S, Goldstein DB and Anyane-Yeboa K (1993) *GNB1 Encephalopathy*, University of Washington, Seattle, Seattle (WA).

Richards KL, Milligan CJ, Richardson RJ, Jancovski N, Grunnet M, Jacobson LH, Undheim EAB, Mobli M, Chow CY, Herzig V, Csoti A, Panyi G, Reid CA, King GF and Petrou S (2018a) Selective Na(V)1.1 activation rescues Dravet syndrome mice from seizures and premature death. *Proceedings of the National Academy of Sciences* **115**:E8077-E8085.

Richerson GB and Buchanan GF (2011) The serotonin axis: Shared mechanisms in seizures, depression, and SUDEP. *Epilepsia* **52**:28-38.

Rogers M, Zidar N, Kikelj D and Kirby RW (2016) Characterization of Endogenous Sodium Channels in the ND7-23 Neuroblastoma Cell Line: Implications for Use as a Heterologous Ion Channel Expression System Suitable for Automated Patch Clamp Screening. *Assay and Drug Development Technologies* **14**:109-130.

Rosker C, Lohberger B, Hofer D, Steinecker B, Quasthoff S and Schreibmayer W (2007) The TTX metabolite 4,9-anhydro-TTX is a highly specific blocker of the Na-v1.6 voltage-dependent sodium channel. *American Journal of Physiology-Cell Physiology* **293**:C783-C789.

Rossie S and Catterall WA (1987) Cyclic-AMP-dependent phosphorylation of voltage-sensitive sodium channels in primary cultures of rat brain neurons. *J Biol Chem* **262**:12735-12744.

Rossie S and Catterall WA (1989) Phosphorylation of the alpha subunit of rat brain sodium channels by cAMP-dependent protein kinase at a new site containing Ser686 and Ser687. *J Biol Chem* **264**:14220-14224.

Rossie S, Gordon D and Catterall WA (1987) Identification of an intracellular domain of the sodium channel having multiple cAMP-dependent phosphorylation sites. *J Biol Chem* **262**:17530-17535.

Rudy B (1978) Slow inactivation of the sodium conductance in squid giant axons. Pronase resistance. *J Physiol* **283**:1-21.

Rush AM, Dib-Hajj SD and Waxman SG (2005) Electrophysiological properties of two axonal sodium channels, Nav1.2 and Nav1.6, expressed in mouse spinal sensory neurones. *J Physiol* **564**:803-815.

Ryvlin P, Rheims S and Lhatoo SD (2019) Risks and predictive biomarkers of sudden unexpected death in epilepsy patient. *Curr Opin Neurol* **32**:205-212.

Saitsu H, Fukai R, Ben-Zeev B, Sakai Y, Mimaki M, Okamoto N, Suzuki Y, Monden Y, Saito H, Tziperman B, Torio M, Akamine S, Takahashi N, Osaka H, Yamagata T, Nakamura K, Tsurusaki Y, Nakashima M, Miyake N, Shiina M, Ogata K and Matsumoto N (2016) Phenotypic spectrum of GNAO1 variants: epileptic encephalopathy to involuntary movements with severe developmental delay. *Eur J Hum Genet* **24**:129-134.

Sakamoto S, Monden Y, Fukai R, Miyake N, Saito H, Miyauchi A, Matsumoto A, Nagashima M, Osaka H, Matsumoto N and Yamagata T (2017) A case of severe movement disorder with GNAO1 mutation responsive to topiramate. *Brain Dev* **39**:439-443.

Sakurai T, Watanabe S, Kamiyoshi A, Sato M and Shindo T (2014) A single blastocyst assay optimized for detecting CRISPR/Cas9 system-induced indel mutations in mice. *BMC biotechnology* **14**:69-69.

Sarno N, Hernandez-Clavijo A, Boccaccio A, Menini A and Pifferi S (2022) Slow Inactivation of Sodium Channels Contributes to Short-Term Adaptation in Vomeronasal Sensory Neurons. *eNeuro* **9**.

Satin J, Kyle JW, Chen M, Bell P, Cribbs LL, Fozzard HA and Rogart RB (1992) A MUTANT OF TTX-RESISTANT CARDIAC SODIUM-CHANNELS WITH TTX-SENSITIVE PROPERTIES. *Science* **256**:1202-1205.

Schaller KL, Krzemien DM, Yarowsky PJ, Krueger BK and Caldwell JH (1995) A NOVEL, ABUNDANT SODIUM-CHANNEL EXPRESSED IN NEURONS AND GLIA. *Journal of Neuroscience* **15**:3231-3242.

Schauf CL, Pencek TL and Davis FA (1976) Slow sodium inactivation in Myxicola axons. Evidence for a second inactive state. *Biophys J* **16**:771-778.

Scheinman RI, Auld VJ, Goldin AL, Davidson N, Dunn RJ and Catterall WA (1989) Developmental Regulation of Sodium Channel Expression in the Rat Forebrain. *Journal of Biological Chemistry* **264**:10660-10666.

Scheuer T and Catterall WA (2006) Control of neuronal excitability by phosphorylation and dephosphorylation of sodium channels. *Biochemical Society Transactions* **34**:1299-1302.

Scheuer T (2011) Regulation of sodium channel activity by phosphorylation. *Seminars in Cell & Developmental Biology* **22**:160-165.

Schorling DC, Dietel T, Evers C, Hinderhofer K, Korinthenberg R, Ezzo D, Bönnemann CG and Kirschner J (2017) Expanding Phenotype of De Novo Mutations in GNAO1: Four New Cases and Review of Literature. *Neuropediatrics* **48**:371-377.

Schreibmayer W, Wallner M and Lotan I (1994) Mechanism of modulation of single sodium channels from skeletal muscle by the beta 1-subunit from rat brain. *Pflugers Arch* **426**:360-362.

Sheets Michael F, Fozzard Harry A and Hanck Dorothy A (2015) Important Role of Asparagines in Coupling the Pore and Votage-Sensor Domain in Voltage-Gated Sodium Channels. *Biophysical Journal* **109**:2277-2286.

Shen H, Zhou Q, Pan X, Li Z, Wu J and Yan N (2017) Structure of a eukaryotic voltage-gated sodium channel at near-atomic resolution. *Science* **355**.

Shen HZ, Li ZQ, Jiang Y, Pan XJ, Wu JP, Cristofori-Armstrong B, Smith JJ, Chin YKY, Lei JL, Zhou Q, King GF and Yan N (2018) Structural basis for the modulation of voltage-gated sodium channels by animal toxins. *Science* **362**:8.

Shen HZ, Liu DL, Wu K, Lei JL and Yan N (2019) Structures of human Na(v)1.7 channel in complex with auxiliary subunits and animal toxins. *Science* **363**:1303-+.

Sigel E and Baur R (1988) Activation of protein kinase C differentially modulates neuronal Na+, Ca2+, and gamma-aminobutyrate type A channels. *Proceedings of the National Academy of Sciences of the United States of America* **85**:6192-6196.

Silva J (2014) Slow inactivation of Na+ channels. *Voltage Gated Sodium Channels*:33-49.

Singh AK, Dvorak NM, Tapia CM, Mosebarger A, Ali SR, Bullock Z, Chen H, Zhou J and Laezza F (2021) Differential Modulation of the Voltage-Gated Na+ Channel 1.6 by Peptides Derived From Fibroblast Growth Factor 14. *Frontiers in Molecular Biosciences* **8**.

Smith MR, Smith RD, Plummer NW, Meisler MH and Goldin AL (1998) Functional analysis of the mouse Scn8a sodium channel. *J Neurosci* **18**:6093-6102.

Smrcka AV (2008) G protein βγ subunits: central mediators of G protein-coupled receptor signaling. *Cell Mol Life Sci* **65**:2191-2214.

Soong TW and Venkatesh B (2006) Adaptive evolution of tetrodotoxin resistance in animals. *Trends in Genetics* **22**:621-626.

Steinrücke S, Lohmann K, Domingo A, Rolfs A, Bäumer T, Spiegler J, Hartmann C and Münchau A (2016) Novel GNB1 missense mutation in a patient with generalized dystonia, hypotonia, and intellectual disability. *Neurology Genetics* **2**:e106-e106.

Stevens M, Peigneur S and Tytgat J (2011) Neurotoxins and Their Binding Areas on Voltage-Gated Sodium Channels. *Frontiers in Pharmacology* **2**.

Stewart M, Silverman JB, Sundaram K and Kollmar R (2020) Causes and Effects Contributing to Sudden Death in Epilepsy and the Rationale for Prevention and Intervention. *Frontiers in Neurology* **11**.

Strittmatter S, Fishman M and Zhu X (1994) Activated mutants of the alpha subunit of G(o) promote an increased number of neurites per cell. *The Journal of Neuroscience* **14**:2327-2338.

Strzelczyk A, Kurlemann G, Bast T, Bettendorf U, Kluger G, Mayer T, Neubauer BA, Polster T, von Spiczak S, Trollmann R, Wolff M, Toward T, Gruenert J, Gibson E, Pritchard C, Carroll J, Rosenow F and Schubert-Bast S (2022) Exploring the relationships between composite scores of disease severity, seizure-freedom and quality of life in Dravet syndrome. *Neurological Research and Practice* **4**:22.

Stühmer W, Conti F, Suzuki H, Wang X, Noda M, Yahagi N, Kubo H and Numa S (1989) Structural parts involved in activation and inactivation of the sodium channel. *Nature* **339**:597-603.

Sudlow LC and Gillette R (1995) Cyclic amp-gated sodium current in neurons of the pedal ganglion of pleurobranchaea-californica is activated by serotonin. *Journal of Neurophysiology* **73**:2230-2236.

Suehiro M (1994) Historical review on chemical and medical studies of globefish toxin before World War II. *Yakushigaku Zasshi* **29**:428-434.

Surmeier DJ, Eberwine J, Wilson CJ, Cao Y, Stefani A and Kitai ST (1992) Dopamine receptor subtypes colocalize in rat striatonigral neurons. *Proceedings of the National Academy of Sciences of the United States of America* **89**:10178-10182.

Surmeier DJ and Kitai ST (1993) D1 and D2 dopamine receptor modulation of sodium and potassium currents in rat neostriatal neurons. *Prog Brain Res* **99**:309-324.

Surve CR, Lehmann D and Smrcka AV (2014) A Chemical Biology Approach Demonstrates G Protein βγ Subunits Are Sufficient to Mediate Directional Neutrophil Chemotaxis *. *Journal of Biological Chemistry* **289**:17791-17801.

Szczałuba K, Biernacka A, Szymanska K, Gasperowicz P, Kosinska J, Rydzanicz M and Ploski R (2017) Novel GNB1 de novo mutation in a patient with neurodevelopmental disorder and cutaneous mastocytosis: Clinical report and literature review. *European Journal of Medical Genetics* **61**.

Tai C, Abe Y, Westenbroek RE, Scheuer T and Catterall WA (2014) Impaired excitability of somatostatin- and parvalbumin-expressing cortical interneurons in a mouse model of Dravet syndrome. *Proc Natl Acad Sci U S A* **111**:E3139-3148.

Takahara K, Yamamoto T, Uchida K, Zhu HL, Shibata A, Inai T, Noguchi M, Yotsu-Yamashita M and Teramoto N (2018) Effects of 4,9-anhydrotetrodotoxin on voltage-gated Na+ channels of mouse vas deferens myocytes and recombinant Na(V)1.6 channels. *Naunyn-Schmiedebergs Archives of Pharmacology* **391**:489-499.

Talvik I, Møller RS, Vaher M, Vaher U, Larsen LHG, Dahl HA, Ilves P and Talvik T (2015) Clinical Phenotype of De Novo GNAO1 Mutation: Case Report and Review of Literature. *Child Neurology Open* **2**:2329048X15583717.

Tang L, Kallen RG and Horn R (1996) Role of an S4-S5 linker in sodium channel inactivation probed by mutagenesis and a peptide blocker. *Journal of General Physiology* **108**:89-104.

Tejedor FJ and Catterall WA (1988) Site of covalent attachment of alpha-scorpion toxin derivatives in domain I of the sodium channel alpha subunit. *Proc Natl Acad Sci U S A* **85**:8742-8746.

Teng S, Zhen F, McRae BR, Zhu E, Frankel WN and Peng Y (2022) Sensory regulation of absence seizures in a mouse model of Gnb1 encephalopathy. *bioRxiv*:2022.2004.2028.489780.

Terakita A, Nagata T, Sugihara T and Koyanagi M (2015) Optogenetic Potentials of Diverse Animal Opsins, in *Optogenetics: Light-Sensing Proteins and Their Applications* (Yawo H, Kandori H and Koizumi A eds) pp 77-88, Springer Japan, Tokyo.

Teramoto N and Yotsu-Yamashita M (2015) Selective Blocking Effects of 4,9-Anhydrotetrodotoxin, Purified from a Crude Mixture of Tetrodotoxin Analogues, on Na(V)1.6 Channels and Its Chemical Aspects. *Marine Drugs* **13**:984-995.

Teramoto N, Zhu HL, Yotsu-Yamashita M, Inai T and Cunnane TC (2012) Resurgent-like currents in mouse vas deferens myocytes are mediated by Na(V)1.6 voltage-gated sodium channels. *Pflugers Archiv-European Journal of Physiology* **464**:493-502.

Terlau H, Heinemann SH, Stuhmer W, Pusch M, Conti F, Imoto K and Numa S (1991) Mapping the site of block by tetrodotoxin and saxitoxin of sodium channel-ii. *Febs Letters* **293**:93-96.

Tidball AM, Lopez-Santiago LF, Yuan Y, Glenn TW, Margolis JL, Clayton Walker J, Kilbane EG, Miller CA, Martina Bebin E, Scott Perry M, Isom LL and Parent JM (2020) Variant-specific changes in persistent or resurgent sodium current in SCN8A-related epilepsy patient-derived neurons. *Brain : a journal of neurology* **143**:3025-3040.

Todt H, Dudley SC, Kyle JW, French RJ and Fozzard HA (1999) Ultra-Slow Inactivation in μ1 Na+ Channels Is Produced by a Structural Rearrangement of the Outer Vestibule. *Biophysical Journal* **76**:1335-1345.

Toib A, Lyakhov V and Marom S (1998) Interaction between Duration of Activity and Time Course of Recovery from Slow Inactivation in Mammalian Brain Na⁺Channels. *The Journal of Neuroscience* **18**:1893-1903.

Toledo G, Hanifin C, Geffeney S and Brodie ED (2016) Convergent Evolution of Tetrodotoxin-Resistant Sodium Channels in Predators and Prey, in *Na Channels from Phyla to Function* (French RJ and Noskov SY eds) pp 87-113, Elsevier Academic Press Inc, San Diego.

Torkkeli PH, Sekizawa S-I and French AS (2001) Inactivation of Voltage-Activated Na+ Currents Contributes to Different Adaptation Properties of Paired Mechanosensory Neurons. *Journal of Neurophysiology* **85**:1595-1602.

Tsuda K, Tachikawa R, Sakai K, Tamura C, Amakasu O, Kawamura M and Ikuma S (1964) On the structure of tetrodotoxin. *Chem Pharm Bull (Tokyo)* **12**:642-645.

Tsukamoto T, Chiba Y, Wakamori M, Yamada T, Tsunogae S, Cho Y, Sakakibara R, Imazu T, Tokoro S, Satake Y, Adachi M, Nishikawa T, Yotsu-Yamashita M and Konoki K (2017) Differential binding of tetrodotoxin and its derivatives to voltage-sensitive sodium channel subtypes (Na(v)1.1 to Na(v)1.7). *British Journal of Pharmacology* **174**:3881-3892.

Tupal S and Faingold CL (2006) Evidence Supporting a Role of Serotonin in Modulation of Sudden Death Induced by Seizures in DBA/2 Mice. *Epilepsia* **47**:21-26.

Ueda K, Serajee F and Huq AM (2017) Exome Sequencing Identifying Dual Mutations in Calcium Signaling Genes GNAO1 and ATP2B3 in a Patient with Early Infantile Epileptic Encephalopathy. *Journal of Pediatric Neurology* **15**:183-186.

Uteshev VV, Tupal S, Mhaskar Y and Faingold CL (2010) Abnormal serotonin receptor expression in DBA/2 mice associated with susceptibility to sudden death due to respiratory arrest. *Epilepsy Research* **88**:183-188.

Valenzuela D, Han X, Mende U, Fankhauser C, Mashimo H, Huang P, Pfeffer J, Neer EJ and Fishman MC (1997) Gα_o is necessary for muscarinic regulation of Ca²⁺ channels in mouse heart. *Proceedings of the National Academy of Sciences* **94**:1727-1732.

Van Keuren ML, Gavrilina GB, Filipiak WE, Zeidler MG and Saunders TL (2009) Generating transgenic mice from bacterial artificial chromosomes: transgenesis efficiency, integration and expression outcomes. *Transgenic Res* **18**:769-785.

Van Wart A, Trimmer JS and Matthews G (2007) Polarized distribution of ion channels within microdomains of the axon initial segment. *Journal of Comparative Neurology* **500**:339-352.

Vassilev P, Scheuer T and Catterall WA (1989) Inhibition of inactivation of single sodium channels by a site-directed antibody. *Proc Natl Acad Sci U S A* **86**:8147-8151.

Vassilev PM, Scheuer T and Catterall WA (1988) Identification of an intracellular peptide segment involved in sodium channel inactivation. *Science* **241**:1658-1661.

Vedantham V and Cannon SC (1998) Slow Inactivation Does Not Affect Movement of the Fast Inactivation Gate in Voltage-gated Na+ Channels. *Journal of General Physiology* **111**:83-93.

Veeramah KR, O'Brien JE, Meisler MH, Cheng X, Dib-Hajj SD, Waxman SG, Talwar D, Girirajan S, Eichler EE, Restifo LL, Erickson RP and Hammer MF (2012) De novo pathogenic SCN8A mutation identified by whole-genome sequencing of a family quartet affected by infantile epileptic encephalopathy and SUDEP. *Am J Hum Genet* **90**:502-510.

Vilin YY and Ruben PC (2001) Slow inactivation in voltage-gated sodium channels: molecular substrates and contributions to channelopathies. *Cell Biochem Biophys* **35**:171-190.

von Schoubye NL, Frederiksen K, Kristiansen U, Petersen AV, Dalby NO, Grunnet M, Jensen HS, Jespersen T, Sohal VS and Perrier J-F (2018) The sodium channel activator Lu AE98134 normalizes the altered firing properties of fast spiking interneurons in Dlx5/6(+/-) mice. *Neuroscience Letters* **662**:29-35.

Wagnon JL, Bunton-Stasyshyn RK and Meisler MH (2016) Mutations of Sodium Channel SCN8A (Na(v)1.6) in Neurological Disease, in *Ion Channels in Health and Disease* (Pitt GS ed) pp 239-264, Academic Press Ltd-Elsevier Science Ltd, London.

Wallace RH, Wang DW, Singh R, Scheffer IE, George AL, Jr., Phillips HA, Saar K, Reis A, Johnson EW, Sutherland GR, Berkovic SF and Mulley JC (1998) Febrile seizures and generalized epilepsy associated with a mutation in the Na+-channel beta1 subunit gene SCN1B. *Nat Genet* **19**:366-370.

Weiser TG, Haynes AB, Molina G, Lipsitz SR, Esquivel MM, Uribe-Leitz T, Fu R, Azad T, Chao TE, Berry WR and Gawande AA (2015) Estimate of the global volume of surgery in 2012: an assessment supporting improved health outcomes. *Lancet* **385**:11-11.

Weiss MM, Dineen TA, Marx IE, Altmann S, Boezio A, Bregman H, Chu-Moyer M, DiMauro EF, Feric Bojic E, Foti RS, Gao H, Graceffa R, Gunaydin H, Guzman-Perez A, Huang H, Huang L, Jarosh M, Kornecook T, Kreiman CR, Ligutti J, La DS, Lin M-HJ, Liu D, Moyer BD, Nguyen HN, Peterson EA, Rose PE, Taborn K, Youngblood BD, Yu V and Fremeau RT (2017) Sulfonamides as Selective NaV1.7 Inhibitors: Optimizing Potency and Pharmacokinetics While Mitigating Metabolic Liabilities. *Journal of Medicinal Chemistry* **60**:5969-5989.

Wengert ER, Miralles RM, Wedgwood KCA, Wagley PK, Strohm SM, Panchal PS, Idrissi AM, Wenker IC, Thompson JA, Gaykema RP and Patel MK (2021) Somatostatin-Positive Interneurons Contribute to Seizures in SCN8A Epileptic Encephalopathy. *The Journal of Neuroscience* **41**:9257-9273.

West James W, Numann R, Murphy Brian J, Scheuer T and Catterall William A (1991) A Phosphorylation Site in the Na+ Channel Required for Modulation by Protein Kinase C. *Science* **254**:866-868.

West JW, Patton DE, Scheuer T, Wang Y, Goldin AL and Catterall WA (1992) A cluster of hydrophobic amino acid residues required for fast Na(+)-channel inactivation. *Proc Natl Acad Sci U S A* **89**:10910-10914.

Westenbroek RE, Hell JW, Warner C, Dubel SJ, Snutch TP and Catterall WA (1992) Biochemical properties and subcellular distribution of an N-type calcium hannel α1 subunit. *Neuron* **9**:1099-1115.

Westenbroek RE, Merrick DK and Catterall WA (1989) Differential subcellular-localization of the ri and rii na+ channel subtypes in central neurons. *Neuron* **3**:695-704.

Weuring WJ, Singh S, Volkers L, Rook MB, van 't Slot RH, Bosma M, Inserra M, Vetter I, Verhoeven-Duif NM, Braun KPJ, Rivara M and Koeleman BPC (2020) NaV1.1 and NaV1.6 selective compounds reduce the behavior phenotype and epileptiform activity in a novel zebrafish model for Dravet Syndrome. *PLOS ONE* **15**:e0219106.

Wickman KD, Iñiguez-Lluhi JA, Davenport PA, Taussig R, Krapivinsky GB, Linder ME, Gilman AG and Clapham DE (1994) Recombinant G-protein βγ-subunits activate the muscarinic-gated atrial potassium channel. *Nature* **368**:255-257.

Wickman KD and Clapham DE (1995) G-protein regulation of ion channels. *Curr Opin Neurobiol* **5**:278-285.

WIPO Patent WO2007110220A1 Use of 4.9-anhydro-tetrodotoxin for the treatment of diseases related to the voltage-gated sodium channel α subunit Na»1.6 (2007).

Wong JC, Makinson CD, Lamar T, Cheng Q, Wingard JC, Terwilliger EF and Escayg A (2018) Selective targeting of Scn8a prevents seizure development in a mouse model of mesial temporal lobe epilepsy. *Scientific Reports* **8**:126.

Woodward RB and Gougoutas JZ (1964) The Structure of Tetrodotoxin. *Journal of the American Chemical Society* **86**:5030-5030.

Wright CF, Fitzgerald TW, Jones WD, Clayton S, McRae JF, van Kogelenberg M, King DA, Ambridge K, Barrett DM, Bayzetinova T, Bevan AP, Bragin E, Chatzimichali EA, Gribble S, Jones P, Krishnappa N, Mason LE, Miller R, Morley KI, Parthiban V, Prigmore E, Rajan D, Sifrim A, Swaminathan GJ, Tivey AR, Middleton A, Parker M, Carter NP, Barrett JC, Hurles ME, FitzPatrick DR, Firth HV and Study DDD (2015) Genetic diagnosis of developmental disorders in the DDD study: a scalable analysis of genome-wide research data. *Lancet* **385**:1305-1314.

Wu L, Nishiyama K, Hollyfield JG and Wang Q (2002) Localization of Na(v)1.5 sodium channel protein in the mouse brain. *Neuroreport* **13**:2547-2551.

Wu YW, Sullivan J, McDaniel SS, Meisler MH, Walsh EM, Li SX and Kuzniewicz MW (2015) Incidence of Dravet Syndrome in a US Population. *Pediatrics* **136**:e1310-e1315.

Wu Y-J, Guernon J, Shi J, Ditta J, Robbins KJ, Rajamani R, Easton A, Newton A, Bourin C, Mosure K, Soars MG, Knox RJ, Matchett M, Pieschl RL, Post-Munson DJ, Wang S, Herrington J, Graef J, Newberry K, Bristow LJ, Meanwell NA, Olson R, Thompson LA and Dzierba C (2017) Development of New

Benzenesulfonamides As Potent and Selective Nav1.7 Inhibitors for the Treatment of Pain. *Journal of Medicinal Chemistry* **60**:2513-2525.

Xu L, Li DY, Ding JJ, Pan L and Ding X (2018) Insight into tetrodotoxin blockade and resistance mechanisms of Na(v)1.2 sodium channel by theoretical approaches. *Chemical Biology & Drug Design* **92**:1445-1457.

Yang X, Niu X, Yang Y, Cheng M, Zhang J, Chen J, Yang Z and Zhang Y (2021) Phenotypes of GNAO1 Variants in a Chinese Cohort. *Frontiers in Neurology* **12**.

Yarowsky PJ, Krueger BK, Olson CE, Clevinger EC and Koos RD (1991) Brain and heart sodium channel subtype mRNA expression in rat cerebral cortex. *Proceedings of the National Academy of Sciences* **88**:9453-9457.

Yin LP, Rasch MJ, He QS, Wu S, Dou F and Shu YS (2017) Selective Modulation of Axonal Sodium Channel Subtypes by 5-HT1A Receptor in Cortical Pyramidal Neuron. Cerebral Cortex 27:509-521.

Yotsu-Yamashita M, Sugimoto A, Takai A and Yasumoto T (1999) Effects of specific modifications of several hydroxyls of tetrodotoxin on its affinity to rat brain membrane. *Journal of Pharmacology and Experimental Therapeutics* **289**:1688-1696.

Yu FH and Catterall WA (2003) Overview of the voltage-gated sodium channel family. *Genome Biology* **4**.

Yu FH, Westenbroek RE, Silos-Santiago I, McCormick KA, Lawson D, Ge P, Ferriera H, Lilly J, DiStefano PS, Catterall WA, Scheuer T and Curtis R (2003) Sodium channel beta4, a new disulfide-linked auxiliary subunit with similarity to beta2. *The Journal of neuroscience : the official journal of the Society for Neuroscience* **23**:7577-7585.

Yu FH, Mantegazza M, Westenbroek RE, Robbins CA, Kalume F, Burton KA, Spain WJ, McKnight GS, Scheuer T and Catterall WA (2006) Reduced sodium current in GABAergic interneurons in a mouse model of severe myoclonic epilepsy in infancy. *Nature Neuroscience* 9:1142-1149.

Yuan Y, O'Malley HA, Smaldino MA, Bouza AA, Hull JM and Isom LL (2019) Delayed maturation of GABAergic signaling in the Scn1a and Scn1b mouse models of Dravet Syndrome. *Scientific Reports* **9**.

Zamponi GW, Bourinet E, Nelson D, Nargeot J and Snutch TP (1997) Crosstalk between G proteins and protein kinase C mediated by the calcium channel α1 subunit. *Nature* **385**:442-446.

Zamponi GW and Snutch TP (1998) Modulation of voltage-dependent calcium channels by G proteins. *Curr Opin Neurobiol* **8**:351-356.

Zamponi GW and Currie KPM (2013) Regulation of CaV2 calcium channels by G protein coupled receptors. *Biochimica et Biophysica Acta (BBA) - Biomembranes* **1828**:1629-1643.

Zhang X, Ren W, DeCaen P, Yan C, Tao X, Tang L, Wang J, Hasegawa K, Kumasaka T, He J, Wang J, Clapham DE and Yan N (2012) Crystal structure of an orthologue of the NaChBac voltage-gated sodium channel. *Nature* **486**:130-134.

Zhang F, Xu X, Li T and Liu Z (2013) Shellfish Toxins Targeting Voltage-Gated Sodium Channels. *Marine Drugs* **11**:4698-4723.

Zhang J, Yuan H, Yao X and Chen S (2022) Endogenous ion channels expressed in human embryonic kidney (HEK-293) cells. *Pflugers Arch* **474**:665-680.

Zhu X, Petrovski S and Xie P (2015) Whole-exome sequencing in undiagnosed genetic diseases: Interpreting 119 trio. *Genet Med*:1-8.

Zurawski Z, Gray ADT, Brady LJ, Page B, Church E, Harris NA, Dohn MR, Yim YY, Hyde K, Mortlock DP, Jones CK, Winder DG, Alford S and Hamm HE (2019) Disabling the Gβγ-SNARE interaction disrupts GPCR-mediated presynaptic inhibition, leading to physiological and behavioral phenotypes. *Science Signaling* **12**:eaat8595.

Zurawski Z, Huynh S, Kaya A, Hyde K, Hamm HE and Alford S (2022) G protein βγ subunits bind to and inhibit the function of multiple Qa- and Qb,c-SNARE isoforms. *bioRxiv*:2022.2005.2030.494040.

Zurawski Z, Page B, Chicka MC, Brindley RL, Wells CA, Preininger AM, Hyde K, Gilbert JA, Cruz-Rodriguez O, Currie KPM, Chapman ER, Alford S and Hamm HE (2017) Gβγ directly modulates vesicle fusion by competing with synaptotagmin for binding to neuronal SNARE proteins embedded in membranes. *Journal of Biological Chemistry* **292**:12165-12177.

Zurawski Z, Rodriguez S, Hyde K, Alford S and Hamm HE (2016) Gβγ Binds to the Extreme C Terminus of SNAP25 to Mediate the Action of Gi/o-Coupled G Protein–Coupled Receptors. *Molecular Pharmacology* **89**:75-83.